

CENTER FOR

ADVANCED NUCLEAR ENERGY SYSTEMS

Massachusetts Institute of Technology
77 Massachusetts Avenue, 24-215
Cambridge, MA 02139-4307

(617) 452-2660
canes@mit.edu
canes.mit.edu



Advanced Nuclear Power Program

ASSESSMENT OF THE LIFECYCLE COST OF NUCLEAR GRADE COOLANTS FOR ADVANCED REACTORS

Lucas Javier Fernandez de Losada^{ab}
Jacopo Buongiorno^b, Annalisa Manera^b

a. *ETH Zurich, Raˆmistrasse 101, Zurich, 8092, Switzerland*

b. *Massachusetts Institute of Technology,
77 Massachusetts Avenue, Cambridge, 02139, MA, United States*

Department of Nuclear Science and Engineering
Massachusetts Institute of Technology

MIT-ANP-TR-203
December 2024

Assessment of the Lifecycle Cost of Nuclear-Grade Coolants for Advanced Reactors

CANES Report

Department of Nuclear Science and Engineering (NSE), Massachusetts Institute of Technology
Department of Mechanical and Process Engineering (D-MAVT), ETH Zurich

Authors:

Lucas Javier Fernandez de Losada | lfernand@ethz.ch | lucasfer@mit.edu

Prof. Dr. Jacopo Buongiorno, NSE

Prof. Dr. Annalisa Manera, D-MAVT

December 2024

Abstract

The vast majority of advanced nuclear energy systems (both fission and fusion) use coolant fluids other than water. While the thermophysical properties of all these coolants are well known, their cost, when the appropriate nuclear-grade characteristics are accounted for, is not. The fluids analyzed in this research are: light water (taken as reference), liquid sodium, liquid lead and lead-bismuth eutectic (LBE), organic coolants (terphenyl derivatives), liquid salt (FLiBe) and helium gas. A credible estimate of all the costs associated with such coolants must include raw material supply, transportation, initial purification to nuclear-grade specifications, chemistry control during operation and disposal.

Here we analyze the current purchase cost of various types of reactor coolants considering the target purity required for the start of the nuclear operations in a nuclear power plant, including the cost of pre-treatment if necessary.

We also perform an analysis of the costs required to control the coolant chemistry and purity throughout the reactor lifetime. To that end, all major expected impurities and the corresponding concentration limits have been identified for each coolant. Consequently, the state-of-the-art purification methods and related systems have been analyzed and their investment and operating costs have been estimated. The cost of coolant makeup has also been considered in the analysis where appropriate. The cost of disposal of the coolants at the backend of the reactor service life has been excluded due to its negligible discounted value.

The final results of the research include the estimate of a CAPEX cost expressed in \$/kg of coolant and an OPEX cost in \$/year per MW.

Contents

Abstract.....	i
CANES Publications.....	iv
List of abbreviations.....	vi
List of Tables.....	ix
List of Figures.....	xi
1. Introduction.....	1
2. Light water.....	5
2.1 Purity requirements.....	8
2.2 Cost of water.....	12
2.2.1 Operating costs.....	12
3. Sodium.....	15
3.1 Purity requirements.....	19
3.2 Purchase cost.....	25
3.3 Purification and chemistry control costs.....	27
3.3.1 Primary sodium purification system.....	27
3.3.2 Secondary sodium purification system.....	30
3.3.3 Inert gas receiving and processing system.....	32
4. Lead and Lead-Bismuth eutectic.....	34
4.1 Purity requirements.....	38
4.2 Lead and Lead Bismuth Eutectic costs.....	41
4.2.1 Purchase costs.....	42
4.2.2 Pre-purification costs.....	44
4.2.3 Purification and chemistry control costs.....	46
5. Organic Fluids.....	53
5.1 Purity requirements.....	59
5.2 Purchase cost.....	61
5.3 Operational and Purification costs.....	62
6. FLiBe.....	69
6.1 Technical Specifications for Nuclear-Grade FLiBe.....	71
6.1.1 Enrichment requirements.....	71
6.1.2 Chemistry requirements.....	74
6.2 Cost of FLiBe.....	77
6.2.1 Purchase cost.....	77
6.2.2 Pre-Purification cost.....	83

6.3	Operating costs	87
7.	Helium.....	89
7.1	Purity requirements	93
7.2	Cost of Helium.....	98
7.2.1	Purchase cost.....	100
7.2.2	Helium make-up cost.....	101
7.2.3	Purification and chemistry control costs	102
8.	Decommissioning costs	115
9.	Conclusion and future work	116
	Bibliography	118
	Appendix A	131
	Appendix B	132
	Appendix C	133
	Appendix D	133
	Appendix E	135

CANES PUBLICATIONS

Topical and progress reports are published under seven series:

Advances in Nuclear Energy Disciplines (ANED) Series
Advanced Nuclear Power Technology (ANP) Series
Nuclear Fuel Cycle Technology and Policy (NFC) Series
Nuclear Systems Enhanced Performance (NSP) Series
MIT Reactor Redesign (MITRR) Series
Nuclear Energy and Sustainability (NES) Series
Nuclear Space Applications (NSA) Series

Please visit our website (mit.edu/canes/) to view more publication lists.

- MIT-ANP-TR-203 Lucas Javier Fernandez de Losada and Jacopo Buongiorno (MIT), Annalisa Manera (ETH Zurich) (**Assessment of the Lifecycle Cost of Nuclear-Grade Coolants for Advanced Reactors** (December 2024).
- MIT-ANP-TR-202 Emile G.R. Germonpre and Jacopo Buongiorno, **A Preliminary Study on the Feasibility of Nuclear Batteries for Offshore Power Generation** (November 2024).
- MIT-ANP-TR-201 Koroush Shirvan, **2024 Total Cost Projection of Next AP1000** (July 2024).
- MIT-ANP-TR-200 Jérémy Mangin, Amaury Le Person, Koroush Shirvan, Jeong Ik Lee, Andrew Whittaker, and Neil Todreas, **Consequence-based security of a sodium-cooled graphite-moderated thermal microreactor (SGTR)** (April 2024).
- MIT-ANP-TR-199 Emile Germonpre and Jacopo Buongiorno, **Feasibility study of decentralized hydrogen production using nuclear batteries** (January 2024).
- MIT-ANP-TR-198 Lucas Lallemand, Jacopo Buongiorno, Shafiqul Islam and Laurent Vernon, **Design of Fission Batteries Process (FIBAPRO) Facility** (October 2023).
- MIT-ANP-TR-197 Matthew Chew and Jacopo Buongiorno, **A Cybersecurity Framework for Nuclear Microreactors** (June 2023).
- MIT-ANP-TR-196 Paul E. Roege(MIT ANPEG), Alexander L. Schoonen(INL), James R. Case (INL), Corey L. Beebe(INL), Ryan Cumings (MIT LL), Zachary A. Collier (Collier Research Systems), **Assessment of Potential Ground Force Capability Enhancement Using Nuclear Microreactors** (August 2022).

- MIT-ANP-TR-194 W. Robb Stewart and K. Shirvan (MIT), **Capital Cost Evaluation of Advanced Water-Cooled Reactor Designs With Consideration of Uncertainty and Risk** (June 2022).
- MIT-ANP-TR-193 K. Shirvan (MIT), **Overnight Capital Cost of the Next AP1000** (March 2022).
- MIT-ANP-TR-192 R. MacDonald and J. Parsons (MIT), **The Value of Nuclear Microreactors in Providing Heat and Electricity to Alaskan Communities** (October 2021).
- MIT-ANP-TR-191 C. W. Forsberg (MIT) and A. W. Foss (INL), **Markets and Economic Requirements for Fission Batteries and Other Nuclear Systems** (March 2021).
- MIT-ANP-TR-190 J. Buongiorno (MIT), **An Economic Evaluation of Micro-Reactors for the State of Washington** (January 2021).
- MIT-ANP-TR-189 C. W. Forsberg (MIT), P. Sabharwall (INL) and A. Sowder (EPRI), **Separating Nuclear Reactors from the Power Block with Heat Storage: A New Power Plant Design Paradigm** (November 2020).
- MIT-ANP-TR-188 X. Zhao and M. Golay, **Symptom-Based Conditional Failure Probability Estimation for Selected Structures, Systems, and Components: Minor Milestone Report: Project on Design of Risk-Informed Autonomous Operation for Advanced Reactors DOE/EXT- DE-NE0008873 Project number: 19-17435** (July 2020).
- MIT-ANP-TR-187 J. Buongiorno, K. Shirvan, E. Baglietto, C. Forsberg, M. Driscoll, W. Robb Stewart, Enrique Velez-Lopez (MIT), H. Einstein (Civil & Environmental Engineering), Iain Macdonald (ArtEZ), Kennard Johnston (Morgan State Univ.) and Go Hashimoto (Univ. of Tokyo), **Japan's Next Nuclear Energy System (JNext)** (March 2020).
- MIT-ANP-TR-186 Y. Cai and M. W. Golay, **A Framework for Analyzing Nuclear Power Multiunit Accident Scenarios and Providing Accident Mitigation and Site Improvement Suggestions** (September 2019).
- MIT-ANP-TR-185 C. W. Forsberg (MIT), P. Sabharwall and H. D. Gougar (INL), **Heat Storage Coupled to Generation IV Reactors for Variable Electricity from Base-load Reactors: Changing Markets, Technology, Nuclear-Renewables Integration and Synergisms with Solar Thermal Power Systems INL/EXT-19-54909** (September 2019).
- MIT-ANP-TR-184 C. W. Forsberg, **Implications of Carbon Constraints on (1) the Electricity Generation Mix For the United States, China, France and United Kingdom and (2) Future Nuclear System Requirements** (March 2019).
- MIT-ANP-TR-183 C. W. Forsberg, **Fluoride-Salt-Cooled High-temperature Reactor (FHR) Temperature Control Options: Removing Decay Heat and Avoiding Salt Freezing** (January 2019).
- MIT-ANP-TR-182 J. Buongiorno, N. Sepulveda and L. Rush, **White Paper: Potential Applications of the Modern Nuclear Fuel Cycle to (South) Australia** (November 2018).

List of abbreviations

ADS: Accelerator Driven System
AEC: Atomic Energy Commission
AGR: Advanced Gas-cooled Reactor
ANL: Argonne National Laboratory
ANP: Aircraft Nuclear Propulsion
ARE: Aircraft Reactor Experiment
AVLIS: Atomic Vapor Laser Isotope Separation
BRS: Boron Recovery (Recycle) System
BWR: Boiling Water Reactor
COLEX: COlumn EXchange enrichment process
CVCS: Chemical and Volume Control System
DOE: (U.S.) Department of Energy
EAEC: European Atomic Energy Community
ELEX: ELectrical EXchange enrichment process
EM: Electromagnetic
FHR: Fluoride-salt-cooled High-temperature Reactor
FOAK: First-Of-A-Kind
FSV: Fort-Saint Vrain
GE: General Electric
GIF: Generation IV International Forum
HB: High Boiler
HLM: Heavy Liquid Metal
HPS: Helium Purification System
HTGR: High Temperature Gas Reactor
HX/IHX: Heat Exchanger/Intermediate Heat Exchanger
IGRPS: Inert Gas Receiving and Processing System
IHTS: Intermediate (or Secondary) Heat Transfer System

INL: Idaho National Laboratory

ISPS: Intermediate Sodium Processing Subsystem

KAIST: Korea Advanced Institute of Science and Technology

LBE: Lead-Bismuth Eutectic

LFR: Lead-cooled Fast Reactor

LOCA: Loss Of Coolant Accident

LWR: Light Water Reactor

MOX: Mixed Oxide Fuel

MIT: Massachusetts Institute of Technology

MOU: Memorandum of Understanding

MRI: Magnetic Resonance Imaging

MSRE: Molten Salt Reactor Experiment

NACC: Nuclear Air-Brayton Combined Cycle

NGNP: Next Generation Nuclear Plant

NPP: Nuclear Power Plant

NRC: (U.S.) Nuclear Regulatory Commission

OCS: Oxygen Control System

OMRE: Organic Moderated Reactor Experiment

OREX: ORganic Exchange enrichment process

ORNL: Oak Ridge National Laboratory

PNPF: Piqua Nuclear Power Facility

PSPS: Primary Sodium Purification System

PWR: Pressurized Water Reactor

R&D: Research and Development

RCS: Reactor Coolant System

SCC: Stress Corrosion Cracking

SFR: Sodium Fast Reactor

SDC: Safety Design Criteria

SDG: Safety Design Guideline

SDT: Sodium Dump Tank

SG: Steam Generator

SS: Stainless Steel

UCB: University of California Berkeley

US and USA: United States of America

USD: U.S. Dollars

USGS: United States Geological Survey

UW: University of Wisconsin-Madison

VCT: Volume Control Tank

List of Tables

Table 1 Planned and potential U.S. Advanced reactor Demonstration Plants (Holt, 2023).	2
Table 2 Recommended values for different control parameters in PWRs (U.S. Nuclear Regulatory Commission) (Kawamura, et al., 2016) (Haas, 2009).	10
Table 3 Possible purification methods to be selected for coolant water preparation for LWR applications (Salam & Rokonuzzaman, 2023) (Singh & Hankins, 2016).	11
Table 4 CVCS cost analysis (Ganda, Hoffman, Taiwo, Kim, & Hansen, 2019) (Ganda, Taiwo, & Kim, Report on the Update of Fuel Cycle Cost Algorithms, 2018).	14
Table 5 Comparison of the physical properties of sodium and water (Schulenberg, 2022) (Ohshima & Kubo, 2023).	15
Table 6 Design parameters of the SFR designs currently pursued in the USA.	18
Table 7 List of the possible impurities in the primary sodium (Kozlov, Bogdanovich, Zagorulko, & Matveev, 2012) (Smith & Holmes, 1975) (Ivanenko, 1996) (Akins, Kultgen, & Heifetz, 2023).	20
Table 8 List of the possible impurities in the secondary sodium (Smith & Holmes, 1975).	22
Table 9 Intensity of sodium impurities based on operational experience of BN-350 and BN-600 reactors.	24
Table 10 Target control limits and detection limits in impurities of the argon cover gas both for primary and secondary coolants (Maeda, Kobayashi, Ishiyama, & Motonaga, 1987).	24
Table 11 Retrieved cost for reactor grade sodium.	25
Table 12 Investment cost associated with coolant initial purchase for different size of reactors based on the necessary quantity of sodium (Prosser, et al., 2023) (Argonne National Laboratory, 2024) (Flanagan, 2019) (Nuclear Energy Agency, 2015).	26
Table 13 Capital investment foreseen for PSPS installation (Prosser, et al., 2023).	29
Table 14 Capital investment foreseen for ISPS installation (Prosser, et al., 2023).	31
Table 15 Capital investment foreseen for IGRPS installation (Prosser, et al., 2023).	33
Table 16 Properties of Lead and LBE compared with other heat transfer fluids commonly considered for nuclear reactors (Nuclear Energy Agency, 2015).	35
Table 17 Comparison of Lead and LBE properties at 500 degrees Celsius (Sofu, 2019).	36
Table 18 Possible impurities present in lead/LBE used for a critical or subcritical reactor system or a spallation target of an ADS. The normal impurity content is taken from data of the MEGAPIE experiment (Nuclear Energy Agency, 2015).	39
Table 19 Lead impurity composition [wt%] for C00 and C2C grades (Levinsky, et al., 2022).	41
Table 20 Retrieved cost for high purity and reactor grade lead and LBE.	42
Table 21 Investment cost associated with coolant initial purchase for different size of LFRs/ADSs based on the necessary quantity of lead/LBE (Nuclear Energy Agency, 2015).	43
Table 22 Investment cost relative to pre-purification systems in a facility of the size of ATHENA.	45
Table 23 Main characteristics of the oxygen control methods in lead-cooled systems (Bassini, 2017) (Brissonneau, et al., 2011).	48
Table 24 Investment cost relative to gas-phase oxygen control systems in a reactor of the size of the BREST-OD-300.	50
Table 25 Investment cost relative to solid-phase oxygen control systems.	51
Table 26 Possible organic coolant options for use in organic cooled and/or moderated reactor and their main properties (Shirvan & Forrest, Design of an Organic Simplified Nuclear Reactor, 2016).	54
Table 27 Completed organic nuclear reactor projects internationally and in the United States (Shirvan & Forrest, Design of an Organic Simplified Nuclear Reactor, 2016).	58
Table 28 Assumed impurities concentrations for new coolant in the Piqua nuclear power plant and the OMRE facility (Makens, 1964) (Atomics International, 1960).	60
Table 29 Cost per kg of various organic fluids useful for nuclear applications.	61

Table 30 Capital and operating costs for the maintenance of a nuclear grade coolant during operation.	67
Table 31 Comparison of water and FLiBe properties respectively at 293 K and 950 K (Sorbom, et al., 2015). As can be seen from the table, FLiBe presents similar thermal-hydraulic features to water.....	69
Table 32 General Chemical Specifications for MSRE Fluoride Mixtures (Shaffer, 1971).	75
Table 33 Classification of 53 impurities possibly present in FLiBe based on a maximum reactivity penalty of 20 pcm (Seifried, Scarlat, Peterson, & Greenspan, 2019).	76
Table 34 Different prices ranges and suppliers for compounds useful for FLiBe cost calculation.	81
Table 35 Calculated cost of FLiBe for different use (fission and fusion applications) based on the assumptions described above.	83
Table 36 Main FLiBe purification methods overview with a short description and their respective advantages/disadvantages.	85
Table 37 Expected capital costs for coolant purchase for different types of reactors.	87
Table 38 Cost estimate of fluoride molten salt chemistry control and testing components for operation (Holcomb, Peretz, & Qualls, 2011).	88
Table 39 A comparison between Helium properties and other coolants at different reactor conditions (Bubelis, 2013).	90
Table 40 Potential risks for the principal reactor internals given by operation of high temperature helium cooled reactor (Bubelis, 2013) (Wright, 2006) (Castle, 2010) (Lee & Pint, 2021) (Cabet & Rouillard, 2009).	94
Table 41 Impurity content of some helium-cooled reactors during operation (Lee & Pint, 2021) (Castle, 2010) (Wright, 2006) (Berka, et al., 2012).	97
Table 42 Impurity concentrations in ppm at the FSV plant during rise to power (Wright, 2006).	98
Table 43 Cost per kg of high purity helium.	100
Table 44 Fronted capital investment of different helium-cooled designs based on the required helium inventory. ...	100
Table 45 Helium make-up cost for different reactor designs.	101
Table 46 List and description of the main subsystems which have been historically considered when designing a helium HPS (Castle, 2010) (Berka, et al., 2012) (Olson, Brey, & Swart, 1980) (Legros, et al., 2006) (Liger, Lefebvre, Ciampichetti, Aiello, & Ricapito, 2011) (Gastaldi, Liger, Robin, & Poletiko, 2006) (Ciampichetti, et al., 2010) (Tincani, et al., 2019) (Shin, et al., 2023) (Idaho National Laboratory, 2010).	103
Table 47 Location of HPS installation in different HTGRs.....	108
Table 48 Capital cost estimation for a HPS capable of filtering a helium flow of 200 kg/h at an input pressure and temperature of 4 MPa and 280 °C.	112
Table 49 Summary of the main results.	117
Table 50 PWR secondary circuit water chemistry indications (Salam & Rokonuzzaman, 2023).	131
Table 51 Control parameters for reactor coolant of BWR during power operations (Kawamura, et al., 2016).	132
Table 52 Materials used in SFRs in different countries (Yoshida & Furukawa, 2012).	132
Table 53 Intensity of impurity contamination in primary sodium for PRISM case (U.S. Department of Energy, 1987).	132
Table 54 Plant Economics for a 400 kg/year Li-7 throughput (Ault, et al., 2012).	134
Table 55 Plant Economics for a 20 ton/year Li-7 throughput (Ault, et al., 2012).	134

List of Figures

Figure 1 PWR (right) and BWR (left) reactor schemes (U.S. Department of Energy, 2015).....	7
Figure 2 CVCS schematic in a Korean APR1400 (Chung, Kim, Lee, & Lee, 2020).....	13
Figure 3 Pool-type (left) and Loop-type (right) SFR models (Cheng, Cheng, & Chen, 2024)	17
Figure 4 PRISM's primary sodium processing system (U.S. Department of Energy, 1987).	28
Figure 5 PRISM's secondary sodium processing system in normal operation configuration (Department of Energy, 1987).....	30
Figure 6 Scheme of a LFR as courtesy of the Generation IV International Forum (Pioro, 2016).....	38
Figure 7 Schematic representation of the ATHENA research facility. Image kindly provided by ENEA (Italy).	45
Figure 8 Oxygen specifications in LBE (Nuclear Energy Agency, 2015).	47
Figure 9 Schematics of the OMRE reactor concept (Parkins & Weisner, 1959).	56
Figure 10 Flow diagram for a flash tank fed hydrocracker as proposed for the Piqua Nuclear Power Facility (Griffith & Russel, 1963)	63
Figure 11 Indirect cost estimate for various size hydrocracker plants (Griffith & Russel, 1963)	66
Figure 12 Operational cost estimate for various size hydrocracker plants (Griffith & Russel, 1963)	67
Figure 13 Mk1 PB-FHR flow schematic (International Atomic Energy Agency, 2016).....	70
Figure 14 Simplified AVILS theory applied to Uranium enrichment (U.S. Nuclear Regulatory Commission).	74
Figure 15 Different possible production processes for naturally enriched FLiBe ("FUSION use") and highly enriched FLiBe ("FISSION use"). As it can be seen from the box scheme for enriched FLiBe, the dashed lines indicate the two possible reactions, either with water and HF or pure F, to produce ${}^7\text{LiF}$. The manufacturing strategy considered in this cost analysis is the one going from ${}^7\text{Li}$ to ${}^7\text{LiOH}$ to finally ${}^7\text{LiF}$ because of the reasons specified in the paragraphs above.	80
Figure 16 Time of oxide removal from a test loop at ORNL MSRE by treatment with H_2 and HF at $565\text{ }^\circ\text{C}$ (Shaffer, 1971).....	84
Figure 17 Difference between prismatic fuel assembly and pebble bed fuel. This difference is at the basis of the two concepts of HTGRs, the pebble-bed HTGR and the prismatic block HTGR (Rahmatullah, et al., 2019)	92
Figure 18 Measured helium leak rate in the HTTR during different periods compared to the restricted rate of 0.3 wt%/day (Tochio, Shimizu, Hamamoto, & Sakaba, 2014).....	102
Figure 19 Schematic of the Fort St Vrain HPS (Olson, Brey, & Swart, 1980).	109
Figure 20 Schematic of the HTTR HPS (Fujiwara, 2021).....	109
Figure 21 Schematic of the HTR-10 HPS (Yao, Wang, Liu, He, & Li, 2002).....	110
Figure 22 Designed HPS considered for subsequent economic evaluation.	110
Figure 23 Decommissioning costs analyzed with FVA and NPV approaches	115
Figure 24 Rate of HB formation in the coolant based on HB equilibrium concentration (J.L. Griffith, 1963).	133
Figure 25 Impurity emission from primary circuit structures in the HTTR at different temperature ranges (Japan Atomic Energy Agency, 2010).	136

1. Introduction

Decarbonization aims at reducing carbon dioxide (CO₂) emissions from energy systems. This process is essential to mitigate climate change, which is driven by the accumulation of greenhouse gases, such as CO₂, in the atmosphere. Carbon dioxide and the other greenhouse gases are important heat-trapping gases which significantly contribute, by their accumulation in the atmosphere, at the increase of the average global temperature affecting Earth's climate equilibrium. At the moment, human activities have raised atmospheric CO₂ by 50% with respect to pre-industrial levels, going from approximately 280 to over 420 ppm (June 2024) (NASA, 2024). To achieve a complete energy decarbonization, the main strategies consist in transitioning from fossil fuels to carbon free energy sources, enhancing energy efficiency, and implementing carbon capture technologies. This approach would be necessary to meet the legally binding international treaty settled by 196 parties at the Paris UN Climate Change Conference in 2015 (United Nations, 2015). The "Paris Agreement" declared the parties' interest of keeping the increase in global average temperature to well below 2 °C above preindustrial levels within this century, further pursuing efforts to limit the increase to 1.5°C (Li, et al., 2020). Given the world's growing demand for electricity driven by population growth, economic development, urbanization, technological advancements, and the electrification of various sectors, providing carbon-free, affordable, and easily accessible electricity to billions of people is anticipated to be one of this century's greatest challenges. A major potential tool in the fight to contain global warming is surely nuclear energy: one of the safest and most reliable forms of carbon-free electricity.

Historically, nuclear energy has been a major contributor to the production of carbon-free electricity. In 2020, it accounted for approximately 10% of global electricity generation. It is the second-largest source of low-emissions electricity (non-fossil-based), following hydroelectricity, and the leading source in advanced economies. In fact, estimations state the world's global emissions from electricity production would have been almost 20% higher and total energy-related emissions 6% higher without nuclear installations within the 1971-2020 period (International Energy Agency, 2022). Looking at the United States, the nuclear power plant fleet is the largest in the world. There are currently (October 2023) 94 nuclear power plants in operation (63 Pressurized Water Reactors and 31 Boiling Water Reactors), which generate about 20% of the nation's electricity (U.S. National Regulatory Commission, 2023). Nevertheless, the nuclear sector has struggled considerably after 2007. In fact, most of the power plants in the United States were highly profitable in the early 2000s and the production costs were lower than the primary competitors: fossil fuels and renewables. Nevertheless, the situation reversed as large quantities of affordable shale natural gas became available in the United States and the Great Recession reduced electricity demand and prices (Massachusetts Institute of Technology, 2018). From that point, the demand for new nuclear reactors has damped and thirteen reactors have closed in the past decade, some of which because of the inability to compete with cheaper generation options (Holt, 2023) (Massachusetts Institute of Technology, 2018). The few new nuclear built in the United States have experienced significant schedule delays and consequent cost overruns, with the Vogtle Units 3 and 4 being the major standout, topping a price tag of 34 billion USD, approximately 17 billion overbudget and seven years behind schedule (Amy, 2023). Due to the high costs and delays associated with large conventional Light Water Reactors (LWRs) construction, along with safety concerns arising from the 2011 Fukushima nuclear disaster in Japan, increasing volumes of nuclear waste, and other issues, there has been a surge of interest for "advanced" nuclear technologies. Advocates of these "new" technologies argue that these could be less expensive, safer, and more fuel-efficient than existing LWRs.

While there exist different definitions for advanced reactors, the definition provided by the One Hundred Fifteenth Congress of the United States of America states: *The term "advanced nuclear reactor" means a nuclear fission or fusion reactor, including a prototype plant (as defined in sections 50.2 and 52.1 of title 10, Code of Federal Regulations (as in effect on the date of enactment of this Act)), with significant improvements compared to commercial nuclear reactors under construction as of the date of enactment of this Act, including improvements such as—*

(A) *additional inherent safety features;*

- (B) significantly lower levelized cost of electricity;
- (C) lower waste yields;
- (D) greater fuel utilization;
- (E) enhanced reliability;
- (F) increased proliferation resistance;
- (G) increased thermal efficiency; or
- (H) ability to integrate into electric and nonelectric applications.

Based on this definition, several reactor types could be included in a potential list such as Small Modular Reactors (SMRs) and the six reactor technologies selected by the Generation IV International Forum (GIF) as the most promising for further research and development. In particular, SMRs were defined by the International Atomic Energy Agency (IAEA) as reactors with a power capacity of up to 300 MW(e) per unit with the possibility of factory-assembling and transporting systems or components as a unit for installation. On the other hand, the six Generation IV technologies selected by the GIF include the Gas-cooled Fast Reactor (GFR), Lead-cooled Fast Reactor (LFR), Molten Salt Reactor (MSR), Supercritical Water-cooled Reactor (SCWR), Sodium-cooled Fast Reactor (SFR) and Very High Temperature Reactor (VHTR). Given the growing interest of the industry towards advanced reactor technologies, several investments have been done by the United States Congress and the U.S. Department of Energy (DOE) to allow the demonstration of these technologies and their commercialization.

In particular, the Nuclear Energy Innovation Capabilities Act of 2017 mandated the DOE to support advanced reactor development by creating the National Reactor Innovation Center for testing and demonstrating private-sector reactor concepts at DOE sites. The Nuclear Energy Innovation and Modernization Act of 2019 required the NRC to develop a regulatory framework for advanced nuclear technologies. The 2020 Energy Act established the Advanced Reactor Demonstration Program (ARDP) within the DOE, allowing it to cover up to 50% of the costs for two commercial demonstration projects and 80% for potential future plants. The program initially received \$230 million from the Further Consolidated Appropriations Act (2020), before allocating \$2.477 billion through FY2025 from the Infrastructure Investment and Jobs. Under the ARDP, the DOE can fund up to 80% of the development costs for advanced reactor concepts for future demonstrations. In 2020, the DOE announced five awards aimed at reducing risks for future demonstration projects potentially licensed and deployed within the next 10-14 years. Under the Energy Act, the Congress also requires the DOE to support the development of High-Assay Low Enriched Uranium (HALEU). HALEU is uranium fuel enriched in fissile Uranium-235 between 5% and 20%, useful for many advanced reactor designs (Holt, 2023). The Department of Defense (DOD) is also involved in the investments. Through Project Pele, the DOD awarded a \$300 million funding for a prototype mobile high-temperature gas-cooled microreactor to be assembled and initially operated at Idaho National Laboratory (INL). The microreactor will not require an official NRC license and will have the capability of being transported by the DOD and able to deliver 1-5 MWe for a minimum of three years of full power operation (U.S. Department of Defence, 2022). Moreover, the CHIPS Act of 2022 authorizes a DOE grant program for advanced nuclear reactor research, development, and demonstration, prioritizing projects located at closed or closing fossil fuel power plants and those planning non-electric applications of nuclear energy. The Inflation Reduction Act of 2022 (IRA) introduced tax credits for zero-carbon power plants, including advanced nuclear reactors. As stated by the IRA, the owners of qualifying plants can receive either a 10-year electricity production tax credit of up to 2.6 cents per kilowatt-hour or a 30% investment tax credit. Additionally, the IRA allocated \$700 million for the DOE to develop supplies of HALEU (Holt, 2023). The currently pursued projects for advanced reactor demonstration in the United States are reported in Table 1 (Holt, 2023).

Table 1 Planned and potential U.S. Advanced reactor Demonstration Plants (Holt, 2023).

Reactor Designer	Technology	Power (MWe)	Plant Owner	DOE Funding	DOE Cost Share	Plant Location	NRC Licensing Status
------------------	------------	-------------	-------------	-------------	----------------	----------------	----------------------

Demonstrations with ARDP funding							
Terra Power	Sodium-cooled fast reactor	345	PacifiCorp	Up to \$2.0 billion	50%	Kemmerer, WY	Pre-application activities
X-energy	High-temperature gas-cooled reactor	80	Energy Northwest	Up to \$1.2 billion	50%	Washington	Pre-application activities
Demonstrations with Other DOE funding							
NuScale	Light water SMR	77	Utah Associated Municipal Power Systems	Up to \$1.4 billion	23%	INL	77 MW standard design application submitted 1/1/2023
Pre-Demonstrations with ARDP funding							
Westinghouse	Heat pipe micro-reactor	5	Westinghouse	Up to \$7 million	80%	-	Pre-application activities
BWX Technologies	Commercial high-temperature gas-cooled micro-reactor	17	BWX Technologies	Up to \$85 million	80%	-	None
Kairos	Fluoride-salt-cooled high-temperature test reactor	35 MWth	Kairos	Up to \$303 million	48%	Oak Ridge, TN	Construction permit application submitted 9/29/2021
Holtec	Water-cooled SMR	160	Holtec	Up to \$116 million	79%	-	Pre-application activities
Terra Power	Molten chloride fast reactor test facilities	-	TerraPower	Up to \$90 million	80%	Everett, WA	Pre-application activities
Prototype Funded by DOD							
BWX Technologies	Defense High-Temperature Gas-cooled microreactor	1.5 MWth	DOD	About \$30 million	funded by DOD	INL	DOE safety oversight
Other Designs with NRC Interactions							
General Atomics	High-Temperature gas-cooled fast reactor	50	-	No demonstration funding	-	-	Pre-application activities
Terrestrial Energy	Molten Salt Reactor	392 MWth	-	No demonstration funding	-	-	Pre-application activities
GE Hitachi	Water-cooled SMR	300	Ontario Power Generation	No demonstration funding	-	Clarington-Ontario	Pre-application activities by NRC and Canadian Nuclear safety Commission
Ultra Safe Nuclear Corporation	High temperature gas-cooled micro-reactor	15 MWth	University of Illinois	No demonstration funding	None	University of Illinois at Urbana-Champaign	Pre-application activities

Given the significant investments dedicated to the Advanced Reactor development and the fact that most of the advanced reactor projects are currently foreseen for the late 2020s or early 2030s, part of the success of the industry is strongly dependent on the ability to build these concepts on time and on budget. Achieving this is essential for making nuclear energy a viable option and enhancing its appeal to investors. In particular, high precision cost estimates,

projections and schedule management will be required by the industry for all the systems and components of the designed concepts. Given that the majority of the advanced reactor concepts currently pursued has never been built in the United States and some of the systems which guarantee their safety and high-performance operation might still have to be developed for some cases, estimating their cost is not a simple task. In particular, the scope of this report is to contribute by focusing on the costs of advanced reactors coolant purification. The cooling fluids analyzed in this research are:

- Light water (taken as reference);
- Liquid sodium;
- Liquid lead-bismuth eutectic (LBE) and lead;
- Organic coolants (terphenyl derivatives);
- Liquid salt (FLiBe);
- Helium gas.

While the thermophysical properties of all these coolants are well known, their cost, when the appropriate nuclear-grade characteristics are accounted for, is not. For each of these coolants, their specific “nuclear grade” requirements are analyzed. In fact, each of these coolants has to comply with high purity standards before they can be used as reactor coolants in advanced concepts, to ensure acceptable neutronic performance, long term reactor safety and high operational reliability. In fact, the presence of excessive impurities in a reactor primary system can significantly reduce reactivity, corrode the primary structures and the fuel cladding, degrade the heat transfer and the heat transportation properties of the coolant, increase the radioactivity levels potentially harming maintenance operations. For this reason, the industry has developed very stringent standards for the coolant’s quality, often referred as “nuclear grade”. In some cases, the primary impurities present in the coolant are also listed. Successively, the cost of the nuclear grade coolants is analyzed considering the specific requirements for every one of them. The quotes included in this report are obtained from a variety of sources, i.e., historical documentation, industry suppliers and buyers, experts in the field at U.S. national laboratories and other nuclear related research facilities. The scope is to provide a range of cost in 2024 USD/kg which may be valid when considering high quantities of coolant, of the same order of magnitude as required for advanced nuclear reactor operation. Moreover, since the report and research activities have been carried out in the United States, the main objective is to identify suppliers within this country, when possible. After identifying the cost for the purchase of the nuclear grade coolants, the cost related to their purification during reactor operation is also assessed in the report. In fact, despite the high purity requirements for the start of nuclear operations, these coolants may degrade over time, change their chemical or physical composition, absorb impurities, especially during maintenance and refueling operations. For these reasons, and to monitor the presence and concentration of possible additives in the coolant to improve their physical and chemical properties, purification systems are required. These systems, which are not relevant for the safety of the reactor, might function continuously or on demand depending on the specific reactor design requirements, the properties of the coolant, the specific operational conditions, etc. Moreover, the functioning of the purification and chemistry control systems together with their main features are described in the report for the scope of completeness. This systems’ operation is based on the specific properties of the coolant as they often leverage on specific chemical reactions to complete the coolant’s purification and maintain the necessary conditions for nuclear operation. The investment costs relative to the purchase and installation of purification systems is normalized to the total quantity of coolant required for reactor operation, so that the final metric included in the report is in 2024 USD/kg. Usually, the purification systems do not require a high level of maintenance and the impact of preservation, reparation and potential regeneration operation is not foreseen to be particularly relevant with respect to the normal operational costs related to reactor operation. Nevertheless, regular maintenance is necessary to ensure the correct functioning of the system. Although it has not been possible to retrieve information for every purification system associated maintenance costs, data based on reactor or experimental facilities experience is included in the report and considered when available. This cost information is normalized with the reactor power (in MWth) and on one year time, so that the final quote is given as \$/MWth·year. Moreover, some of the advanced reactor

coolants considered in the report need make-up coolant during their lifetime, as the initial properties of the coolant could be degraded during operation given the high radiation and temperature operating conditions, or due to the specific properties of the coolants which allow it to escape from the primary system boundaries. These make-up requirements are also considered as operational costs. Other operating costs are also accounted and considered when available and retrievable from the literature. Finally, the costs relative to the decommissioning of the coolant are also evaluated in this report and assessed separately in a specific chapter. In fact, although there is much uncertainty on the decommissioning requirements for some of these coolants as regulations might significantly differ within the U.S. and other countries or might not be completely developed, the impact on decommissioning costs is expected to be very limited with respect to the other costs.

2. Light water

Water, the most abundant compound on Earth's surface, is a remarkable substance with unique properties that make it essential for life and invaluable in various industrial applications. In its liquid form, water can be classified as "light water" and "heavy water" based on the isotopic composition of its hydrogen atoms. Light water, which comprises about 99.98% of naturally occurring water on Earth, has an atomic mass of approximately 18 amu. Heavy water, on the other hand, contains a higher concentration of deuterium—a hydrogen isotope with one proton and one neutron—giving it an atomic mass of about 20 amu. In light water reactors (LWRs), which constitute the majority of nuclear power plants worldwide, water serves a dual purpose: it acts as both a coolant to remove heat from the reactor core and as a neutron moderator to facilitate the fission process. From a nuclear perspective, water's ability to slow down fast neutrons through elastic scattering, transforming them into thermal neutrons, is crucial for sustaining nuclear chain reactions in thermal reactors. When used as a coolant, light water offers several advantages. First, its thermal-hydraulic properties are well-understood, which is one reason LWRs have become the most widely commercialized reactor type globally. Additionally, water has an excellent heat capacity (around 4000 kJ/m³ at 75 atm), enabling it to absorb and transport large amounts of heat efficiently (World Nuclear Association, 2024). When pressurized, water can operate over a wide temperature range, and effectively transfers heat through vaporization and condensation due to its high latent heat of vaporization. While its thermal conductivity is not as high as that of liquid metals, it is sufficient for effective heat transfer in reactor systems. Moreover, water is abundant and inexpensive. Other advantages include the ability to provide inherent safety features, such as a negative temperature coefficient of reactivity, where increased temperatures lead to decreased reactivity, and the adaptability to natural circulation, which is facilitated by density changes. Water also offers significant radiation shielding, adding an extra layer of protection in reactor systems. Finally, water's transparency facilitates refueling operations and maintenance activities.

On the other hand, using water as a coolant in light water reactors (LWRs) also presents some drawbacks. The primary issue is the need to maintain high pressures in the coolant circuits to keep water in its liquid state and achieve sufficient thermodynamic efficiency. Additionally, water and steam can oxidize metals commonly used in reactors, such as steel and copper, leading to degradation of internal structures, especially at high pressures. The relatively high neutron absorption cross section of light water necessitates the use of enriched uranium to improve neutron economy and sustain chain reactions. Neutron absorption also results in the production of tritium, a radioactive isotope with a half-life of 12.3 years. The presence of tritium complicates maintenance operations and imposes stringent containment requirements. Nonetheless, LWRs have historically been the most commercially adopted design of nuclear power plants (NPPs) and have demonstrated high reliability. In fact, since 2013, Boiling Water Reactors (BWRs) have achieved a worldwide median capacity factor of 89.3%, while Pressurized Water Reactors (PWRs) have reached 82.7% (International Atomic Energy Agency, 2024).

The use of light water as a coolant for commercial nuclear reactors began in 1954 with the operation of Obninsk Unit 1, a 6 MWe Russian graphite-moderated light water reactor, marking the world's first practical-scale reactor for power generation. Shortly after, in 1957 and 1958, the United States launched the first Boiling Water Reactor (BWR) at Vallecitos (24 MWe) and the first Pressurized Water Reactor (PWR) at Shippingport (68 MWe), supplied by General Electric and Westinghouse, respectively (Murakami, 2021). These American reactors were developed based on the operational experience gained from the U.S. Navy's nuclear submarine program, which, despite not considering water as the ideal coolant technology for submarine applications, adopted light water reactor technology. This decision gave PWR technology a significant "head start" in operational experience compared to other designs, though research and development continued on alternative technologies such as liquid metal, gas-cooled and molten salt reactors (Ferguson, 2015).

Nevertheless, LWR technology had to wait for several years, until the 1970s, before they would be the most commercially deployed reactor design. The primary reason for this delay was the high neutron absorption cross section of light water, which, despite being a more effective moderator than graphite and heavy water, could not sustain a nuclear chain reaction with naturally occurring uranium. This limitation was overcome in the 1970s when enriched uranium became commercially accessible, enabling the broader adoption and further development of LWRs. In fact,

the URENCO enrichment company started using centrifuge separation for uranium enrichment in the 1970s, causing a sharp decrease of enrichment costs. Previously, these costs stayed high due to the use of gaseous diffusion technology, which was highly energy-intensive. Since then, the proportion of gas cooled reactors dropped from a 38% to a 6% while LWRs went from 42% to 76% (Murakami, 2021). The introduction of enriched uranium allowed new plant's burnup to be increased by two or three times and to perform fewer core refueling outages. This, combined with improved plant management practices and operator training, allowed for a great improvement of the plant's capacity factors. From this point on, aside from the main exceptions of the United Kingdom and Canada, which chose gas-cooled reactors and CANDU reactors for their NPP fleet, most of the countries chose the LWR technology for further improvement (Murakami, 2021).

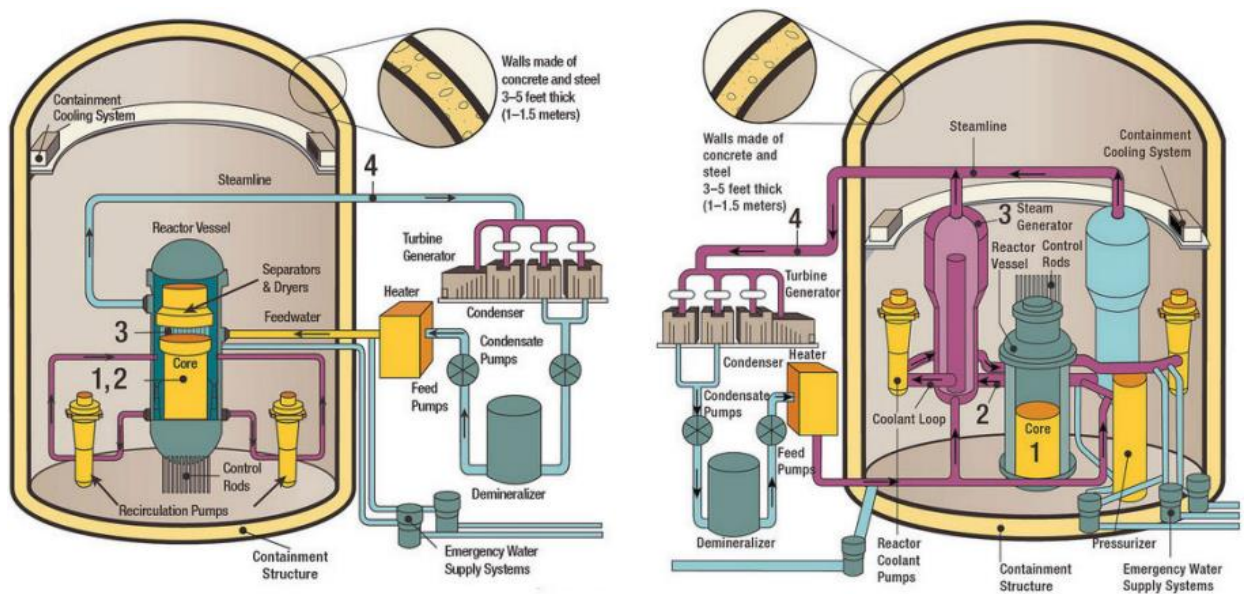


Figure 1 PWR (right) and BWR (left) reactor schemes (U.S. Department of Energy, 2015).

Thus, the deployment of LWRs arose after 1970. In particular, the Browns Ferry and Peach Bottom units started operation during these years, becoming the first plants to break the 1 GW barrier in the United States. Despite a record breaking 41 nuclear power plants ordered by utilities in 1973 in the U.S., the trend was reversed after the TMI (Three-Mile Island) accident in the United States in 1979 (U.S. Department of Energy). The TMI accident represented a turning point for the US nuclear industry. In fact, not only nuclear power plants were targeted by the public as “unsafe” but new stricter safety regulations were introduced, especially for the bigger reactors, and concerns over rising construction costs became apparent in the 1980s. In response to the TMI incident, there was a strong focus on achieving economies of scale in nuclear power plant design. The Nuclear Energy Agency (OECD/NEA) identified increasing plant size as an effective strategy for reducing construction costs per unit power installed. As a result, LWR designs evolved to include larger and more efficient systems, balancing cost-effectiveness with enhanced safety standards. This trend was driven by the recognition that economies of scale could significantly reduce costs. Further cost reductions were expected in the United States by constructing multiple plants of the same type, allowing for improvements in construction methodology and shorter construction periods. Though those expectations never materialized in the US, cost-saving trends were observed in France and Japan during the 1980s and in South Korea in the 2000s. These reductions were also facilitated by cross-border lesson learning and the sharing of information among countries (Murakami, 2021).

More than 40 years after the TMI accident, there are 442 operating nuclear reactors worldwide, with 96% being water-cooled (International Atomic Energy Agency, 2024). The United States operates the largest fleet of commercial nuclear reactors of which approximately two thirds are PWRs and one third are BWRs. In 2023, these reactors achieved an average capacity factor of 93.1% (U.S. Department of Energy, 2015) (Statista, 2024). The industry is currently deploying Generation III+ LWRs, which feature passive safety systems that rely on gravity or natural convection to mitigate the impact of off-normal events on plant safety. An example of Gen III+ reactor is the Westinghouse's AP-1000. Moreover, nuclear reactor vendors have turned towards the possibility of commercializing the so-called "Small Modular Reactors" or SMRs. SMR developers attempt to counter on the drawbacks of building large, complex LWRs to deploy simpler and smaller concepts. Despite not being able take advantage of economies of scale, which have historically been proven in several countries worldwide, SMRs avail of the following (Murakami, 2021):

- Power output flexibility and small demand areas accommodation;
- Modularization of construction with pre-fabrication of the components necessary for reactor construction before local assembly;
- Lower reliance on active safety systems due to smaller scale of the core and lower residual heat after shutdown;
- Possibility of proving the same economies of scale achieved by increasing the size of the LWRs by mass-production of SMRs and their relative components.

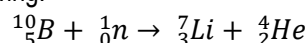
The U.S. is currently working towards the commercialization of the light water SMR technology by allocating significant funds, grants and cost-share agreements with various companies, providing regulatory support and supporting demonstration projects (World Nuclear Association, 2024).

2.1 Purity requirements

To ensure the integrity, reliability, and availability of the main plant structures, systems, and equipment that are essential for safety, the chemistry of the primary coolant has to be monitored and carefully controlled. The main risks associated with coolant chemistry include stress corrosion cracking (SCC) of piping and other components, leakage of radioactive materials from the fuel, and high occupational radiation exposure. In particular, corrosion has to be controlled as its rate can be worsened considering the high temperature and pressure conditions of PWR/BWR operation (Lister & Uchida, 2014). Thus, the primary objectives of coolant chemistry control in LWRs are to maintain the material integrity of primary system structures, components, and fuel cladding, and to minimize radiation exposure. In this report, while analyzing the requirements for water purity and their relative costs, the focus is placed on pressurized water reactors. In PWRs, maintaining proper coolant chemistry is crucial to prevent SCC in the steam generator's nickel-alloy tubing, other nickel-based alloy components, and stainless steel weld metal. This careful management helps to ensure the longevity and safety of the reactor systems (Kawamura, et al., 2016).

While the reactor coolant for a BWR is high purity water, the primary coolant in a PWR is an alkaline solution supplemented with several chemical additives to maintain an equilibrium between the chemistry and physics of the solution and achieve operational safety. In particular, the required additives are:

1. Boric acid (H_3BO_3). Boric acid is used in PWR plants as a reactivity control agent. In particular, Boron-10 has a very high absorption cross-section for thermal neutrons (>3800 barns), making it a perfect candidate as a reactor burnable absorber and for potential emergency reactivity control (Wiedenmann & Cook, 2020). The neutron absorption reaction is the following:



Given the natural abundance of Bo-10 being set at 19.6%, more and more enriched boric acid (commercially enriched at quantities higher than 99.9%) is used by modern PWRs. The main reason is because of the possibility of reducing the total quantity of boric acid in the coolant while maintaining the same absorption performance and solubility. Its concentration in the reactor coolant ranges between 0 and approximately 0.2 weight percent.

2. Lithium hydroxide. LiOH with an enriched concentration of Li-7 (99.99%) is added to the PWR reactor coolant to maintain the coolant's pH at optimum levels. Natural lithium, which contains about 6% Li-6, is not used because Li-6 can produce tritium through neutron capture. The use of LiOH also reduces the deposition of corrosion products on heat transfer surfaces. To accomplish a pH specification range between 4.2 and 10.5, lithium concentration is maintained between 0.7 and 2.0 ppm (U.S. Nuclear Regulatory Commission). It is important to note that the amount of lithium hydroxide added should not solely compensate for the total boric acid introduced, as the coolant's pH can vary due to factors such as the dissociation of water molecules at high temperatures and the introduction of Li-7 via neutron absorption of B-10 (see equation above). Proper management of these chemical processes is important to maintain the desired pH balance and ensuring the safe and efficient operation of the reactor.
3. Hydrogen or hydrazine (N_2H_4). It is recommended to keep oxygen levels as constant as possible, ideally at or below 50 ppb. At this level, ferric hydroxide and ferrous hydroxide combine to form a protective film that reduces corrosion of the primary structures. However, if oxygen levels increase, ferrous hydroxide can convert to ferric hydroxide, which does not adhere well to surfaces and can result in increased corrosion. To maintain appropriate oxygen levels in PWRs, a slight excess of hydrogen can be used, and oxygen scavengers like hydrazine may be added, especially during reactor startup when the temperature range allows for their effective use. Nevertheless, at very low oxygen concentrations (below 5 ppb), a significant amount of ferrous iron can be produced, leading to higher corrosion rates and increased iron release into the solution (U.S. Nuclear Regulatory Commission).
4. Zinc. Zinc injection in PWR coolant is part of the long term strategy for chemistry control and has been applied to 21 Japan reactors to reduce the radiation field. In fact, zinc oxide deposits in the corrosion film on piping. This creates competition to other metals' accumulation and reduces the buildup of Co-60, etc (U.S. Nuclear Regulatory Commission). The Japanese have proved no adverse effects for Zinc injection, and have obtained excellent dose rate reduction for zinc quantities of 2-8 $\mu\text{g/L}$ during normal operation (Kawamura, et al., 2016).

Given the presence of such additives, it is expected that the chemistry of the coolant would have to be controlled regularly to check that the most important water parameters are in line with the requirements for reactor operation. Consequently, some specific key parameters have been defined to evaluate the chemistry, volume conditions and to guarantee optimal plant operation. These parameters, called "control parameters" are those parameters which require strict control due to material integrity or fuel integrity considerations, and have been defined based on power plant experience and the state-of-the-art scientific knowledge. On top of the main control parameters, conditioning and diagnostic parameters can be also defined. Conditioning parameters are defined for chemical additives such as lithium, boron etc. while diagnostic parameters should assist the chemistry team in interpreting changes in the primary coolant chemistry that could impact radiation buildup, corrosion behavior of system materials, or fuel performance (Kawamura, et al., 2016) (Haas, 2009). Based on the defined control parameters for water chemistry, some recommended values can be defined for PWRs. The recommended chemical conditions for optimal water chemistry and corrosion control are achievable and were established based on extensive field experience from PWR operations. These values are intended to enhance safety and reliability. If a utility does not meet these recommended values, water chemistry experts are supposed to identify and assess the root cause of the deviation and discuss appropriate corrective actions. For the purpose, different action levels can be defined based on the deviation from the standard value and the potential consequences on operation. Those can require immediate evaluation and corrective action with a frequency based on the severity of deviation. While it is not the purpose of this report to discuss

the necessary action levels based on the measured plant parameters, the recommended values for plant operation are reported in Table 2.

Table 2 Recommended values for different control parameters in PWRs (U.S. Nuclear Regulatory Commission) (Kawamura, et al., 2016) (Haas, 2009).

Control parameter	Recommended value	Monitoring frequency	Comments
Conductivity at 25 °C, $\mu\text{mhos/cm}$	1.0	Daily	Conductivity is index to check the impurities and lithium ions in the primary coolant. For most applications in nuclear facilities, water specification is "Very Pure". Ultra-Pure demineralized water (0.1-0.2 $\mu\text{mhos/cm}$) is normally only required in laboratory situations.
pH at 285 °C	7.2 – 7.4		The pH specification range set by the NRC at 25 °C is in the range of 4.2 to 10.5. If pH is measured at a higher temperature, the reading may show an increase in hydrogen ions, resulting in a lower pH. This could misleadingly suggest that the water is more acidic than it actually is. Therefore, it is important to always measure pH at the reference temperature of 25°C to ensure accurate results.
Chloride, $\mu\text{g/L}$	< 10	Weekly	Chloride, fluoride, and sulfate are designated as control parameters because they are harmful chemical species that can adversely affect the integrity of coolant system components by causing corrosion issues such as SCC. The limits on these three are usually plant specific.
Fluoride, $\mu\text{g/L}$	< 10		
Sulfate, $\mu\text{g/L}$	< 10		
Lithium, mg/L	-		Lithium and dissolved hydrogen concentrations are key parameters for controlling primary coolant conditions and are closely associated with the use of chemical additives. Although no specific recommended values were found, as the values are usually set by plant specifics, limits action levels are at <0.2 and >3.5 for lithium and <25 for hydrogen.
Dissolved Hydrogen, cm^3/kg	-		
Dissolved Oxygen, $\mu\text{g/L}$	-	Monthly	Although no specific recommended values were found for oxygen, limits action levels are set at >5 $\mu\text{g/L}$.

For the purpose of report's completeness, recommended guidelines for secondary circuit coolant in PWRs and BWRs primary circuit are reported in the Appendix A.

Having analyzed the composition of PWR's primary circuit water and the guidelines set for the operation, the focus now falls on the techniques used for water purification. In fact, the values of raw water are very far from the recommended values of NPP operation and water needs to be treated before it can be filled in the Reactor Pressure Vessel and allow the start of nuclear operations. The multiple techniques that can be potentially used for water purification are described in Table 3.

Table 3 Possible purification methods to be selected for coolant water preparation for LWR applications (Salam & Rokonzaman, 2023) (Singh & Hankins, 2016).

Purification method	Description
Distillation	Water distillation usually has several advantages such as process simplicity, the possibility of generating water with a resistivity of around 1.0 MΩ/cm (2.0 micromhos conductivity equal to a specific resistance of 500,000 Ω), and the technique's affordability. Disadvantages rely on the high energy and water use other than the high maintenance and cleaning requirements due to the feedwater deposits. Moreover, distillation requires planning and cannot be done on demand.
Deionization	Most deionization systems are composed of one to four cartridge cylinders connected to plumbing lines and positioned opposite a sink. These systems work by exchanging hydrogen ions with cationic pollutants and hydroxyl ions with anionic impurities in the input water. The desalination process involves small spherical plastic beads, known as resins, that filter the feed water. Over time, the cations and anions in the water displace the hydrogen and hydroxyl groups in the resin, necessitating either replacement or regeneration of the resin. The maximum water resistance achievable after treatment is 18.2 MΩ per centimeter. One significant advantage of deionization over distillation is its ability to produce purified water on demand. However, deionization cannot guarantee contaminant-free water, as small particles of ion exchange resin may be released during operation, and stagnant water in the cartridges can encourage bacterial growth. Additionally, deionization cartridges are typically expensive, and regular regeneration is required.
Reverse Osmosis	Osmosis is the process of water moving from the less concentrated side of a semipermeable membrane to the more saturated side. On the other hand, reverse osmosis works by applying pressure (greater than the osmotic pressure) to the more concentrated solution so that water molecules are driven back over the membrane to the less concentrated side, resulting in purified water. Reverse osmosis can typically remove up to 99% of contaminants. This process is often used in combination with deionization to extend the lifespan of the cartridges by significantly reducing the levels of bacteria and pyrogens in the water.
Activated carbon filtration	Activated carbon filtration is typically used for the removal of chlorine and soluble organic substances using the strong interaction and desorption properties of carbon.
Ultrafiltration	Ultrafiltration simply employs a filter with a pore size in the range of 0.001-0.05 μm. Pyrogens and other big-chain biological substances or organic compounds such are removed from cleaned water using an ultrafilter. The main disadvantage is the need of applying a considerable pressure and of maintaining the filter because of rapid pore clogging.
Ultraviolet oxidation	Ultraviolet oxidation kills bacteria by emitting ultraviolet light at a biocidal wavelength of 254 nm. It also splits and ionizes certain organic compounds at 185 nm, which are subsequently removed by the deionization and organic adsorption cartridges in a subsequent polishing loop. Ultraviolet filtration is widely employed for producing drinking water.
Electrodialysis	Electrodialysis (ED) uses charged membranes and electrical energy to move ions against a concentration gradient, resulting in separation and purification. A direct current electric potential is applied perpendicular to the flow, causing cations to move toward the cathode and anions toward the anode. This process removes salts or demineralizes water. The process is rarely used for water purification in laboratories because it cannot remove pollutants with weak or no charge, such as certain organics, pyrogens, and elemental metals. Larger molecules with significant charges, like colloids and detergents, can clog the membrane pores, reducing their ion transport capacity and requiring frequent cleaning. Additionally, ED can potentially produce hazardous hydrogen gas. The process is also relatively expensive as the water's electrical resistance increases during the process, necessitating a higher electrical current to maintain the purification process.

2.2 Cost of water

While analyzing the cost of water purification, our primary focus is on operating costs linked to the installation of a chemical and volume control system. In fact, the cost per kg of water is expected to be very low (between 0.21 and 0.32 cents per kg) (Kwon, Lee, & Jang, 2018) and for large quantities (almost 260,000 kg for the PWR12-BE) on-site installments allow PWRs to maintain high purity involving processes such as demineralization, filtration, and distillation. For this reason, this section focuses mainly on the costs related to chemistry control and the machinery related to it.

2.2.1 Operating costs

The main operating costs analyzed in this report are related to the installation of the chemical and volume control system (CVCS). The main goals of the CVCS systems are to regulate the chemistry of the reactor coolant so that it maintains the proper water inventory within its design radioactivity and chemistry limits. Moreover, it should provide the necessary borated water (and emergency boration if required) and corrosion-inhibiting chemicals. It is classified as a Seismic Category I system. Before evaluating the capital investment needed for the CVCS installation, let us first provide a brief overview of the key operating systems involved, while taking into account that the strategy for reactor purification can potentially differ between reactor models and designs (U.S. Nuclear Regulatory Commission). The main CVCS subsystems are (U.S. Nuclear Regulatory Commission):

- The Letdown System. The letdown system extracts coolant from the Reactor Coolant System (RCS) for purification and chemical adjustments. It includes several components: isolation valves to prevent depressurization of the letdown piping, a "delay pipe" to allow the decay of highly radioactive nitrogen-16 after it exits the containment, a heat exchanger that cools the flow to a temperature suitable for purification via a mixed bed demineralizer (ion exchanger). The demineralizer (which is usually redundant) removes ionic impurities from the reactor coolant using a mixture of anion and cation resins (Li-OH or H-OH resins), provided the temperature is not too high. Additionally, a filter is included to remove any resin fines (broken resin beads) that may escape from the ion exchangers.
- A Volume Control Tank (VCT). The volume control tank collects the coolant released from the system and acts as a storage reservoir for the charging pumps. The tank is over pressurized with hydrogen gas, which dissolves into the coolant. This dissolved hydrogen helps reducing oxygen in the primary coolant, helping to prevent corrosion.
- The Reactor Makeup and Chemical Addition System. It provides concentrated boric acid, demineralized reactor makeup water, or a mixture to the VCT. It can eventually add lithium hydroxide and hydrazine to control the coolant chemistry.
- The Charging system. It returns processed coolant to the RCS and provides seal injection to reactor coolant pumps. It usually consists of two redundant centrifugal charging pumps and a positive displacement pump. The centrifugal charging pumps serve as high head safety injection pumps during the actuation of the emergency core cooling system. The system is also composed of some filters, control, isolation valves and a regenerative heat exchanger which preheat the charging flow.
- The Excess Letdown System. The excess letdown system simply consists of an additional letdown system which is actuated during certain plants evolution such as RCS heat-up (for volume expansion accommodation), RCS depressurization or the inoperability of the normal letdown path.
- The Boron Recovery (Recycle) System (BRS). The primary function of the Boron Recycle System (BRS) is to collect excess borated water that results from the dilution of reactor coolant. This dilution compensates for core burnup, potential load-following operations, RCS heat-up from cold shutdown to hot standby, and

refueling operations. The BRS receives the coolant directly in the holdup tanks from the volume control tank via the letdown line. After a certain amount of liquid is accumulated, the processing begins. It starts when the liquid passes through a preheater and successively a stripper column where the dissolved gases can be redirected to the waste disposal system. After the stripper column, an evaporator separates the solution into water vapor and a concentrated boric acid solution. The water vapor goes through an absorption tower, condenses in the condenser and is pumped to the monitor tanks after being demineralized and filtered. On the other hand, any boric acid carryover is blocked at the absorption tower and remains at the lower part of the evaporator. Both the water in the monitor tanks and the concentrated boric acid solution (concentrated up to 4 wt%) have to be sampled and tested before respectively being pumped to other tanks or to the boric acid tanks where it will be used as boric acid makeup. As mentioned, this process is not always the standard as the concentration of boric acid in the holdup tanks can also vary, going from the just-after-refueling concentration of 2000 ppm to essentially zero ppm at the end of the core cycle. As the BRS is not always considered as part of the CVCS system but it may be considered as an additional system, its cost would not be included in the successive cost analysis.

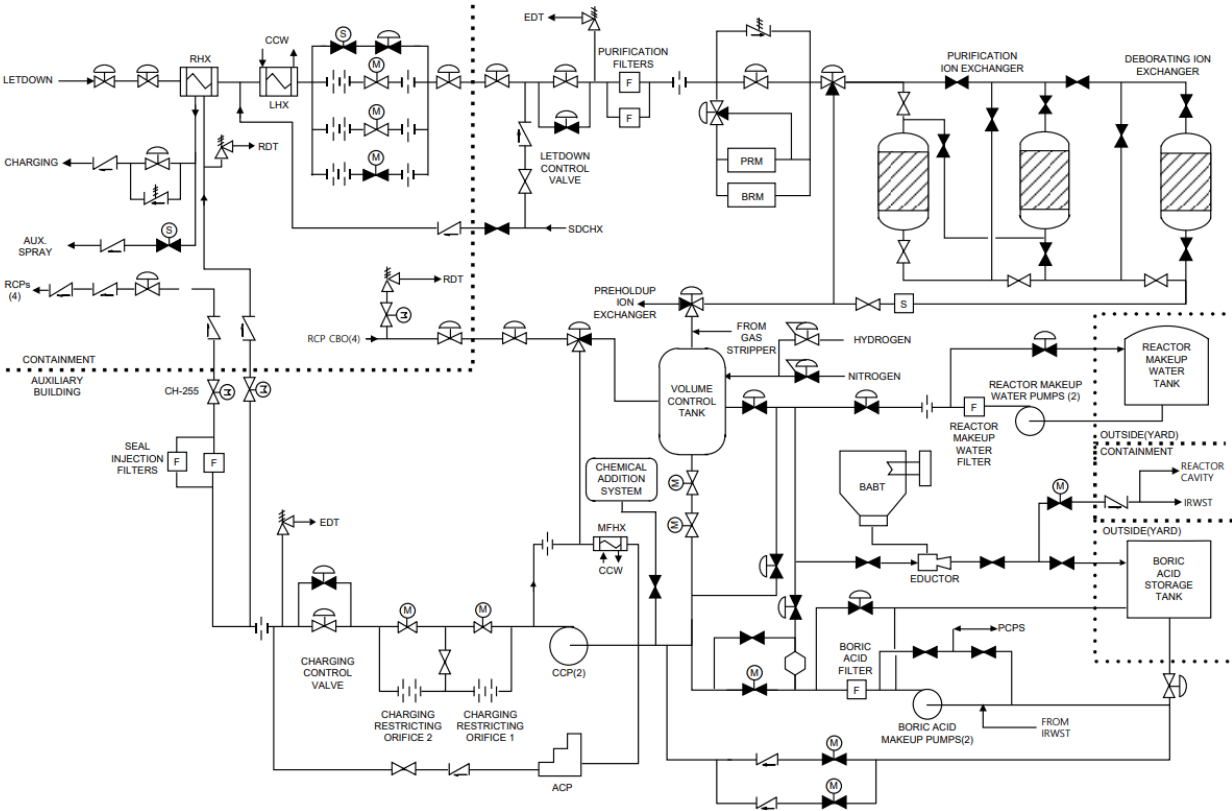


Figure 2 CVCS schematic in a Korean APR1400 (Chung, Kim, Lee, & Lee, 2020)

Having discussed the main objectives of the CVCS and the features of the main systems that compose it, we now focus on its respective costs. As mentioned, the cost relative to the BRS are not considered in this report. The majority of the quotes is retrieved from (Ganda, Hoffman, Taiwo, Kim, & Hansen, 2019) and (Ganda, Taiwo, & Kim, Report on the Update of Fuel Cycle Cost Algorithms, 2018) and reported in Table 4.

Table 4 CVCS cost analysis (Ganda, Hoffman, Taiwo, Kim, & Hansen, 2019) (Ganda, Taiwo, & Kim, Report on the Update of Fuel Cycle Cost Algorithms, 2018).

Description	Quotation year	Factory equipment	Site labor	Site material	Total
Rotating machinery	2017-1987 USD*	2,223,207	54,031	5,403	2,282,641
Heat transfer equipment		2,450,735	9,754	977	2,461,466
Tanks & press vessels		1,145,785	125,746	137,514	1,409,045
Purification & filtration equipment		2,451,849	74,635	7,464	2,533,948
Piping	1987 USD	2,225,867	4,688,361	420,195	7,334,423
Chem. & vol. control valves		734,132	0	0	734,132
Piping - miscellaneous items		167,440	8,708	871	177,019
Instrumentation + control		187,938	21,681	1,084	210,703
Foundations/skids		5,094	3,652	366	9,112
Total	2017-1987* USD	11,592,047	4,986,568	573,874	17,152,489
Inflated Total	2024	20,000,000	14,000,000	1,600,000	35,600,000
Normalized total**	2024 [\$/kg]	77.5	54.5	6	138

*When the quotation year is displayed as 2017-1987 it refers to the fact that the Factory equipment costs have been calculated in (Ganda, Hoffman, Taiwo, Kim, & Hansen, 2019) in 2017 USD while the rest of the quotes (Site labor, site material) are from a 1987 cost analysis.

**The normalized total costs refer to the PWR12-BE, which has a primary coolant inventory of 0.57 million lb (approx. 260,000 kg) (Ganda, Hoffman, Taiwo, Kim, & Hansen, 2019).

To sum up, the total 2024 cost for the installation of a CVCS system in the 3,400 MWth PWR12-BE is around 35,600,000 considering site labor and materials. That accounts for a normalized cost of about 138 \$/kg (considering almost 260,000 kg of primary system coolant).

3. Sodium

Sodium is a soft, silvery-white, highly reactive metal belonging to the alkali metal group in the periodic table. With the symbol Na and atomic number 11, it is abundant in nature, predominantly found in its compounds (as sea salt, rock salt, carbonates, nitrates), and it is the sixth most abundant element on earth (Cacuci, 2010). Despite having several isotopes, the only stable form being 100% abundant is ^{23}Na . In the nuclear field, sodium is used as a liquid metal coolant for a fast spectrum reactor thanks to a small enough neutron cross section and a rather high atomic mass number, making it an attractive choice. Sodium melts at about 98 °C (~208 °F) and boils at of 881 °C (approximately 1617 °F) under atmospheric pressure. Being a stable metal liquid under such a big range of temperatures makes it attractive for high temperature reactor operation at about 500-550°C (higher values are not achieved because of materials limit).

The main advantages of using sodium as coolant are its exceptional heat transfer properties. On one hand, sodium has a density like water and a higher viscosity, but only about a quarter of water's specific heat capacity. The higher viscosity and lower heat capacity can be seen as drawbacks since these worsen heat transfer. On the other hand, the liquid metal has outstanding thermal conductivity—five times greater than stainless steel and more than ten times that of water. This feature, makes sodium highly effective for cooling high power density fuel assemblies (Schulenberg, 2022). Thanks to its properties, a sodium-cooled reactor core can be specifically designed to safely operate with high power density without pressurization both under normal and accidental conditions. From the point of view of safety and accident management, the natural circulation capabilities of sodium are excellent and have been experimentally proven (Lucoff, Waltar, Sackett, Salvatores, & Aizawa, 1992). A great circulation can be achieved in the coolant thanks to the high thermal conductivity, high allowable system temperature, and large temperature difference between the core inlet and outlet coolant (Ohshima & Kubo, 2023).

Table 5 Comparison of the physical properties of sodium and water (Schulenberg, 2022) (Ohshima & Kubo, 2023).

Features	Sodium	Water
Melting temperature at atmospheric pressure (1 bar) [°C]	97.8	0
Boiling temperature at atmospheric pressure (1 bar) [°C]	883	100

Absorption cross section of thermal neutrons at 0.025 eV [mbarn]	530		660	
Total cross section of thermal neutrons at 0.025 eV [barn]	3.9		104	
Important material data for core entry and exit conditions:				
Temperature [°C]	400	550	290	320
Pressure [bar]	1	1	155	155
Density [kg/m ³]	856	820	746	680
Viscosity [μPa·s]	277	220	92	81
Thermal conductivity [W/m·K]	70	62	0.58	0.52
Specific heat capacity [kJ/kg·K]	1.28	1.26	5.24	6.14

Another advantage of using sodium as fast reactor coolant is its compatibility with structural materials. Excellent results have been registered under the deoxidization condition (Ohshima & Kubo, 2023). In fact, by controlling the concentration of impurities during operation, a very low level of corrosion and surface changes can be obtained. As proof, the EBR-II has been left *looking as good as new* after 30 years of operation as the sodium did not cause any corrosion on the pipelines and internal structures of the reactor (Schulenberg, 2022).

On the other hand, the main disadvantage of using liquid sodium as a coolant is its high reactivity with water and air. Sodium has a strongly exothermal reaction with water, producing sodium hydroxide and hydrogen, whereas, it burns in contact with air. In case of a pipe leakage and consequent sodium dripping, burning drops will be seen. The fire is not extinguishable with water, but rather using a metal plate which rapidly dissipates the heat coming from the reaction, blocking the flame (Schulenberg, 2022). Counter-measures in case of sodium fire and sodium-water reaction should be taken into account when designing a system involving pure liquid sodium such as a Sodium Fast Reactor (SFR). Another drawback of using sodium as a coolant is its opaqueness. Sodium, in contrast to water, does not allow for visual inspection and this could complicate the procedures in case of damage detection and repair in the primary/secondary side of a SFR. Nevertheless, several sodium-cooled reactor concepts have been pursued since the 1950s and the SFR industry currently accounts for more than 390 reactor-year experience over five decades (Cheng, Cheng, & Chen, 2024).

The first nuclear reactor to produce electricity, the Experimental Breeding Reactor I (EBR-I), was operated starting from 1951 and used a sodium-potassium alloy (NaK) as a coolant. The EBR-I together with its successor, the EBR-II, demonstrated that operating with sodium presents no insuperable obstacles and that there is no practical reason to forego the advantages of sodium as a coolant (The American Society of Mechanical Engineers, 1979). During the following years, between the 1960s and 1970s, several SFRs models have been built around the world. Examples can be found in the United States [Fermi-1, EBR-II, the Fast Flux Test Facility (FFTF)], the former Soviet Union (BR-5/BR-10, BOR-60), France (Rapsodie), the United Kingdom [Dounreay Fast Reactor (DFR)], Germany (KNK-II), and Japan (Joyo) (Aoto, et al., 2014) (Ohshima & Kubo, 2023). The building and operation of these facilities allowed their respective countries and regulations to gain significant experience with sodium and the related technology. This valuable knowledge led to the deployment of some bigger concepts, considered as prototype or demonstration SFRs. The countries involved in such commitment were the former Soviet Union (BN-350, BN-600), the United Kingdom (PFR), France (Phenix, Super-Phenix), and Japan (Monju) (Aoto, et al., 2014) (Cheng, Cheng, & Chen, 2024). From the design, construction, and operation of these reactors, extensive engineering knowledge and understanding of SFR technology was accumulated. This experience includes insights into plutonium fuel performance, fissile material breeding, fuel handling for refueling, operation and maintenance, the related nuclear fuel cycle process, and safety features (Cheng, Cheng, & Chen, 2024). Given that a great effort was also dedicated to the control of incidental situations such as sodium coolant leakage, it was recognized that the SFR concept could have been a feasible

technology in the near-term future (Ohshima & Kubo, 2023). However, the development of SFRs decelerated during the 1980s because of four main reasons (Cheng, Cheng, & Chen, 2024) (Ohshima & Kubo, 2023):

- Accidents. Public opinion on SFRs was influenced by accidents in SFR facilities such as sodium leaks and fires as the ones happened at the Monju plant in Japan.
- Incorrect estimates over uranium resource depletion. SFRs were developed so that they could work with MOX and have a high breeding ratio. This would allow expansion of nuclear energy use even though uranium resources were expected to be depleted soon. Being the demand-supply balance for uranium more stable than what initially predicted when LWRs were introduced to the market, SFR development slowed down.
- Fast LWR development. LWRs imposed less financial risk in short term and their technology (which initially was parallelly developed) had foreseen a greater growth.
- Nuclear non-proliferation policy. Being the plutonium technology deeply involved with SFRs and with the enhancement of the non-proliferation policy, the SFR development was interrupted in some countries.

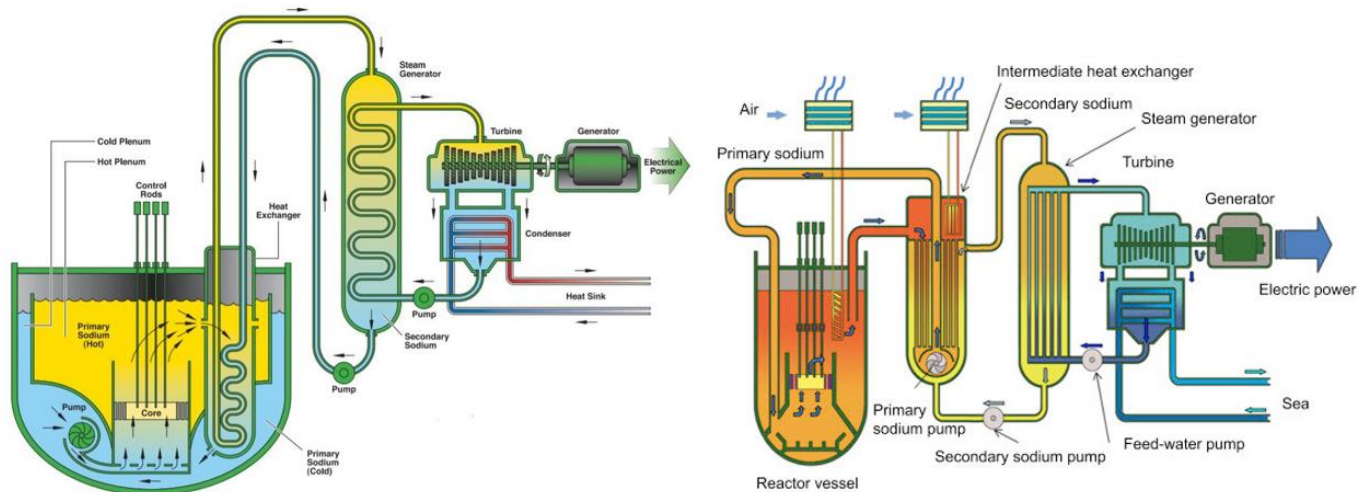


Figure 3 Pool-type (left) and Loop-type (right) SFR models (Cheng, Cheng, & Chen, 2024)

At the start of the 2000s nuclear energy claim increased again given a raising attention to global warming, the necessity to lower the carbon emissions worldwide and because of a growing disposal problem of LWRs waste. Therefore, some of the countries which already had developed great competence with nuclear and LWR technologies other than SFRs some years before, launched SFR R&D campaigns with the goal to design a nuclear reactor with enhanced economic competitiveness and safety. The main investors into this Gen-IV technologies were: United States, Russia, France, South Korea, Japan, China, and India.

In Russia, the BN-600, a 1470 MWth reactor, has been operational for over 40 years. During its first years of operation, there were twelve incidents of steam and water leaking into sodium, even though none of which led to emergencies. However, since the last SG leak in 1991, the plant has operated smoothly, demonstrating both its safety and reliability, as well as the high manufacturing quality of its SGs (Aoto, et al., 2014). After 2014, the BN-600 plant achieved a capacity factor of 85-88% (Ohshima & Kubo, 2023) and obtained an operating permit extending until 2025 (Aoto, et al., 2014). Currently, Rosatom is considering extending the life of the BN-600 fast reactor to 2040 (Nuclear Engineering International, 2020). Parallel to the operation of the BN-600, Russia has built a larger plant, the BN-800, at Beloyarsk (Cacuci, 2010). This plant has been operational since 2014, reached 100% power in 2016, and achieved a 68%

capacity factor in 2019 (Ohshima & Kubo, 2023) Building on the well-developed BN technology, Russia is now developing a commercial 1200 MW SFR called the BN-1200 (Cheng, Cheng, & Chen, 2024), which is also planned for construction at the Beloyarsk site (World Nuclear News, 2022).

In China, a large increase of internal energy demand in the last decades has pushed the research on new reactor designs. The experimental pool-type SFR named CEFR (65 MWth) has been connected to the grid in 2011 and reached 100% power in 2014 (Ohshima & Kubo, 2023) (Huang, 2021). Based on CEFR operational experience, China is currently building two units of a 600 MWe SFR design called the CFR-600 at the Xiapu County, in China's Fujian province (World Nuclear News, 2017) (World Nuclear News, 2020). The CFR-600 development is part of China's ambitions to close the fuel cycle and to demonstrate a high SFR economic performance. The CFR-600 project will lead to the building of a bigger plant, the CFR-1000 or CFR-1200, set to be operational by 2035 (Huang, 2021).

France launched a SFR project called Advanced Sodium Technological Reactor for Industrial Demonstration (ASTRID) in 2006 before backing off in 2019 following a decision from the French government due to its nuclear energy and investment policy (Cheng, Cheng, & Chen, 2024). Nevertheless, France is still pursuing R&D for the development of a SFR and the closure of the fuel cycle (Ohshima & Kubo, 2023). On the other hand, despite of the closure of the Monju NPP and its current ongoing decommissioning (World Nuclear News, 2022), Japan and South Korea are proceeding with the development of the Japanese Sodium-cooled Fast Reactor (JSFR) and Prototype Gen-IV Sodium-cooled Fast Reactor (PGSFR), respectively. India has managed to develop a 13 MWe SFR named FBTR even without signing the Nuclear Non-Proliferation Treaty to this day and being thus excluded from international cooperation (Schulenberg, 2022). A 500 MWe larger reactor has been under construction in India since 2003 and has recently undergone fuel loading (Patel, 2024).

In the United States, the pursued concepts are: the Power Reactor Innovative Small Module (PRISM), the 250-MWt Advanced Reactor Concept (ARC-100), the Traveling Wave Reactor-Prototype (TWR-P), and a sodium-cooled fast spectrum test reactor (FASTER) (Kim, Grandy, Natesan, Sienicki, & Hill, 2018). All these concepts are potentially deployable by 2030 and they are all characterized by some features inherited by the EBR-II reactor: metal fuel, a pool-type primary system, and passive-decay heat removal systems. Among these reactors, some will use experience from the same demonstration projects. Table 6 compares the main design features of the four (Kim, Grandy, Natesan, Sienicki, & Hill, 2018):

Table 6 Design parameters of the SFR designs currently pursued in the USA.

Design Parameter	PRISM	ARC-100	TWR-P	FASTER
Primary system type	Pool*	Pool*	Pool*	Pool*
Fuel form	Metal	Metal	Metal	Metal
Fuel composition - Start-up core	U-Zr	U-Zr	U-Zr	U-Pu-Zr
- Eq. core	U-TRU-Zr	U-Zr	U-Zr	U-Pu-Zr
Coolant outlet temperature [°C]	~500	550	510	510
Power conversion	Steam	Steam or S-CO ₂ Brayton	Steam	Steam
Ave. driver burnup [GWd/t]	66	TBD	150	34
Cladding material	HT-9	HT-9	HT-9	HT-9
Primary sodium pump	EM	Mechanical	Mechanical	Mechanical

*The designs presented are all “pool-type” SFRs, as the EBR-II was. The SFRs are divided in two categories: either pool-type or-loop type. Pool-type SFRs have intrinsically higher safety and economic efficiency while being difficult to design and repair. Loop-types are easier to maintain and have a high natural circulation capacity while having a relatively lower safety. Some examples of pool type SFRs are the EBR-II, Phenix, Super Phenix, BN-600 and BN-800, PFBR and CEFR. Some examples of loop type SFRs are the EBR-I, Fermi 1, SEFOR, CRBR, FFTF, Rapsodie, BN-350, Joyo and Monju.

On top of the reactors previously presented and currently developed in the USA, the Sodium reactor is also being developed by TerraPower. The reactor is a 345 MWe pool type sodium fast reactor using HALEU metal fuel and combining features from the GE PRISM and TerraPower Traveling Wave designs. The SFR design features a molten salt energy storage system for integration with renewable energies. In May 2024, the U.S. Nuclear Regulatory Commission (NRC) accepted TerraPower’s construction permit application for review, marking the first time in more than 40 years that the NRC has accepted this type of application for a commercial non-light water reactor. TerraPower is now working for the construction of other non-nuclear buildings at the plant location in Wyoming so that the site will be ready to build the reactor as soon as the company received the final construction permit from NRC which is expected in two-year time (Nuclear Engineering International, 2024).

Internationally, the Generation IV International Forum (GIF) was founded in the early 2000s. The GIF is a multilateral cooperation to promote SFR and Gen-IV development while balancing international competition and cooperation. The GIF member states have developed Safety Design Criteria (SDC) for SFRs in 2013 and released them officially. The GIF is currently working at the development of Safety Design Guidelines (SDGs) to support the practical application of the SDC in the process of reactor design (Ohshima & Kubo, 2023).

3.1 Purity requirements

The purity of sodium has to be maintained to a nuclear-grade level during operation. This is to prevent that the thermophysical, technological, nuclear-physical, and corrosion properties of metallic sodium, which is used as a coolant in nuclear power facilities, could exhibit inadmissible variations due to impurities (Kozlov, Bogdanovich, Zagorulko, & Matveev, 2012). On this regard, one of the main advantages is that sodium has an excellent chemical compatibility with stainless steel which is usually used as structural material in SFRs; in particular 304SS, 321SS and 316SS have been historically used as can be seen in Table 51 of the Appendix B. In fact, stainless steel is unlikely to corrode significantly up to the temperature range of reactor operation (400–550 °C) (Yoshida & Furukawa, 2012). This compatibility has experimentally proved to lead to low levels of corrosion to the internal structures such as pipes and internal structures (Schulenberg, 2022) and consequently does not promote the chemical contamination of the coolant, whose properties can remain unaltered. Nevertheless, this is valid for pure sodium while the corrosion of stainless steel structures cannot be considered as negligible at higher impurities concentration. On this topic, data over sodium purity requirements has been gathered thanks to years of operation experience of sodium experimental facilities and pool-type, loop-type SFRs. The chemistry control requirements and purity limits are based on an accurate study over the properties of the sodium itself, the sodium impurities, the construction materials, the structural materials with which sodium will interface, and the protective cover gas.

In this chapter, the analysis of the impurity levels is divided in purity requirements for the primary and secondary sodium. The “primary sodium” refers to the liquid sodium interfacing with the reactor core and the primary circuit while the “secondary sodium” refers to the liquid sodium interfacing in the secondary circuit and the sodium-water heat exchanger. The chemistry of the two coolants significantly differs given that the structural materials they are in contact with are different and the primary side directly cools the fuel which may release some radionuclides. Nevertheless, the

analyzed documentation mentions that some of the impurities can be present both within the primary and secondary sodium because of possible points of contact in the Intermediate Heat Exchanger (IHX).

The data in the successive tables is retrieved by documentation and literature released from the operational experience of the BN-600 in Russia, the EBR-II in the United States and the Monju reactor in Japan.

Table 7 List of the possible impurities in the primary sodium (Kozlov, Bogdanovich, Zagorulko, & Matveev, 2012) (Smith & Holmes, 1975) (Ivanenko, 1996) (Akins, Kultgen, & Heifetz, 2023).

Primary sodium			
Metallic impurities			
Impurity	Normal concentration in EBR-II [ppb or ppm]	Concentration of impurities in sodium transport tank delivered to FEI* for BN-600 use [wt%] / Recommendations [wt%]	Source and comments
Ag	60 ppb	< 0.000001 / 0.00001	Unknown. The concentration in EBR-II stayed constant at 60 ng/g of sodium.
Al	< 0.6 ppm	≤ 0.0003 / 0.0001	Seals of the primary pumps. The concentration is usually below detection limits.
B	< 0.05 ppm	≤ 0.0023 / 0.0001	Potential sources are the boron carbide in CRs and borated graphite in the SS neutron shielding surrounding the reactor vessel.
Ba	-	< 0.00002 / 0.001	Unknown.
Bi	2 ppm	< 0.00005 / 0.001	Plug seals alloy.
Ca	< 20 ppb	< 0.001 (to 0.0019) / 0.001	Calcium impurities could derive from the high purity bulk sodium. Ca is probably removed in the form of CaO via the cold trap.
Cd	80 ppb	-	Unknown. Cd concentration has to be closely monitored because of its high capture cross section for thermal neutrons. Most of EBR-II analyses showed concentrations below 20 ng/g.
Co	< 20 ppb	≤ 0.00008 / 0.0005	Impurities in SS, stellite bearings. Can be found in fuel cladding.
Cr	< 20 ppb	< 0.001 (to 0.0018) / 0.001	Fe-18Cr-8Ni steels, if included in the primary system. Concentration is usually below detection limits. Can be found in fuel cladding as well.
Cu	< 20 ppb	0.00001 / -	Auxiliary pump. In EBR-II, it was normally under the detection limit of 20 ng/g.
Fe	0.2 ppm	≤ 0.0013 (to 0.0022) / 0.005	Primary system SS. Data for Fe was very scattered in EBR-II.
K	140 ppm	0.0075 – 0.08 / 0.1	No source and usually not detected.
Li	0.5 ppb	≤ 0.0003 / 0.001	Principal metallic impurity. It comes directly from the NaK from which Na is manufactured by electrolysis. Low NaK concentration is no threat to reactor operation though.

Mg	10 ppb	$\leq 0.0004 / 0.001$	Original sodium or maintenance and operation. Concentration is very low though.
Mn	< 5 ppb	$\leq 0.0001 / 0.001$	304SS and 316SS which contain a 2% maximum of Mn. Can be found in fuel cladding.
Mo	< 70 ppb	-	316 SS (2-3 %wt). Very rarely found.
Ni	< 40 ppb	< 0.00002 (to 0.00025) / 0.003	Seldom detected in the primary system. Nevertheless, it is potentially a big threat since it comprises 8% of the SS weight in the primary system.
Pb	10 ppm	0.0001 – 0.0005 / 0.0005	Unknown. It has not created significant corrosion problems in EBR-II and has been detected at around 10 $\mu\text{g/g}$.
Si	0.3 ppm	≤ 0.001 (to 0.0046) / 0.001	304SS and 316SS which contain a 1% maximum of Si and stellite bearings (1.75%). Generally, the concentration is very low and less than 0.5 $\mu\text{g/g}$.
Sn	38 ppm	$< 0.0004 / 0.002$	Eutectic alloy that seals the rotating shield plugs. It has initially been a problem in EBR-II operation even though it does not represent a threat for operation.
U	< 4 ppb	-	Reactor fuel.
Non-metallic impurities			
Impurity	Normal concentration in EBR-II [ppb or ppm]	Other sources limits**	Source and comments
H	50 ppb	50 ppb	1. Diffusion of hydrogen from the secondary side. The source of hydrogen from the secondary side is corrosion on the steam side of the SG; 2. Leaks into the primary side cover gas, especially during fuel handling and transfer. Hydrogen in the form of NaOH and NaH precipitates in the cold trap.
C	0.1 ppm	≤ 0.0012 (to 0.0022) / 0.003	1. Decarbonization of stainless steel; 2. Grease used to lubricate the pump; 3. Leakage of carbonaceous gases in the cover gas; 4. Carbon in the original sodium; 5. Contamination of assemblies entering the tank.
N	< 0.1 ppm	$< 0.001 / 0.001$	Cover gas or nitrides formed with lithium and alkaline-earth metals dissolved in sodium. The main issue with nitrogen is that it can lead to nitriding of SS, which alters the physical properties of the steel contributing to added corrosion.
O	0.7 ppm	1 ppm	Impurities in the reactor cover gas. It forms Na_2O which is removed by precipitation in the cold trap.
F	< 0.1 ppm	-	No known source except possible residues from cleaning or components entering the primary system.
Cl	< 0.5 ppm	≤ 0.0012 (to 0.0035) / 0.003	
Radionuclide impurities			
Impurity	Normal activity		Source and production
^3H	60 nCi/g		Fission or $\text{B}^{10}(\text{n},\alpha)^3\text{H}$ in the CRs

²² Na	75 nCi/g	²³ Na(n,2n) ²² Na
²⁴ Na	2.5 mCi/g	²³ Na(n,γ) ²⁴ Na
⁵⁴ Mn	100 pCi/g	⁵⁴ Fe(n,p) ⁵⁴ Mn in the SS
¹¹⁰ Ag	1 nCi/g	¹⁰⁹ Ag(n,γ) ¹¹⁰ Ag (probable)
¹¹³ Sn	18 nCi/g	¹¹² Sn(n,γ) ¹¹³ Sn in the seal alloy
¹¹⁷ Sn	10 nCi/g	¹¹⁶ Sn(n,γ) ¹¹⁷ Sn in the seal alloy
¹²⁵ Sb	1 nCi/g	¹²⁴ Sn(n,γ) ¹²⁵ Sn(β-) ¹²⁵ Sn in the seal alloy
¹³¹ I	60 pCi/g	Fission
¹³⁷ Cs	27 nCi/g	Fission
²¹⁰ Po	58 pCi/g	²⁰⁹ Bi(n,γ) ²¹⁰ Bi(β-) ²¹⁰ Po in the seal alloy
²³⁹ Pu	< 0.3 pCi/g	Fuel

*FEI is the Russian Physics and Power-Engineering Institute.

** (Ivanenko, 1996)

Table 8 List of the possible impurities in the secondary sodium (Smith & Holmes, 1975).

Secondary sodium		
Metallic impurities		
Impurity	Normal concentration in EBR-II [ppb or ppm]	Source and comments
Ag	0.1 ppm	Unknown.
Al	< 0.6 ppm	Extraneous materials entering the system. The limit of 0.6 μg/g was never reached for EBR-II.
B	< 0.05 ppm	Unknown.
Bi	< 0.1 ppm	Unknown. The limit of 100 ng/g was never reached for EBR-II.
Ca	20 ppb	Original filling sodium. The normal concentration in the EBR-II was of < 40 μg/g
Co	< 20 ppb	SS304 which Co concentration is 0.08%.
Cr	50 ppb	SS304 (18% chromium) and chromium-molybdenum steel (2.25% chromium).
Cu	< 20 ppb	Unknown apart from a possible original concentration. Copper is removed by the cold trap.
Fe	0.3 ppm	SS304 and chromium-molybdenum steel. Concentration is still generally low and under 1 μg/g.
K	140 ppm	Original sodium.
Mg	20 ppb	Unknown.
Mn	5 ppb	SS304 (2% manganese) and chromium-molybdenum steel (0.3-0.6% manganese).
Mo	70 ppb	Cr-I-Mo steel.
Ni	50 ppb	Major constituent (8 %wt) of 304 SS.
Pb	0.4 ppm	Unknown. Concentration is low and under 0.5 μg/g.
Si	0.3 ppm	SS304 (1% max. silicon) and chromium-molybdenum steel (0.5% max silicon).
Sn	< 0.5 ppm	Unknown.

Non-metallic impurities		
Impurity	Normal concentration in EBR-II [ppb or ppm]	Source and comments
H	0.2 ppm	Hydrogen formed on the steam side by metal corrosion. It is normally removed by the cold trap, which is 100% effective.
C	0.8 ppm	<ol style="list-style-type: none"> 1. Decarburization of 304 SS and chromium-molybdenum steel (no evidence); 2. In-leakage of carbonaceous gases in the secondary side cover gas; 3. Impurities in newly installed components. This source is negligible usually; 4. Carbon in the original sodium. Graphitic carbon is the most probable.
N	< 0.1 ppm	Impurities in the inert gas.
O	2 ppm	<ol style="list-style-type: none"> 1. Air which may enter during maintenance operations; 2. Oxygen in the cover gas supply system; Both are considered very limited and not problematic.
Radionuclide impurities		
Impurity	Normal activity	Source and production
³ H	2 nCi/g	Diffusion from the IHX.
²⁴ Na	30 nCi/g	Formed at the IHX by the ²³ Na(n,γ) ²⁴ Na reaction

As it can be seen from the Tables 7 and 8 there is a great variety of impurities which can be detected from the initial sodium and during the systems operation. All of them have a different origin and a different potential consequence on reactor operation. The impurities which are given a higher attention are oxygen, hydrogen, carbon, products of corrosion of the constructional materials, and radionuclides (Ivanenko, 1996). As previously mentioned in this chapter, hydrogen and oxygen can cause corrosion of the metallic structures because of SFR high temperatures. Moreover, minimizing hydrogen impurities in the coolant can help control tritium activity and aiding in the identification of sodium-water interactions (in the secondary/intermediate circuit) through hydrogen sensors (Grabaskas, 2019). The main problem associated with these two impurities is the formation of sodium oxide (Na₂O) and sodium hydride (NaH), respectively having melting temperatures of 1132 and 425 °C (inlet and outlet temperatures in the SFR are 400 and 550 °C). Therefore, crystallization and precipitation of Na₂O and NaH can cause plugging of sodium lines in subcooled areas the remediation of which involves SFR shut-down for maintenance (Akins, Kultgen, & Heifetz, 2023) (Grabaskas, 2019). The principal method to avoid this scenario is to use a cold trap to purify sodium during operation or maintenance. The cold trap, cools sodium to a temperature range between 110 and 150 °C (still well above the melting point of the coolant) so that sodium oxides and hydroxides solubility would decrease. At impurities supersaturation, nucleation and impurity crystal growth happens allowing solid particulates to be filtered out with a mesh filter. This allows the purification system to keep impurity concentration levels under five ppm (Akins, Kultgen, & Heifetz, 2023). Other risks raised by impurities are related to radioactive corrosion products and fission products from failed fuel. The release of those in the primary coolant normally increases the system's and components' dose rates, raising the risk for personnel during reactor operation and maintenance activities (Grabaskas, 2019).

To quantify the amount of impurities being filtered out of a sodium cooled reactor, Table 9 is given from BN-350 and BN-600 operation (PRISM data has been also added for completeness, in the Appendix B):

Table 9 Intensity of sodium impurities based on operational experience of BN-350 and BN-600 reactors.

Source	Oxygen	Water [kg/year]	Hydrogen	Products of corrosion [kg/year]	Tritium [g/h]
Shielding gas	1 kg/year*	0.1 – 0.5*	$3.6 \cdot 10^{-2}$ g/m ²	20**	$6.3 \cdot 10^{-5}$
Maintenance work	6 kg/year*	0.6*	0.5-1 g/h**	60*	-
X18H10T steel	0.01 g/m ²	-	$4.4 \cdot 10^{-3}$ g/kg	-	-
1X2M steel	0.01 g/m ²	-	$6.4 \cdot 10^{-3}$ g/kg	-	-

*Based on BN-600 data.

**Based on BN-350 data.

To avoid that the reactor coolant would lose its purity during operation and during the filling of the reactor before nuclear power start, it is important to control the surfaces of contact and make sure that the impurity limits on them would be within the ones described in the previous tables. In particular, the molten sodium interfaces the fuel rods (which have to be leak tight), the structural materials and the cover gas. The coolant's inert gas purity maintenance influences directly the operating conditions of sodium and especially the hydrogen, nitrogen and oxygen concentrations. For this reason, an active system is operated to make sure that the cover gas purity (usually argon or helium) is maintained throughout the reactor lifetime. Since the purification of the primary and secondary inert gas entails a relatively significant cost for a SFR and it is strictly linked with the costs of coolant operation, they are taken into account in the following sections analyzing closely the economic aspects. Therefore, the target control limits as well as the detection limits based on the Monju reactor operational experience are explicated in Table 10.

Table 10 Target control limits and detection limits in impurities of the argon cover gas both for primary and secondary coolants (Maeda, Kobayashi, Ishiyama, & Motonaga, 1987).

Element or isotope	Target control limits		
	Primary argon [ppmv]	Secondary argon [ppmv]	Detection limits [ppmv]
N ₂	2500	5000	2.5
O ₂	30	50	1.6
CO	10	20	4.7
CO ₂	20	30	7.0
H ₂	20	30	0.16
CH ₄	10	20	1.2
He	-	-	0.2
¹⁸⁵ Kr	-	-	$1.0 \cdot 10^{-4}$ μCi/Ncm ³
¹³³ Xe	-	-	$1.8 \cdot 10^{-6}$ μCi/Ncm ³
Tritium	-	-	$2.0 \cdot 10^{-7}$ μCi/Ncm ³

To conclude this section, it is important to note that the evaluated sodium purity which is assumed for economic considerations in the next paragraphs is 99.9%. This value is considered as reference as the SFR purification system would be able to purify the coolant down further in case needed for nuclear operations. This possible strategy, confirmed by some information exchange with industry professionals and by historical literature (Ivanenko, 1996) (Mechanisms Engineering Test Loop Facility, 2018), consist in purchasing 99.9% purity (R-grade) sodium first and operate it under cold environment (at temperatures right above the melting temperature in which sodium is molten while the oxides and hydroxides are not) for a specific amount of time with the purification system operating. Thanks to the instrumentation, the impurities concentration can be monitored and when the purity would meet the established requirements for operation the nuclear heat and can be started.

Given the high efficiency of the purification system and its capability to maintain a low level of impurities throughout operation and potentially before it, this strategy seems to be economically convenient. In fact, the cost of higher purity sodium (> 99.9%) tends to increase significantly. One of the advantages of a lower purity sodium (~99.9%) is that it shares the market with other sectors such as pharmaceuticals, metallurgy, agrochemical, batteries, biodiesel and poly-silicon industries. Given the higher request from other sectors for a lower quality of sodium, more facilities are equipped to meet these requirements while guaranteeing a competitive cost. Given the capital investment required for the purification system of sodium coolant and its efficiency, it is not really convenient to acquire sodium of a quality higher than 99.9%. On the other hand, buying a lower quality of sodium can also be non-convenient. This is because the cold trap and the subsystems being part of the coolant purification loop may necessitate additional maintenance before the start of nuclear operations leading to higher costs. Between the two cases, there is an optimum value, which minimizes the sodium purity and maintenance expenses. This optimum is identified in 99.9% sodium purity, which is considered in the next chapters as reference for economic calculations.

3.2 Purchase cost

The price of sodium is investigated in this paragraph taking into account the assumptions made in the last chapters. The cost per kg of sodium is derived from literature and from industry conversations, having a sodium quantity in the order of the thousands of tons as target. This is because thousands of tons are the minimum required amount of liquid sodium to be used in a SFR (Prosser, et al., 2023) and the cost per kg of sodium is expected to decrease with the increase of quantity purchased. Nevertheless, also quotes for different quantities are added to the analysis. The target purity of sodium considered for cost estimations is 99.9%. The retrieved quotes for such metal are grouped in Table 11:

Table 11 Retrieved cost for reactor grade sodium.

Supplier/Buyer	ANL	MSSA Metaux Speciaux	KAIST	ALMR*	ANL
Year of purchase	2016	2013	2006	1994	1978
Original cost	4.65 \$/lb	3.75 \$/lb	7 \$/kg	1.5 \$/lb	0.57 \$/kg
Inflated cost in 2024**	13.6 \$/kg	11.3 \$/kg	9.5 \$/kg	7.1 \$/kg	2.6 \$/kg
Comments	The order quantity was of 55 gallons (~ 0.21 m ³).	-	-	(Gokcek, Babka, Pavlenco, & Kemmerer, 1995)	The cost has been retrieved from (Vaaler, 1979) and has been used in INL

					SFR cost estimation (Prosser, et al., 2023).
--	--	--	--	--	--

*The U.S. Advanced Liquid Metal Reactor Program.

**All costs are inflated using the CPI Inflation calculator of the U.S. Bureau Of Labor Statistics as in the rest of the report.

Based on the quotes retrieved and properly inflated as of May 2024, the cost range of R-grade sodium (99.9%) is between 2.6 – 13.6 \$/kg. Nevertheless, the cost estimations shown in Table 11 differ not only for the reference year but also for quantity purchased which can significantly influence the cost per kg. Given that the quote coming from the ANL purchase in 2016 refers to a quantity of only 55 gallons (approximately 0.21 m³) and the coolant volume necessary for a reactor varies in the order of hundreds and thousands of cubic meters, this quote is not considered when estimating the necessary front capital investments for a potential SFR (considered cost range is then 2.6 – 11.3 \$/kg in Table 12). The 2016 cost estimation can be still used for cost estimates calculations of smaller facilities such as testing facilities or experiments. The results of the analysis are displayed in Table 12:

Table 12 Investment cost associated with coolant initial purchase for different size of reactors based on the necessary quantity of sodium (Prosser, et al., 2023) (Argonne National Laboratory, 2024) (Flanagan, 2019) (Nuclear Energy Agency, 2015).

Source	(Argonne National Laboratory, 2024)	(Prosser, et al., 2023)	(Prosser, et al., 2023)	(Nuclear Energy Agency, 2015)	(Prosser, et al., 2023)	(Nuclear Energy Agency, 2015)	(Nuclear Energy Agency, 2015) (Flanagan, 2019)
Reactor name	EBR-II	-	-	Phenix	-	EFR	Superphenix
Plant Nominal Power [MWe]	62.5	165	311	350	1,243	1470	1500
Power Block Nominal Power [MWe]	62.5	165	311	350	622	1470	1500
Reactor Nominal Power [MWe]	62.5	165	311	350	311	1470	1500
Sodium Price [\$/kg]	2.6 – 11.3						
Total Sodium Coolant Quantities							
Volume [gallons]	112,600	100,338	259,930	254,259	1,039,718	635,647	983,740
Volume [m ³]	~ 430	380	~ 985	~ 960	~ 3,940	2,370	3,725
Mass [kg]	372,000	331,489	858,735	840,000	3,434,938	2,100,000	3,250,000

Total Cost [2024 USD]	967,000 – 4,200,000	860,000 – 3,750,000	2,230,000 – 9,700,000	2,180,000 – 9,500,000	8,930,000 – 39,000,000	5,460,000 – 24,000,000	8,450,000 – 37,000,000
Nominal cost [2024 USD/MWe]	15,400 – 67,300	5,220 – 22,700	7,180 – 31,200	6,240 – 27,200	7,180 – 31,200	3,710 – 16,200	5,630 – 24,500

As can be seen from Table 12, the cost range for sodium initial purchase investment normally increases with increasing plant nominal power. While performing such calculations, the cost range was considered to be within 2.6 – 11.3 \$/kg. Nevertheless, it could be normally expected to face a cost range closer to the minimal values (thus 2.6 \$/kg) for bigger reactors such as Super Phenix.

3.3 Purification and chemistry control costs

The operating costs are evaluated by analyzing the cost of the purification systems in a SFR. The sodium purification system is crucial for maintaining the quality and performance of the liquid sodium coolant both in the primary and secondary (or intermediate) circuits. The primary objectives of the sodium purification system are to remove impurities that can affect the reactor's operation by corrosion, scaling, etc. and to ensure the long-term stability and safety of the reactor. In this chapter, the capital costs related to the installation of the purification systems for the primary and secondary coolant are analyzed together with the cost of the cover gas purification system. In fact, even though the inert gas does not act as a coolant and has a different purpose with respect to the primary and secondary sodium, whose main scope is to cool the reactor fuel, it does play a role in maintaining the chemistry of the sodium coolant throughout its lifetime. Therefore, the cost related to the cover gas purification is accounted for in this chapter as well.

The cost analysis performed in this chapter is based on the 165 MWe U.S. SFR PRISM (Power Reactor Inherently Safe Module) designed by GE under the sponsorship of the U.S. Department of Energy (DOE). The PRISM model is a compact modular SFR which presents unique passive safety features to enhance the safety of the pool-type design. The reactor and its subsystems have been described in the PRISM-Preliminary Safety Information Document released by GE for DOE in a 1987 report (U.S. Department of Energy, 1987). The document has been later used by INL in collaboration with Strategic Analysis, Inc. in 2023 to complete a report assessing the possible cost of the PRISM reactor (Prosser, et al., 2023).

In the following chapters, each system whose cost is analyzed (primary sodium purification system, intermediate sodium purification system and inert gas receiving and processing system) has its own section in which the functioning of the subsystem is explained as well.

3.3.1 Primary sodium purification system

The primary sodium purification system has the main scope to maintain the chemistry of the primary coolant at the required purity levels, other than to provide storage for the sodium used in the reactor vessel. The primary sodium purification system (PSPS) operates only during the reactor refueling shutdown periods. This is because the continuous cold trapping is not necessary as the reactor is completely sealed during normal operation and the in-leakage of impurities is usually negligible. In the unlikely event that purification of the reactor sodium becomes necessary during operation, the reactor has to be shut down to hot standby condition and cold trapping must be performed. Before the

initial plant startup, the strategy is to use the PSPS to purify the fresh sodium to “clean” the internal surfaces of the reactor vessel. Given that the operation of this system is intermittent, the same PSPS can be used for three different PRISM reactor modules (thus sharing the costs) given that each one of them is provided a submerged sodium EM pump to allow the circulation of the coolant to the PSPS. Thanks to this pump the PSPS can also transfer the primary sodium to a specific storage vessel which can temporarily store the coolant during replacement of the PRISM’s reactor module. The PSPS is designed to comply with seismic category 1. The main components of the PSPS are:

- EM pumps (one every reactor module);
- Nitrogen cooled cold trap: It cools sodium below saturation temperature of the impurities. This allows them to crystallize on the cold trap vessel or internal meshes. The scope is to remove oxygen, hydrogen, tritium, carbon, and some corrosion products (Grabaskas, 2019). One of the main problems and risks of using a cold trap is that nucleation and growth kinetics are faster for hydrogen than for oxygen. Oxygen supersaturation could exist in the cold trap when hydrogen is not supersaturated. This creates the risk of sodium oxide deposits which can lead to plugging of the cold trap sodium lines. Therefore, temperatures and flow rates in the cold trap subsystem need to be closely monitored and controlled while used. The ability to rapidly detect malfunctions, so that operators can rectify the system before a total freeze occurs, is therefore crucial to reduce SFR operation and maintenance costs. The cold trap includes the economizer and the crystallizer.
- Nitrogen blower;
- Air blower;
- Impurity/Plugging Monitor and Analyzer;
- Interconnecting piping and valves;
- Sodium sampling station, glove box and other instrumentation.

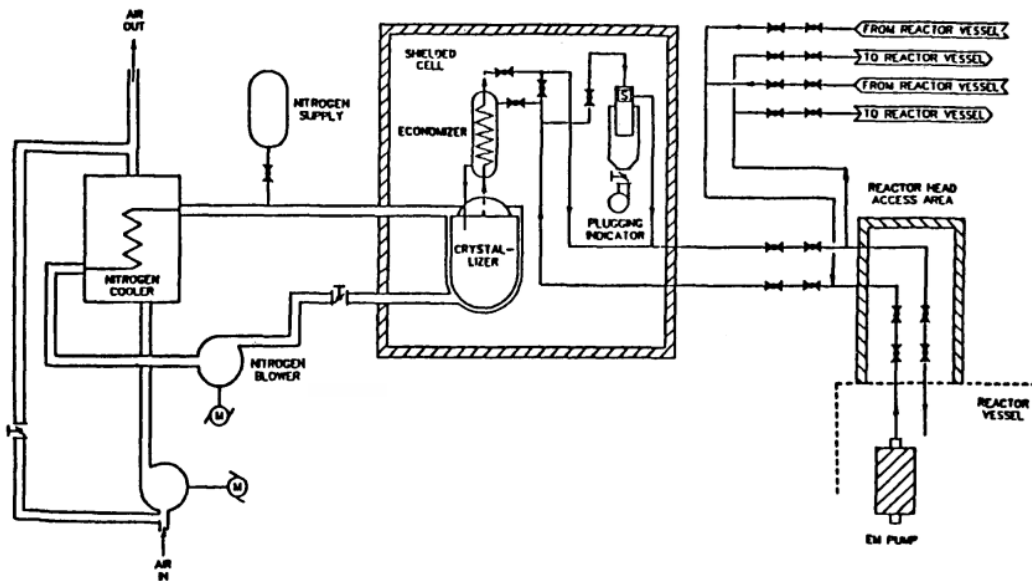


Figure 4 PRISM’s primary sodium processing system (U.S. Department of Energy, 1987).

The purification system is operated when the reactor vessel temperatures approach 400 °F (205 °C), during SFR refueling. The PSPS is heated before operation so that it can be ensured the coolant remains in molten state. The

discharge line and return line (which can be seen in Figure 4) start from below the reactor vessel (more precisely beneath the primary sodium surface), go through the reactor head access area to the PSPS shielded cell. Double isolation valves are also used inside the reactor head access area as well as in the primary sodium service building to minimize the chances of sodium leak to the environment in case of pipeline break. When the PSPS is actioned, primary sodium from the pool-type reactor is pumped via the EM pump. The EM pump circulates the sodium at 60 gpm (approx. 0.2 cubic meters per minute), discharging it through a pipe near the reactor lower head. The sodium temperature in the crystallizer can be controlled by the nitrogen flow which transfers the heat to the environment thanks to the nitrogen-to-air-cooler. Cold trapping operation can be ceased when the oxygen concentration in the sodium is measured at 2 ppm. To make the measurements and monitor the operation of the PSPS, a small portion of the sodium flow (almost 4 liters per minute) is syphoned off the loop after the cold trap to monitor the operating parameters of the sodium cold trap and determine the coolant quality. Thanks to the PSPS, all the oxygen which leaked in through the metal surfaces of the internal structures or the cover gas and the one which was absorbed during refueling, will be removed. The sodium will then be contaminated again once reactor operation restarts and the temperature get to 800 °F (~ 426 °C). In fact, this is the temperature at which the oxygen present in the newly installed fuel will dissolve again into the coolant. Assuming a capacity factor of 17%, (U.S. Department of Energy, 1987) estimated a cold trap of 750 gallons (2.83 m³) could serve three reactor modules throughout a lifetime of 60 years.

The cost of the PSPS, based on INL and Strategic Analysis, Inc. analysis in 2023 (Prosser, et al., 2023) is summarized in Table 13, which assumes a project contingency of 30%.

Table 13 Capital investment foreseen for PSPS installation (Prosser, et al., 2023).

Primary Sodium Processing System	Cost [2023 USD]	Inflated cost [2024 USD]*
Sodium Processing Pump	19,318	20,200
Air Blower	18,183	19,000
Nitrogen Blower	18,183	19,000
N2-Cooled Cold Trap	9,091	9,500
Economizer	4,546	4,750
Crystallizer	18,183	19,000
Impurity/Plugging Monitor & Analyzer	27,274	28,500
Sodium Sampling Station	3,637	3,850
Shielded Cell/Glove Box	272,738	285,000
Piping	24,774	25,900
Valves	24,774	25,900
Other Instrumentation & Controls	9,910	10,350
Total System Cost	450,611	471,000
Total Plant Cost	450,611	471,000
Contingency (Excluding Pump)	30%	30%
	129,388	135,000
Total	579,999	596,000
Normalized total	3.52 [2023 USD/kWe]**	3.61 [2024 USD/kWe]**

*Reference month for inflation is February 2023.

**The normalization is done considering 165 MWe of the PRISM module.

3.3.2 Secondary sodium purification system

Contrary to the Primary Sodium processing System, the Secondary or Intermediate Sodium Processing Subsystem (ISPS), provides continuous purification of the sodium coolant in the secondary circuit during all modes of operation including normal operation, hot standby, and refueling other than initially purifying the fresh filled coolant. The reason of this difference between the operation mode of the primary and secondary systems lies in the presence of constant sources of oxygen, hydrogen, and tritium leakage into the Intermediate Heat Transfer System (IHTS) of the PRISM SFR. Their source, which is also mentioned in the previous paragraphs, is:

1. Oxygen: O_2 enters the secondary sodium via argon cover gas at the pump and the expansion tank. The pump seal for PRISM is also purged with argon (potentially a source of oxygen due to impurities);
2. Hydrogen: H_2 results from the diffusion through the sodium-water heat exchanger. The H_2 reacts with Na to form NaH whose concentration has to be kept to very low levels as it can promote further corrosion of the HX;
3. Tritium: being the primary purification system in stand-by during reactor operation, tritium diffuses to the secondary circuit via the sodium-sodium IHX. Due to the difference in concentration, the tritium which will most entirely be produced in the primary circuit will potentially diffuse to the secondary.

Each of the IHTSs has its own Intermediate (or Secondary) Sodium Purification System (ISPS). The ISPS is composed by:

- EM Pump;
- Cold Trap (Economizer Plus Crystallizer);
- Cold Trap Air Blower;
- Interconnecting Piping and Valves;

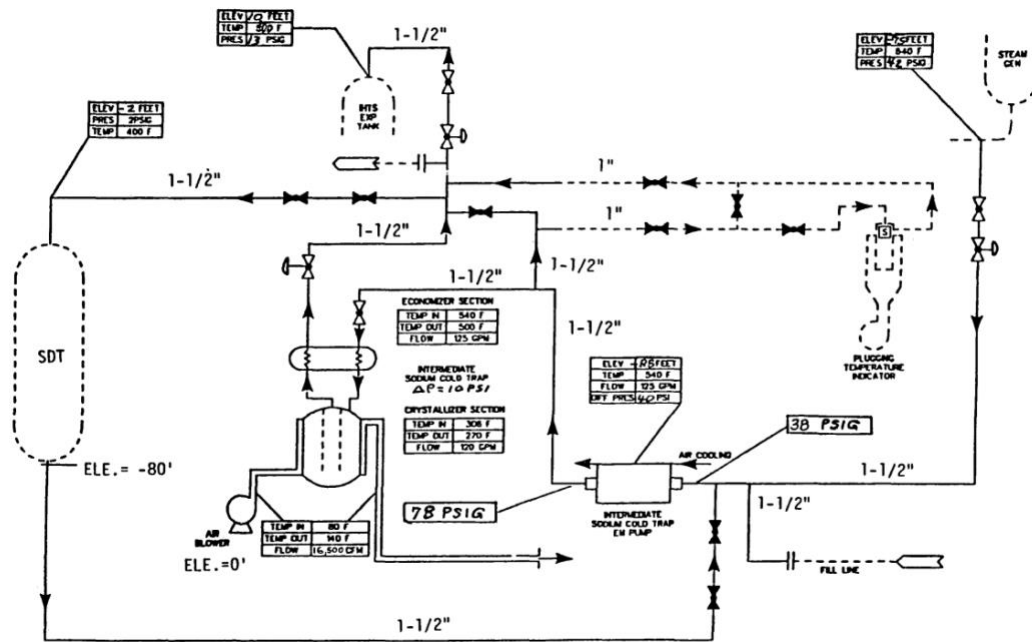


Figure 5 PRISM's secondary sodium processing system in normal operation configuration (Department of Energy, 1987).

During continuous operation, sodium is extracted from the IHTS at a rate of 120 gpm (approx. 0.4 cubic meters per minute) thanks to the EM pump, circulated in the cold trap to remove impurities, and then returned to the IHTS expansion tank.

The ISPS is connected to the IHTS from the cold leg upstream of the IHTS sodium pump near the steam generator and at the IHTS expansion tank. The cold trap and the air blower are located in the cold trap equipment vault in the steam generator building. This eases the maintenance and replacement of the ISPS. Remote operated valves are located at each of the ISPS interfaces.

Other than purifying the intermediate sodium, a connection from the ISPS to the Sodium Dump Tank (SDT) allows to purify that coolant reserve as well. Sodium is kept in the SDT for temporary storage until a system charge has been unloaded. In the meantime, sodium held in the SDT can be circulated through the intermediate cold trap by the ISPS EM pump in order to remove impurities in the sodium collected from the inner surface of the dump tank. The supply line from the dump tank is connected to the main piping of the ISPS which goes at the suction of the EM pump, going directly to the cold trap. Then, the sodium goes back to the SDT after passing through the cold trap. Both lines (supply and drain) have double isolation valves usually closed. The ISPS can also receive sodium from other tank cars or drums which can be connected to the suction of the EM pump as well. Another connection is located after the cold trap and can serve to initially pump sodium in or to take non-radioactive secondary sodium from the IHTS to the tank cars. In fact, in the PRISM reactor the transfer of sodium in and out of the intermediate system is done through the same lines. During this operation, the filters, or filter elements, are removed.

The ISPS can also be used at the start of operations to purify the primary sodium coolant as well. Reactor vessel fill can be temporarily facilitated by connecting a supply line to the ISPS. Fresh non-used sodium is pumped from the SDT to the reactor vessel using the ISPS EM pump. Upon completeness of the fill operation, the reactor sodium supply line is disconnected to prevent any further interface between primary and secondary sodium systems. The ISPS lines cannot be used for the removal of radioactive primary sodium.

The cost of the ISPS, based on INL and Strategic Analysis, Inc. analysis in 2023 (Prosser, et al., 2023) is summarized in Table 14, which assumes a project contingency of 30%.

Table 14 Capital investment foreseen for ISPS installation (Prosser, et al., 2023).

Intermediate Sodium Processing System	Cost [2023 USD]	Inflated cost [2024 USD]*
Sodium Processing Pump	19,318	20,200
Air Blower	18,183	19,000
Air-Cooled Cold Trap	9,091	9,500
Economizer	4,546	4,750
Crystallizer	18,183	19,000
Impurity/Plugging Monitor & Analyzer	27,274	28,500
Sodium Sampling Station	3,637	3,800
Shielded Cell/Glove Box	272,738	285,000
Piping	22,297	23,250
Valves	22,297	23,250
Other Instrumentation & Controls	8,919	9,300
Total System Cost	426,482	445,550
Total Plant Cost	426,482	445,550
Contingency (Excluding Pump)	30%	30%
	127,945	133,650

Total	554,427	579,000
Normalized total	3.36 [2023 USD/kWe]**	3.51 [2024 USD/kWe]**

*Reference month for inflation is February 2023.

**The normalization is done considering 165 MWe of the PRISM module.

3.3.3 Inert gas receiving and processing system

The Inert Gas Receiving and Processing System (IGRPS) receives, stores, transfers, distributes and processes inert gas used on site. In particular, it delivers inert gases of specified composition and purity at regulated flow rates and pressures to points of usage throughout the PRISM plant, accepting the contaminated gases through its vacuum and compressor facilities for storage and transfer to the gas radwaste system. Since the IGRPS plays a fundamental role in controlling the chemistry and maintaining the purity of the sodium coolant, its cost has been accounted for in this section. In fact, the PRISM reactor as well as other SFRs normally work at atmospheric pressure and, since they cannot interact with air because of the high reactivity between air and sodium, they have to face an inert gas. The purity of the inert gas has to be kept at very high levels so that impurities such as oxygen, hydrogen and others are not absorbed by the coolant.

The inert gases used in the PRISM reactor are argon, nitrogen and helium. Argon gas is provided as a cover gas for both the IHTS and the auxiliary sodium systems. Nitrogen gas is used as a cover gas for controlling and mitigating sodium-water reactions and serves as a coolant in the primary sodium processing subsystem. Helium gas is used for evacuation and as a cover gas for the reactor, in addition to providing inert atmospheres in the reactor service building, spent fuel shipping casks, fuel transfer casks, ports, and floor valves. The IGRPS has to be able to satisfy the design requirements of inert gas for 15 days. It includes five 2-pound (~ 1 kg) cylinders of helium, two 1,500 gallons (5.67 cubic meters) of liquid argon and two 3,000 gallons (11.35 cubic meters) of liquid nitrogen.

For each of the three inert gases, the IGRPS has a different distribution subsystem:

1. The helium distribution subsystem; It maintains a purity of helium of 99.9945% by volume as minimum value in the PRISM design. It is composed of helium gas storage tanks, pressure regulatory valves, stop valves, piping, gas bottles, filters, and relief systems.
The system includes a portable helium gas supply subsystem (plus a backup) called the Reactor Helium Distribution Subsystem. It is used to evacuate, purge and establish the reactor system cover gas prior to reactor startup and during refueling and maintenance (primary system purification does not happen continuously). The portable, motor truck mounted supply also manages the flow and pressure control of the reactor cover gas and receives recycled helium from gaseous radwaste. It is conservatively sized to handle the radioactive isotopes released from failure of ten fuel pins four days after reactor shutdown. Other than that, it supplies helium to fuel handling cells and sends radioactive helium from the cell to radwaste for cleanup. It also provides helium by some gas bottles to the fuel transfer casks and the fuel shipping canisters to maintain their purity. The distribution subsystem also includes instrumentation and control for the monitoring of the system operation.
2. The argon distribution subsystem; It is composed of liquid argon supply tanks, pressure regulating valves, stop valves, piping, gas cylinders, filters, and relief systems. Its main function is to distribute purified argon at a minimum purity of 99.996% to the cover gas of the IHTS (one distribution system is used per reactor power block) and the auxiliary liquid metal systems for system evacuation and backfill. The distribution subsystem also pumps argon to be used as cover gas into the reactor containment vessel for inerting purposes. The primary sodium service vault is supplied with argon as cover gas for the sodium processing and sampling

systems, and primary sodium storage vessel. The distribution lines of the argon subsystem run alongside the ones used for nitrogen in the PRISM SFR.

3. Nitrogen distribution subsystem; It is composed of liquid nitrogen supply tanks, vaporizers, pressure control valves, stop valves, piping, filters, and relief systems. It principally distributes fresh nitrogen (minimum 99.998% pure) to inert and pressurize the Steam Generator (SG) and to purge the sodium water reaction pressure relief system following a sodium water reaction involving gaseous reaction products. Nitrogen is also used as an inert cooling gas for the primary sodium processing subsystem. The nitrogen is stored as liquid in two, redundant gas generators. The liquid nitrogen is vaporized by heat transfer to ambient air as it is withdrawn. Nitrogen gas is generated from one unit during normal use and a connection to the second unit provides a backup source of nitrogen in case of low level or when the generator is being serviced.

The cost of the IGRPS, based on INL and Strategic Analysis, Inc. analysis in 2023 (Prosser, et al., 2023) is summarized in Table 15, which assumes a project contingency of 30%.

Table 15 Capital investment foreseen for IGRPS installation (Prosser, et al., 2023).

Inert gas receiving and processing system	Cost [2023 USD]	Inflated cost [2024 USD]*
Helium Distribution	29,750	31,100
Argon Distribution	546,000	570,000
Nitrogen Distribution	642,250	670,500
Tag Gas Recovery & Analysis	300,000	313,000
Reactor Cover Gas Cleanup	657,500	686,500
Total System Cost	2,175,500	2,271,000
Total Plant Cost	3,363,750	3,512,000
Contingency	30%	30%
	1,009,125	1,054,000
Total Plant Contingent Cost	4,372,875	4,566,000
Normalized total	26.53 [2023 USD/kWe]**	27.67 [2024 USD/kWe]**

*Reference month for inflation is February 2023.

**The normalization is done considering 165 MWe of the PRISM module.

Overall, considering a total sodium mass of 331,489 kg, the total operating coolant's costs can be estimated. Summing up the inert gas receiving and processing system cost together with the primary and intermediate sodium processing system, we obtain a normalized cost of approximately 17.32 \$/kg (in 2024 USD).

4. Lead and Lead-Bismuth eutectic

Lead is a dense, bluish-gray metal that has been used for thousands of years due to its malleability, corrosion resistance, and low melting point. When associated with Bismuth at their eutectic point (44.5% lead, 55.5% bismuth), it can form an alloy called LBE or Lead-Bismuth Eutectic. Both liquid lead and LBE are prime candidates for liquid metal cooling in nuclear reactors due to their intrinsic advantages. These include (Luo & Zhang, 2024):

- Excellent coolant properties. Lead and LBE allow reactors to operate at approximately atmospheric pressure and high temperature due to their high boiling and low melting points, and high heat of vaporization. The possibility of core voiding is also eliminated due to the high boiling point. Higher operating temperatures can also potentially increase the efficiency of the reactor and allow the production of other energy products (Nuclear Energy Agency, 2015). Given that the coolant can operate in an un-pressurized environment, there is much reduced concern over a potential LOCA accident or no need to have a high-pressure injection system (Sofu, 2019).
- Chemical inertness. The two coolants are inert and exhibit just minimal reactivity with high-temperature water or steam (no risk of hydrogen build-ups). This allows the elimination of an intermediate circuit between the primary circuit and the steam generator, as it would be required in an SFR.
- High heat capacity. In case the heat sink would be lost during an accident transient, lead and LBE coolant would respond well due to their high thermal inertia (Smith & Cinotti, 2023). Compared to SFRs, Lead Fast Reactors (LFRs) would have a longer grace period due to a 40% higher heat capacity per unit volume.
- Shielding capacity. Lead and LBE can effectively shield against gamma rays and retain actinides and fission products like Iodine and Cesium up to 600 °C (Smith & Cinotti, 2023) (Nuclear Energy Agency, 2015). The two coolants also allow a relatively low energy dispersion when neutrons undergo elastic scattering. This makes them good candidates for fast reactor development.
- Low moderating and absorption cross section. Thanks to a moderation power being more than 400 times smaller than that of light water, lead assemblies can accommodate bigger spacing between the pins without excessively affecting the neutron economy. This reduces the pressure head of the core, promoting passive natural circulation and reducing the risk of channel obstruction (Smith & Cinotti, 2023).

At the same time, they also present various drawbacks (Sofu, 2019):

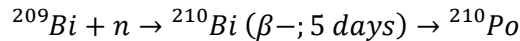
- Coolant corrosiveness. Lead and LBE can degrade typical structural steels and cause coolant slugging (lead oxide) if oxygen levels are not controlled.
- Melting point. Both melting points for LBE (125 °C) and lead (327 °C) are above room temperature. This is a safety concern and requires the installation of appropriate systems to guarantee heating of the piping and the primary structures in every operating condition (Nuclear Energy Agency, 2015).
- Lead and LBE density. Lead and LBE have a very high material density requiring a great pumping power and strong mechanical supports for components.
- Lead toxicity. Even though it is unlikely to deposit on cold metal surfaces, lead still has to be treated appropriately as the worker's exposure has to be limited.

Table 16 Properties of Lead and LBE compared with other heat transfer fluids commonly considered for nuclear reactors (Nuclear Energy Agency, 2015).

Coolant	Atomic mass [g/mol]	Relative moderating power	Neutron absorption cross-section (1 MeV) [mbarn]	Neutron scattering cross-sections [barn]	Melting point [°C]	Boiling point [°C]	Chemical reactivity (with air and water)
Pb	207	1	6.001	6.4	327	1737	Inert
LBE	208	0.82	1.492	6.9	125	1670	Inert
Na	23	1.8	0.23	3.2	98	883	Highly reactive
H ₂ O	18	421	0.1056	3.5	0	100	Inert
D ₂ O	20	49	0.000212	2.6	0	100	Inert
He	2	0.27	0.007953	3.7	-	-269	Inert

Despite both being considered as coolants for fast reactors (LFR) operation, lead and LBE exhibit differences in their physical properties. As shown in Table 16, LBE has a lower melting point compared to pure lead. Consequently, several designed and built LFRs use LBE as a coolant. Notably, it has been used in Soviet/Russian Alpha-class submarines and chosen for the SVBR-100 and CLEAR-1 designs, as well as the MYRRHA Accelerator Driven System (ADS) (Smith & Cinotti, 2023). However, the primary focus of the Generation IV International Forum has shifted to pure lead for several reasons (Smith & Cinotti, 2023):

- The biggest drawback related to LBE use is the large production of Polonium-210. Polonium, is generated by the following reaction:



Polonium successively decays emitting a 5.3 MeV α particle with a half-life of 138.4 days. The presence of polonium is a threat in case of its release to the environment while also contributing to the reactor's heat load. Such Polonium-210 heat load is equal to the fuel decay power after five days of cooling in an 80 MW LBE cooled ADS (Luo & Zhang, 2024). The presence of Polonium is not excluded in case pure lead would be adopted as coolant option as it could still be forming from the impurities of Bismuth. Nevertheless, the creation of Po-210 would be about 10,000 times less than in LBE and does not represent a major threat. So far, in spite of the experience gained by the Russians in dealing with polonium contaminated LBE, no publication describing industrially established and proven polonium extraction technology exists (Ortiz Amaya & Braet, 2009). For this reason, the cost relative to polonium de-contamination in LBE-cooled reactor, will not be included in this report.

- Bismuth scarcity contributes to the higher cost of LBE with respect to pure Pb (Sofu, 2019). This cost difference can be noticed in the investment required for huge quantities of materials as required for NPP operation (Luo & Zhang, 2024).
- LBE is more corrosive than lead (when compared at the same temperature). This is due to the fact that the growth of a protective oxide layer is more stimulated in a lead pure environment, and steel components are less soluble in lead (Nuclear Energy Agency, 2015).
- LBE has a lower thermal conductivity at 500 °C;
- LBE has a slightly lower heat capacity.
- LBE expands when freezing meaning the vessel walls would be subject to high stresses in case freezing happened.
- Other disadvantages are the formation of solid and macroscopic oxide slags in LBE-cooled reactors. Those may become a potential cause of accidents.

Table 17 summarizes the principal differences between lead and LBE.

Table 17 Comparison of Lead and LBE properties at 500 degrees Celsius (Sofu, 2019).

	Lead	Lead-Bismuth
Melting point [°C]	330	125
Boiling point [°C]	1735	1670
Conductivity [W/m·K]	18	15
Density [g/cm]	10.45	10
Specific heat (c_p) [J/K·kg]	145	140
Specific heat (ρc_p) [J/K·cm]	1.5	1.4
Viscosity [10^{-4} Pa·s]	18	13
Thermal expansion [10^{-6} K ⁻¹]	122	128

The use of lead-based coolants for nuclear reactor cooling was proposed in the 1950s in the USA despite being abandoned early because of the corrosive nature of the coolant (Cacuci, 2010). Parallely during the same timeframe, the Soviets (and later the Russians) developed the technology for usage in their nuclear Alpha-class submarines. They were able to achieve 80 years of LBE-cooled reactor experience thanks to the deployment of a total of 12 reactors and 15 reactor cores, including two reactors and three reactor cores onshore (Alemberti, Smirnov, Smith, & Takahashi, 2014). Russia's interest on LFR development did not end with the Soviet Union but was rather strengthened by increasing international attention towards environmental concerns. In fact, the possibility of closing the fuel cycle and enhancing uranium utilization brought the world's interest towards fast reactors (Luo & Zhang, 2024). Current Russian research on this field has concentrated on some ADS systems and two LFR concepts. The first one is the SVBR (Svintsovo Vismutovyi Bystryi Reaktor), a 100 MWe LBE-cooled reactor designed to address the energy requirements of small grids and rural areas considered to be the successor of the prior submarine technology (Alemberti, Smirnov, Smith, & Takahashi, 2014) (Smith & Cinotti, 2023). The second major initiative is the BREST-OD-300 (Bystryi Reaktor Estestrennoy Bezopasnosti) reactor, a 300 MWe lead-cooled multipurpose reactor able to produce electricity while consuming and producing plutonium, producing radioisotopes for industry and medical applications, and transmuted long-lived fission products and actinides (Cacuci, 2010). Despite the Russian support towards the SVBR-100 development was stopped in 2018, the BREST-OD-300 will be the first Gen IV LFR to begin operation (Smith & Cinotti, 2023). In fact, the steel reactor base plate was recently installed at the construction site in Russia and it is expected to start operation in 2026 (World Nuclear News, 2024). The plan for Rosatom (the Russian State Atomic Energy Corporation) is to develop a 1200 MWe model, called the BR-1200, in case BREST-OD-300 is able to demonstrate a good performance both in operational and financial terms.

In Western Europe, research on LFRs was mainly concentrated on ADSs for the transmutation of plutonium and minor actinides (Alemberti, Smirnov, Smith, & Takahashi, 2014). The major steps were done during the sixth and seventh European framework program plans organized by the European Atomic Energy Community (EAEC). Firstly, the EAEC funded a research project aiming to develop a 600 MWe LFR called ELSY in 2006. The ELSY project was later followed by the LEADER in 2010. The LEADER initiative focused on the study of two concepts: an industrial-sized reactor under the name ELFR and a 100 MWe demonstration LFR called Advanced Lead Fast Reactor European Demonstrator or ALFRED. The latter is planned for construction in Romania and several parties are currently involved in its development. On the other hand, SCK-CEN has carried on the development of a Multi-purpose Hybrid Research Reactor for High-tech Applications (MYRRHA) since 1997. The goal is to prove the feasibility of a both subcritical and critical operation of a research reactor driven by an accelerator, where LBE is used as spallation target and coolant, for the burning of minor actinides (Cacuci, 2010) (Smith & Cinotti, 2023). Presently, the European LFR development

program counts 34 experimental facilities (operating or being built), in 10 of their research institutions (Alemberti, Smirnov, Smith, & Takahashi, 2014). The Italian company NewCleo is also developing a lead-cooled LFR, having raised more than 400 million euros in investments. The company plans to build a first prototype of their 300 MWe reactor in France before the end of this decade.

In Asia, Korea, Japan and China lead the way. Nevertheless, while the Koreans and the Japanese started their research on LFR development in the 1990s, the Chinese focused on it in recent times (Alemberti, Smirnov, Smith, & Takahashi, 2014). In Korea, the LBE-cooled Proliferation-resistant, Environment-friendly, Accident-tolerant, Continual and Economical Reactor (PEACER) was proposed by Seoul National University in 1996. Korea is currently actively involved in LFR development with efforts focused mainly on thermal-hydraulics and corrosion experiments. In Japan, the Tokyo Institute of Technology proposed several interesting LFR projects starting from 1991. Between those, it is possible to name the LSPR (small reactor with long-life core), the PBWFR (an exotic reactor concept eliminating the need of steam generators and primary pumps by direct injection of water into the hot LBE) and the CANDLE (originally a sodium-cooled design adapted for lead use). Regarding China, they started ADS development effort in 2009 at the Chinese Academy of Science. Moreover, they launched a strategic research program for the development of the China LEAd-based Reactor (CLEAR) which included three development steps from a 10 MWth reactor towards a 1000 MWth one (Alemberti, Smirnov, Smith, & Takahashi, 2014). The design of the 10 MWth prototype, CLEAR-I, has been completed (Wu Y. , 2016).

In the United States, the Accelerator Transmutation of Waste (ATW) program was launched in the 1990s to close the fuel cycle by burning plutonium, minor actinides, and long-lived fission products in a lead-bismuth-eutectic (LBE)-cooled subcritical ADS. Additionally, the Small, Secure Transportable Autonomous Reactor (SSTAR) was designed by Argonne National Laboratory in collaboration with other organizations. SSTAR is a 45 MWth lead-cooled reactor engineered to eliminate the need for on-site refueling and to be easily transportable. It features a very long-life core design, capable of operating for 15 to 30 years and following the load with minimal operator intervention (Smith, et al., 2008). The SSTAR has been included by the Generation IV International Forum (GIF) in the list of the three reference designs together with the 300 MWe BREST-OD-300 reactor and the 600 MWe ELFR. In fact, LFRs were identified in 2002 as one of the six promising nuclear energy technologies to be considered for future advanced systems by the GIF. This later led to the formation of a Provisional System Steering Committee in 2005, which was formalized as the System Steering Committee through the initiation of a Memorandum of Understanding (MOU) in 2010. Several countries have joined this cooperation for LFR development as the GIF-LFR-MOU was strongly proposed and promoted by Europe (Alemberti, Smirnov, Smith, & Takahashi, 2014).

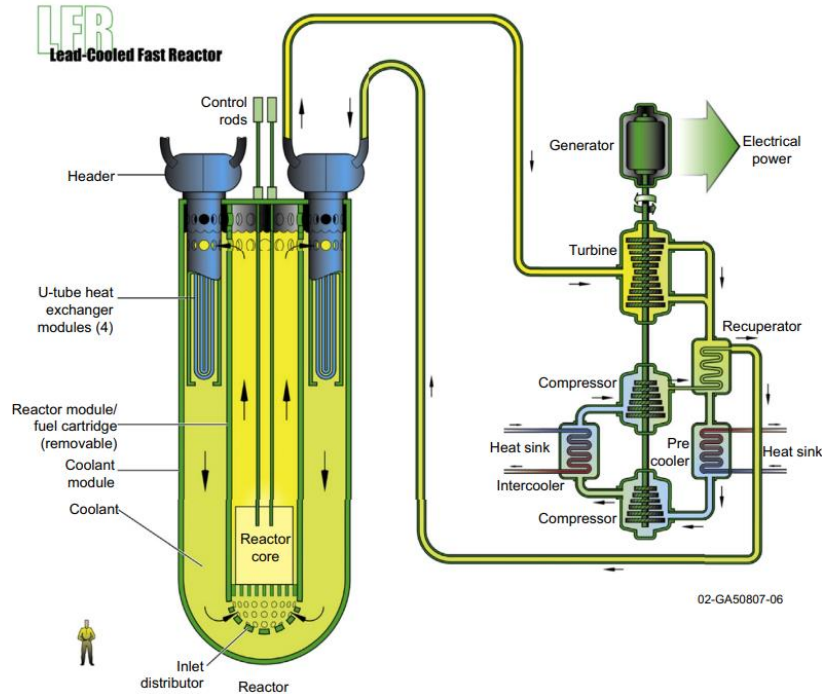


Figure 6 Scheme of a LFR as courtesy of the Generation IV International Forum (Piro, 2016).

4.1 Purity requirements

In this paragraph, the purity requirements for nuclear operation of lead and LBE are explored. Both coolants have to comply with some purity requirements during reactor operation. The main reasons for this are the following (Nuclear Energy Agency, 2015):

1. Impurities activate. Due to their passage through the core, the coolant's impurities can activate forming radioactive elements that can contaminate the primary circuit and the structural components. This represents an increase of volume of material that will have to be disposed and additional constraints when performing maintenance or other activities surrounding the nuclear environment involving human operators. This often translates to higher costs of operation. Moreover, radioactive element's formation could alter the physical parameters of the LFR.
2. Corrosion issues. If the level of impurities in the coolant is higher than a certain threshold, the structural materials may degrade faster because of corrosion phenomena. To preserve the long-term use of structural steels, the lead/LBE chemistry requirements must be accurately monitored and controlled.
3. Impurities react. Some impurities can react with elements generated under irradiation, eventually inducing solid precipitation in the circuit's cold parts (leading to the risk of flow blockage) and affecting polonium formation.

Table 18 lists the possible impurities that can be found in a critical or subcritical reactor system and ADS/spallation target taking the MEGAPIE experiment (an LBE-cooled neutron spallation target) as a reference (Nuclear Energy Agency, 2015).

Table 18 Possible impurities present in lead/LBE used for a critical or subcritical reactor system or a spallation target of an ADS. The normal impurity content is taken from data of the MEGAPIE experiment (Nuclear Energy Agency, 2015).

Species	Content [µg/g]	Impact	Operation*	System**	Comments		
Ag	25.6	Grade definition	B	3	These impurities trace from the intrinsic pollution of the lead material and might stay within the coolant during operation if not removed.		
Cd	2.2						
Cu	26.5						
In	14.4						
Sn	5.9						
Fe	1.4	Plugging/deposits	A		Fe, Cr and Ni are typical corrosion products. These are continuously generated at a rate dependent on the operational temperature, flow rate, etc.		
Cr	0.19						
Ni	2						
O	-	Plugging and cover gas pressurization	A-B-C		Oxygen can be introduced in different ways to the primary cooling system. It could enter through the cover gas, by the coolant when changed, via primary circuit surface adsorption during maintenance, because of air inlet or SG leak (water can be split in H and O due to high temperature). To allow the presence of an oxide film on the steel structures of the primary system, the oxygen level must be carefully controlled. Some alloys make oxygen control less critical than others though.		
H ₂ O	-					Release to the environment	A
H	-			Plugging/deposits			
Oil	-	A	2		Possible sources are leakages and causal pollution of the primary circuit.		
Hg	-						
Po	-						

Au		Release in case of loss of confinement			
Os/Ir					
Pu		Activation on the long term	C	1	These derive mostly from fuel cladding failure and consequent release to the coolant.
U					
FPS (I, Cs, ...)					
Mn		Coolant activation	A	1	Possible impurities deriving from the fuel or the cladding.
Co					
^{110m} Ag					

*Operation refers to the conditions in which the impurity is normally introduced into the coolant. The possible options are normal operating conditions (A), initial start-up, restart after maintenance or repair (B), off-normal pollution sources (C).

**System classifies whether the impurity is relevant for the coolant system of a critical or subcritical reactor system (1) or a spallation target of an ADS (2) or both (3).

As shown in Table 18, various impurities can be present in lead-bismuth eutectic (LBE) or lead-cooled systems. These impurities may include metallic contaminants from new lead ingots, corrosion and erosion products formed due to the interaction of the coolant with structural materials during operation, fission products released by cladding rupture or generated through beam interactions with structures, and impurities resulting from the coolant's interaction with cover gas, among others. Most impurities in the primary system are expected to maintain a constant concentration during operation, except for oxygen and corrosion products. Over time, corrosion products can accumulate, potentially leading to pipeline clogging. Oxygen, on the other hand, is the most significant contaminant when nuclear operations restart after maintenance and repairs. The potential rate of oxygen contamination, along with its impact on corrosion processes and the formation of solid oxides, makes oxygen the most critical impurity in lead-cooled nuclear systems (Nuclear Energy Agency, 2015).

Oxygen concentration in lead/LBE coolant must be accurately monitored throughout nuclear operations. In particular, a lower and upper threshold must be set. The upper threshold for oxygen contamination is set based on the lead monoxide (PbO) solubility (which varies with temperature) as solid PbO might accumulate in the primary system cold spots clogging the circuit, depositing on pipes or heat exchanger surfaces, affecting the overall heat transfer (Martinelli, Courouau, & Balbaud-Célérier, 2011). On the other hand, the lower threshold for oxygen concentration is set by assuring that the oxygen potential in the liquid metal is above the potential for a protective film formation on the structural materials for use in the high temperature range (> 450°C). The formation of an oxide film can be beneficial for structural steels and alloys as it has been proved to be able to protect the materials from corrosion. For these reasons, an oxygen control system must be installed in the primary circuit to allow oxygen purification during start-up (highest level of oxygen can be expected at this point) and during operation to promote the formation of a protective oxide layer. However, it has been observed that even with a few weight percent of solid lead oxide in the metal coolant, the system remains compatible with flowing conditions. This indicates a surprising operational flexibility compared to other liquid metal coolants, such as sodium. The problem still remains the long-term operation as the accumulation of the un-treated oxide might cause operational problems. In particular, solid PbO and deposits of LBE with iron traces were recorded up to 5% of the coolant mass in the circuit. Their dissolution into the coolant has been proven to be difficult (Martinelli, Courouau, & Balbaud-Célérier, 2011).

Given that it has been clarified that a great part of the impurities present in the liquid lead/LBE comes from the initial ingots, it is of our interest to delineate the requirements in terms of purity for lead-based coolants. On this topic, it must be noted that according to the (Nuclear Energy Agency, 2015) and some private conversations held with Nathan Trotter & Company and Westinghouse, no nuclear specifications currently exist for lead or LBE. However, standard commercially available grades would meet the requirements for nuclear operations as commercial grades up to 99.98%

(or even 99.99%) are available on the market. In fact, reactor conditions would not need ultra-pure C0 or C00 (respectively 99.992%, and 99.9985%) as even a C2C grade (99.97%) could be considered suitable for reactor operation. Westinghouse conducted research to determine if the decommissioning acceptance conditions for coolant could be met using C2C grade lead (Levinsky, et al., 2022). The findings revealed that naturally occurring impurities in lead significantly contribute to lead activation, with Antimony-124, produced by neutron activation, being the primary contributor. The study indicates that lead coolant will likely need to be disposed of mostly as Low-Level Waste and partially as Intermediate-Level Waste as planned for the UK. Despite this, the higher impurity levels in C2C compared to C00 have a minimal impact on activation and do not affect plant operations. However, the initial impurity levels can significantly impact neutronics, influencing Lead Fast Reactor (LFR) core behavior and fuel requirements. The study does not specify the level of lead purity required to meet regulatory standards, which may vary by country as each regulator may have specific criteria. Finally, since no findings have contradicted the use of C2C quality lead, a purity level of 99.97% is considered the "nuclear grade" quality required for reactor operations involving lead and LBE in this report.

For completeness purposes, the level of impurities normally present in C00 and C2C lead are illustrated in Table 19 (Levinsky, et al., 2022).

Table 19 Lead impurity composition [wt%] for C00 and C2C grades (Levinsky, et al., 2022).

Element	Lead Grade		Element	Lead Grade		Element	Lead Grade	
	C00	C2C		C00	C2C		C00	C2C
Pb	99.99852	99.97	Sn	0.0001	0.001	Na	0.0001	0.003
Ag	0.00001	0.002	Sb	0.0001	0.005	Cd	0.00005	Not regulated**
Cu	0.00001	0.002	Mg	0.0001	0.003	Al	0.00005	Not regulated**
Zn	0.0001	0.002	Fe	0.0001	0.001	Hg	0.00005	Not regulated**
Bi	0.0005	0.02	Tl	0.0001*	-	In	0.00001	Not regulated**
As	0.0001	0.002	Ca	0.0001	0.003	Mg+Ca+Na	-	-

*Indicated by the literature but not confirmed.

**Not regulated, thus data from C00 could be used in case this lead grade would be considered for activity calculations.

4.2 Lead and Lead Bismuth Eutectic costs

In this section, the cost relative to the use of the lead/LBE coolants is analyzed. In particular, capital expenditures are divided in:

1. Purchase costs: the cost associated with the purchase of the lead/LBE in nuclear grade quality and quantity before the start of the nuclear operations.
2. Pre-purification costs: the cost of the installation of the necessary facilities to melt and purify the lead ingots before the start of the nuclear operations.
3. Online purification costs: Capital investment required for the installation of an Oxygen Control System (OCS) and other impurities purification systems.

As mentioned in the previous paragraphs, since no commercial method for the extraction of Po-210 from LBE has been developed so far, the costs relative to the extraction of Polonium are not analyzed in this report.

4.2.1 Purchase costs

In this section, the price for lead and LBE coolants is investigated considering a purity of 99.97% based on the assumptions made in the last chapters. The cost per kg of lead/LBE derives from literature and from industry conversations, having considered a minimum target quantity of tons. This is because thousands of tons are the expected amount of liquid metal to be used in a LFR (Nuclear Energy Agency, 2015) and the cost per kg of lead and bismuth is expected to decrease with the increase of quantity purchased. The retrieved quotes for such liquid metals are grouped in Table 20 including some others considering a different purity.

Table 20 Retrieved cost for high purity and reactor grade lead and LBE.

Lead					
Supplier/Buyer	Westinghouse	Nathan Trotter & Company	USGS	INL	Thermo Fisher Scientific
Purity	99.97%			Unknown	99.999%
Cost [2024 USD/kg]	2.2 – 3		2.5	6 – 7.7	1920
Comments	The price for large quantities of lead results to be very low. The price for commercial lead is usually driven by the London Metal Exchange quotation (currently at 2.06 \$/kg) to which a market-driven physical premium based on the metal quality and quantity is then added to the to determine final pricing. Current premiums are approximately 0.4 \$/kg for the C2C quality, meaning large quantities (~ 20 metric tons) of lead would cost today around 2.5 \$/kg.		The United States Geological Survey (USGS) quantified the cost of commercial grade lead at <i>115 cents per pound (253 cents/kg) during the first 10 months of 2023</i> (United States Geological Survey, 2024)	The price indicated has been shared via private conversation by INL. The quantity and the purity of lead are unknown though.	The cost is extrapolated from a quote for 250 grams from Thermo Fisher Scientific. The scope is to highlight that the cost of ultra-high purity lead can be some orders of magnitude higher than the commercial one, adapt for nuclear applications.
Lead Bismuth Eutectic					
Supplier/Buyer	USGS	Westinghouse	INL		
Purity	99.98%	99.97%	Unknown		
Cost [2024 USD/kg]	6 – 6.3	15	25.5 – 35.5		
Comments	Taking into account the retrieved price of 2.2 – 3 \$/kg for 99.97% lead, the price for LBE is calculated using data for Bismuth from the USGS. USGS mentions a price of 4.10 \$/lb (~ 9.0 \$/kg) for	Suggested price for future purchases. No quantity of reference is mentioned in the conversations though.		The price indicated has been shared via private conversation by INL. The quantity and the purity of lead are unknown though.	

	99.99% purity metal at warehouse (Rotterdam) in minimum lots of 1 ton, as published by Fastmarkets (United States Geological Survey, 2024). Using the two quotes, and knowing the eutectic point has a share of 44.5% of lead, the quote is retrieved.		
--	--	--	--

Considering the quotes for lead and LBE which are reported in Table 20, a cost range of 2.2 – 3 \$/kg for lead and 6 – 15 \$/kg for LBE is considered for subsequent calculations. Some of the quotes are not further considered as data because the target quantity of metal and/or the purity are missing. Based on the retrieved cost range for the two coolants, some additional calculations are performed in Table 21 to show how the capital requirements for coolant purchase escalate for different reactors and systems.

Table 21 Investment cost associated with coolant initial purchase for different size of LFRs/ADSs based on the necessary quantity of lead/LBE (Nuclear Energy Agency, 2015).

Source	(Brissonneau, et al., 2011) (Van den Eynde, Malambu, Stankovskiy, Fernandez, & Baeten, 2015)	(Brissonneau, et al., 2011) (Liu, et al., 2009)	(Nuclear Energy Agency, 2015) (Dragunov, Lemekhov, Moiseyev, & Smirnov, 2015)	(Nuclear Energy Agency, 2015) (Dragunov, Lemekhov, Moiseyev, & Smirnov, 2015)	(Nuclear Energy Agency, 2015) (Stepanov, et al., 1998)	(Nuclear Energy Agency, 2015) (Waltar, Todd, & Tsvetkov, 2012)
Reactor name	XT-ADS	EFIT	BREST-OD-300	BREST-OD-1200	NPHP Angstrom	SVBR
Coolant	Pb	Pb	Pb	Pb	LBE	LBE
Plant Nominal Power [MWth]	57	400	700	2800	30	210
Coolant Price [\$/kg]	2.2 - 3				6 - 15	
Total Lead/LBE Coolant Quantities						
Volume [m³]*	~ 190	~ 570	600	2500	3	18
Mass [kg]**	2,000,000	6,000,000	6,300,000	26,250,000	~ 30,500	182,500
Total Cost [2024 USD]	4,400,000 – 6,000,000	13,200,000 – 18,000,000	13,800,000 – 19,000,000	57,500,000 – 79,000,000	180,000 – 460,000	1,100,000 – 2,800,000
Nominal cost [2024 USD/MWth]	77,000 – 106,000	33,000 – 45,000	19,500 – 27,000	20,500 – 28,500	6,100 – 15,500	5,200 – 13,100

*The volume for the XT-ADS and EFIF is calculated using a density of 10,500 kg/m³ as indicated in (Nuclear Energy Agency, 2015) for the BREST-OD-300 and BREST-OD-1200 reactors.

**The mass of LBE is calculated by using the following correlations: $\rho_{Pb} = 11367 - 1.1944T$ and $\rho_{LBE} = 11096 - 1.3236T$ which can be found in (Nuclear Energy Agency, 2015). Firstly, the temperature at which Pb density is 10,500 kg/m³ is calculated. Successively, the retrieved temperature can be plugged in the second formula to retrieve the density for LBE at the same temperature conditions.

As can be seen from Table 21, the absolute cost range for lead/LBE initial purchase investment normally increases with increasing plant nominal power while the normalized cost (to the plant MWth) decreases with plant's size. While performing such calculations, the cost range is considered to be within 2.2 - 3 \$/kg for lead and 6 – 15 \$/kg for LBE. Nevertheless, it could be normally expected to face a cost range closer to the minimal values (thus 2.2 and 6 \$/kg) while the plant size escalates to bigger thermal outputs.

Based on a report published by the International Atomic Energy Agency in 2012, the cost of bismuth, estimated by the USGS to be \$4.10 per pound (~ 9.0 \$/kg) in 2024, represents approximately 1% of the capital investment required for constructing a Lead Fast Reactor. Consequently, the technical and economic parameters of an LBE-cooled LFR are unlikely to be significantly affected by substantial increases in bismuth costs. The future use of a non-eutectic lead-bismuth alloy may be considered if bismuth prices rise, though this would involve a trade-off concerning the melting temperature. Non-eutectic lead-bismuth alloys with reduced bismuth content have higher melting points; for instance, reducing the bismuth content by 10% raises the melting point from 125 °C to 250 °C. However, this change is not expected to pose insurmountable operational challenges for the reactor (International Atomic Energy Agency, 2012).

4.2.2 Pre-purification costs

In this section, the cost of pre-purification is analyzed. In fact, before the start of nuclear operations, pre-purification facilities are required to ensure an appropriate level of oxygen and other impurity concentration in the coolant. The procedure starts with the melting of the lead ingots in a melting tank. The melting operations are performed at a relatively low temperature in the range of 350-380 °C. This is done in order to minimize the oxygen content in the lead/LBE as oxygen solubility is minimized close to the melting temperature. At this relatively low temperature the impurities will float on the melting tank and will not go into the storage tank. The lead/LBE can be then transferred to a storage tank. While moved between the two tanks, the coolant is filtered from the possible oxides and impurities. Once all the liquid metal is in the storage tank, gas phase oxygen control can be performed to achieve the required level of oxygen content in the coolant for the start of nuclear operations. In the HELENA-2 facility, built for ALFRED reactor development, the deoxygenation is performed using Ar/H₂ gas mixtures in which the hydrogen is directly supplied by a hydrogen generator to prevent possible explosions or fires.

As a reference for our cost estimations, the pre-purification systems of the ATHENA research facility are taken into account. ATHENA or Advanced Thermo-Hydraulics Experiment for Nuclear Application, is an electrically heated, 2.21 MW pool type multipurpose facility representative of LFR systems. The facility, installed in Mioveni (Romania), aims to perform experimental studies over different aspects related to LFR operation, being able to fully characterize a single 1:1 ALFRED fuel assembly. In particular, several aspects related to the oxygen control in large pool, corrosion and erosion of materials and coatings, lead flow dynamic and stratification will be analyzed there.

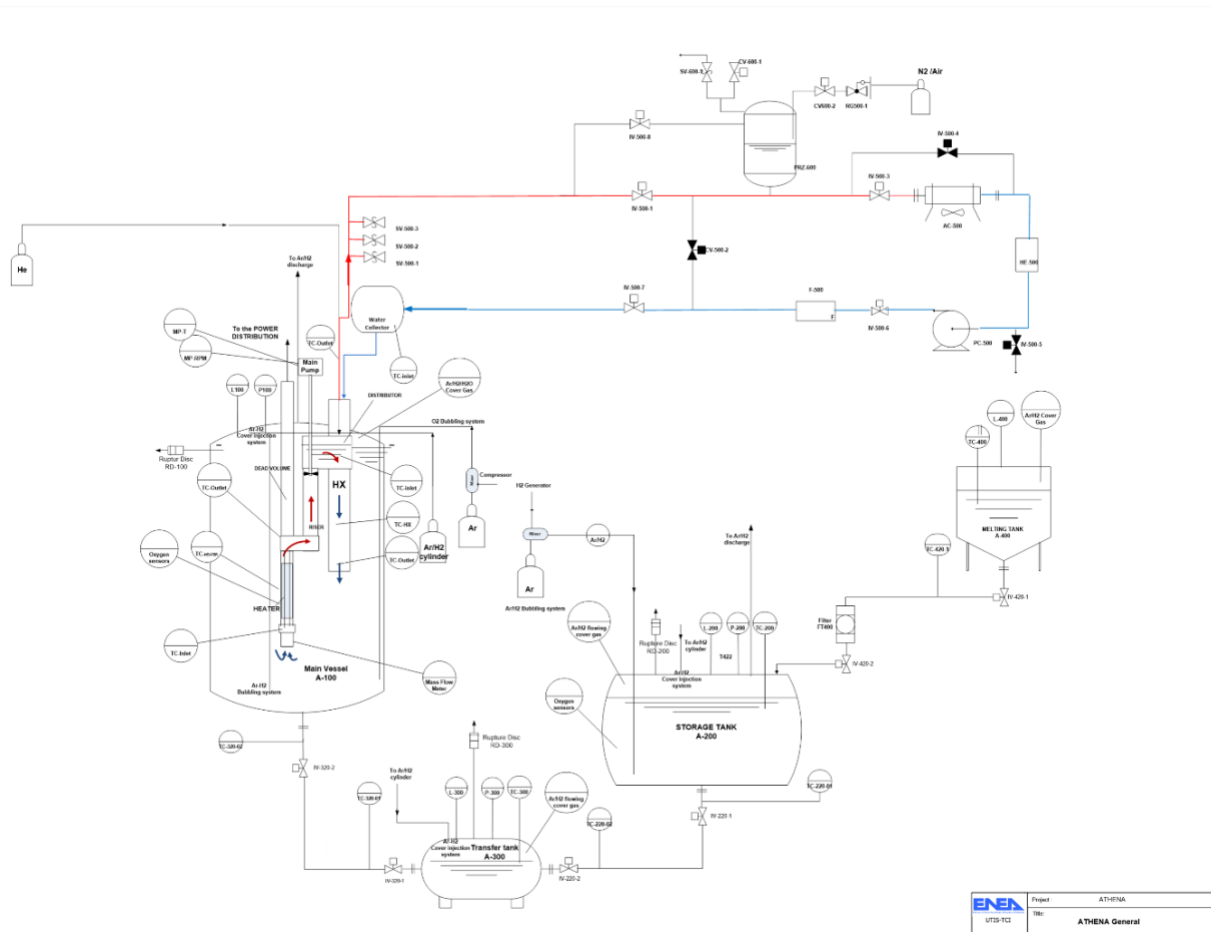


Figure 7 Schematic representation of the ATHENA research facility. Image kindly provided by ENEA (Italy).

The ATHENA facility, depicted schematically in Figure 7, features a large vessel measuring 3.2 meters in diameter and 10 meters in height, capable of holding 800 tons of liquid lead. Due to the scale of the facility and its pre-purification vessels, a similar capital investment would be required for an LFR such as ALFRED. The projected costs for pre-purification for the 300 MWth reactor are expected to be comparable to those of ATHENA. The expenses associated with the pre-purification facilities at ATHENA are detailed in Table 22. It should be noted that the costs related to oxygen removal, particularly hydrogen production, are addressed in the following section, "Purification and Chemistry Control Costs".

Table 22 Investment cost relative to pre-purification systems in a facility of the size of ATHENA.

System	Subsystem	Cost [2024 USD]	Comments
Pre-purification	Pump	210,000	-
	Storage vessel	425,000	-
	Transfer vessel	105,000	-
	Melting tank	59,000	-

	Control valves, Isolation Valves, Relief Valves	48,000 – 67,000	-
	PbO filter	3000 – 4000 /unit	-
Control*	Lead/LBE Sampling Station	3,850	Sampling and control cost consider sodium as a reference.
	Shielded Cell/Glove Box	285,000	
Cost calculations	Total	1,150,000 – 1,190,000	-
	Contingency	30%	-
	Total (with contingency)	1,490,000 – 1,550,000	-
	Normalized total**	1.86 – 1.94 \$/kg	The total costs are normalized considering a mass of 800 tonnes of lead as in the ATHENA facility. Nevertheless, as previously mentioned, the same costs for pre-purification are expected to be faced for a 300 MWth LFR like ALFRED.

4.2.3 Purification and chemistry control costs

The cost related to lead purity maintenance during operation is being analyzed in this chapter. Before discussing the cost information, it is important to present a brief introduction of the methods of lead purification. It should be considered that chemistry control is generally not critical for operation of lead/LBE-cooled systems, if properly addressed during the early design stages and throughout the start-up and shutdown procedures. However, neglecting this aspect in the design phase can lead to significant operational difficulties. Therefore, it is crucial not to overlook chemistry control in the design of any system. Well-designed and well-operated facilities can be run with a high degree of confidence, even under low-oxygen conditions. However, higher operating temperatures necessitate the long-term validation of oxygen control systems at specific medium-range concentrations, particularly in larger systems and when using pure lead coolant (Nuclear Energy Agency, 2015).

As discussed in previous chapters, oxygen is the most critical impurity in lead and LBE-cooled nuclear systems, as its control is crucial for ensuring long-term operational safety. The oxygen concentration must be carefully balanced to prevent the massive formation of lead and bismuth oxides and to mitigate the risk of fouling the heat-transfer surfaces, causing the pumps' failure, the increase of hydraulic resistance on the coolant flow path, and other problems (Orlov, et al., 2007). This is achieved by maintaining oxygen levels well below the solubility limits. On the other hand, lead and LBE are highly corrosive to conventional structural steels, with pure lead being less corrosive than LBE at equivalent temperatures. To protect the structural integrity of the materials, it is essential to promote the formation of a protective Fe-Cr oxide layer on the surfaces. This requires maintaining the oxygen potential in the liquid metal above the threshold needed for protective film formation on structural materials, especially at high temperatures. However, the effectiveness of this oxide layer is limited to temperatures below 480 °C, as it loses its protective properties at higher temperatures. For steel surfaces exposed to temperatures above 480 °C, alternative solutions such as high-performance coatings must be considered. Still, proper oxygen regulation will ensure the long-term viability of components operating at lower temperatures. In summary, contamination and corrosion issues can be minimized by maintaining oxygen concentrations within a range between the oxygen solubility at the coldest point and the minimum level required for forming Fe-Cr oxides at the hottest point (Bassini, 2017).

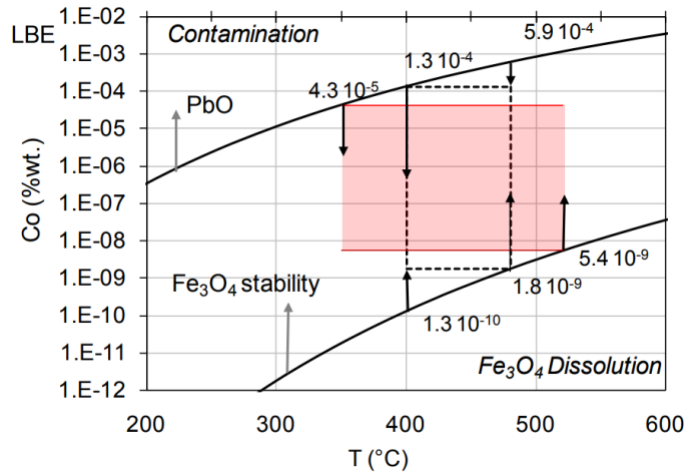
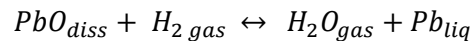


Figure 8 Oxygen specifications in LBE (Nuclear Energy Agency, 2015).

For every nuclear system that uses lead or LBE as coolants, the oxygen control strategy shall include oxygen control systems and oxygen measurements systems. The methods by which oxygen control can be maintained in an LFR/ADS system are two. The first one is called “gas phase oxygen control”. Gas phase oxygen control is based on the creation of a gas/liquid equilibrium between the cover gas and the liquid metal, controlling the oxygen partial pressure in the gas to set the dissolved content when the liquid is below saturation (Nuclear Energy Agency, 2015). The following can be achieved using two strategies (Bassini, 2017):

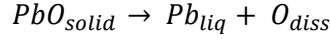
1. Injection of H₂ and O₂. Pure oxygen and hydrogen diluted with an inert gas (argon) can be either supplied to the cover gas or the liquid metal using some bubbling lines which increase the surface exchange area ensuring an equilibrium can be stabilized. The reaction happening would be then the following:



The efficiency of the system can be enhanced by increasing the exchange area, which can be achieved by reducing the size of bubbles using spargers or impellers, or by adjusting the temperature of the liquid metal. Hydrogen gas is particularly useful for recovering from significant oxygen contamination, which can occur during startup or maintenance. It also helps purify newly melted lead ingots before the filling procedure begins. Typically, the hydrogen concentration starts at 30% H₂/70% Ar at the beginning of operations and is then reduced to 5% H₂/95% Ar during operation. This reduction is feasible because oxygen sources are minimal during operation, and the oxygen concentration in the cover gas can be maintained at ppb levels using oxygen getters.

2. Injection of a H₂/H₂O mixture. An H₂/H₂O mixture diluted with Argon can be prepared bubbling a mixture of argon and hydrogen in water (controlling the temperature) to create an H₂O-saturated Ar-H₂ mixture. The concentration of oxygen can be varied in the liquid metal by varying the ratio of H₂ and H₂O.

The second method for oxygen control in lead/LBE is called “solid-phase oxygen control”. Solid phase control of the oxygen concentration can be achieved by meticulously controlling the temperature and flow rate conditions (and so the dissolution rate) in a specific device containing stable solid lead oxide. The solid PbO is usually in the form of spheroids, which gradually dissolve over time, accordingly to the formula:



Mass transfer primarily occurs at the PbO/HLM interface, specifically within the boundary layer surrounding the solid PbO spheroids. However, some internal transfer by diffusion within the porous solid can also occur (Bassini, 2017). Other factors influencing mass transfer include the size of the PbO spheroids and the mass exchange area even though temperature and the flow rate of the liquid metal are the primary determinants. A strategy for the use of the mass exchanger might be to install it in a loop type LFR or as part of an external loop. It should syphon off part of the coolant to re-insert it where it is predominantly consumed during operation such as in the core or steam generators (Brissonneau, et al., 2011). For solid-phase oxygen removal, oxygen getters such as Mg, Zr, and Ti-based alloys can be used. While Mg has been tested in lead/LBE systems, Zr and Ti have primarily been used in sodium systems. These getters oxidize according to their surface area and the operating temperature, forming solid oxides. To prevent contamination of the coolant, these oxides must be contained in cartridges.

Table 23 summarizes the principal methods for oxygen control, considering each option advantages and disadvantages (Bassini, 2017) (Brissonneau, et al., 2011).

Table 23 Main characteristics of the oxygen control methods in lead-cooled systems (Bassini, 2017) (Brissonneau, et al., 2011).

Type	Method	Advantages	Disadvantages
Gas-phase	Injection of O ₂ and H ₂ gases (oxygen supply and removal).	Simple operation, especially using H ₂ ; rapid adjustment of concentration.	Potential PbO contamination during O ₂ supply. In fact, the use of O ₂ is not recommended except in case of abrupt decrease of O ₂ concentration in the coolant; precise control is difficult.
	Injection of H ₂ /H ₂ O mixture.	Set the desired oxygen concentration by controlling H ₂ /H ₂ O ratio in the gas; good results in experimental facilities.	Long time to reach equilibrium; difficulty in restoring large deviations; low effectiveness when used in large pools where the ratio between the surface area and the volume may not be enough to promote the mass transfer.
Solid-phase	PbO mass exchanger (oxygen supply).	Simple operation; efficiency due to solid/liquid contact; no PbO contamination of the coolant; avoid having a gas circuit in the system enhancing the confinement of radioactive gases like Po-210.	Replenishment after consumption; No indication of the state of the PbO pebbles during use, at least for the designs developed outside of Russia; poor experience in large-scale experiments.
	Oxygen getters addition (oxygen removal).	Simple operation; efficiency due to solid/liquid contact.	Lead/LBE contamination with metal-oxides; replenishment after consumption; poor experience with lead/LBE systems.

Generally speaking, maintaining precise oxygen control in liquid lead or lead-bismuth is one of the most significant challenges. The targeted oxygen concentration must be consistently maintained throughout the entire coolant system at all times during operation. In industrial-scale reactors, this involves managing liquid metal volumes around 1,000 metric tons, compared to the much smaller 0.1–1 metric tons typically handled in most of today's experimental facilities

(Brissonneau, et al., 2011). Both solid-phase and gas-phase control methods have their own advantages and disadvantages, making the choice for reactor operation dependent on several factors. These factors include the reactor type (loop or pool), the methods employed in experimental facilities, and prior experience. Historically, the Russians have cumulated the most experience with loop type LFRs thanks to their use in nuclear submarines and have developed complex types of oxygen mass exchangers (Martynov, Askhadullin, Simakov, Chaban', & Legkikh, 2008). On the other hand, gas phase control has been tested in several experimental facilities Europe-wide such as the Karlsruhe Institute of Technology (KIT) and ENEA (Italy) for ALFRED oxygen control development. In this report, both types of oxygen control are analyzed with particular focus on gas phase control.

To accurately control the oxygen concentration in LFRs and ADSs, reliable devices must be installed. Over the past decade, potentiometric ceramic-based sensors have been developed and studied for monitoring dissolved oxygen concentration in Pb and LBE. The developed sensors work with an oxygen-conductive ceramic and a reference electrode contained within a one-hand closed tube. The oxygen-conductive ceramic is a doped zirconia stabilized with Y_2O_3 and MgO. The goal of the additive compounds is to stabilize up to room temperature the crystalline cubic form of zirconia, which is the conductive form of oxygen ions (Bassini, 2017). The solid electrolyte separates the lead or LBE coolant, where the oxygen concentration is to be measured, from a reference system (either gas or metal/metal-oxide) where the oxygen concentration is known and stable. This difference in oxygen concentrations between the two media generates an electromotive force across the ceramic element, which enables precise measurement of the oxygen concentration. These sensors have demonstrated high accuracy and reliability and have been successfully employed in small-scale experimental setups, such as small vessels and facility loops. However, when it comes to large-scale experiments, like large pool facilities, the main challenge lies in the ceramic's fragility. In fact, the ceramic electrolyte should be able to withstand great pressures (several bars of gas pressure could also be present on top of lead/LBE head in storage tanks) and flow velocities, requiring high mechanical resistance to compression and shear stresses to provide long-term reliability. Moreover, a major limitation is the temperature of operation. In fact, ceramic sensors have demonstrated a scarce performance at temperatures below 300 - 400 °C. Other than that, these sensors have been tested to be chemically compatible with lead/LBE and to be able to withstand the neutron flux without any damages to the crystalline structure. Thus, the key technological challenge is ensuring adequate protection of the ceramic components within the extensive lead/LBE mass (Bassini, 2017).

To enhance the stability of ceramic sensors under high pressures, several strategies can be considered. One approach is to add small amounts of aluminum oxide ($\leq 2\%$ wt.) to improve the mechanical strength of zirconia. Another option is to design a protective metallic sheath around the ceramic tube to mitigate mechanical and thermal shock caused by the thermal expansion of the liquid metal and air within the electrolyte. A steel sheath could effectively distribute heat along the tube, thereby reducing thermal stresses. Alternatively, using a shorter ceramic thimble instead of a long, one-end closed tube can help prevent failure of the solid electrolyte. The limitation of liquid metal/metal-oxide reference systems could also be overcome by using solid metal/metal-oxide electrodes. For example, Cu/Cu₂O and Fe/Fe₃O₄ are potentially usable systems in which the metal phase is solid throughout the entire working temperature range. The research over these systems has only begun recently and shows promise (Bassini, 2017).

During their latest tests, ENEA has developed reliable detectors up to 1.5 meters of length. For reactor operation, oxygen sensors should get to a length of 10 meters approximately. Developing a reliable sensor of this length is very challenging as the lead pressures it should withstand are high (up to 10 bar). Nevertheless, having probes of different lengths inside the vessel can help monitoring the oxygen concentration in the different zones: stagnant locations, mixed zones and points close to coated and non-coated steels. If coupled with a model that simulates the oxygen concentration in the total volume as a function of temperature and stagnation, multiple detectors can help drawing a complete distribution of the zones of homogeneity and inhomogeneity of the primary circuit. In this case, the sensors should be additionally supported to mitigate Archimedes thrust, for example, by reinforcing the electrode support and guide tube with a thicker tube. Nevertheless, other strategies could be adopted for oxygen control not involving the development of 10-meter-long oxygen sensors. For our analysis, we have considered that several probes would be

used during pre-purification and operation, some of them able to reach 10 meters long. Given that the cost of 1.5 meters probes is around 6000/7000 USD, the cost of a longer probe would include the addition of a longer and thicker support steel tube. Based on advice from experts at ENEA, the cost of long sensors to be used in a pool type LFR is extrapolated to be 10,000 USD each. At least four of these sensors are hypothesized to be used in the reactor, being placed in hot, cold leg, expansion vessel and storage tank (considering stagnation points are excluded by design).

Having introduced the methods currently used for gas-phase oxygen control, the costs can be analyzed. One of the main considerations is about the strategy for hydrogen supply. For a reactor like ALFRED with a capacity of 125 MWe, the use of an electrolyzer is planned as advised by experts at ENEA. The size of the electrolyzer can be conservatively estimated using de-oxygenation tests performed by ENEA on the HELENA facility as a reference (Bassini, 2017). The considered electrolyzer would be able to withstand a large intrusion of oxygen bringing the reactor from a “contaminated condition” to a “safe zone”. In these tests, the HELENA storage tank, containing over 3000 kg of lead, was de-oxygenated using various Ar-H₂ mixtures with different hydrogen concentrations. These tests reduced the oxygen concentration in the lead from $3.4 \cdot 10^{-4}$ wt%—considered a contaminated condition—to approximately $1.6 \cdot 10^{-7}$ wt%, placing it within the “safe zone” as can be seen from Figure 8. The transient was managed with a concentration of 26.7% of H₂ and lasted around 45 hours. Considering the same transient for a reactor like the BREST-OD-300, with a mass of coolant of 6,300 tons, the hydrogen requirement to compensate the large oxygen contamination is approximately 267 kg. Considering a de-oxygenation time of 45-50 hours and a rule of thumb of 50 kWh per kg of hydrogen, the needed electrolyzer should have a capacity of approximately 265-300 kW.

Considering the aforementioned assumptions, the costs related to gas-phase oxygen control for an LFR of the size of BREST-OD-300 are listed in Table 24.

Table 24 Investment cost relative to gas-phase oxygen control systems in a reactor of the size of the BREST-OD-300.

System	Subsystem	Cost [2024 USD]	Comments
Gas phase OCS	Electrolyzer	908,000 – 1,015,000	The electrolyzer cost is calculated considering a price of 3500 \$/kW for small (<50 MW) electrolyzers including installation costs (Gilbert, Penev, O'Dell, Howe, & Wu, 2024).
	Closed argon loop, purification	7,000 – 8,000	A 20-30 m ³ Argon loop is considered, 99.999% pure.
	Air filtration system	negligible	-
	Detectors	40,000 – 60,000	Between four and six 10-meter-long oxygen probes are considered for the cost calculation, located in hot, cold leg, expansion vessel and storage tank.
	Oxygen getters	20,000 – 30,000	-
	Material cost	310,000 \$/ton stainless steel 75,000 \$/ton carbon steel	(Ganda, Hoffman, Taiwo, Kim, & Hansen, 2019)

	Mass flow controllers	24,000 – 60,000	Between 6 and 10 mass flow controllers are used for ATHENA. The same amount could be expected in a reactor.
	Filters on gas cylinders	5,000 – 15,000	-
	Filters on gas control panel	8,500 – 17,000	-
Cost calculations	Total	1,010,000 – 1,590,000	-
	Contingency	30%	
	Total (with contingency)	1,310,000 – 2,070,000	
	Normalized total	0.20 – 0.33 \$/kg	6300 tons of lead as used in the BREST-OD-300 reactor are considered.

As it can be seen from Table 24, the normalized cost of Oxygen Control System (OCS) is very low as the mass of lead in an LFR is very high with respect to the mass of coolant of other technologies.

Next, we analyze the costs associated with an OCS if a mass exchanger would be installed. As previously mentioned, solid-phase oxygen control is theoretically more suitable for a loop-type LFR. Historically, most expertise in this technology is held by Russian organizations and SCK-CEN in Belgium. In the United States, the DELTA (DEvelopment of Lead Alloy Technical Applications) loop at Los Alamos National Laboratory (LANL) utilized a mass exchanger for forced LBE convection (Wang, et al., 2022). However, detailed cost information on these systems is often proprietary, particularly among the companies and Russian entities that possess this expertise. As a result, only rough financial estimates are available. Moreover, to accurately estimate the cost of a solid-phase oxygen control system, it would be necessary to model and design a specific loop tailored to the application.

The costs related to solid-phase oxygen control for an LFR are listed in Table 25.

Table 25 Investment cost relative to solid-phase oxygen control systems.

System	Subsystem	Cost [2024 USD]	Comments
Solid-phase OCS	Pump	Around 50,000	An electromagnetic pump with external permanent magnets, 20 kg/s flow rate and a prevalence of 1 bar is estimated around 50,000 USD. The final cost of the pump is strongly dependent on the system's design, flow rate and size of the loop. Possible suppliers are KSB (Germany) and GREENPUMPS Srl (Italy).
	Control valves	4730 - 6660 /each	The number of control valves is strongly dependent on the system's design.
	Mass exchanger	From 350,000	The cost of the mass exchanger refers to the cost of a Russian design mass-exchanger sold to the Italian party ENEA in 2008 for

			installation and testing at the CIRCE facility. The cost of the mass-exchanger comprehends the detectors, the related software and hardware (Martynov, Askhadullin, Simakov, Chaban', & Legkikh, 2008).
	PbO pebbles	-	The cost of the PbO pebbles is not estimated here. Nevertheless, the cost related to the purchase of this custom pebbles is expected to be the highest contribution for solid-phase oxygen control systems.
	Mass flow controllers	4000 – 6000 each	The number of control valves is strongly dependent on the system's design.
	Material cost	310,000 \$/ton stainless steel	(Ganda, Hoffman, Taiwo, Kim, & Hansen, 2019)
		75,000 \$/ton carbon steel	

After examining the costs associated with installing systems for oxygen control in lead/LBE-cooled nuclear reactors, we also considered the expenses related to managing corrosion products and possible lead oxide accumulation. Corrosion products can have long-term and cumulative effects due to the dynamic mass transfer equilibrium in a non-isothermal system. If not properly managed, impurities can cause clogging in the colder sections of the primary circuit, a problem observed in several test loops. For instance, during hot and cold standby modes, the redistribution of deposited impurities can quickly clog cold pipes, as seen in the CICLAD loop. In lead alloy coolant systems expected to operate for 30 years or more, as well as in target loop systems with shorter operational lifespans due to specific conditions, it is essential to continuously trap impurities in a dedicated unit. The dedicated unit is a bypass line connected to the lower operating temperature parts of the circuit in which filters, crystallizers and settling units can be placed to capture the impurities. In this bypass line, different temperature-dependent chemical processes could remove the impurities, thus minimizing the amount of impurity species dissolved in the coolant. One other option is to install a specific sedimentation vessel for startup purification. In fact, existing particles could accumulate at the gas/liquid interface of a cold quasi-stagnant auxiliary vessel by providing sufficient time for them to sediment and crystallize in the tank. Despite presenting some issues, this purification technique has been used in the MEGAPIE experiment prior to filling operation. Nevertheless, validation will be still required for larger systems (Nuclear Energy Agency, 2015).

While validation is necessary for the mentioned purification methods, filtration appears to be the most suitable method for continuous impurity removal in lead/LBE-cooled reactors. Filtration should be implemented at the coldest point in the facility with the specific approach depending on factors such as particle size distribution and operating conditions. The most widely supported filtration mechanisms include (Nuclear Energy Agency, 2015) (Beauchamp, et al., 2010):

- “Cake bed” filters. These “pile-up” the impurities at the surface of the filtration medium to then form multiple layers of impurities which resemble a cake. These are particularly suitable for filtration and accumulation of PbO excessively formed.
- “Deep bed” filters. These trap impurities at the pores of the filtration medium. These are particularly suitable for thin particles of non-reducible lead, iron and chromium oxides.

Currently, no definitive design rules or selection criteria have been established for filtration in lead/LBE-cooled reactors. However, some initial tests have been conducted: a pressed and sintered fiber metal medium was tested during the

development of the BREST-OD-300 reactor, and Pall Corporation filters were tested in the STELLA loop. These efforts represent the initial steps towards demonstrating the feasibility of continuous coolant purification in lead/LBE systems. However, sustained research using representative liquid metal loops is necessary to develop the design parameter relationships required for designing purification process units for larger-scale systems (Nuclear Energy Agency, 2015).

Given the uncertainty over the possible methods of purification and corrosion product control, our research focuses mainly on the possible cost of cake bed and deep bed filters. These filters, which have still to be tested in large systems, and whose operational reliability over time still needs to be proven together with their maintenance and regeneration, are estimated to cost in the range of 3,000 – 4,000 USD each. The quote has been shared by experts at ENEA, based on their current experience at the ATHENA research facility and in the development of ALFRED. Their cost is expected to vary based on their length, pore size, material composition and temperature resistance, etc. To be able to extract the exact amount useful for reactor operation and the related cost, the amount of filters required should be estimated together considering their effective lifetime.

5. Organic Fluids

Despite not being included in the list of 4th generation designs, organic nuclear reactors can offer several advantages with respect to other advanced designs. Due to their low vapor pressure, organic fluids can be used as a coolant in a

nuclear reactor at pressures slightly above atmospheric reaching temperatures in the range of 260 – 370 °C. This strongly limits the risk of suffering severe loss of coolant accidents, eliminating the need of heavy forgings for pipelines, RPV and fittings (Shirvan & Forrest, Design of an Organic Simplified Nuclear Reactor, 2016). Organic fluids have a very low corrosion rate which allows the use of standard materials such as aluminum and low carbon steels. Such chemical compatibility also applies to the uranium fuel (UO₂, UC, U, Thorium-Uranium) allowing just few of the fission products to get to the coolant even in case of cladding failure accident. Moreover, the radioactivity of the coolant due to oxygen and carbon activation is almost null, meaning low shielding requirements and easier maintenance of the system with respect to light water reactors (Parkins & Weisner, 1959). Organic fluids also have higher moderation properties than light water which allows to use just slightly enriched uranium as fuel. Other advantages are given by the considerable experience of the petroleum and chemical industries in handling organic fluids and the fact that no exothermic chemical reactions have been noticed under any possible conditions between the organic fluid and any materials used in the reactor system (Makens, 1964).

Nevertheless, several disadvantages can be also pointed out. The main drawback is that the high heat and radiation coming from the core alters the composition of the organic coolants. The fluid would decompose yielding hydrogen, light hydrocarbon gases and higher molecular weight compounds, also called “High Boilers” (HBs). These impurities, and especially the high boilers, must be continuously removed and maintained at some equilibrium value in the core (Parkins & Weisner, 1959). Therefore, continuous injection of make-up coolant is required. Organic coolants also have worse heat exchange properties with respect to water necessitating large heat transfer areas in the core and in the steam generating equipment to maintain the temperature stable (Makens, 1964). Terphenyls and diphenyls, the organic coolants class which has been historically chosen for nuclear applications, exhibit a spontaneous ignition temperature around 1,000 °F (~ 540 °C). Another drawback is that terphenyls and diphenyls have melting points above room temperature. This feature makes it necessary to provide steam tracing or some form of electric heating for the piping and other components of the organic system (Parkins & Weisner, 1959).

Several organic coolants have historically been identified as suitable for reactor applications. Polyphenyl compounds are the most attractive class, of which diphenyl and terphenyl are, as mentioned, the main candidates. Those can be present in different chemical forms and eventually mixed to create low volatility, highly stable organic fluids useful for nuclear applications (Makens, 1964). The potentially adapt organic coolants for use in an organic cooled and/or moderated reactor have to be defined. These are shown in Table 26 based on information from (Shirvan & Forrest, Design of an Organic Simplified Nuclear Reactor, 2016).

Table 26 Possible organic coolant options for use in organic cooled and/or moderated reactor and their main properties (Shirvan & Forrest, Design of an Organic Simplified Nuclear Reactor, 2016).

Fluids	Santowax OM	Santowax OMP	HB-40	Dowtherm A	Syltherm 800
Fluid type	15–25% o-terphenyl; 60–80% m-terphenyl; 4% p-terphenyl.	< 0.1% biphenyl; 10–13% o-terphenyl; 55–62% m-terphenyl; 27–34% p-terphenyl; < 1% HBs	~0.2 to 1.9% biphenyl; ~18% o-terphenyl; ~82% hydro-terphenyl.	73.0% diphenyl oxide; 27.0% biphenyl.	Polydimethyl-siloxane.
Freezing or pour point (°C)	~85 (liquidus)	~175 (liquidus)	-24 (pour point)	12 (freeze)	-60 (freeze)
Atm. boiling point (°C)	~315	~350	342	257	~205

Max. recommended film temperature (°C)	N/A	N/A	N/A	427	427
Density (kg/m³)	813 (371°C)	823 (371°C)	737 (371°C)	1,056 (20°C)	936 (20°C)
Thermal conductivity (W/m-K)	0.11 (371°C)	0.11 (371°C)	0.11 (371°C)	0.138 (25°C)	0.135 (20°C)
Specific heat capacity (J/kg-K)	2,529 (371°C)	2,508 (371°C)	2,387 (371°C)	1,587 (25°C)	1,608 (20°C)
Dynamic viscosity (mPa-sec)	0.23 (371°C)	0.27 (371°C)	0.26 (371°C)	3.71 (25°C)	9.1 (20°C)
Flash point (closed cup, °C)	172	190	170	113	> 160
Autoignition temperature (°C)	578	> 538	374	599	385
Toxicity	Moderate toxicity to humans. Highly toxic to aquatic life.	Moderate toxicity to humans. Highly toxic to aquatic life.	Moderate toxicity to humans. Highly toxic to aquatic life.	Slight toxicity to humans. Highly toxic to aquatic life.	Essentially nontoxic to humans and aquatic life.

The firsts to introduce the possibility of using organic fluids as coolant/moderator in a nuclear reactor were Enrico Fermi and Leo Szilard. During the times of the Manhattan Project, they filed a patent application for a “neutronic reactor” stating (United States of America Patent No. 2,708,656, 1944):

...diphenyl can also be used as a moderator and closely resembles light water giving a gain of from .2 to .4 percent in K. With either, a slight enrichment of the uranium with one of the fissionable isotopes such as, for example U²³³, U²³⁵, Pu²³⁹ will provide a K sufficiently greater than unity, to enable the construction of operating reactors...

Nevertheless, the organic coolant reactor concept has not been explored further in the 1940s. Despite their enhanced moderation, these fluids would still require the use of enriched uranium as a fuel, which was still not available for civilian use at the time. Moreover, there was no proof of their stability at high temperature and irradiation (Makens, 1964). Both these challenges were overcome in the 1950s as uranium enriching for power applications started and the decomposition rate of organic coolants was defined within a range acceptable for power reactor operation. To start the research on organic coolants and organic-cooled/moderated reactors, the Atomic Energy Commission initiated the construction and operation of the Organic Moderated Reactor Experiment (OMRE) at the National Reactor Testing Station in 1955.

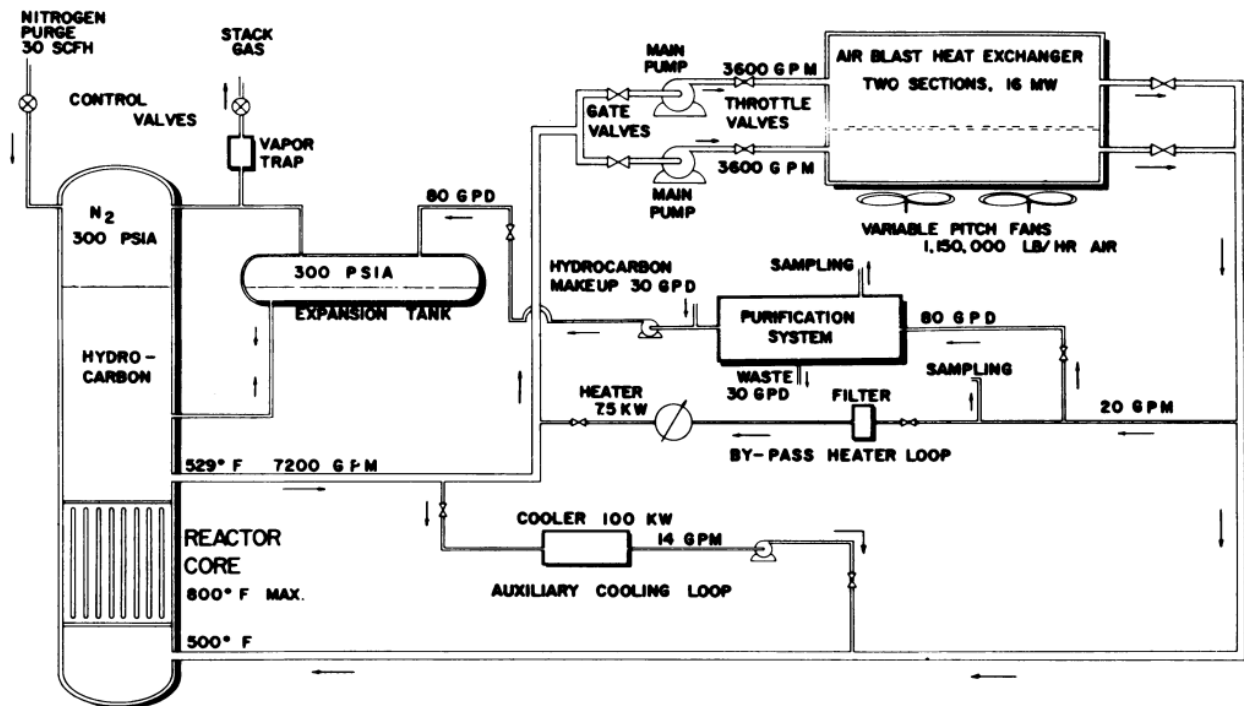


Figure 9 Schematics of the OMRE reactor concept (Parkins & Weisner, 1959).

The OMRE was designed to be used in different operating conditions (without any electric power provision) up to 16 MW (Bosworth & Parkins, 1960). The OMRE was a “quick and dirty” tentative to demonstrate the technical feasibility of the organic reactor concept and was constructed as a “minimum cost facility” (Parkins & Weisner, 1959) (Makens, 1964). The principal topic of investigation and goal of the project was to analyze the rate of polymer formation as a function of various operating conditions (Parkins & Weisner, 1959). The first two cores tested at the OMRE facility were equipped with insufficient purification systems and the terphenyls coolants (Santowax OM and Santowax R) were also exposed to the atmosphere during outage. Due to coolant polymerization and consequent coolant channel blockage, some of the experimental fuel elements failed (Shirvan & Forrest, Design of an Organic Simplified Nuclear Reactor, 2016). The fouling problem was partially addressed when the operation of the third core started, by increasing the ingress flow rate of the used distillation system. However, the operation was later interrupted to further upgrade the purification system by installing a glass spool filtration system and an activated clay adsorption system (Makens, 1964). Thanks to these improvements, excellent performance and fuel burnup was obtained.

From the experience gained with the OMRE project, the Atomic Energy Commission (AEC) authorized an engineering and technical development program in 1958 for the building of a bigger scale organic-cooled reactor in the United States. The program led to construction operations which started in July 1959 at the site of Piqua, Ohio. The Piqua Nuclear Power Facility (PNPF), which went critical in 1963, was a 45.5 MWth (11.4 MWe) organic-cooled and moderated concept using Santowax OMP. It had an installed distillation and glass spool filtration system and a nitrogen gas blanket with which it was able to minimize the exposure of the hot coolant to the atmosphere during fuel handling (Makens, 1964). Parallely to the construction of the PNPF, the AEC presented a report stating that the organic cooled and moderated reactor concept had shown a lower perspective of economic improvement and thus the development program for this technology was shut down. From that point on, all the economic efforts on the organic concept concentrated on the PNPF and a relatively small research project at MIT (Makens, 1964). This decision also affected the EOCR (Experimental Organic Cooled Reactor), a 40 MWth facility built to complement the research done at OMRE.

In fact, despite the facility being entirely built, it was never fueled. The PNP full-power operation started successfully in 1964 with no significant problems during the test period apart from two superheater tube leaks caused by steam corrosion on the secondary side (Makens, 1964). Nevertheless, after the first refueling, it was noted that some carbonaceous materials accumulated in the reactor, preventing fuel elements from seating properly. Later analyses demonstrated that the carbonaceous material was formed by coolant degradation in some part of the fuel elements due to flow stagnation. The accumulation of these impurities was leading to hotspots in the fuel and polymerization of the coolant. Given the technical difficulties encountered, the AEC ordered the cease of operations at Piqua in 1966, leading to its decommissioning in the next years (Shirvan & Forrest, Design of an Organic Simplified Nuclear Reactor, 2016).

Despite the United States abandoning the perspective of further developing organic reactor concepts, other international programs had arisen at that time. In Europe, the Reattore Organico Sperimentale a Potenza "O" (ROSPO) was built in Italy with the purpose of developing the technology for a 30-60 MWth reactor experiment called PRO (Makens, 1964) (Bitelli, Martinelli, Orestano, & Santandrea, 1967). The ROSPO concept was both cooled and moderated with Santowax R. On the other hand, organic cooled and heavy water moderated concepts were also developed in Denmark and at Euratom respectively with the EXPO research reactor and the ORGEL power demonstration reactor (Shirvan & Forrest, Design of an Organic Simplified Nuclear Reactor, 2016).

The possibility of building a heavy water moderated and organic cooled reactor was also pursued by Canada and Russia. Several were the recognized advantages of this concept (Makens, 1964):

1. The possibility of using naturally enriched uranium as well as Th-U²³³ fuel due to the enhanced moderation of heavy water instead of slightly (1.9%) enriched uranium used at Piqua.
2. Utilization of carbides and metallic fuel as alternative to oxide for extended burnup. The higher density of the fuel in form of UC and U with respect to UO₂ allows a better neutron economy which is extremely valuable when using naturally enriched fuel. Neither of the two can be used in heavy water-cooled reactors because of the potential chemical energy release deriving from the reaction of water and the fuel in the event of a fuel cladding rupture.
3. The use of organic coolants eliminates the need of a pressure boundary normally present in D₂O cooled designs as the coolant and the moderator can work at near atmospheric pressures, simplifying operation and refueling. This represents also an improvement in terms of safety in the eventuality of a LOCA accident.
4. Minimization of losses. Low pressure of the D₂O moderator allows the decrease of losses of costly heavy water due to leakage. At the same time, given the reduced size of the organic coolant inventory, the make-up costs due to terphenyls degradation with heat and irradiation are much more limited.
5. Cost savings due to reduced quantities of heavy water needed and the possibility of using low-pressure carbon steel as main material for the primary coolant system, thus minimizing capital costs.
6. Possibility of providing superheated steam (coolants can safely operate to 370 °C approximately).

Recognizing the several advantages of the concept, the Soviets started exploring the possibility of coupling heavy water moderation and organic fluids cooling by commissioning the Arbus reactor in 1963. The reactor, which initially operated at 5 MWth, was able to operate successfully for 25 years. Arbus demonstrated all the advantages of this concept including some innovations over the possibility of pre-fabricate the reactor by assembling several easily transportable low-weight units (Polushkin, et al., 1964). On the other hand, the Atomic Energy of Canada Limited started building the 40 MWth Whiteshell Reactor-1 (WR-1) in 1962. The WR-1 operated for 20 years with an average capacity factor of 85%. Similarly to the Arbus, also the WR-1 proved the intrinsic advantages of adopting a heavy water moderated organic cooled design, achieving remarkable simplicity of operation and minimal operator exposure (due to the lower organic coolant activation with respect to water) during primary circuit maintenance (Shirvan & Forrest, Design of an Organic Simplified Nuclear Reactor, 2016). Despite the large success of the Arbus and WR-1, the research has mainly focused on other concepts after the end of their operation. The main reason was the uncertainty

over the future uranium availability and the consequent need to develop breeding reactors as well as reprocessing technologies in the 1980s (Shirvan & Forrest, Design of an Organic Simplified Nuclear Reactor, 2016). Very limited research has been done on organic-cooled reactor concepts since then.

All U.S. and international organic nuclear reactor projects are summarized in Table 27 (Shirvan & Forrest, Design of an Organic Simplified Nuclear Reactor, 2016).

Table 27 Completed organic nuclear reactor projects internationally and in the United States (Shirvan & Forrest, Design of an Organic Simplified Nuclear Reactor, 2016).

Reactor	OMRE	EOCR	PNPF	Arbus	WR-1
Year of operation	1957–1963	Construction in 1962	1963–1966	1963–1979 (NPS) 1979–1988 (AST-1)	1965–1985
Location	Natl. Reactor Testing Station, Idaho	Natl. Reactor Testing Station, Idaho	Piqua, Ohio	Melekest, Russia	Whiteshell Nuclear Research Establishment, Canada
Purpose	Expt. reactor	Expt. reactor	Power reactor	SMR prototype for electricity gen. (NPS); process heat (AST-1)	Materials test reactor
Power	15 MWth	40 MWth	45.5 MWth / 11.4 MWe	750 kWe [5 MWth] (NPS); 12 MWth (AST-1).	60 MWth
Coolant	Santowax OM (Core I); Santowax R (Core II).	Terphenyl	Santowax OMP	GSG; HTpH; DTM	HB-40 (OS84)
Moderator	Santowax OM (Core I); Santowax R (Core II).	Terphenyl	Santowax OMP	GSG; HTpH; DTM	D ₂ O
Fuel type	UO ₂ /SS cermet (Core I-III); U-3.8 Mo-0.2 Al (Core IV)	UO ₂ /SS cermet, SS cladding	U-3.5Mo-0.2Al/Si alloy, Al-finned cladding	UAl alloy; UO ₂ /Al cermet	UC, Zr-2.5 Nb cladding
Coolant temp.	260–371°C / 271–377°C	260°C / 274°C	271°C / 302°C	230°C / 243°C	280–400°C / 320–425°C

Comments	- At least three cores and a fourth prototype over operating history to test different fuels and conditions	- Reactor never fuel loaded - Shift of AEC priorities to LWRs and fast breeders	- Excessive film buildup on cladding from coolant degradation led to shut down.	- The plant use was changed from nuclear power station to heat supply in 1979.	- Used natural uranium.
-----------------	---	--	---	--	-------------------------

Among the other possible uses of organic fluids in the nuclear field, fusion technology must be cited. In fact, these fluids have also been evaluated along the 1980s and 1990s as first wall and breeding blanket coolant (Romero, 1980) (Sze, et al., 1991) (Gierszewski & Hollies, 1987).

5.1 Purity requirements

In this section, the purity requirements for the use of organic coolants in nuclear facilities are analyzed. As mentioned in the paragraphs before, the major problem identified with the operation of organic nuclear reactors was related to the degradation of the coolant. The interaction between the organic coolant with the heat and radiation coming from the core can lead to the pyrolytic (temperature-dependent) and radiolytic (radiation-dependent) decomposition of the coolant. In fact, both thermal energy and radiation (gammas, neutrons and electrons) can break the bonds of the organic chains freeing hydrogen, methane and other light hydrocarbon gases as well as other organic compounds within a whole spectrum of volatility and molecular weight (Makens, 1964). The organic compounds can polymerize to form larger, more complex molecules with higher boiling points (Shirvan & Forrest, Design of an Organic Simplified Nuclear Reactor, 2016). These are called high boilers or HBs, as mentioned before in the report. High boilers are scientifically defined as *the organic materials boiling above triphenylene ((C₆H₄)₃), and in most cases residue remaining after micro-sublimation at 240 °C, 0.20 mm, and 30 minutes time* (Griffith & Russel, 1963). The accumulation of high boilers in the coolant leads to the decrease of the heat transfer coefficient as well as the coolant viscosity requiring a higher pumping power (Gardner & Hutchinson, 1964). Moreover, the high boilers can contribute to the deposition and fouling of thermally insulating films at the surface of the fuel elements other than partial plugging of the coolant channels (Makens, 1964). These phenomena were the main reasons behind the problems encountered during operation of core-I and core-II configurations at OMRE.

Given the possible difficulties in operating with excessive high boiler concentration, their concentration has to be limited during operation by using a continuously operating coolant purification system. Although a recommended equilibrium high boiler concentration in the coolant was not explicitly mentioned in the historical literature, several sources mention an equilibrium operational concentration range between 10 and 30% for existing facilities including the PNP (Griffith & Russel, 1963) (Gardner & Hutchinson, 1964) (Parkins & Weisner, 1959) (Atomics International, 1960).

On behalf of the initial purity requirements, data from the operation of the Piqua Nuclear Power Plant considers some impurities in the new organic coolant to calculate the possible activity of the fluid after the nuclear power is started (Atomics International, 1960). Data from OMRE initial purity has also been retrieved (Makens, 1964). The list of impurities, completed with some additional information from other retrieved sources, is shown in Table 28.

Table 28 Assumed impurities concentrations for new coolant in the Piqua nuclear power plant and the OMRE facility (Makens, 1964) (Atomic International, 1960).

Element	Maximum Allowable Impurities at OMRE [ppm]	Unirradiated OMRE coolant [ppm]		Circulating* OMRE Coolant Dec. 1960 [ppm]	PNPF activation calculations [ppm]	Purification Efficiency
		Typical Core I Santowax OM Coolant	Santowax OMP Range			
Copper	2	0.53	0.07 - 0.32	0.38	0.50	0.97
Sodium	0.2	0.11	0.17 - 0.58	0.38	0.20	0.97
Manganese	0.1	0.05	0.006 - 0.25	0.22	0.10	0.98
Chlorine**	2	1.5	0.24 - 0.84	1.5	2.00	0.75
Sulfur	60	64	36 - 75	54	60.0	0.73
Phosphorus	8	< 0.3	0.5 - 12.0	0.5	80.0	0.97
Aluminum	1	0.27	0.25 - 18.0	0.22	-	0.98
Arsenic	0.5	< 0.3	Not Detected	0.008	0.30	0.96
Barium	2	< 0.5	< 0.5	0.03	-	0.98
Boron	0.5	0.5	0.09 - 0.52	0.008	-	0.98
Calcium	10	0.3	0.06 - 6.0	0.08	-	0.98
Chromium	1	0.05	< 0.005	0.38	-	0.98
Cobalt	0.1	0.005	0.005 - 0.1	0.08	0.10	0.98
Iron	10	4	1.0 - 11.0	53	-	0.98
Lead	4	0.15	0.48 - 1.7	0.38	-	0.98
Magnesium	1	0.17	0.05 - 0.25	0.22	-	0.98
Mercury	0.1	< 0.001	Not Detected	ND	-	0.9
Molybdenum	1	< 0.04	0.35 - 0.92	0.22	-	0.98
Nickel	3	0.18	0.10 - 2.8	0.15	-	0.98
Silicon	3	0.4	0.51 - 45.0	1.14	-	0.98
Silver	0.1	< 0.005	Not Detected	0.008	-	0.98
Tin	1	1.2	0.19 - 0.23	0.22	-	0.98
Titanium	5	0.05	< 0.02 - 5.5	< 0.08	-	0.98
Zinc	1	< 0.05	< 0.2 - 0.81	1.52	-	0.98
Zirconium	1	< 0.05	< 0.03 - 0.05	< 0.10	-	0.98
Selenium	0.5	0.05	Not Detected	0.06	-	0.73

*The circulating OMRE coolant has already been irradiated. This data should not be considering when analyzing initial impurities concentrations and purity requirements for new coolant.

**Chlorine in combined form can contribute to the fouling problem when present in concentrations higher than 5 ppm (Kasten, et al., 1967).

Based on data from Table 28, the initial coolant target purity for reactor operation is of approximately 99.98% in the Piqua Power Plant and slightly higher in the OMRE facilities (almost 99.99%). It should be also noted that the 96 to 98% of the of the impurities listed above (apart from Cl, Se and S, at approximately 75%) can be removed through a distillation purification system before the start of nuclear power as indicated in the column "Purification efficiency" of Table 28. By installing a hydrocracker purification system instead of a distillation system (considered a more modern and better option as it allows the recovery of the high boilers), it has been experimentally shown that at least 75% of

the iron both soluble and in the particulate form can be removed by the catalyst. It is also believed that the hydrocracker will remove at least 75% of the other impurities (Griffith & Russel, 1963). It would be therefore possible to purchase a coolant with a quality of 99.98 – 99.99% as done at the OMRE and PNPf and purify the coolant further before starting the nuclear operations activating the coolant purification system.

Other possible impurities accumulated during operation are oxygen and water. Oxygen was present in very low concentrations during normal operation of organic-cooled reactors and the OMRE. At OMRE, the concentration of oxygen increased rapidly (by factors between 2 and 6) when air was admitted to the system during reactor shutdown, as the facility did not dispose of an inert gas cover (Makens, 1964). The presence of oxygen decreases the thermal stability of the reactor, contribute to a greater degradation and marked loss of fluidity and causes the formation of compounds corrosive to metal components (e.g., acids, phenolic compounds and water). Moreover, oxygen possibly contributes to the fouling phenomenon as a higher formation of polymers and lighter gaseous organic compounds was noticed when oxygen was present in biphenyl pyrolysis (Makens, 1964). Nevertheless, its presence in the primary circuit can be limited significantly adopting a strategy to not expose the primary coolant to air during operation and refueling/maintenance operations. The presence of water in the coolant could lead to the loss of chemical inertness between the organic coolant and the structural materials. Nevertheless, values up to 400 ppm were measured to have no corrosion effect on a number of different steels but aluminum alloys. Water concentrations of 1000 to 2000 ppm corroded aluminum seriously (Kasten, et al., 1967).

5.2 Purchase cost

The cost of purchase of different organic “nuclear grade” fluids is shown in Table 29.

Table 29 Cost per kg of various organic fluids useful for nuclear applications.

Source	Product	Quantity	Year	Original cost [Year USD/kg]	Cost [2024 USD/kg]***
(Gardner & Hutchinson, 1964)	Santowax OMP	-	1963	0.22	2.27
(Gardner & Hutchinson, 1964)	Santowax OMP	-	1964	0.38	3.81
(Griffith & Russel, 1963)	Generic organic fluid	-	1963	0.38	3.88
(Kasten, et al., 1967)	Santowax OM	1,040,000 kg	1967	0.27	3.63
(Makens, 1964)	Terphenyl coolant	-	1964	0.38	3.81
Chempoint	Dowtherm A*	55 gallons (almost 210 liters)**	2024	22.5	22.5

*Dowtherm A is an organic heat transfer fluid for liquid- and vapor-phase processes for applications between 15 °C and 400 °C.

**A density of 1.064 g/cm³ is considered here.

***The prices are inflated to 2024 USD prices using the official CPI inflation calculator from the US Bureau Of Labor Statistics.

As can be seen from Table 29, the current price for organic heat transfer fluids seems to have increased with respect to the prices considered in historical literature written during the development program of the organic cooled reactor in the United States. Also, some of the historical alternatives considered for organic-cooling are currently no longer produced.

5.3 Operational and Purification costs

In this chapter, the investment cost relative to the installation of a purification system is analyzed together with some operational costs. The operational costs considered are also linked to the maintenance of the purification system and the necessary make-up due to coolant degradation. Before quantifying the required investment, it is important to understand what are the options in terms of coolant purification technologies for an organic reactor.

The scope of the organic coolant purification system is to remove the high-molecular weight compounds (the high boilers), thus maintaining the desired HB concentration in the main heat transfer system. By removing the high boilers and other impurities which may be present in the organic fluid (with the efficiencies explicated in Table 28), most of the radioactivity in the coolant can be removed. Part of the purification system is also the coolant make-up injection line as the new coolant which is pumped in must be filtered to remove possible impurities (Atomics International, 1960). The purification method which was used for the OMRE and PNP facilities is a distillation process. During this process, the coolant is siphoned off at a controlled, continuous rate from the pressurizing pumps and directed toward the column feed heater. The heater raises the coolant's temperature to the required 700 °F (~ 370 °C) before it enters the distillation column. The coolant enters the upper section of the column, where it undergoes flashing. The gases at the top of the distillation column are condensed in the column condenser, then flow to a receiving tank and subsequently to a degasifier tank. Once in the degasifier tank, the coolant is pumped back into the primary circulation system and the core. Meanwhile, the high boilers accumulate at the bottom of the distillation column. These are periodically withdrawn, cooled, and pumped to specific decay tanks where they are allowed to decay and further cool down. Finally, they are transferred to the waste disposal system (Atomics International, 1960). The described distillation method inevitably requires large amounts of makeup and necessitates the disposal of large amounts of waste material (Griffith & Russel, 1963). To be able to reduce the necessary makeup demand and the volume of waste material, a hydrocracking process was developed. This method, is based on the possibility of breaking down complex hydrocarbon molecules into simpler chains which can be re-used in the primary coolant circuit. The process requires the use of a catalyst at high temperatures (450 – 510 °C) and pressures (around 70 bar), and a high hydrogen flow to saturate the broken hydrocarbon chains and prevent the formation of coke (solid carbon deposits) (Gardner & Hutchinson, 1964). Of the high boilers which enter the hydrocracker, some high boiler material is processed into light ends in the hydrocracker and some is lost as a coke deposit on the hydrocracker catalyst (Griffith & Russel, 1963). The catalytic hydrocracker can be linked to a distillation column (as was proposed for Piqua given that a distillation column was already present as main purification device) or a flash tank. The two would have the same scope: to cause some of the liquid to flash into vapor by sudden depressurization so that the less volatile components (the high boilers) can accumulate in the lower zones. This way, the flow rate at the inlet of the hydrocracker contains a higher share of HBs, increasing the efficiency of the process.

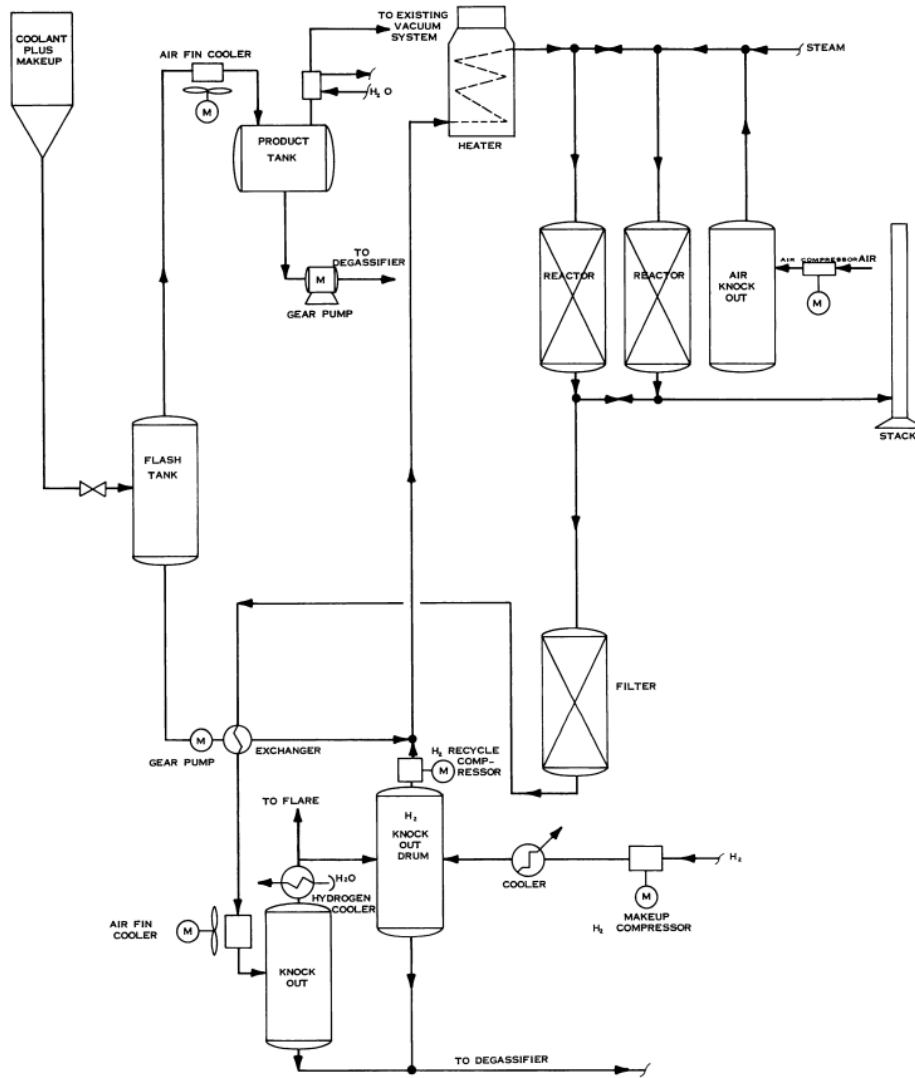


Figure 10 Flow diagram for a flash tank fed hydrocracker as proposed for the Piqua Nuclear Power Facility (Griffith & Russel, 1963)

To estimate the economics of the purification system, the hydrocracker system is chosen due to its several advantages over the distillation system such as reduced costs, lower make-up needs and HBs waste disposal. In fact, modern organic reactors are expected to incorporate a hydrocracking system rather than a distillation system (Shirvan & Forrest, Design of an Organic Simplified Nuclear Reactor, 2016).

Consequently, the major capital and operational costs associated with the coolant purification are:

- Investment cost related to the catalytic hydrocracker system installation (capital);
- Investment cost for the purchase of a flash tank (capital);
- Periodical cost due to the degradation of the hydrocracker catalyst (operational);
- Cost related to the provisioning of hydrogen for the correct functioning of the hydrocracker (operational);
- Make-up costs related to the inevitable loss of coolant due to pyrolysis and radiolysis;
- Other operational costs associated with the hydrocracker's operation: Utilities, operating labor, maintenance, supplies (operational);

- Other indirect costs associated with the hydrocracker's operation: General expenses, social security and other taxes, direct overhead and services and insurance (operational).

All the above-mentioned costs are calculated using the 45.5 MWth Piqua Nuclear Power Facility as a reference. In fact, before the permanent shutdown at PNPf, a detailed cost analysis over the possible installation of a hydrocracker system at Piqua was done considering different possibilities and comparing their convenience (Griffith & Russel, 1963). The calculated costs displayed in the report are useful to compare our calculations with the inflated costs. Firstly, the target HB concentration and production rate must be analyzed to properly scale the hydrocracker. At Piqua, the HB production rate was set to vary linearly between 50 and 90 lb/h (22.7 and 40.8 kg/h), depending on the equilibrium concentration of HBs in the coolant. The production rate would be 22.7 kg/h if the coolant has a 30% HB concentration and 40.8 kg/h if the coolant has a 10% HB concentration (more information in the Appendix C). Two hydrocrackers were considered for PNPf (Case 1 and Case 2 in the report). The first hydrocracker would process 40.8 kg of high boiler per hour (inlet flow 172 kg/h), maintaining the equilibrium high boiler concentration in the primary system at 10% and the ash concentration at about 0.4 ppm. The second hydrocracker would process 68.0 kg of high boiler per hour (inlet flow 277 kg/h), maintaining the equilibrium high boiler concentration in the primary system at less than 10% and the ash concentration at approximately 0.3 ppm (Griffith & Russel, 1963). The second hydrocracker installation price was calculated to be around 300,000 in 1963 including the additional costs related to the concrete slab to mount the unit, addition to the previous Piqua aqueous waste holdup capacity, radionuclide monitoring equipment, manual preparation and other miscellaneous items. The price, inflated to 2024 USD, is of approximately \$ 3,060,000.

Given that the hydrocracker technology has tremendously improved thanks to the oil and gas refining industries (Shirvan & Forrest, Design of an Organic Simplified Nuclear Reactor, 2016), it is considered necessary to investigate the actual costs for such systems. Therefore, the costs relative to the two proposed hydrocrackers (inlet flow rates of 172 and 277 kg/h) are analyzed by scaling the cost of a bigger plant used for refining purposes in the oil and gas industry. For price scaling, data shared from the MIT Energy Initiative reports is used. Calculations are performed based on the following equation (Jones, et al., 2009):

$$C = C_0 \left(\frac{f}{f_0} \right)^n$$

Where C_0 represents the cost of a reference plant built in 2005, estimated to be around \$ 5,700,000 (in 2005 USD). The term $\frac{f}{f_0}$ is the ratio of the hydrocracker feed inlets, and n is the scaling factor, set at 0.65. The cost is also adjusted for inflation from 2005 and an installation cost factor of 2.47 is considered. Based on the calculations, the total cost for purchasing and installing a hydrocracking system suitable for PNPf is expected to range between \$ 2,600,000 and \$ 3,600,000, depending on the inlet flow requirements (either 172 or 277 kg/h). Notably, the inflated cost of the PNPf system from 1963 to 2024 falls within our calculated range.

The same formula and procedure are used to calculate the flash tank costs. Cost and feature data for the flash tank are provided by members of the MIT Energy Initiative, based on 2013 cost data. In this case, the scaling factor n is set to 0.7, while the installation cost factor is set to 2.56. For the flash tank, the term $\frac{f}{f_0}$ again represents the ratio of the feed inlet between the PNPf flash tank and the reference tank. The reference flash tank cost and inlet feed are \$ 52,500 and 673.25 tonnes/day, respectively. The feed for the PNPf flash tank is calculated considering an equilibrium HB concentration of 10% and a HB processing of 40.8 – 68.0 kg/h in the hydrocracker (Griffith & Russel, 1963). This assumption, which allows the calculation of the coolant inlet feed in the flash tank, is not entirely accurate. This is because, with the installation of a hydrocracker processing 277 kg/h, the HB concentration is expected to be lower than 10%, even though no specific data is available for this scenario. Using a hydrocracker HB feed inlet of 40.8 and 68.0 kg/h and an equilibrium HB concentration of 10% as assumed in (Griffith & Russel, 1963), the obtained cost range for the flash tank varies between \$ 10,000 and \$ 14,000. Despite the assumptions for the flash tank cost estimate might

not be entirely correct and conservative, the flash tank has just a small impact on the required capital investment for the purification system as the costs related to the hydrocracker installation are at least two orders of magnitude higher. The relatively small impact of the flash tank on the total costs is also confirmed by (Griffith & Russel, 1963) when comparing the investments required for the installation of a hydrocracker with or without a flash tank.

Having calculated the capital investment required for the purification system installation in a plant of the size of Piqua, the focus shifts now to operational costs.

Although having high efficiencies, catalytic hydrocrackers are not able to recover all of the coolant. Moreover, a portion of light products formed by radiolysis and pyrolysis will not be recovered as well. Therefore, although the rate is not comparable to the one required in case a distillation purification system would be installed instead of a hydrocracker, continuous make-up injection would be needed. For the calculation of the make-up required for the PNPf, the following assumptions are done:

- The hydrocracker efficiency is assumed at 98% based on data from (Shirvan & Forrest, Design of an Organic Simplified Nuclear Reactor, 2016). The efficiency refers to the recovered coolant out of the total inlet, having a HB concentration of 75%.
- It is assumed that of the total coolant destroyed in a nuclear reactor, 4 weight per cent is light ends (non-recoverable) and 96 weight per cent is high boiler material (Griffith & Russel, 1963).

Based on this information, the total make-up costs are calculated with the following formula, also used in (Griffith & Russel, 1963):

$$\text{total yearly losses} = Cd h F (I\alpha + \beta r)$$

Where C is the cost of the coolant, set at \$22.5/kg, d is the number of days in a year, and h is the number of hours in a day. F represents the capacity factor, conservatively (to maximize the losses) set at 0.9. I is the flow inlet in the hydrocracker, with values of 172 and 277 kg/h. α denotes the hydrocracker efficiency, set at 98%, β is the HB formation rate at Piqua, which is 40.8 kg/h, and r is the ratio between the creation rates of light boilers and high boilers (4% on 96% as assumed before). The calculated make-up costs for a plant with the same features as the PNPf varies between 20,000 and 28,300 \$/year·MWth.

Other operational costs include the periodic replacement of the catalyst and the continuous use of hydrogen to prevent coke accumulation on the catalyst. The preferred catalysts for this operation are of the CoMoO₄-Al₂O₃ type, with a composition of 4.0 wt% Co and 14.0 wt% Mo and a low surface area. The optimal conditions are identified as 480 °C, 1000 psig (69 bar), and a high boiler feed rate of 0.5 volumes per volume of catalyst per hour (Gardner & Hutchinson, 1964). Given that a catalyst life of at least one year can be expected, the volume of catalyst required can be calculated based on the volume of high boilers (HBs) processed by the hydrocracker in one hour. The volume of HBs is determined considering a formation rate of 40.8 kg/h in the Piqua reactor and a density of 0.829 g/cm³. This density refers to the organic fluid at 30% HB and 425 °C, as data for the density of pure HBs at 480 °C and 1000 psig (69 bar) are unavailable (Kasten, et al., 1967). Once the required volume of catalyst is calculated, its mass can be determined using a catalyst density range of 1.14 to 1.18 g/cm³. The price for cobalt oxide-molybdenum oxide on alumina is approximately 600 \$/kg for small quantities (~ 500 grams), based on online sources. On the other hand, the required hydrogen quantity was assumed to be between 3.2 and 10 moles per mole of high boiler considering data from (Gardner & Hutchinson, 1964) for the higher bound and from (Griffith & Russel, 1963) for the lower bound. Considering HBs to be mostly hexaphenyls (C₄₂H₃₀) (Gardner & Hutchinson, 1964) and an inflated price of delivered hydrogen at 15-17 \$/kg (Rustagi, Elgowainy, & Vickers, 2018), the operational costs related to hydrogen purchase can be calculated. The obtained operational costs relative to catalysts and hydrogen yearly purchase are between 1,300 and 1,500 \$/year·MWth and 1,400 and 5,000 \$/year·MWth respectively. The cost related to hydrogen storage was also accounted at 700 \$/kg considering the price of an industrial 1500 kg steel with liner pressurized at 350 atm (Burke, Ogden, Fulton,

& Cerniauskas, 2024). It must be considered that the catalyst yearly costs could be decreased by regenerating them as $\text{CoMoO}_4\text{-Al}_2\text{O}_3$ were proven to retain their activity and selectivity after repeated air regenerations (up to 36 cycles!). Nevertheless, our cost calculation assumes no regeneration is performed for conservative reasons and because regenerating such catalysts, which operate in close contact with radioactive HBs, might be more costly than installing a new bed every year and disposing of the old one. To determine whether regeneration operations might be cost-effective, a specific analysis must be performed, considering the end-of-life catalyst activity, potential regeneration strategies, and associated costs. To minimize the hydrogen cost, a hydrogen recovery system could be installed. The economic conveniency of the unit was investigated in the 1960s for PNPf installation. Nevertheless, a study proved that the front capital costs related to the setting up of such machinery would be convenient only in case it would be placed on a large hydrocracker unit on relatively large organic or organic - heavy water reactors (Griffith & Russel, 1963).

The final evaluated costs are related to operational and indirect costs associated with hydrocracker operation. On one hand, indirect costs include general expenses, social security and other taxes, direct overhead and services and insurance. On the other hand, operational costs include utilities, operating labor, maintenance, supplies for the catalytic hydrocracker. Such costs are calculated based on data from (Griffith & Russel, 1963).

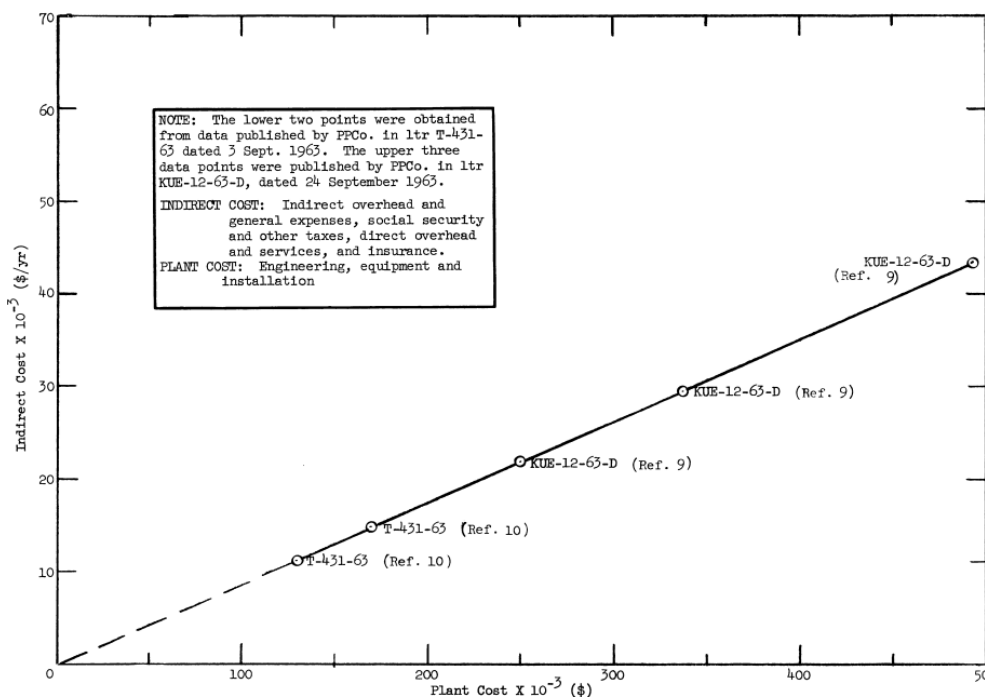


Figure 11 Indirect cost estimate for various size hydrocracker plants (Griffith & Russel, 1963)

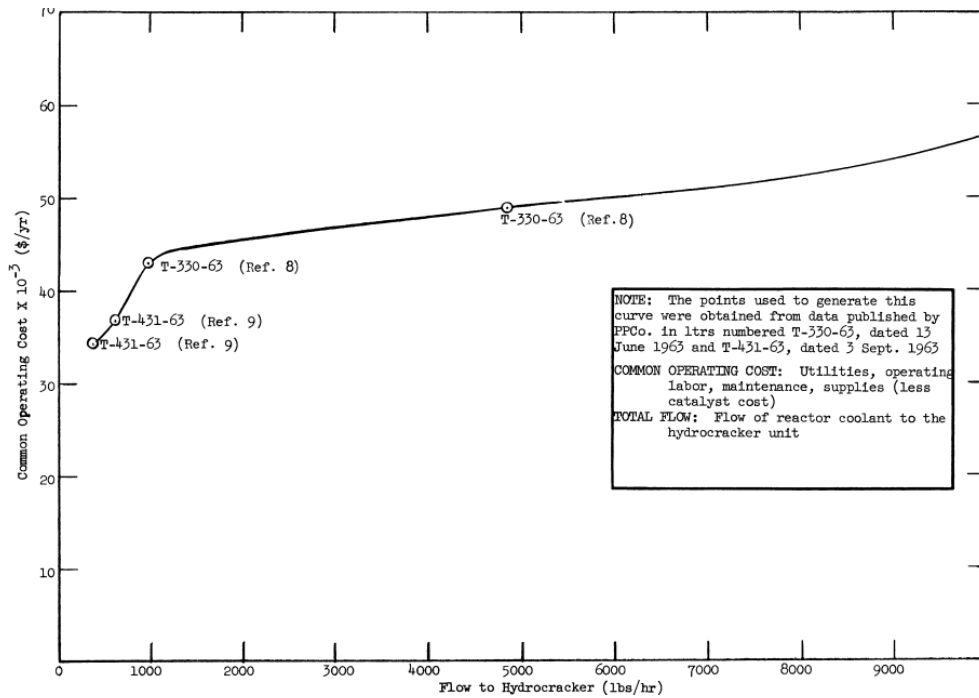


Figure 12 Operational cost estimate for various size hydrocracker plants (Griffith & Russel, 1963)

By interpolating such graphs and appropriately inflating the costs to 2024 USD when necessary, we can obtain the indirect and operational costs associated with catalytic hydrocracker operation. Those are calculated to be between 2,200 – 3,900 \$/year·MWth and 6,500 – 8,000 \$/year·MWth respectively.

Table 30 summarizes the capital and operational costs related to PNPf operation, including the costs relative to a 500 MWe Organic cooled - Heavy Water moderated Reactor (OHWR) analyzed in (Griffith & Russel, 1963). Cost data for the OHWR is retrieved by calculating the HBs production rate based on the information contained in (Griffith & Russel, 1963) and by using the same assumptions used for the PNPf.

Table 30 Capital and operating costs for the maintenance of a nuclear grade coolant during operation.

Reactor	Piqua (US)	OHWR
Power [MWe]	11.4	500
HB formation rate [lb/h]	90 (~ 40.8 kg/h)	286 (~ 22.7 kg/h)
Coolant makeup [\$ /MW·year]	20,000 – 28,300	1,900
Hydrocracker cost [\$]	2,600,000 – 3,600,000	5,500,000
Hydrogen supply [\$ /MW·year]	1,400 – 5,000	140 - 480
Catalyst required [\$ /MW·year]	1,300 – 1,500	115 - 130
Flash tank cost [\$]	10,000 – 14,000	21,000 – 22,000

Storage cost [\$/kg]	700	700
Indirect costs* [\$/MW·year]	2,200 – 3,900	130 -170
Operating costs** [\$/MW·year]	6,500 – 8,000	280 - 320

*Indirect costs refer to social security and other taxes, insurance.

**Operating costs refer to utilities, operating labor, maintenance, supplies (excluding catalyst).

6. FLiBe

Li_2BeF_4 is a molten salt mixture composed of lithium fluoride (LiF) and beryllium fluoride (BeF_2) in a 2:1 molar ratio. Also named lithium tetrafluoroberyllate, or simply “FLiBe”, it appears as a colorless or white crystalline solid at room temperature, becoming a completely clear liquid when melted. The properties of this molten salt make it a good candidate for use in the nuclear fields. FLiBe has some inherent advantages such as high temperature stability (Moriyama, Sagara, Tanaka, Moir, & Sze, 1998), transmutation characteristics, good radiation shield and moderating ratio, other than having modest to good fluid flow properties (Cadwallader & Longhurst, 1999) (Lam, Li, Ballinger, Forsberg, & Li, 2021). These features, make FLiBe the favorite coolant of choice for the Fluoride-salt-cooled High-Temperature reactor (FHR) (Seifried, Scarlet, Peterson, & Greenspan, 2019). Its melting temperature is 459 °C (~858 °F) while it boils at over 1430 °C (2606 °F) (Romatoski & Hu, 2017). FLiBe can be used at high temperature, but low pressure (atmospheric) in a reactor. Due to its relatively low viscosity, it necessitates a pumping power which is negligible with respect to the reactor thermal power (Seifried, Scarlet, Peterson, & Greenspan, 2019).

Table 31 Comparison of water and FLiBe properties respectively at 293 K and 950 K (Sorbom, et al., 2015). As can be seen from the table, FLiBe presents similar thermal-hydraulic features to water.

Property	FLiBe	Water
Melting point (K)	732	273
Boiling point (K)	1700	373
Density (kg/m ³)	1940	1000
Specific heat (kJ/kg/K)	2.4	4.2
Thermal conductivity (W/m/K)	1	0.58
Viscosity (mPa·s)	6	1

The first work studying salt coolants for nuclear reactors was performed by Oak Ridge National Laboratory (ORNL), specifically the Aircraft Nuclear Propulsion (ANP) project in the 1950s (Romatoski & Hu, 2017). The ANP project was a comprehensive program initiated by the United States Army Air Forces in 1946 to develop a nuclear-powered aircraft. The project aimed to create a nuclear reactor that could power a jet engine, providing a significant increase in range and endurance compared to conventional chemically-powered aircraft. The application of fluoride molten salts to nuclear technology was successfully demonstrated during the preparation of fluoride mixtures and their loading into the Aircraft Reactor Experiment (ARE) beginning October 23, 1954 (Shaffer, 1971). Despite the ANP program being cancelled due to the high costs, technical challenges, and concerns about safety and radiation exposure, the Molten Reactor Experiment (MSRE) project was initiated throughout the 1960s. The 8 MWth MSRE was operated by ORNL during the period June 1, 1965, to December 12, 1969, for experimental purposes and as a demonstration of the molten-salt nuclear reactor concept. The reactor fuel mixture was to contain nominally (in mole %) 65 LiF, 29.1 BeF_2 , 5 ZrF₄ and 0.9 UF₄ (liquidus temperature of 450°C). The actual fuel composition was dependent upon the amount of uranium required to bring the system to criticality, and then to the operating condition. The secondary coolant was FLiBe (2LiF- BeF_2) (Shaffer, 1971). During the 1970s and 1980s, interest in salt coolants suited for nuclear applications waned, as a consequence of the excessive corrosive behavior of molten salts due to the dissolved fission products and the high temperature.

However, in the 2000s, a resurgence of interest in using fluoride salts as nuclear coolants yielded assessments of candidate coolant thermophysical properties. Several reviews or summaries of the existing literature emerged studying the properties of FLiBe especially focusing on heat transfer performance for energy applications (Romatoski & Hu,

2017). The growing interest and research effort led to the proposal of a new reactor concept, the FHR by ORNL in 2003 (Forsberg, Peterson, & Pickard, 2003). In the FHR concept, fluoride salt is only used as a coolant and not as a nuclear fuel solvent, as was firstly proposed by the MSRE experiment. In fact, the planned fuel for the first FHR design was TRISO particles loaded into a prismatic graphite-matrix fuel assembly. Being high-temperature plants able to achieve a core outlet temperature up to 700 °C, FHRs have the potential to support either high-efficiency electricity generation or industrial process heat production (Holcomb, Peretz, & Qualls, 2011). Their major advantage with respect to the high-temperature gas-cooled reactors (HTGRs) is the possibility of operating at atmospheric pressure. Moreover, the chemical stability of its constituents, LiF and BeF₂, is much higher than the fluoride forms of the structural materials' constituent elements (Ni, Fe, Cr, etc.). This means that most common structural materials are well compatible with FLiBe itself (Moriyama, Sagara, Tanaka, Moir, & Sze, 1998). From the initial proposal of the FHR in the 2003 ORNL project, several improvements and studies were published to demonstrate the convenience of the design from an engineering, physics and financial point of view (Jiang, et al., 2022).

In 2014, the Mark-1 pebble bed FHR (Mk1 PB-FHR) was launched. The concept, developed by the University of California Berkeley (UCB) together with Westinghouse Electric, ORNL, and MIT (Jiang, et al., 2022), differs from previous FHR designs developed and published by other parties. It uses a Nuclear Air-Brayton Combined Cycle (NACC) based upon a modified General Electric 7FB gas turbine, designed to produce 100 MWe of base-load electricity when operated with only nuclear heat, and to increase this power output to 242 MWe using gas co-firing for peak electricity generation. Due to the high thermal efficiency of the NACC system, the steam-bottoming condenser of the Mk1 PB-FHR requires only 40% of the cooling water supply that is required for a conventional light water reactor (LWR), for each MWh of base-load generation. As with conventional natural-gas combined cycle plants, this makes the efficiency penalty of using dry cooling with air-cooled condensers much smaller, enabling economic operation in regions where water is scarce (Andreades, et al., 2014).

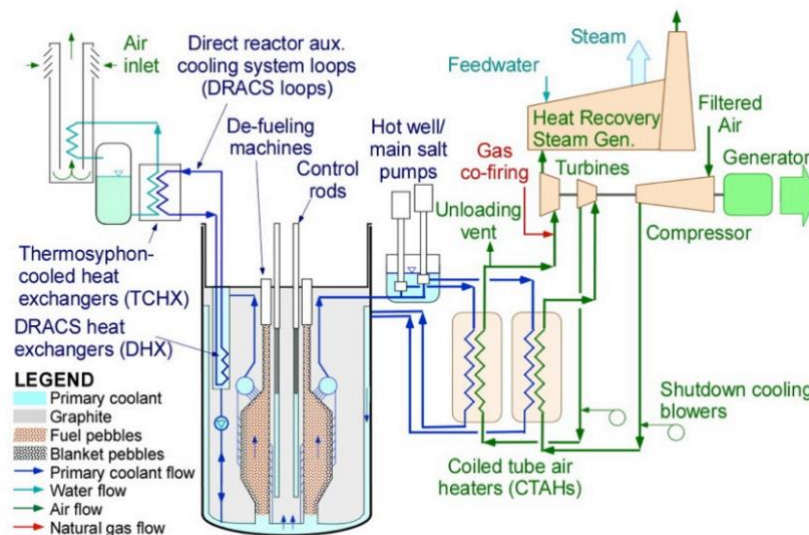


Figure 13 Mk1 PB-FHR flow schematic (International Atomic Energy Agency, 2016)

After only 2 years, in 2016, Kairos Power was founded. The company absorbed the past research done with FLiBe coolant and FHR development for the launch of their Kairos Power FHR (KP-FHR) in 2018 (Jiang, et al., 2022). The company has recently received the license to build their Hermes demonstration reactor in Oak Ridge (TN) to be used

for the development of the company's fluoride salt-cooled high-temperature reactor. Kairos is planning to have Hermes operational as early as 2026 (U.S. Department of Energy, 2023).

Most of those reasons for selecting fused fluoride salt for fission are also applicable to fusion, though there are some specific requirements for fusion reactor coolant/blanket materials concerned with the magnetohydrodynamic force, tritium breeding ratio, tritium confinement and so on. FLiBe has been explored in magnetic fusion energy reactors as a regenerative surface for plasma interaction in high-flux regions and as a coolant capable of breeding tritium. Additionally, in inertial fusion energy designs (such as HYLIFE II), FLiBe has been considered for its potential as a shielding medium, protecting against both neutron radiation and the intense hydrodynamic blast generated by inertial fusion energy targets (Cadwallader & Longhurst, 1999) (Moir, House, & Leber, 1994). In particular, it has been used as coolant and as a plasma-facing material by the Advanced Liquid Plasma Surface and Advanced Power Extraction projects within the US DOE Office of Fusion Energy Sciences (Cadwallader & Longhurst, 1999). FLiBe is also a potential candidate to be used as breeding blanket and its currently being pursued within the ARC project at the Massachusetts Institute of Technology (MIT). In their concept, FLiBe flows slowly into a channel within the double-walled elliptical torus for cooling and tritium breeding. FLiBe also has a function of radiation shield for the Poloidal Field pull coils of the reactor (Sorbom, et al., 2015).

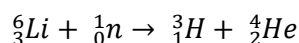
Other applications of FLiBe as a molten salt are for advanced battery technologies (Attarian, Morgan, & Szlufarska, 2022).

One of the main drawbacks of using FLiBe as a coolant or other applications in the nuclear field, is the toxicity of its pure constituents: fluorine, lithium, beryllium. Exposure to Beryllium could lead to an inflammatory reaction of the entire respiratory tract and, in extreme cases, it can produce acute fulminating pneumonitis. Beryllium can also potentially accumulate in the lungs over time leading to granulomas. On a similar note, Fluorine exposure leads to skin burns and pulmonary diseases such as edemas. Prolonged exposure to Fluorine could, in extreme cases, lead to death. Being potentially harmful for human health, fluorine and beryllium exposure is strictly regulated by limited thresholds for airborne exposure. During FLiBe purification, hydrogen fluoride needs to be handled. Hydrogen fluoride is a highly hazardous gas, converting into hydrofluoric acid, which is both corrosive and penetrating. This acid is a contact poison that can cause deep, initially painless burns, eventually leading to tissue destruction. Personnel dealing with FLiBe should be properly trained in handling hydrogen fluoride and hydrofluoric acid safely (Ames & Hu, 2013). On behalf of lithium, none of the reactions normally involving FLiBe in nuclear reactors environments is expected to produce free lithium, which is highly pyrophoric in its free form. Moreover, when the FLiBe components react together to form its constituents, LiF and BeF₂, it does not show a relevant chemical activity, showing a passive behavior. Qualitatively, the molten salt hazards appear to be manageable, since similar hazards have been, or are currently being, managed in other industries. In addition to the experience in conventional industrial facilities, review of experience by MSRE maintenance personnel indicated that handling the molten salt was not difficult and that the maximum radiation exposure any maintenance personnel received was < 0.5 rem per year (Cadwallader & Longhurst, 1999).

6.1 Technical Specifications for Nuclear-Grade FLiBe

6.1.1 Enrichment requirements

One of the main drawbacks of using natural lithium in a thermal reactor such as the FHR is the high absorption cross section of Lithium 6, which is naturally present in a concentration of approximately 7.5% of lithium isotopic composition. In a thermal neutron spectrum, the following reaction is likely to occur:



As it can be seen, one of the products of the reaction is tritium. Tritium is a radioactive gas that is famously difficult to contain, and its levels are closely monitored by regulatory agencies. Tritium in the coolant is not only a radiological concern but presents also other significant threats (Mohamed & Parks, 2017):

- Significant corrosion issues because of the initial production of tritium fluoride, which is a strong oxidant.
- Tritium gas. Depending on the salt's chemical redox potential and the occurrence of chemical reactions, tritium can also exist as tritium gas (T_2). Unlike tritium fluoride, which does not diffuse through metals, tritium gas permeates most metals at typical FHR operating temperatures ($\sim 700^\circ\text{C}$), potentially releasing into the atmosphere and causing off-site concerns.

To prevent the formation of tritium and thus reduce radiation exposure, lithium needs to be enriched to very high levels of Li-7 (naturally present at 92.5%). Given the high concentration of lithium as a coolant in FHRs, the ORNL recommends a Li-7 enrichment of 99.995% (Ault, et al., 2012).

There exist also other applications of Li-7 both in the nuclear and non-nuclear fields. Li-7 in the form of hydroxide (${}^7\text{LiOH}$) is also used in pressurized water reactors (PWRs) for chemistry control at a concentration of 2.2 ppm, to regulate the corrosive effects generated by boric acid and the degradation of the steam generator tubes. The requirement in terms of enrichment for ${}^7\text{LiOH}$ to be used in PWRs is of 99.99% (Reister, 2013) (United States Government Accountability Office, 2013). Moreover, it is used for the production of chemical reagents for nuclear power engineering, and as a basic component for preparation of nuclear grade ion-exchange membranes which are used in PWR coolant water treatment facilities. For use in the nuclear fusion industry, given that one of the main scopes of the blanket is tritium breeding, the need would be to have a higher enrichment of lithium 6 (about 30%). Nevertheless, given the very limited availability of Li-6 worldwide and its concerns caused over proliferation, the option of designing a blanket which uses natural lithium has arisen even though the technological challenge is surely more significant (Pearson, 2022). Outside of the nuclear industry, the chemically pure tails coming from Li-7 enrichment process have been used to enhance the performance of the lithium-ion batteries, used for electric cars and other applications (World Nuclear Association, 2022).

At present, there appears to be no active lithium enrichment capability in the United States, which was importing its needs of lithium 7 from China at least until 2013 (University of California, Berkeley, 2013). The last program for production of lithium 7 was the mercury-based COLEX (COlumn EXchange) process, which stopped operation in 1963. In that process, Li-7 was a byproduct of Li-6 enrichment for weapons programs (Reister, 2013). Given that the US do not currently possess the internal capabilities to enrich lithium on a scale necessary for FHR development, the calculated cost of FLiBe is estimated based on the cost of PWR grade enriched lithium (about 99.99%) instead of FHR grade (99.995%).

A literature review of the enrichment process of lithium is also included in the following paragraphs for the purpose of completeness, and to obtain a better understanding of the production processes of FLiBe to inform its cost calculation.

6.1.1.1 Overview of the lithium enrichment process

As part of the research done for the development of thermonuclear weapons (and the so-called hydrogen bomb) in the United States during the cold war years, different techniques for lithium 6 enrichment were studied and developed at the Y-12 plant at the ORNL between the 1950s and 1960s.

In particular, the first ever used method was the ELEX process, whose pilot plant was built at Y-12 in 1951. The ELEX (ELEctrical EXchange) was an electrically driven chemical exchange process using a method similar to the one used for chlorine gas and sodium hydroxide production by the chlor-alkali plants (Ragheb, 2015). The ELEX process, though, was classified as inadequate for increasing demand of lithium 6 and ceased operations as early as 1956 (Y-12 National Security Complex, 2014).

The two subsequent enrichment methods which were developed are the so called OREX (ORganic EXchange) and COLEX processes and are based on mercury exchange processes. These methods involve an amalgam of lithium and mercury made via electrolysis and a solution of lithium hydroxide. Having Li-7 a slightly lower affinity to mercury than Li-6, it diffuses out of it more quickly than Li-6 increasing (or “enriching”) the quantity of Li-6 in the amalgam. Therefore, the Li-6 can be later separated from the amalgam while the tails of Li-7 are electrolyzed from the aqueous solution of lithium hydroxide which can be later re-used (Ragheb, 2015). In particular, the OREX process used an organic solution of lithium instead of the LiOH, called Propylene-di-amine. The two processes, COLEX and OREX, were developed in parallel and quite intensively in response to a Soviet explosion on August 12, 1953, of a hydrogen bomb which intensified the need for lithium 6 at the Y-12 laboratory (Y-12 National Security Complex, 2014). The COLEX process was demonstrated to be the most efficient and this led to the dismantling of the OREX facility in building 9202 of the Y-12 between 1957 and 1959. On the other hand, numerous parts of the Y-12 were converted to be suitable for Li-6 production via COLEX, with the creation of the Alpha-4 and Alpha-5 facilities (Y-12 National Security Complex, 2014). The production of lithium 6 for military purposes stopped in 1963 and produced the necessary stockpiles of lithium 7 necessary to cover the requirements of the nuclear industry until today (Reister, 2013).

Overall, lithium separation operations at ORNL between the 1950s and 1960s required almost 11 million kilograms of mercury which would sometimes be released into the environment causing considerable damage. In particular, the COLEX process facilities were the most intense in terms of mercury releases but also other sources were documented as coming from the test facilities, nuclear weapon components, chemical recovery or decontamination plants and burned coal on site (ChemRisk, 1999). The contamination due to mercury has been accounted in a study done in 1983 which estimated 330,000 kg to have been lost in waste streams, evaporation, and spills. The mercury released in the air was accounted for approximately 23,300 kg while the releases to a local pond connected to the Y-12 plant were in the range of 239,000 – 350,000 pounds (~ 108,000 – 159,000 kg). Moreover, 193,000 kg of mercury were lost in eight accidental spills (Ragheb, 2015) (Oak Ridge National Laboratory, 2020).

Today, Russia and China are the only countries that continue enriching lithium 6 via COLEX process, although China has also developed a centrifugal extraction process at SINAP facilities. The United States, which extensively used COLEX during the last century, have banned it (World Nuclear Association, 2022). Given that China has stopped exporting lithium 7 due to increasing internal requirements and Russia capability of scaling up production for exporting has not been proven, the Department of Energy has been investigating other methods for lithium 7 production in the US (Reister, 2013). In 2012, a report from UCB has been released describing two of the most promising techniques for lithium separation and their economics (Ault, et al., 2012).

The first method is called Crown Ether (CE) Enrichment and represent the most promising alternative to mercury-based enrichment methods. CEs and cryptands are cyclic derivatives of ethylene oxide characterized by the recurring unit, –CH₂CH₂O. Certain ethers exhibit ring structures that preferentially bond with specific isotopes. When resin columns or a water-insoluble solvent containing these crown ethers are introduced to an aqueous lithium mixture, Li-6 is selectively concentrated in the solvent phase, allowing for its extraction (World Nuclear Association, 2022). Studies have demonstrated some of the CEs to have a separation factor (defined as the final relative abundance of the heavier and lighter isotopes on the initial one) which can go up to 1.068 (Pei, Yan, Liu, He, & Li, 2024), being comparable to the COLEX process (having separation factors around 1.05). As described in a published report from UCB, two crown ethers appear economically attractive: benzo-15-crown-5 and dicyclohexano-18-crown-6 (World Nuclear Association, 2022). In particular, the use of this technique has been applied to two economic cases based on the production request

either mainly coming from the U.S. PWRs (about 400 kg/h) or the build of 10 FHRs/year (200 metric tonnes per year of FLiBe). For PWRs supply, the cost of installation of such unit would be \$ 11,500,000 and \$ 402,000,000 for the bigger plant for FHR supply (both figures in 2012 USD). The payback times are respectively 7.2 and 12.4 years for the two facilities and those targets are possibly achievable thanks to the elevated price of lithium 7. In those cost analyses, it was emphasized that over 50% of the capital expenses and over 75% of operating expenses are attributed to the crown ether purchase. Therefore, a study on the production of benzo-15-crown-5 and detailed analysis as to the economics of large-scale benzo-15-crown-5 must be done before better economic estimates can be made (Ault, et al., 2012). The full cost analysis including the cost breakdown of the two different cases can be found in the Appendix D.

On the other hand, a second possible method for natural lithium enrichment is called Atomic Vapor Laser Isotope Separation (AVLIS). The method leverages hyperfine structure differences between isotopes to selectively ionize one of them. When subjected to an electromagnetic field, the ionized particles drift, while the neutral isotopes remain unaffected, allowing the ionized isotopes to be collected (Ault, et al., 2012). The AVLIS method was originally designed for weapon-grade enrichment of Uranium but was subsequently considered as an alternative of the COLEX process for lithium enrichment even though not much research has been done on the topic. Nevertheless, optimism over feasibility of lithium separation via AVLIS is given by the fact that it uses components from technologies already in use for other older applications. The main issue is represented by the scalability of the process which must be resolved first (Ault, et al., 2012). Just a few papers have been published on the use of AVLIS for lithium before the report published by UCB in 2012 (Scheibner, 2004) (Strydom, 1999). The economics of the process have been studied and the cost of lithium enrichment to PWR levels (99.92%) has been accounted at 185 2012 USD/year (Ault, et al., 2012) as it has been delineated as more appropriate for production of small quantities of lithium 7 mainly to supply the current fleet of PWRs in the US. Given its possible application use for uranium enrichment, the technology is also subject to proliferation concerns, even though it has been described as *unclear* whether the use of this technique for uranium enrichment would be feasible. In the case it can be commercialized, uranium enrichment can be easily recognizable by an inspector due to the different wavelengths used with respect to lithium and the need of extra instrumentation and equipment, which is not needed for the separation of lithium (Ault, et al., 2012).

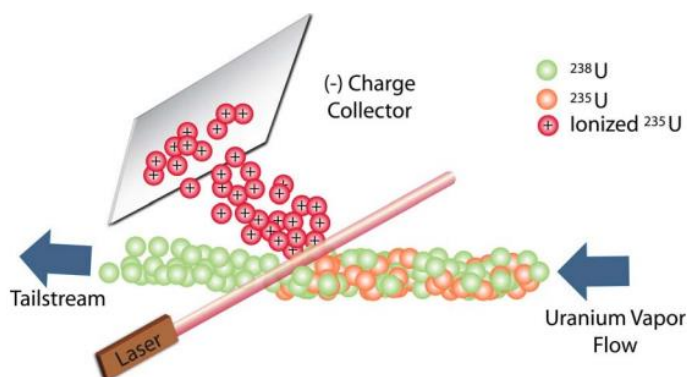


Figure 14 Simplified AVLIS theory applied to Uranium enrichment (U.S. Nuclear Regulatory Commission).

6.1.2 Chemistry requirements

One reason FLiBe was chosen as the primary fuel solvent for the MSRE experiment is its ability to dissolve fuel and fission products. This characteristic can be especially beneficial in the event of fuel failure in the FHR, as FLiBe, acting as a coolant, can serve as the first retention barrier against the release of radioactive elements. However, this also

implies that FLiBe has a high affinity for impurities, which could potentially impact salt chemistry control, coolant activity, system reactivity, component corrosion, and ultimately the fluid's thermophysical properties (Seifried, Scarlet, Peterson, & Greenspan, 2019).

Impurities can be introduced to the salt during different processes throughout the coolant's lifetime. These can be either manufacturing, transport, storage, reactor operations and maintenance. Focusing on the specific methods of contamination, impurities can be mixed in FLiBe in different ways: either because of contamination of the elements useful for the production of the molten salt, during manufacturing and handling, because of salt contact with structures (such as Hastelloy N and SS316) and gases (O₂, H₂O, N₂ can be introduced by the cover gas which will most likely be argon), neutron activation or intentional addition (such as zirconium, cerium and europium are added to control the corrosion of the structural materials) (Seifried, Scarlet, Peterson, & Greenspan, 2019) and many others.

In order to guarantee the safety of operation, the maximum allowable levels of impurities in fluorides were studied during the MSRE experiment. The program documented a total of 31 impurities, 15 of which were rare earths. The presence of some of these rare earth elements may be of concern with respect to neutronics for an FHR (Ames M. R., 2015). The results of the program are visible in Table 32.

Table 32 General Chemical Specifications for MSRE Fluoride Mixtures (Shaffer, 1971).

Impurity	Allowable concentration (wppm)	Derivation
H ₂ O	1000	Raw materials, plays an important role in corrosion
Cu	50	-
Fe	100	Present in SS316, present in graphite
N	25	Present in SS316
S	250	Raw materials, present in graphite, accelerates corrosion
Cr	25	Present in SS316, Acts as indicator of the metal's corrosion
Al	150	Present in graphite
Si	100	Present in SS316
B	5	Present in graphite
Na	500	-
Ca	100	Present in graphite
Mg	100	-
K	100	-
Li (natural)	50	Present in Li
Zr (natural)	250	Present in Zr (if FLiBe used as fuel solvent)
Cd	10	-
Rare earths (total)	10	-

Based on the results shown in Table 32, the purity requirement for FLiBe is approximately 99.76% in weight.

As for the nuclear poisons, whose impact on neutronics is the highest, only hafnium in zirconium was added. Moreover, iron concentrations of 250 and 500 wppm were allowed in BeF₂ and LiF together with some carbonaceous impurities whose origin was identified to come from the manufacturing process and could eventually be easily removed by gas sparging (Shaffer, 1971).

A more recent analysis based on a subsequent impurity classification provided by MIT using FLiBe manufactured at University of Wisconsin-Madison (UW), allowed the documentation of additional 22 impurities which had not been detected by MSRE. New methods such as delayed-gamma neutron activation analysis, cold-neutron prompt-gamma activation analysis, inductively coupled plasma optical emission spectrometry, inductively coupled plasma mass spectrometry, combustion infrared analysis, glow discharge mass spectrometry, and electrochemical techniques can theoretically provide measurements of concentrations up to the ppm level even though not every one of these methods has been tested on FLiBe yet. It has to be noted that, even though the techniques to detect additional impurities in FLiBe have evolved during the years and from the MSRE ONRL program, the salt purification methods have not (Seifried, Scarlet, Peterson, & Greenspan, 2019).

All the impurities found in the MSRE and MIT studies and the possible impurities that could eventually be found on the salt or migrate to it were considered in a study by University of California Berkeley (UCB) and UW to perform additional analysis on acceptance criteria for salt impurities. In particular, the neutronics effect of the impurities delineated by MSRE were analyzed based on the effect of coolant temperature coefficient of reactivity, on the excess reactivity and on the achievable burnup (Seifried, Scarlet, Peterson, & Greenspan, 2019). As a result of the study, a range of allowable impurity concentrations has been also proposed to limit the reactivity penalty to 20 pcm. The results are summarized in Table 34.

Table 33 Classification of 53 impurities possibly present in FLiBe based on a maximum reactivity penalty of 20 pcm (Seifried, Scarlet, Peterson, & Greenspan, 2019).

Precision (wppm)	Impurities
0.1	B, Cd, Sm, Eu, Gd
1	Dy, Ho, Er, Lu, Hf, Ta, Au, Hg
10	Cl, Sc, Mn, Co, As, Se, Br, Mo, Sb, Cs, Nd, Tb, Tm, Yb, W, Th, U
100	H ₂ O, Na, S, K, Ti, V, Cr, Fe, Ni, Cu, Zn, Rb, Sr, Y, Ba, La, Pr
1000	Mg, Al, Si, Ca, Zr, Ce

As it can be seen from Table 33, the impurities with the strongest reactivity effect are B, Cd and the rare elements Sm, Eu and Gd - their concentration was anyways detected at values <0.01 wppm in hydro-fluorinated batches. Those have to be given particular attention during salt purification and their extraction has to be ensured. The same is valid for H₂O, O₂ and H₂, which influence the reactivity of the system. In particular, H₂O concentration must be studied before the absorption behavior of other possible impurities, as it strongly influences the neutron spectrum by moderation (Seifried, Scarlet, Peterson, & Greenspan, 2019).

6.2 Cost of FLiBe

In this section, the cost of FLiBe purchase and maintenance throughout its lifetime is described. The study is divided in three main sub-categories, each of them indicating three different stages of the coolant lifetime:

- **Purchase cost**, indicating the cost to first acquire the constituents of FLiBe;
- **Pre-purification cost**, indicating the cost of pre-purifying FLiBe prior to reactor use;
- **Operating cost**, the cost of maintaining the FLiBe purity throughout the reactor lifetime to ensure the correct functioning of the system.

6.2.1 Purchase cost

In this section, we analyze the production costs of FLiBe. To ensure accuracy, we assess one of the methods for producing enriched FLiBe and compare it to the method used for non-enriched FLiBe (referred to as 'fusion FLiBe'), which served as a benchmark to validate our cost model and verify the accuracy of the data retrieved and utilized. The reason why the method for FLiBe production is included in this chapter and described hereafter is strictly linked to the cost calculations of the molten salt. In fact, to be able to provide the most reliable cost estimation on the cost of enriched FLiBe, it is considered appropriate to follow the possible steps of the production process of its bare components, LiF and BeF₂. Using this approach, the final price could reflect the real path of a possible fabrication procedure instead of summing the cost of the elemental components (Li, F, Be) taking into account the stoichiometric proportions of the three. Summing the costs of raw elements is not the optimal solution as it is far from what a possible strategy for FLiBe manufacturing would be, both from an economic and technical point of view. This is because of the extreme difficulty in handling and retrieving pure Fluorine and Beryllium (pure metallic lithium 7 is also problematic), and the cost of the two. Also, it is important to note that the possible paths from the mining of lithium brine to the production of high purity FLiBe, both containing enriched lithium and not, are multiple. The possible options chosen during manufacturing strictly depend on the financial aspects of the project as well as other engineering challenges such as initial brine purity, available facilities for treatment and purification and so on. The two paths which are described in the following paragraphs start from the mining process of lithium and are recognized as the shortest paths from the initial product to the final output required: naturally enriched FLiBe (for fusion use) and highly enriched FLiBe (for fission use). These methods of manufacturing were partly described in a United States patent from Sammy C. Honeycutt and Ricardo O. Bach, dated 1971 and are explained in the next paragraph. Moreover, given that there is yet no large-scale facility for lithium enrichment in the United States that could internally supply enough Li-7 for a possible FHR development at 99.995% enrichment levels, the economic estimation is based on the COLEX process for which it has been possible to produce 99.99% enriched ⁷LiOH for PWR pH control. This choice is identified as the closest possible to the real case to most accurately predict the cost.

Both production processes start with electrolysis of the purified lithium brine. In the context of lithium mining and processing, "purified brine" refers to the lithium-rich brine solution that has undergone pretreatment steps to remove impurities, contaminants, or unwanted constituents. The feed aqueous chloride brines to be used in the first steps of the process contains mainly LiCl and NaCl in the quantity of about 8 to 30% of LiCl and from 2 to 15% NaCl. The LiCl-NaCl feed is electrolyzed in some interconnected steps in a diaphragm cell separated by chlorine gas (United States Patent No. 3597340, 1971). During the electrolysis process, a significant portion of the lithium chloride undergoes a transformation, resulting in the formation of lithium hydroxide monohydrate (LiOH·H₂O). Typically, this conversion accounts for approximately half of the initial LiCl content, while the remaining portion stays in its original form. The sodium chloride (NaCl) and other salt compounds present in the solution remain largely unaffected by the electrolysis process, retaining their original state. At the anode, chlorine gas is generated as a byproduct, while a small quantity of

hydrogen gas is produced at the cathode and subsequently discharged from the electrolytic cell. A portion of the water molecules present in the initial brine solution combines with the lithium hydroxide formed during electrolysis, resulting in the formation of $\text{LiOH}\cdot\text{H}_2\text{O}$ through a process known as hydration or crystallization. Subsequent to the electrolysis stage, the impure solid lithium hydroxide monohydrate ($\text{LiOH}\cdot\text{H}_2\text{O}$) is isolated from the electrolyzed solution through filtration or other conventional solid-liquid separation techniques. The remaining liquid filtrate or the recovered solution can undergo one of two processes:

1. Evaporation: The filtrate can be subjected to evaporation, where the liquid is completely vaporized, leaving behind only dissolved solids or salts.
2. Recycling: Alternatively, the recovered solution can be recirculated and reused in the initial electrolysis step, effectively closing the loop and minimizing waste.

This separation and processing of the solid lithium hydroxide monohydrate and the liquid solution components allows for further purification and refinement of the desired lithium compound, as well as the potential for efficient recycling and reuse of the remaining solution (United States Patent No. 3597340, 1971). The percentage of lithium recovery from the process is evaluated in the range between 38–98% with a final purity achievable of 98% (Dahlkamp, Quintero, Videla, & Rojas, 2024). It should be noted that this first part of the production process described is just one of the possible (and among the shortest) paths from the purified lithium brine which is extracted from concentrated lithium-containing brine deposits, to the final product, either naturally enriched FLiBe or 99.995% enriched FLiBe. Other processes can be possibly identified and have been described in the literature (Dahlkamp, Quintero, Videla, & Rojas, 2024).

At this point of the process, the two production methods for fusion FLiBe and fission FLiBe will start to differ because of the difference in enrichment levels and consequently in the treatment of lithium. Focusing on the path to produce enriched FLiBe, the LiOH obtained from the process and eventually mixed in an aqueous solution can be used as feed to the following step of the process (Ragheb, 2015), the COLEX enrichment method, which is described in the section above called *Enrichment requirements*. In the COLEX process the two lithium isotopes are separated using natural lithium dissolved in mercury (to form an amalgam) and lithium hydroxide. Lithium-6 is more attracted to the mercury than lithium-7, which is more attracted to the hydroxide, thus separating the two isotopes (United States Government Accountability Office, 2013). As the principal output of the process, Li-6 is extracted while we also get an aqueous LiOH enriched solution, from which the Li-7 can be electrolyzed (Ragheb, 2015).

Based on a literature review, it has not been possible to identify whether the 7-Li has been stored in the form of metallic lithium or lithium hydroxide as tail product of the ORNL program for lithium 6 enrichment. On the one hand, the COLEX process finishes with the electrolysis of lithium-7 as described by (Ragheb, 2015) which may suggest that it could have been stored in the form of metal. The entirety of the quotes which were collected regarding enriched lithium 7 are also referring to the pure metal form which may indicate that the US stocks of Li-7 were maintained as metallic. On the other hand, there are some counter arguments. The first one is that lithium is pyrophoric (Cadwallader & Longhurst, 1999) in its elemental form, complicating its storage and maintenance. The second one is that for PWR use the required form of Li-7 is ${}^7\text{LiOH}$, as base to equilibrate the acid environment created by the use of boric acid for reactivity control purposes. This may indicate that the stocks of Li-7 could have been converted to hydroxide during the time of storage especially in case they were additionally enriched from tails to PWR grade. Furthermore, examining the production process of FLiBe for use in Fluoride-salt-cooled High-temperature Reactors (FHRs), it is financially more advantageous to synthesize ${}^7\text{LiF}$ via the reaction of ${}^7\text{LiOH}$ with HF, rather than through the reaction of lithium 7 with pure fluorine. From a technical perspective, although HF poses severe health risks, pure fluorine gas is also highly hazardous and challenging to handle. Therefore, for both PWR and FHR use, storing enriched lithium is more convenient in its hydroxide form. Nevertheless, the analyzed literature references do not provide an answer to the issue. As stated in a report over the purification of the salt, lithium 7 was available in the form of hydroxide in 1971 and had to be transformed to fluoride at Y-12 to conduct some tests and experiments (Shaffer, 1971). In 2013, the United States Government

Accountability Office affirms that the National Nuclear Security Administration had approximately 1300 kg of lithium hydroxide enriched to 99.99% (PWR grade) and 400 kg of lithium-7 enriched to 99.99 percent lithium-7, but in a different chemical form (United States Government Accountability Office, 2013).

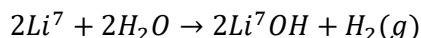
Given that it is not possible to establish with certainty the chemical form of lithium-7 in the US stocks at ORNL Y-12 facilities, it is assumed that Li-7 had been electrolyzed out of the hydroxide compound during the COLEX process to later re-use the LiOH in the process as described by (Ragheb, 2015). Given the difficulties in stocking metallic lithium, the electrolyzed enriched Li-7 is then assumed to react with water via an exothermic reaction involving hydrogen as product and later stocked in its hydroxide form to be used in PWRs. In fact, the use of the Li-7 given as output of the COLEX enrichment process is not enough to be used for FHR FLiBe as further enrichment is needed. Nevertheless, since there is no information of any other facility for lithium enrichment in the US at the moment, the cost is calculated starting from the ORNL produced Li-7. To summarize, the selection of this two-step process, converting Li-7 to ${}^7\text{LiOH}$, and the assumption that DOE's stocks of enriched lithium might have been converted into hydroxide at some point are justified by the following reasons:

- The difficulties of storing metallic ${}^7\text{Li}$ because of its pyrophoric nature;
- The current main market demand of Li-7 from the 65 US PWRs which use up to 300 kg of ${}^7\text{LiOH}$ per year (2-4 kg each) (Reister, 2013).
- The fact that the Y-12 facility had some of the stocks in the form of hydroxide (Shaffer, 1971) (United States Government Accountability Office, 2013).
- Other chemical forms could be potentially more convenient for storage than ${}^7\text{LiOH}$ but given that the shortest path from purified lithium brine to enriched FLiBe has been previously taken as a reference for the FLiBe production process, the same approach, based on the shortest paths, is used in this case. It might be also taken into account that there is some economic convenience in going from ${}^7\text{Li}$ to ${}^7\text{LiOH}$ and finally ${}^7\text{LiF}$ instead of from ${}^7\text{Li}$ to ${}^7\text{LiF}$ directly as the cost per kg of pure fluorine is much higher than the one of water and HF, which act as reagents in the first case.

It is possible that the DOE might have stored the ${}^7\text{Li}$ in other forms, making the production process different than the one indicated in this report. On this topic, the choice of calculating the cost of non-enriched FLiBe goes in the direction of verifying the assumptions made for enriched FLiBe, given that the cost of its pure constituents is known and the final cost has been retrieved as well from a market supplier. Fusion FLiBe, not having to go through the enrichment process, can directly go through the next steps of the reaction after the crystallization in the form of LiOH.

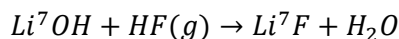
The following steps, both for fusion and fission FLiBe processing can be described through the following chemical reactions, given that the starting compound is LiOH (enriched or not) in both cases:

1. Reaction between Li-7 and water (process valid also for naturally enriched lithium):



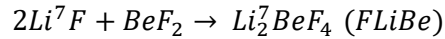
The reaction is intensively exothermic and forming lithium hydroxide and highly flammable gaseous hydrogen.

2. Reaction between LiOH and HF (process valid also for naturally enriched lithium):



This is a simple reaction between an acid and a base.

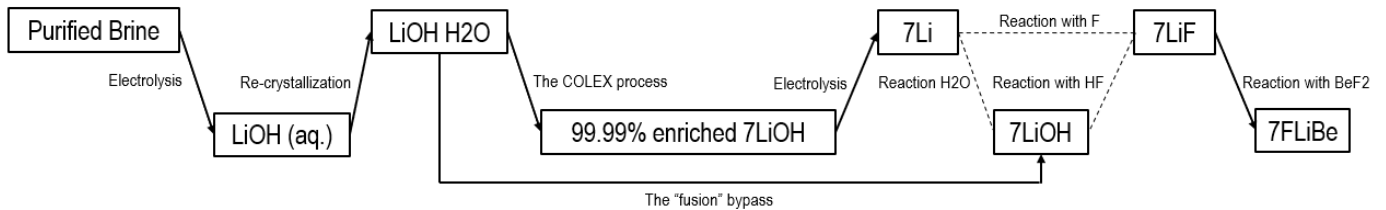
3. Reaction between LiF and BeF₂ (process valid also for naturally enriched lithium):



This is the last reaction needed for both enriched and non-enriched FLiBe production (fission and fusion). The production process of BeF₂ is not explored in further depth as done for lithium because we have a direct quote for it in \$/kg (whose price includes the production processes), thus there is not a pressing need to explore the manufacturing process to justify the cost calculations.

Both the assumed production process for naturally enriched FLiBe and 99.99% enriched FLiBe are in Figure 15 starting from the lithium purified brine (lithium-rich brine solution that has undergone pretreatment steps to remove impurities, contaminants, or unwanted constituents):

1. Enriched FLiBe (for FISSION use):



2. Non-enriched FLiBe (for FUSION use):

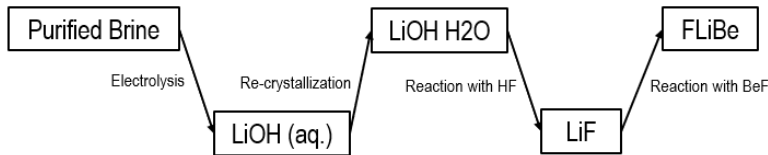


Figure 15 Different possible production processes for naturally enriched FLiBe ("FUSION use") and highly enriched FLiBe ("FISSION use"). As it can be seen from the box scheme for enriched FLiBe, the dashed lines indicate the two possible reactions, either with water and HF or pure F, to produce ⁷LiF. The manufacturing strategy considered in this cost analysis is the one going from ⁷Li to ⁷LiOH to finally ⁷LiF because of the reasons specified in the paragraphs above.

To determine the cost of FLiBe for both fission and fusion applications, we need to obtain the cost of the raw materials. Table 34 lists the cost of each component, considering a target purity equal to or higher than that of the final FLiBe product. All the prices are given in 2024 USD. Due to varying factors such as the time of quote retrieval during the year, quantity ordered, and supplier pricing differences, cost information from suppliers varies. Therefore, Table 34 presents a cost range with the lowest and highest prices found, even though multiple quotes are obtained in some cases (included in the range). The lowest and highest boundaries of the price range are given in \$/kg as our target cost for FLiBe is also in \$/kg. It is important to note that these price estimates do not include shipping costs, which can be significant depending on the supply location, transportation methods, delivery schedule, and urgency. The most cost information is coming from suppliers based, or having subsidiaries, in the USA, although some quotes are also obtained from overseas companies. For these international suppliers, shipping costs might be higher, and delivery times might be longer. The quotes aim to provide information for a high quantity of product of the order of tens of tons. This is based on information from the Mk-1 design, a 100 MWe reactor designed by UCB, which would need approximately 47 m³

(91,970 kg) of FLiBe as its main salt, or 0.92 kg/kWe (International Atomic Energy Agency, 2016). Obtaining information for high quantities of raw materials certainly means higher accuracy in the final estimation, as it is observed that some cost estimations vary significantly based on the quantity of product purchased, sometimes by orders of magnitude. Nevertheless, it is not always possible to retrieve information for quantities in the order of tens of tonnes, as the suppliers sometimes cannot provide such estimations given their production of certain raw materials is limited to lower quantities for other non-nuclear applications. The necessary scaling-up costs that the supply chain has to incur to supply enough high-purity materials for such nuclear applications can be significant and are not evaluated in this report, as it is not within the scope of our current research.

Table 34 Different prices ranges and suppliers for compounds useful for FLiBe cost calculation.

Element or compound	Lowest Price [\$/kg]	Highest Price [\$/kg]	Source/Supplier	Comments
BeF ₂	56	250	Materion (US), AChemicals (CAN), Hebei Yanxi Chemical Co. (CHN), Shaanxi Dideu Medichem Co. Ltd (CHN).	The price for BeF ₂ for a quantity of 2000 kg comes from Materion for around 500,000 \$ (250 \$/kg). Being Materion the biggest supplier in the US for Beryllium fluoride and fluoride products and given their recent collaboration with Kairos Power towards molten salt reactor development, their quote is highly trustable. Nevertheless, other companies in China and Canada can provide lower prices for similar quantities of high purity material purchased.
⁷ Li	14377	24828	(Reister, 2013), (Ault, et al., 2012), (Fruzzetti, 2017), Nukem Isotopes (US).	It has to be noted that the prices for lithium 7 refer to an enrichment of approximately 99.99%, useful for PWR chemistry control. Having no literature source of higher enrichment costs and given that there is currently no facility in the USA for industrial production of FHR enrichment grade (99.995%), these values are used as benchmark for our calculations. The quotes for ⁷ Li are all coming from US suppliers, as China and Russia (the only other producers in the world) might have different prices. They are all inflated to 2024 USD prices using the official CPI inflation calculator from the US Bureau Of Labor Statistics as some of them are retrieved from past public documentation released. The lower boundary is given from (Reister, 2013) inflated cost of 10,000 \$/kg in 2010. The higher boundary is inflated from the information given by (Fruzzetti,

				2017) estimating 90,000 \$/year of savings for each PWR in 2017 in case of KOH use for pH control. From that quote, the 2017 FLiBe price per kg can be calculated given a usage of 300 kg for the 65 PWRs present in the USA. The result obtained is 19,500 2017 USD/kg. The price of Li-7 is expected to increase by 3-5% every year.
HF	1	2	Online resources: businessanalytiq.com intratec.us	HF price per kg is identified to be generally pretty low. The price for hydrogen fluoride/hydrofluoric acid in North America is predicted to be stable around 1.2-1.3 \$/kg until June 2025 (Business Analitiq, 2024).
H ₂ O	1		(Shirvan, et al., 2023)	Price for water is assumed to be 1 \$/kg as done in the paper recently published at MIT analyzing costs of different micro-reactor types.
Li (natural)	13	15	Online resources: intratec.us dailymetalprice.com	Prices per kg for metallic lithium and lithium hydroxide can be found in numerous resources online. For high quantities the cost of the two is found to be similar.
LiOH (natural)				
F	660	1900	Online resources and calculations	The price per kg of pure fluorine is not really useful for the price calculations done in this section but is added rather to compare its high cost with the one of HF and demonstrate the cost-effectiveness of reacting lithium hydroxide with hydrogen fluoride for LiF production rather than pure metallic lithium and fluorine.
FLiBe (not enriched)	600		MIT purchase from Kairos Power	The cost of non-enriched FLiBe (approx. 92.5% Li-7) for fusion blanket use is retrieved from Kairos Power to verify the calculations made for enriched FLiBe. It has to be noted that the price of 600 \$/kg refers to quantities in the order of 10-100 kg so considering the same prices for quantities in the order of tens of tonnes could represent an overestimation. Moreover, this FLiBe quote refers to purified FLiBe meaning that the cost of purification is already included in the cost. This last point has to be accounted when first comparing this quote with the one calculated in the following paragraphs as it is important to first sum the cost of

				purification in \$/kg to our quote before addressing the quality of our calculation. Other quotes can also be retrieved for small quantities (1-10 kg) of fusion FLiBe from other suppliers and the prices are around 5500 \$/kg.
--	--	--	--	---

Given the price ranges indicated in Table 34, some calculations to evaluate a price range for the cost of FLiBe are performed. The calculations take into account the assumptions and the production process described above, its different steps and the stoichiometric relation between the different components in each of the steps. The results are provided in Table 35.

Table 35 Calculated cost of FLiBe for different use (fission and fusion applications) based on the assumptions described above.

Component	Cost range [\$/kg]
Non-enriched FLiBe (92.5%) for fusion use	20 - 130
Enriched FLiBe (99.99%) for fission use	1,200 – 2,200

As mentioned, the calculated price of non-enriched FLiBe is still not comparable with the quote retrieved from Kairos Power as the price of purification must be accounted for as well before comparing them. Regarding the cost estimate of 99.99% lithium 7 enriched FLiBe, we must also consider the price of purification which is analyzed in the next section.

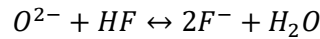
6.2.2 Pre-Purification cost

As described in the previous section, *Chemistry requirements*, FLiBe presents different types of impurities. Those can come from different process throughout the coolant lifetime such as manufacturing, transport, storage, reactor operations and maintenance, and others. The origin of impurities in FLiBe can be various but some of the major sources can be identified in the imperfect removal of impurities present in the raw materials, the contact with the structural materials (metal alloys and graphite) and the gaseous phases (cover gas) during operation and handling (Seifried, Scarlet, Peterson, & Greenspan, 2019). Given that those impurities may generate penalties in the operation parameters such as the coolant temperature coefficient of reactivity, excess reactivity, and achievable burnup, they have to be controlled and the salt must be purified before the reactor loading.

One of the first experiments treating FLiBe purification was done for the loading of the ORNL MSRE with 99.99% enriched FLiBe coolant and fuel solvent. Performing such operations, the molten salt solvent and coolant was treated with different gases to volatize and remove the impurities. The process has been described in ORNL document 4616. In 2015, the largest batch of Li_2BeF_4 since the ORNL testing has been treated and purified at the facility of University of Wisconsin-Madison to produce a high-quality coolant. During the most recent purification, UW included technological advancements that simplify the purification and analysis process. The two processes, which are partially similar, are summarized and reported hereafter in their main steps focusing on the purification of the salt for coolant applications and not for fuel solvent (as it also was in the MSRE program).

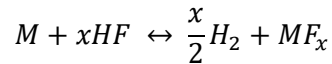
The first of the targeted impurities are the oxides. Oxides mainly arise from the incomplete evaporation of absorbed water during the melting of the FLiBe components leading to hydrolysis. These oxides may alter the heat transfer

properties of the reactor components, ultimately creating localized temperature peaks by uranium oxide deposition. Just before the MSRE FLiBe purification efforts, they were removed from the molten fluoride melt using only anhydrous hydrogen fluoride. The reaction used is the following:



And the water vapor could be then removed as reaction product from the system. This reaction has been proved to be very effective in particular at low temperatures (Shaffer, 1971).

Possibly the main drawback of using hydrogen fluoride for this process is that it would chemically attack the structural materials by the following reaction:



As it can be seen, one of the products of this reaction are metal fluorides which will be created in the external layer of the structural purification vessel/container. Given the high solubility of these fluoride forms into the molten salt melt, they will detach from the external layers and dissolve into the FLiBe. This sequence of reaction of oxidation and reduction of the salt container materials would eventually cause severe corrosion and possibly failure of the vessel.

The solution to this problem was defined by the study of the thermodynamics corrosion mechanisms, which suggested using together hydrogen fluoride and hydrogen gases at specific partial pressures so that the redox potential of the reaction will be stabilized. In fact, the redox potential can be adjusted to an optimal level by mixing a reducing agent with a fluorinating agent and sparging it through the salt. This process facilitates the removal of oxides while reducing the equilibrium concentration of dissolved metal fluorides in the salt (Kelleher, Dolan, Brooks, Anderson, & Sridharan, 2015). The materials used as containment structure are typically inert such as carbon, molybdenum, or tungsten even though nickel is the one preferentially used, allowing ratios of hydrogen fluoride to hydrogen in the range of 1:5–1:10 to prevent rapid oxide removal without damaging the purification vessel (Kelleher, Dolan, Brooks, Anderson, & Sridharan, 2015).

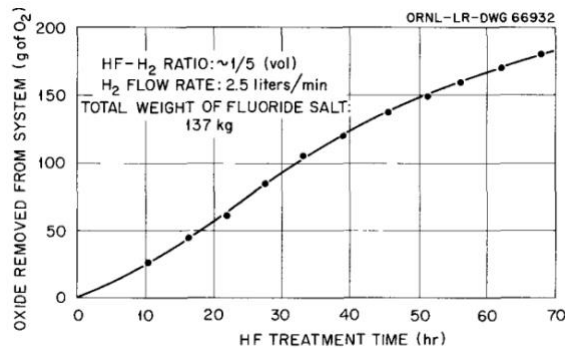


Figure 16 Time of oxide removal from a test loop at ORNL MSRE by treatment with H₂ and HF at 565 °C (Shaffer, 1971).

After the hydro-fluorination process with the appropriate HF and H₂ ratio has been executed, the hydro-fluorinated salt is hydrogen-sparged at a specific rate for a certain duration to complete the purification process. This allows to control the redox potential of impurities like oxides while minimizing the concentration of dissolved metal fluorides in the salt. The hydrogen flow was sometimes maintained overnight (Kelleher, Dolan, Brooks, Anderson, & Sridharan, 2015) or for several hours/days (Ames M. R., 2015) during FLiBe purification.

Other than oxides, the purification process at ORNL focused on sulfur impurities (in the form of SO_2 and SO_3) which must be kept at concentrations lower than 10 ppm to avoid their high-temperature aggressive corrosive behavior on nickel based structural materials especially during the first hours of operation. One of the advantages of introducing hydrogen is about exploiting its reducing capabilities. In this case, it can continuously reduce the sulfate which would react with HF to form H_2S which can be removed from a gas effluent stream in a minimum treatment time (Kelleher, Dolan, Brooks, Anderson, & Sridharan, 2015) (Shaffer, 1971).

In case other metal impurities would be present in the solution, the addition of hydrogen will reduce dissolved metal fluorides, mainly nickel fluoride and iron fluoride, to nickel and iron (Kelleher, Dolan, Brooks, Anderson, & Sridharan, 2015). Those metal impurities have low solubility in the molten salt and they can precipitate out of the solution as metallic powder which is then filtered (Seifried, Scarlat, Peterson, & Greenspan, 2019).

Other purification methods for FLiBe theoretically exist and have been described by the literature. An overview of the main techniques with their respective advantages/drawbacks is reported in Table 36 (Seifried, Scarlat, Peterson, & Greenspan, 2019).

Table 36 Main FLiBe purification methods overview with a short description and their respective advantages/disadvantages.

Method of purification	Description	Advantages	Disadvantages
HF + H_2	Treatment of salt with HF and H_2 followed by filtration.	Method effectiveness has been demonstrated for a relatively large scale (ORNL MSRE); Required gas and instrumentation is cheap; High chance of success.	Corrosiveness of HF and difficulties of operational handling.
Active metal exposure	Treatment of salt impurities with active metal (alkali metal, zirconium, etc.) which react with it forming less soluble species later separated by a cold trap or filtration.	Method effectiveness has been explored.	Difficulty of separation of the active metal and of the metal fluoride produced by the reaction between HF and the active metal; difficulties of operational handling.
Electrolysis	Reduction of impurities to the metal state which is insoluble and will attach to the surface of the electrodes.	Some success in FLiBe purification; avoid using HF.	Technique can only be applied to compounds with a reduction potential higher than the one of BeF_2 .

Other methods not described here include high temperature and vacuum distillation, fractional solidification and directional solidification, but have not yet been applied to FLiBe purification even though they could potentially be employed for it (Seifried, Scarlat, Peterson, & Greenspan, 2019).

Regarding the economics of the purification facility, ORNL estimated that re-installing a FLiBe production and purification facility, similar to the one used in 1971, would cost between \$300,000 and \$500,000 in 1971 USD. However, actual costs at that time were reportedly higher (Shaffer, 1971). The inflated cost of the facility (2024 USD) is in the range of 2,350,000 \$ and 3,950,000 \$, without accounting the cost of the materials (lithium fluoride, beryllium fluoride, etc) themselves.

The facility produced and purified approximately 15,964 lb (7,240 kg) of FLiBe coolant (salt) and 10,545 lb (4,780 kg) of fuel solvent mixture (${}^7\text{LiF}-\text{BeF}_2-\text{ZrF}_4$). In total, it handled 26,509 lb (12,020 kg) of material. The operations for production of the coolant lasted 191 days (83.58 lb/day or 37.91 kg/day of production considering outages and maintenance) and 126 days for the fuel solvent (83.69 lb/day or 37.96 kg/day of production considering outages and maintenance). The operating costs of the facility were estimated at 20,000 1971 USD per month which nearly correspond to 157,000 \$/month in 2024. Therefore, the total operational cost was almost 1,659,000 \$ for the total duration of the program, considering 317 days of operation. The estimated total cost for FLiBe production from its bare constituents and its purification for MSRE use (target operational purity 99.76%) is estimated in the range of 4,009,000 and 5,609,000 \$ in 2024 USD.

Given the cost range necessary to build a facility like the one used by MSRE, we performed a simple calculation to account the time it would take for a facility like the one used for MSRE coolant and fuel production to supply enough FLiBe for a power reactor like an FHR. Given the production rate obtained at MSRE, to produce a quantity of FLiBe necessary for the operation of the 100MWe FHR Mk-1 (91,970 kg, 202,760 lb) they would have taken approximately 6.64 years of operation considering a production rate of approximately 38 kg/day. To ramp up the production of coolant it would be possible to install more than the two salt-treatment and processing vessels present at the MSRE facilities. Considering the FLiBe requirement of 0.92 kg/kWe for the Mk-1, the produced salt in the 1960s experiment could be potentially useful for a reactor up to 13 MWe of power (MSRE experiment was only 7.4 MWth).

Inflating the MSRE data, the cost of production and purification can be accounted between 306 \$/MWe and 329 \$/MWe for a reactor of a small size (like the MSRE demonstration program was) and the purification cost per kg of FLiBe is between 333 and 466 \$/kg for the 12,020 kg batch. The purification cost per kg of FLiBe is calculated considering the total amount of coolant and fuel solvent produced at the MSRE would be 2:1 stoichiometric LiF–BeF₂ without accounting the additional costs related to the production of the fuel solvent (${}^7\text{LiF}-\text{BeF}_2-\text{ZrF}_4$). This assumption overestimates the calculated cost. The cost range reported here would be expected to decrease for a higher production as the cost of machinery and components installation would be amortized on a higher total production. Summing the calculated purification costs and the prices reported in Table 35, we get that the final cost of non-enriched FLiBe (92.5%) for fusion use varies within 350 – 600 \$/kg while the cost for enriched FLiBe (99.99%) for fission use ranges between 1,530 and 2,670 \$/kg.

As observed, the cost range for fusion FLiBe aligns with the upper boundary of the cost range for Kairos Power FLiBe when considering quantities around 10-100 kg. This alignment at the higher end is likely due to the difference in quantities considered in the two quotes. On one hand, our cost estimation is based on quotes for tens of tons of raw materials (BeF₂, lithium, HF, etc.) and purification costs derived from the MSRE values, which involved over 12,000 kg of purified FLiBe used as coolant or solvent. On the other hand, Kairos Power's cost estimation is for quantities that are two orders of magnitude lower. Consequently, it can be expected that the Kairos quote would be close to the highest end of our calculated range of prices.

Nevertheless, since the cost of naturally enriched FLiBe from Kairos Power falls within our predicted cost range, it confirms the reasonableness of our calculation method and the assumptions made about the production scheme of fusion FLiBe. These results should also verify the accuracy of the calculation done with fission enriched FLiBe given the similarities of the two production processes (especially for the BeF production) except for the procedures linked to the enrichment of Li-7. Some uncertainties in our results remain, including the normalization of the cost considering the fuel solvent, the enrichment level being non-FHR grade but rather PWR grade, the cost range of the raw elements, and other factors. The obtained price for enriched FLiBe reflects the current capabilities of the U.S. industry given that most of the quotes were obtained from suppliers operating mainly in the country. For comparison, the calculated cost of 99.995% enriched FLiBe in 2019 by the Chinese Academy of Science was of approximately 125 \$/kg (Zhu, et al., 2019). The possibility to achieve figures remarkably lower with respect to the USA market is due to the cost per kg of 99.995% Li-7, standing at 558 \$/kg in the Chinese market. Prices two orders of magnitude lower than the ones obtained

from U.S. based studies (which refer to a PWR enrichment grade) appear to be possible thanks to internal enrichment facilities.

For the sake of completeness, the cost of purification and for the whole setup at University of Wisconsin-Madison in 2015 is also quantified. The experiment, which purified 57 kg of FLiBe and whose main goal was to validate the purification and treatment theory, was quoted around a total of 250,000 USD in 2015. The corresponding quote in 2024 USD is about 330,000. This cost estimate is not taken into consideration when accounting purification costs for multiple reasons. First, some instrumentation and facility components were re-used at the time from other facilities present at UW, making it harder to account for the total capital investments of the project. Secondly, being the scope of our research the quantification of purification costs on a reactor scale, the quantity produced and purified by UW makes the quote unreliable, given that it refers to a purified quantity of FLiBe some orders of magnitude lower than the one considered here (tens of tons of FLiBe for the Mk-1). The cost of purification (in \$/kg) is expected to scale down with the quantity of FLiBe treated as the costs of operation of these facilities are two orders of magnitude lower than the expenses related to the initial capital investment for the installation of the treatment plant (Shaffer, 1971).

The capital investment required for various types of reactors are summarized on Table 37 (cost of purification are included):

Table 37 Expected capital costs for coolant purchase for different types of reactors.

Reactor name	Power [MWth]	Required coolant for start-up [tonnes]	Capital cost of coolant [2024 USD]	Normalized cost [2024 USD/MWth]	Sources used
MSRE*	7.4	12.02	18,300,000 – 32,000,000	2,485,000 – 4,340,000	(Shaffer, 1971)
Mk-1 FHR	236	91.97	140,000,000 - 250,000,000	590,000 - 1,050,000	(International Atomic Energy Agency, 2016)
AHTR**	3400	2,950	415,000,000	125,000	(Holcomb, Peretz, & Qualls, 2011)

*The cost data seen on this table for the MSRE are not referring to the capital investments faced during its construction but rather an estimation of what today's financial efforts would be considering a similar model would be built in 2024 based on our calculations.

**The data for the AHTR is taken from the ORNL/TM-2011/364 report and inflated to 2024. The previously calculated FLiBe cost is not used for this case as the price for such quantities of coolant would be expected to scale down significantly from the cost specified by our calculations (tared on tens of tonnes of coolant and not on thousands of tonnes).

6.3 Operating costs

There is currently little information on the possible strategies for coolant chemistry control during operation in a FLiBe cooled reactor.

One of the possible strategies for FLiBe purification is to have two batches of FLiBe, one of them loaded into the reactor and the other one loaded into a drain tank, linked to the primary system. The primary salt could operate during a reactor

cycle from outage to outage before being pumped to a drain vessel while the other one being pumped again into the reactor. While in the drain vessel, the FLiBe would be left untouched for a certain amount of time so that the decay of the main fission products would happen before it can be treated and purified. Then, the purification method would be a hydro-fluorination technique similar to the one described for pre-operation of FLiBe. This strategy presents some complications such as:

- The need to pump out a great amount of FLiBe while pumping in also a great amount from the drain vessel without leaving the core uncovered and allowing constant decay heat removal.
- The need of constantly monitor the level of impurities at all critical points in the coolant in the primary system to ensure that stable operation can be achieved considering an increase of impurities could alter the heat exchange properties of the fluoride molten salt and lead to an increase of temperature in the fuel. This is considering that purification of the coolant would be done only during outages.

The hypothetical costs of FLiBe chemistry maintenance during operation has been described by a report produced by ORNL taking a 3400 MWth AHTR as reference (Holcomb, Peretz, & Qualls, 2011). The AHTR is an Advanced High Temperature Reactor within the FHR family. The data is summarized in Table 38. As it can be seen, some of the costs were compared with the one expected from the PWR12 BE model, a typical Westinghouse four-loop plant with a core power of 3417 MWth and net electrical power to the generator step-up transformer of 1144 MWe (Holcomb, Peretz, & Qualls, 2011). The PWR12 reflects typical building and equipment sizes that are useful for comparison to the AHTR concept.

Table 38 Cost estimate of fluoride molten salt chemistry control and testing components for operation (Holcomb, Peretz, & Qualls, 2011).

Component	PWR12 BE cost [2011 USD]	AHTR cost [2011 USD]	AHTR cost [2024 USD]
Inert gas system - primary salt cover gas	0	20,000,000	27,680,000
Primary salt drain and storage system	0	8,000,000	11,070,000
Intermediate/DRACS* salt drain and storage system	0	8,000,000	11,070,000
Primary salt treatment system	0	50,000,000	69,210,000
Intermediate/DRACS* salt treatment system	0	30,000,000	41,530,000
Fluid leak detection system	415,210	415,210	574,750
Maintenance equipment	3,426,113	3,426,113	4,742,565
Sampling equipment	1,542,533	1,542,533	2,135,237
Total	5,383,856	121,383,856	168,012,552
Normalized total**	-	41.15 \$/kg	56.95 \$/kg

*DRACS stands for Direct Reactor Auxiliary Cooling System.

**2,950 metric tons of FLiBe are considered for the calculation.

To sum up, the total 2024 cost for the coolant maintenance and chemistry control during operation is around 168,000,000 \$. That translates to a normalized cost of about 56.95 \$/kg (considering 2,950 metric tons of FLiBe and 2024 USD).

7. Helium

Helium, the second most abundant element in the universe and second lightest element, is a colorless, odorless, and tasteless noble gas. It exists primarily in two stable isotopes: helium-3 (He-3) and helium-4 (He-4), with He-4 being the most prevalent as it constitutes 99.999% of the total helium gas (Danabalan, 2017). Helium is non-toxic, non-reactive, and has the lowest boiling point among all elements, making it invaluable for a variety of applications, including cryogenics.

Helium is also used as a coolant for nuclear applications and especially for High Temperature Gas Reactors (HTGRs). The use of helium is quite convenient because of its inertness which guarantees excellent compatibility with structural materials (Ricapito, Aiello, Galabert, Poitevin, & Tincani, 2017). It does not react chemically with graphite, and has good compatibility with fuel and metal construction materials, so that no corrosion products and corresponding reactive products are generated in the primary coolant system (Wang & Zhong, 2024). Being a monoatomic gas, it does not decompose under irradiation. Under reactor operation, helium does not change phase and it does not cause changes in reactivity as its neutron absorption cross section is practically zero and the moderation is also not appreciable (Wang & Zhong, 2024) (Schulenberg, 2022). In fact, a loss of helium does not lead to a change in reactivity. Because of its low interaction with neutrons, a helium-cooled reactor can also feature a hard spectrum, which may be used to breed new fuel. Helium thermal conductivity is good with respect to other gases like CO₂ (10 times higher) and has an important advantage on liquid metals as it is transparent, which facilitates internal vessel components and primary system inspection during operation making it possible to visualize failures or debris (Schulenberg, 2022).

Table 39 A comparison between Helium properties and other coolants at different reactor conditions (Bubelis, 2013).

Coolant	Water	CO ₂	He	Ar	Na
Pressure, Temperature	150 bar, 300°C	60 bar, 500°C	60 bar, 500°C	60 bar, 500°C	1 bar, 500°C
ρ [kg/m ³]	725.53	40.86	3.7	37.29	857
C_p [J/kg/K]	5476	1182	5190	525	1262
λ [W/m/K]	0.56	0.006	0.303	0.037	66.3
μ [10 ⁻⁵ Pa·s]	8.83	3.33	3.73	4.54	24.3
1/Pp* (normalized to water)	1	6·10 ⁻⁵	2.8·10 ⁻⁵	5·10 ⁻⁶	0.02
HTC** (normalized to water)	1	0.7	0.99	0.65	21
1/P*** (normalized to He)	-	5.5	1	2.8	-

*1/Pp represents the inverse of the pumping power. A higher value indicates less pumping power is required, which is desirable for reactor efficiency.

**HTC stands for Heat Transfer Coefficient. A higher HTC value indicates better heat transfer capabilities of the coolant, which is important for efficient reactor cooling.

***1/P represents the inverse of the power under natural circulation conditions. A higher value in this column suggests better natural circulation capabilities of the coolant, which is beneficial for passive safety systems in reactors.

Table 39 compares helium coolant properties with other coolants used in thermal and fast reactors (helium is considered for both). As it can be seen, helium is indeed a good gas coolant but presents several drawbacks. In fact, requires a high pumping power and it does not have high natural circulation properties (Ricapito, Aiello, Galabert, Poitevin, & Tincani, 2017) (Bubelis, 2013). Moreover, it has a heat transfer coefficient lower with respect to other coolants even at very high pressures. To maintain acceptable cladding temperatures, the reactor core must therefore be cooled at much higher flow rates and the power of the fuel rods must be reduced (Schulenberg, 2022).

Helium was firstly used as coolant in thermal reactors when the concept of HTGR was introduced. These thermal gas-cooled reactors came into the market in the 1960s after the operational AGRs (Advanced Gas-cooled Reactors) had

reported issues with their coolant, CO₂. In fact, carbon dioxide dissociates into CO and O₂ under the combined action of heat and radiation at about 600°C due to a phenomenon called radiolytic dissociation. The free oxygen radical can oxidize metal structures and graphite damaging the reactor internals at a rate which is considered *unacceptable* at high temperatures (Bubelis, 2013). Therefore, helium was adopted to avoid the radiolytic dissociation problems associated with carbon dioxide. Helium is currently considered as an option for both thermal and fast reactors even though helium-cooled fast reactor have not been built yet (Schulenberg, 2022).

The Dragon test reactor was the first HTGR to be developed and it was built in Winfrith, UK. The Dragon reactor operated at 20 MWth and used helium as the primary coolant with an inlet and outlet reactor temperature of 350°C and 750°C, respectively. These temperatures were considerably higher than the ones reached with the second AGR generation (1960s onwards) which got to an outlet temperature of about 650°C. The operating pressure was 2 MPa and the core was of a prismatic block design (Rennie, 1978). In Germany, the Arbeitsgemeinschaft Versuchsreaktor reactor (AVR) was built. It produced 46 MWth and it remained operational for 20 years testing the technology for the pebble-bed reactor concept.

In the USA, a 40 MWe HTGR was built at Peach Bottom. Peach Bottom reactor stayed operational approximately 8 years and tested different types of fuel including the BISO fuel particles. The BISO fuel had an inner layer that acted as a buffer from recoiling fission products and an outer layer to retain the noble fission gasses. The BISO operation led to development of TRISO, later used in other HTGRs and in the Fort St. Vrain power station. The TRISO concept had an improved fission product retention thanks to an external layer of Silicon Carbide (SiC). The Fort St. Vrain power station was a medium size reactor (842 MWth) using Peach Bottom as design basis. It was able to operate for slightly more than a decade before being decommissioned due to significant problems encountered during operation and related to moisture intrusion in the reactor. The large moisture intrusions directly affected the plant safety and led to the degradation of the control rod drives and reserve shutdown systems (Oak Ridge National Laboratory, 2004). During the 1970s and 1980s the concept of modular HTGR flourished in response to a requirement of higher safety standards imposed by the U.S. Congress after the accidents at Three Mile Island and Chernobyl. The modular HTGR was developed to be *simpler and safer* and to be economically competitive (Beck & Pincock, 2011). The reactor design was created to generate a power of 200 MWth at a core outlet temperature of 700°C, allowing applications like electricity production with high efficiency or process heat application like cogeneration (Kugeler & Zhang, 2018). The concept can be divided in two categories:

1. The Pebble bed HTGR: This particular thermal reactor design uses spherical elements called “pebbles” which contains TRISO fuel particles embedded in a graphite matrix. During operation, the pebbles move slowly downward in the reactor core allowing continuous refueling of the reactor. The advantages of this concept include increased reactor availability due to continuous refueling, a relatively uniform power distribution and fuel burn-up depth, and the absence of a large excess reactivity, which facilitates reactor control (Wang & Zhong, 2024)
2. The Prismatic block HTGR: It uses stationary stacked hexagonal graphite blocks with cylindrical fuel channels containing fuel compacts made of TRISO particles. This stationary fuel arrangement allows for higher power density and a more predictable and easier-to-model core physics.

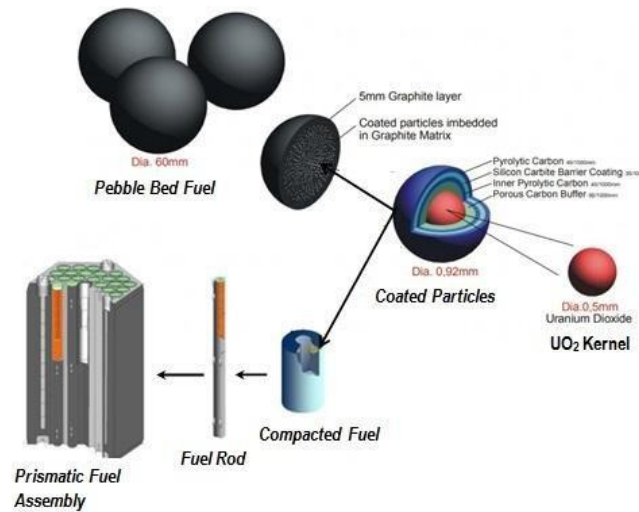


Figure 17 Difference between prismatic fuel assembly and pebble bed fuel. This difference is at the basis of the two concepts of HTGRs, the pebble-bed HTGR and the prismatic block HTGR (Rahmatullah, et al., 2019)

In China, the HTR-10 was built in the late 1990s. It was a pebble-bed HTGR with a thermal power of 10 MWth developed from the 1979 German design called “HTR-Module” (Wu, Lin, & Zhong, 2002). The HTR-10 was the first HTGR to simulate unprotected transients in 2004 by performing a nuclear safety test demonstration of the loss of reactor cooling without inserting the control rods (Wang & Zhong, 2024). It further simulated the mis-lifting of the control rods without scram, the shutdown of the main helium fan without scram, and the non-closing of the fan stall without scram to verify the inherent safety of the reactor looking forward to the HTR-PM development (Wang & Zhong, 2024). The HTR-PM comprises two small size pebble-bed reactors (250 MWth each) driving a single 210 MWe steam turbine. It was completed in 2015 after 3 years of construction, reaching criticality for the first time in September 2021 and grid-connected in December 2021 (World Nuclear News, 2022).

On the other hand, Japan developed a prismatic block HTGR called the High Temperature Engineering Test Reactor (HTTR) with a thermal power of 30 MWth. It was built between 1991 and 1998. The reactor has been used for testing of the direct sulfur-iodine for hydrogen production thanks to the high temperatures which could be reached (between 850 – 950°C). The reactor had also been used for accident safety demonstration (Fujiwara, 2021) before being shutdown in February 2011 after the Fukushima accident. The JAEA has reportedly been developing the subsequent model, a GTHTTR300 which will be able to achieve an efficiency of 50.4% (Sato, Yan, Tachibana, & Kunitomi, 2014). Such prismatic block HTGRs have also been explored in the USA at the turn of the 1980s and 1990s when the MHTGR was conceptually designed.

In the United States, the Department of Energy (DOE) initiated the NGNP Project at Idaho National Laboratory (INL) in 2006 as mandated by the Energy Policy Act of 2005. The goal was to commercialize the HTGR technology for use in the United States and internationally. Preliminary designs for pebble-bed and prismatic-based plants were developed, leveraging previous work done in previous designs such as the MHTGR. These new NGNP designs aimed to produce electricity and hydrogen, with thermal power ratings between 500 and 600 MWth and reactor outlet temperatures of 900 to 950°C. Following the initial design phase, extensive interaction with potential industrial end users and tradeoff studies concluded that the NGNP should serve as a source of high-temperature process heat to meet industrial energy needs in forms such as electricity, steam, high-temperature gas, hydrogen, and oxygen. This interaction helped refine the configurations and operating conditions of the pebble-bed and prismatic reactor-based plants to ensure they met industrial energy requirements. However, the project was halted by the DOE in 2011. The NGNP did not advance to the detailed design and license application phases due to cost-sharing impasses between

the DOE and the NGNP Industry Alliance for the required public-private partnership mandated by the U.S. Congress (Beck & Pincock, 2011) (U.S. Nuclear Regulatory Commission, 2024).

In 2009, X-energy was founded. The company flagship project, the Xe-100 HTGR small modular reactor, is designed to produce 80 MW of electricity and be scaled up to a “four-pack” configuration for a total output of 320 MW. X-energy has made progress towards commercialization, signing agreements with various partners and receiving significant funding and support from both private sources and government grants, including a notable selection for the Department of Energy's Advanced Reactor Demonstration Program (ARDP) in 2020 (X-energy, 2021).

Other notable uses of helium, both in the nuclear industry and not, are:

1. Magnetic Resonance Imaging (MRI) scanners used for organs, muscles, and blood vessels examinations. This is the major application of helium and it is used for the cooling of the superconducting magnets. The low temperature helium cooling is crucial to the operation of these devices as it allows the magnets to operate in the superconductive region and generate strong magnetic fields. 22% of the global helium consumption is for this application (Berganza & Zhang, 2013).
2. Fusion applications. Liquid helium will be used as coolant for some proposed breeding blanket and divertor concepts for ITER and DEMO and other fusion reactors worldwide. It has also been considered as vacuum vessel coolant (Tillack, Humrickhouse, Malang, & Nygren, 2014).
3. Semiconductor manufacturing. Helium creates an inert environment around silicon to prevent unwanted reactions generally gas- or liquid-based. Moreover, it helps monitoring the temperature around the silicon by cooling heat allowing semiconductor miniaturization. According to projections, the semiconductor industry's revenue is expected to continue growing, which could significantly increase the helium market for semiconductor and optic fiber production in future (Serra Leal, Incer-Valverde, & Morosuk, 2023) (Institute for Energy Research, 2021).
4. Welding purposes. Helium's properties such as its chemical inertness and heat transfer make it a good candidate to protect a weld point from oxygen and water intrusion. Helium acts as shielding gas to allow fast welding speeds and efficiency. It is usually mixed with argon at different percentages depending on the particular application and weld required partly because of argon's lower cost. If the mixture of the two is not calibrated properly weak or porous welds can be created as well as a metallic spatter (Leiden, 2015) (Bite, 2021).

7.1 Purity requirements

Controlling the purity of helium in a helium-cooled reactor is essential for maintaining the reactor's integrity and performance. Helium, being an inert gas, does not react with other materials. However, impurities in helium can lead to significant issues especially considering the pressure and temperature conditions in which the helium coolant operates in HTGRs. For instance, contaminants like oxygen, water vapor, and carbon compounds can cause oxidation, carburization, or decarburization of the reactor's structural materials depending on several factors such as the target material, the impurity levels, temperature, and so on. In particular, corrosion is the main issue for the integrity of the graphite moderator and for internal metallic components while alloy oxidation is a risk for the Intermediate Heat Exchanger (IHX) and the Reactor Pressure Vessel (RPV) steels. These chemical interactions can degrade materials, leading to loss of mechanical strength, increased corrosion, and potential failure of critical components. If helium purity is not properly managed, it can result in reduced efficiency of heat transfer and neutronics, increased maintenance

costs due to abnormal activation, and even catastrophic failures, compromising both safety and economic viability of the reactor.

Table 40 summarizes the potential effects in terms of corrosion and material degradation to the principal structural materials/components of the reactor (Bubelis, 2013) (Wright, 2006) (Castle, 2010) (Lee & Pint, 2021) (Cabet & Rouillard, 2009):

Table 40 Potential risks for the principal reactor internals given by operation of high temperature helium cooled reactor (Bubelis, 2013) (Wright, 2006) (Castle, 2010) (Lee & Pint, 2021) (Cabet & Rouillard, 2009).

Component	Potential risk	Selected materials	Comments
Reactor Pressure Vessel (RPV)	Oxidation*, carburization*, decarburization, radiation embrittlement, and changes in emissivity.	Steel (Peach Bottom), Pre-stressed Concrete Reactor Vessel (FSV), G22 (HTTR), SA 508/533B, 2-¼ Cr – 1 Mo (NGNP) and G91 (HTR-10) steels. The G22 and G91 are chromium molybdenum alloy steels that ensure excellent high temperature strength and creep resistance.	The RPV can benefit from a slightly oxidizing environment. In fact, such environment allows the development of a slow growing external oxide (Cr ₂ O ₃) beneficial for long-term durability. In an inert environment, there is no oxygen available to repair the oxide layer if it is damaged. Without the oxide layer the material properties would be reduced in limited time at the HTGR conditions. On the other hand, an oxidation layers reduces the surface emissivity of the RPV limiting the vessel capability to “cool off” in case of accidents events in which RPV cooling and decay heat removal are not possible. No lifetime model has been proposed yet. Ni-Cr-Mo materials have a specific temperature over which the oxide layer and the base metal will start to react removing the oxide. This is called “microclimate” reaction and can be stopped adding CO and H ₂ O in the coolant.
Intermediate Heat Exchanger (IHx)	Oxidation, carburization*, decarburization*, radiation embrittlement.	Iron based alloy 800H considered for temperatures up to 1033 K while Nickel based alloys 617, X (or XR) used for the highest temperatures.	The possible alloys considered as candidates for IHx use require superior oxidation and creep properties at temperatures between 750 and 1000°C. Also, they have to comply with ASME Boiler and Pressure Vessel Code (BPVC) Section III Div. 5 for high-temperature reactors.
Graphite moderator	Oxidation, formation of graphite “dust” which can change the free surfaces emissivity and might react	Graphite evaluated for NGNP: IG-430, NBG-17, NBG-18, PCEA, PGX, and 2020	Graphite is one of the impurity sinks in a helium-cooled reactor together with the HPS as it can capture and adsorb maintaining gas chemistry.

	<p>with the C_2O_3 oxide layer at high temperatures according to:</p> $Cr_2O_{3(s)} + 3C_{(s)} \rightarrow 3CO_{(g)} + 2Cr_{(s)}$ <p>This reduction of chromia leaves the alloy unprotected and susceptible to further corrosion phenomena like carburization* or decarburization*.</p>		<p>Three levels of oxidation regimes exist for graphite depending on temperature: the chemical regime (<500°C), the in-pore diffusion-controlled regime (500-900°C) and the boundary layer regime (>900°C). The oxidation rate is controlled by the chemical reactivity of the graphite which is a function of the temperature and of the metallic impurities present which can act as catalysts. To maintain the integrity of the graphite moderator it is essential to control the level of oxygen in the primary circuit.</p>
Structural metallic components	<p>Oxidation, carburization*, decarburization*, radiation embrittlement, and changes in emissivity.</p>	<p>Iron based alloy 800H considered for temperatures up to 1033 K while Nickel based alloys 617, X (or XR) used for the highest temperatures.</p>	<p>The helium environment within the primary circuit must always sustain a continuous, self-healing chromium oxidation which protects the metal structures against gases corrosiveness and reactivity.</p>

*Carburization is the phenomenon for which carbon atoms are able to diffuse into the base metal due to lack of oxide layer protection. Decarburization stands for the movement of the carbon atom into the interface between the oxide level and the base metal potentially leading to the formation of surface carbides.

As mentioned, the inertness of helium could be altered in a HTGR environment due to the presence of impurities. The mechanisms that control the level of impurities in the coolant are the graphite core and the Helium Purification System (HPS). The graphite core is the main sink and acts passively achieving a dynamic balance which tends to a low steady state impurity level while the HPS acts actively and continuously during operation (Castle, 2010). Nevertheless, some impurities can be intentionally added or originated to prevent the damage caused by graphite oxidation. The impurities can originate from air by charging/discharging fuel elements or in-leakage, core outgassing, proton diffusion, and reactions in the gas phase due to the high temperature and pressure conditions. For long term operation, it is important to maintain an oxidizing environment in the primary circuit so that the oxidizing impurities can form a protective oxide layer, thermally grown, which can act as a barrier against solid state diffusion of oxygen and carbon. The impurities present in a HTGR can be classified as radioactive and non-radioactive impurities, as explained next.

Both prismatic and pebble bed HTGRs are designed to work with TRISO particles. This type of tri-structural isotropic fuel has been accurately tested before and has been demonstrated to be able to contain the release of fission products through multiple containment barriers, integrated in its design. Nevertheless, it can happen that a certain number of TRISO fuel particles could get damaged during operation eventually leading to the release of fission products in the primary circuit will be also present in the primary circuit. Tritium impurities must be also controlled. The potential origins of tritium are multiple and consist of different path with respect to noble gases (Castle, 2010):

1. Ternary fission. It is expected to be the major source of tritium in the NGNP reactor even though having a yield of just 0.2 to 0.4%.
2. Helium-3. This is expected to be the second greatest source by NGNP since it can be found in *significant quantities* in purified Helium.
3. Lithium-6. It is usually present as a minor impurity in graphite but given the high quantities of moderator present it is likely to be a source by thermal neutron absorption.

4. Boron-10. It can be used as burnable poison for reactivity control in HTGRs (Rittenhouse & Morgan, 1976) and can generate tritium via two pathways depending on the number of neutrons absorbed.

The main mechanism of tritium removal is via the graphite moderator which will remove it and other impurities via chemisorption, as was proven via some experiments at the Arbeitsgemeinschaft Versuchsreaktor (AVR) in Germany (Castle, 2010). The total amount of impurities that can be adsorbed in graphite is inversely proportional to the core temperature and directly proportional to the concentration or pressure of the impurities in the gas phase (Trester, Johnson, Simnad, Burnette, & Roberts, 1982). The HPS will also contribute to tritium removal in the molecular sieve.

Tritium will be introduced into the secondary circuit via diffusion because of the concentration gradient at the helium-water heat exchanger. Given that the tritium concentration will be higher in the helium given the sources mentioned above, the secondary circuit will act as a sink. The removal of tritium from the water must be ensured to reduce hazards associated with leaks, maintenance, and downstream emissions. The extraction of it is anticipated to be technically complicated and there is limited experience with the possible methods which can be adopted. The candidates to be used on a periodic basis or continuously to maintain tritium concentrations below an established value are isotope exchange columns, H₂O/HTO distillation, electrolysis and cryogenic distillation, combined electrolysis and catalytic exchange, and catalytic exchange and cryogenic distillation (Castle, 2010). HTGRs has also been considered for high-temperature heat transport applications such as: hydrogen production, ammonia production from natural gas, ammonia production from coal, natural gas to liquids, coal to liquids, coal to gasoline, coal to substitute natural gas, and steam-assisted gravity drainage (Castle, 2010). During the transport to the users and costumers, the HTGR heat has to respect certain limitations in terms of quality and that is the main reason why a tritium control system will be required at the secondary circuit.

Regarding non-radioactive impurities, they can be generated from different sources in a HTGR. These can be already present in the coolant, on the structural materials, on the fuel, on the graphite moderator or leak in through the primary system piping, the circulator (as it was for FSV lubricant (Wright, 2006)) or be generated through some chemical reaction due to the high pressure and temperature conditions of the primary system. In particular, hydrogen is produced via oxidation of metallic surfaces, decomposition of water or methane due to the high temperature. CH₄ levels have been a problem in FSV (Wright, 2006) because of the leakage coming from the lubricant from the helium circulators. The leaking bearings could be replaced in newer HTGRs using modern lubricant-free electromagnetic bearings, therefore reducing the level of methane in the primary circuit which would be still dependent on radiolytic reactions of H₂. The CH₄ concentration has a relationship with temperature as its level is expected to be reduced in the hotter parts of the core due to thermal cracking. CO is produced by the reaction of the water impurities (potentially coming from the HX) with the core. The CO₂ is instead produced from the degassing of the graphite reflectors (impurities which are trapped there are freed with temperature increase) (Natesan, Purohit, & Tam, 2003). Regarding CO and CO₂, it has been demonstrated that a higher temperature yields a higher level of CO with respect to CO₂ and there seems to be a relationship between the two based on temperature (Castle, 2010), i.e., the higher the temperature, the higher the CO concentration. Lastly, N₂ does not seem to pose a threat for operation of HTGRs as it is minimally reactive and would not cause a major impact to the chemistry. Oxygen levels are extremely low given the high number of different reaction possibilities within the primary system.

Table 41 summarizes the impurities present in some operational reactors or designed plants during steady state operation in wppm (Lee & Pint, 2021) (Castle, 2010) (Wright, 2006) (Berka, et al., 2012) (Priambodo, Pancoko, Sriyono, & Setiadipura, 2018). Caution should be exercised when comparing data on impurities for different plants, as varying values are sometimes reported for the same plant in different publications. This is likely associated with conversion from partial pressure of impurities (favorite unit for corrosion studies) to ppm by volume (typical units used for comparison of one plant to another) (Wright, 2006).

Table 41 Impurity content of some helium-cooled reactors during operation (Lee & Pint, 2021) (Castle, 2010) (Wright, 2006) (Berka, et al., 2012).

Reactor	Impurities [wppm]						
	H ₂ O	H ₂	CO	CO ₂	CH ₄	N ₂	O ₂
GT-MHR	2.0	-	CO + CO ₂ < 6.0		-	-	-
Peach Bottom	0.5	10.0	0.5	< 0.5	1.0	0.5	-
FSV	1.0	7.0	3.0	1.0	0.1	-	-
AVR	0.2	9.0	45.0	0.25	1.0	22.0	-
PMBR	< 0.2	2.0 – 11.0	2.0 – 11.0	< 0.2	< 0.1	3.0 - 115	-
Dragon	0.05 – 0.1	0.8 - 2	0.5 – 1.0	< 0.02	0.15	0.15	-
THTR	< 0.01	0.8	0.4	0.2	0.1	0.1	-
HTTR (upper limit)	0.2	3.0	3.0	0.6	0.5	0.2	0.04
HTR-10	<= 1.0	<= 9.0	<= 9.0	<= 1.0	<= 3.0	<=2.0	1.0
RDE*	<= 0.2	<= 5	<= 3	<= 0.6	<= 1	<= 1	<= 0.02
NGNP approximated	1 - 2	2 - 10	2 - 4	0.1 - 1	0.1 - 1	0.1 - 2	-

*Impurities concentration for the RDE (Reaktor Daya Eksperimental) are given in volume per million (Priambodo, Pancoko, Sriyono, & Setiadipura, 2018).

In Table 41, the main impurities present in different HTGRs are reported. As it can be seen, the values are mostly similar within different designs. It should be noted that on historically operated plants, no components of the primary circuit have failed because of impurity levels in the helium coolant even though there exist reports of some oxidation and at least one report of massive carbonaceous deposits on the reactor internals (Wright, 2006). In fact, the production of carbon dust is one of the main risks for the alteration of the primary alloys emissivity factor during operation. The AVR total yearly dust production was accounted to be 3 kg corresponding to an average density of 5 µg/m³ and an average quantity of 8 mg in the primary circuit over time. The dust was found to settle in low flow areas of the AVR's primary circuit with an estimated deposition of 60 kg every 20 years (Wright, 2006). Moreover, studies have proven that graphite dust could accumulate at a rate of 0.1 kg/MW at the reactor's end of life, depending on the core geometry and format (Lee & Pint, 2021). Nevertheless, dust has not been categorized as an operational showstopper for the AVR system.

As it can be seen from Table 41, the impurities in modern HTGR reactors and especially in the projected values for NGNP, are in the order of 1 – 10 ppm. Therefore, a helium purity of 99.999% will be considered in the next paragraphs as target for economic cost estimations of coolant purchase.

The impurity sources during steady state are reduced with respect to those associated with maintenance or outage periods. Possible examples are adherence of impurities on metallic surfaces during fuel handling, possible in-leakages and contamination of newly installed components, etc. For the sake of completeness, the impurity levels at the start of operation (during power rise) have been reported using data from FSV reactor in Table 42 while the impurities released at different temperatures from the primary coolant circuit internal structures are being displayed in the Appendix E.

Table 42 Impurity concentrations in ppm at the FSV plant during rise to power (Wright, 2006).

Date	Power [%]	Outlet Temperature [K]	H ₂	H ₂ O	CO	CO ₂	CH ₄	H ₂ /H ₂ O
July 3-6, 1976	2	490	2 - 15	70 - 240	0.2	1.8 - 2	0.6	0.01-0.2
July 24-28, 1976	11	590	35 - 45	2 - 50	2 - 4	1 - 6	3 - 5	0.9-1.4
July 28-30, 1976	21	700	40 - 90	80 - 180	2 - 4	4 - 10	3 - 6	0.2-1
July 30 – Aug 2, 1976	26	785	30 - 85	76 - 140	3 - 4	6 - 10	2 - 6	0.4-0.6
Dec 10 – Jan 9, 1977	28	895	10	40 - 4	1.5 - 3	3.5 - 1	0.5 - 0.6	0.25
Sept 16 – Oct 24, 1977	38	895	2 - 3	<1	2 - 4	2 - 3	0.2	>3
Oct 29-31, 1977	50	945	3	0.2	5 - 6	1 - 1.5	0.2 - 0.4	15
Apr 28 – May 4, 1978	65	980	4 - 5	<1	7 - 10	2 - 3	0.4 - 0.8	>5
Dec 10 – Jan 27, 1979	63	945	2 - 7	<1	1 - 3	0.5 - 1	0.1 - 0.2	>3

7.2 Cost of Helium

In this section, the different costs related to the initial purchase of helium and its purification system as well as some of the operational costs, are analyzed. Before going to the details of the actual costs, a brief introduction on the origin of helium reserves and the methods of helium extraction has been added for completeness, and to justify future and present price fluctuations of the gas.

Helium is one of the most common elements of the universe despite being very rare on Earth and being in high demand from different industries, some of them described in previous sections. Helium is generated within the Earth's crust by the very slow decay of elements such as Thorium and Uranium (National Research Council, 2000) (Nordrum, 2024) and does not usually remain on the planet but rather escapes into outer space shortly after as it is unleashed from the crust (Brumfiel, 2019). This is due to the fact that helium does not react chemically with any other elements and is pulled upwards by buoyancy forces. Nevertheless, it usually gets trapped in natural gas deposits from where it can be extracted. From these reserves, helium can be extracted with natural gas and it is normally economical to do so when concentrations are as high as 0.3% though it also depends on other products concentration in natural gas and the reservoir conditions. In fact, sometimes helium extraction might be unfavorable in case the natural gas reserve would be too limited given the considerable costs related to the installation of the appropriate machinery for helium extraction. The maximum helium concentration in natural gas is about 8% (National Research Council, 2000). Helium is extracted using drill rigs that bore deep into the Earth's crust. These rigs penetrate through a layer known as the "Cap Rock" to access natural gas reserves. Upon discovery, both natural gas and helium ascend and fill the rig. Subsequently, they are directed through a network of pipelines to a refining facility where the natural gas and raw helium undergo

processing (Rocky Mountain Air Solutions, 2024). In some cases, helium is a by-product of nitrogen's removal from the gas stream to increase its heating value or some processing systems can be specifically designed to remove it (National Research Council, 2000). It usually has to go through a multi-step "scrubbing process" to remove possible impurities. Amine and glycol absorption, dry desiccant adsorption, and/or other extraction processes typically remove water, carbon dioxide, and hydrogen sulfide from the gas (National Research Council, 2000). Nitrogen and methane can be separated via cryogenic units which cool the gases to their liquifying temperature. This way, N₂ and CH₄ are removed and hydrogen can be also extracted with the addition of oxygen in a reaction to produce water. Afterwards, helium can be additionally purified to reach the commercial target purity of 99.99% or further ones (as the one of interest for the nuclear industry: 99.999%) (Rocky Mountain Air Solutions, 2024). The final purification is done using activated charcoals (similarly to what is done in HTGR HPS) and high pressure or pressure-swing adsorption (PSA) processes (a gas separation technique that uses pressure changes to selectively adsorb and desorb gases from a mixture) (National Research Council, 2000).

There is limited amount of helium on Earth and the largest reserves are in Qatar, Russia, Algeria and the U.S, administered by less than 15 companies worldwide (Hopkins, 2024) (Nordrum, 2024). The United States are currently the world's largest producer of helium (55% globally) as well as one of the top consumers (Siddhantakar, et al., 2023). Historically, the helium global market has been closely tied to the U.S. government (Nordrum, 2024) and the two most important reserves are the Hugoton-Panhandle field complex, which is located in Texas, Oklahoma, and Kansas, and ExxonMobil's LaBarge field, which is located in the Riley Ridge area of southwestern Wyoming. Most production from the Hugoton-Panhandle complex is connected to or could be connected to the BLM (Bureau of Land Management) helium pipeline and Cliffside storage facility near Amarillo, Texas (National Research Council, 2000). Amarillo's pipeline and storage facility is administered by the BLM department of the U.S. Department of the Interior and it supplies over 20% of the domestic and 9% of the global demand for helium (Bureau of Land Management, 2024). After initial stockpiling happened for military use (initially used for airships), the U.S. government has started selling part of its helium reserves for private uses and has auctioned off the Federal Helium Reserve in Amarillo to an industrial company called Messer (Bureau of Land Management, 2024). The change of ownership could lead to a facility shutdown of almost three years stressing on an existing gas shortage which has a high demand currently mainly because of usage in MRIs (Hopkins, 2024).

The helium's demand is likely set to rise due to high request from new fast progressing sectors such as chip manufacturing (set to become the biggest application in the oncoming years), quantum computers, rockets, fiber-optic cables, etc (Nordrum, 2024). Given actual shortage of the gas and lack of supply, the gas cost is expected to rise in the next years as it has done in the last two, approximately doubling its price from 2021 to 2023 (Nordrum, 2024). To respond at this price increase, most of the industries in which helium is currently used will phase out in case it is non-essential and the MRI industry has started to commercialize machines able to use between 1 and 7 liters of helium. This is extremely low with respect to what traditional MRIs use: around 1700 and 1800 liters of liquid helium which require constant replenishment. Nevertheless, the transition between new generation and old generation MRIs will not happen overnight as they are currently used in more than 6000 hospitals in the U.S. alone (Hopkins, 2024). Other countries such as Russia and Qatar will expand their production to cope with increasing export demand and the supply is set to expand by 50% in the upcoming years (Nordrum, 2024). An increase of supply in other countries would not necessarily determine lower costs in the United States as it has been estimated that up to 50% of the helium extracted is lost before usage (Siddhantakar, et al., 2023) and long-distance import of helium from countries overseas to the U.S. would not be always economical due to the gas high volatility, which implies potentially high gas losses.

The current market instability and the rapidly increase of demand of a limited resource like helium will likely lead to highly volatile prices (whose average trend has been noted to be increasing so far) in the future and therefore the prices reported in this report might be subject to some changes based on demand-supply equilibrium and market evolution.

7.2.1 Purchase cost

The cost of helium initial purchase for reactor operation is analyzed in this chapter. The cost of helium refers to the cost of pure gas which does not include the cost of transportation, purchase/rent of the helium cylinders, shipping method and schedule. These factors are highly dependent on the case study and could influence the costs reported in the following table. As mentioned previously in this report, the target purity for which the following quotes refer to is of 99.999%. Table 43 lists helium Grade 5 cost.

Table 43 Cost per kg of high purity helium.

Supplier	USGS* (U.S. Geological Survey, 2024)	AirGas	Linde	Advanced Specialty Gases
Purity [%]	99.997	99.999	99.999	99.999
Cost [2024 USD/kg]	78.45	205	170	545
Comments	The price refers to the cost of one cubic meter. Since the purity is lower than the target for HTGR use, this quote could be used as lower boundary for cost estimations.	The price refers one cylinder only.	The price refers to a quantity of 3000 cylinders and has been used for further calculations. 3000 cylinders correspond approximately to a 4 tonnes of helium gas.	The price refers one cylinder only.

*U.S. Geological Geological Survey.

When extrapolating the cost to get the potential total price for helium purchase for a reactor, the quote given by Linde is used. This choice considers that the other quotes may not reflect the real price per kg for high quantities of gas (and thus subject to a cost reduction with respect to the cost per kg of single cylinders or lower quantities) or do not match the target purity for our application.

Table 44 Fronted capital investment of different helium-cooled designs based on the required helium inventory.

Reactor name	Source	Power [MWth]	Helium inventory [kg]	Front capital investment for coolant purchase [2024 USD]	Normalized capital investment [2024 USD/MWe]
--------------	--------	--------------	-----------------------	--	--

HTR-10 (China)	(Castle, 2010)	10	210	36,000	3,600
Dragon (UK)	(Feng, et al., 2021) (Rainer, 2005)	21.5	355	61,000	2,850
HTTR (Japan)	(Castle, 2010)	30	2,000	345,000	11,450
Peach Bottom (US)	(Castle, 2010)	115	425	73,000	635
HTR-PM (China)	(Bubelis, 2013)	250	2,440	419,000	1,675
MHTGR (US)	(Castle, 2010)	350	5,515	945,000	2,700
PMBR (South Africa)	(Bubelis, 2013)	400	4,000	687,000	1,715

As it can be seen from Table 44, different reactor designs may face different helium investment cost depending on the volume of the primary system and the pressure requirements. Nevertheless, the trend underlines a higher nominal investment cost for smaller plants with respect to bigger units. To calculate the cost of helium purchase in a HTGR for which the required volume of helium is unknown, the rule of thumb is of 1 ton of helium per 100 MW of thermal power, or ~25 tons per GW of electricity, assuming the overall efficiency of the reactor at 40% (Bubelis, 2013).

7.2.2 Helium make-up cost

The use of helium as a primary coolant in HTGRs presents unique operational challenges and associated costs. One of these, is associated with the size and properties of helium. In fact, the helium atom is very small and can easily penetrate through tiny gaps and imperfections in materials. Its small size makes it particularly prone to leakage compared to other gases. The high pressure at which HTGRs operate, up to 100 atmospheres (Wang & Zhong, 2024), makes it particularly challenging to limit the leak rate of helium. Moreover, the gas can also diffuse through metal, leaking to the external, non-pressurized environment especially at high temperatures (Cowgill, 2018). Potential leakage points during normal operation in a HTGR are represented by the multiple components and connections in the primary coolant system, including valves, seals, and other penetrations. Significant helium losses can also be accounted for during maintenance or other auxiliary operations such as fuel handling and purification of the coolant. Even though the nature of helium as an element makes it an impossible engineering challenge to achieve a null leak of helium outside of the primary circuit boundaries, its leakage rate must be controlled.

There are two main reasons why excessive helium losses must be prevented. Firstly, to restrict the release of radioactive materials to the environment. Secondly, to be able to check the primary system pressure boundary integrity during operation (Tochio, Shimizu, Hamamoto, & Sakaba, 2014). To be able to maintain a controlled leak rate during operation, the joint between the helium pipelines and/or the equipment has been welded in the Japanese HTTR (Tochio, Shimizu, Hamamoto, & Sakaba, 2014) (Beck & Pincock, 2011).

Table 45 summarizes the target/allowed helium leak rate for different reactor designs and the related costs associated to the coolant make-up.

Table 45 Helium make-up cost for different reactor designs.

Reactor	Source	Reactor Thermal	Helium inventory [kg]	Target/restricted helium leakage rate [wt%/day]	Helium make-up cost [2024 USD/MW·year]
---------	--------	-----------------	-----------------------	---	--

		power [MWth]			
Dragon	(Bubelis, 2013)	21.5	355	0.1	1,000
HTTR	(Tochio, Shimizu, Hamamoto, & Sakaba, 2014) (Japan Atomic Energy Agency, 2010)	30	2,000	0.3	6,300*

*The calculations consider a leak rate of 0.15 wt%/day as periodic inspections at the HTTR have registered a lower loss rate than the maximum allowed (0.3 wt%/day), as can be seen from Figure 18.

As it can be seen in Table 45, the cost for helium make-up can differ significantly between two different reactor designs. Generally speaking, the make-up cost is highly influenced by the allowed leak-rate and the helium inventory into the reactor. Those parameters are strictly dependent on material selection, reactor design, welding techniques and accuracy, helium coolant availability, operational safety, etc. From an economic point of view, an optimum point can be found between the capital investment in structural materials development, welding, and investment in helium make-up (always taking into account safety limitations). This is because a higher investment in metallic alloys and welding techniques could yield a higher capital cost during reactor construction but consequently lead to lower make-up investments faced during operation due to a lower leak rate of the primary coolant. The leakage data, respectively 0.1 wt%/day for Dragon and 0.3 wt%/day for the HTTR, is valid during normal operation. No data has been found about allowed helium leaks during maintenance and other outage activities. Outside of the normal operation range the helium losses are expected to be higher even though they could not be economically quantified in this study. Although the HTTR would accept a higher loss rate, some periodic inspections have registered a lower loss rate, as can be seen from the next picture.

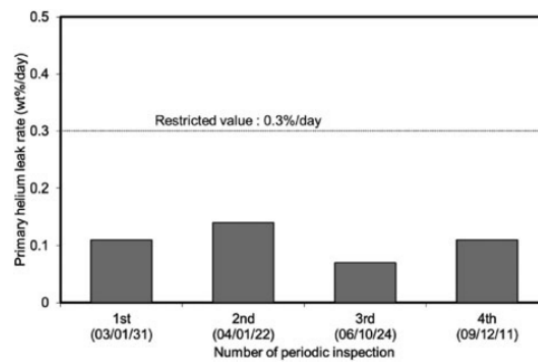


Figure 18 Measured helium leak rate in the HTTR during different periods compared to the restricted rate of 0.3 wt%/day (Tochio, Shimizu, Hamamoto, & Sakaba, 2014).

7.2.3 Purification and chemistry control costs

In this section, the cost of the purification of the primary helium coolant is estimated. As described in the previous sections of the report, the presence of large quantities of graphite in the core makes it the largest sink for collecting

and holding impurities in all HTGR designs (Wright, 2006). The other most important system for helium purification is the Helium Purification System (HPS). By design, the HPS should be able to execute the following actions (Castle, 2010):

1. Remove all the targeted impurities using a bypass loop whose location and flow rate have to be analyzed and determined. As a rule of thumb, it must be considered that a HTGR requires the whole helium inventory in the primary circuit to be purified in the HPS every 24 hours.
2. Control the oxygen potential so that the chemistry of the primary circuit can be left unaltered and the free metal surfaces can be protected from the harsh temperature conditions in the reactor.
3. Allow the depressurization of the primary loop in 24 hours after shutdown. The required purification fraction is $2.9 \cdot 10^{-5}$ per second (syphoned off mass flow rate divided by the total circulating helium mass).

Before analyzing the capital costs related to the installation of the HPS, the functioning of the system is described, presenting the current solutions and some of the choices that must be done from an engineering and economical point of view. It must be considered that the HPS is one of the key subsystems for reactor operation but it is not considered safety grade because it can be fully isolated in case of a leak (Yao, Wang, Liu, He, & Li, 2002). However, it is one of the most important support systems for HTGR operation, and it is useful for post-accident management such as during a water ingress into the primary circuit (Priambodo, Pancoko, Sriyono, & Setiadipura, 2018).

The HPS purifies helium from its impurities in a multi-step process that exploits the physical and chemical properties of helium as well as of its diverse impurities. Various subsystems are present in a HTGR HPS and each of them serves a different scope. In this regard, there have been different approaches to the purification of the helium coolant and consequently the design of the HPS has varied in time. The different HTGRs which have been built in the U.S. and worldwide present different subsystems and components based on the chemistry requirements as well as the developed commercial techniques of the time and location. Some of the different strategies adopted have been more successful than others as in some cases HPS constituents have been proven less effective than expected and are currently not foreseen to be used anymore in future builds. Nevertheless, the majority of the subsystems have proven reliable within different helium-cooled reactors and are expected to be used again in the next installations. Those components have been identified and highlighted in this section. Table 46 presents the specifics of all the subsystems used in the HPS of a HTGR and every component function is being described. Operationally successful and unsuccessful components are included in the Table and the approach for helium purification used in the nuclear fusion research has also been included. Note that the components are analyzed in the order which follows the sequence the helium flow encounters when entering a HPS loop.

Table 46 List and description of the main subsystems which have been historically considered when designing a helium HPS (Castle, 2010) (Berka, et al., 2012) (Olson, Brey, & Swart, 1980) (Legros, et al., 2006) (Liger, Lefebvre, Ciampichetti, Aiello, & Ricapito, 2011) (Gastaldi, Liger, Robin, & Poletiko, 2006) (Ciampichetti, et al., 2010) (Tincani, et al., 2019) (Shin, et al., 2023) (Idaho National Laboratory, 2010).

Component or subsystem	Performed operation	Temperature	Reactor/loop	Comments
Particle filter	Mechanically remove debris.	< 280 °C	HTTR, HTR-10, FSV, MHTGR, NRI	The mechanical filter is usually 5 μm so that corrosion products, dust and radioactive particles (including ⁵⁹ Fe, ⁶⁰ Co) can be trapped. FSV had a specific potassium hydroxide impregnated charcoal

			Rez, HELITE, RDE.	filter designed to remove FPs and particulate matter larger than a few microns. Some tritium was also removed there. The mechanical filter can be present both at the beginning and at the end of the circuit, before the circulator. Adopting this configuration both the traps and the blower can be protected from possible debris and dust coming from the molecular sieve and the other adsorbers.																
Pre-charcoal trap	Adsorption of FPs.	280 °C	HTTR.	Few information is known about the pre-charcoal trap and its chemistry principles as adopted in the HTTR.																
Copper oxide fixed catalyst beds	H and CO are converted to H ₂ O and CO ₂ .	250 °C – 280 °C	HTTR, HTR-10, MHTGR, NRI Rez, HELITE, RDE, Peach Bottom.	<p>The copper oxide bed is usually designed for 2000 hours of operation. Some of the CuO bed characteristics have been reported below:</p> <table border="1"> <tr> <td>Molar mass</td> <td>79.5 g/mol</td> </tr> <tr> <td>Relative density</td> <td>6390 kg/m³</td> </tr> <tr> <td>Bed Apparent density</td> <td>1810 - 1813 kg/m³</td> </tr> <tr> <td>Bed porosity</td> <td>0.6</td> </tr> <tr> <td>Internal particle porosity</td> <td>0.5</td> </tr> <tr> <td>Pore diameter</td> <td>1.2 × 10⁻¹⁰ m</td> </tr> <tr> <td>Particle mean diameter</td> <td>0.8 - 2 × 10⁻³ m</td> </tr> <tr> <td>Grain mean diameter</td> <td>1.9 × 10⁻⁷ m</td> </tr> </table> <p>On the efficiency of the CuO bed, experiments performed in CEA have highlighted a complete oxidation of hydrogen. The regeneration of the copper oxide is quite complicated and it is performed by oxygen injection. Part of the complication is due to the need to remove the residual hydrogen to avoid potential explosive reactions when in contact with O₂. A prior flush using helium or vacuum is performed to remove traces of H₂ and the same process is repeated after regeneration (with helium or vacuum) to remove O₂. The regeneration process will lead only to a maximum yield of regeneration of 55% in weight. This issue can be potentially solved by bed size overestimation. Another problem during CuO regeneration is the agglomeration of Cu and CuO during the different reaction–regeneration phases that, over a long time, could lead to big pressure drop in the system. A possible supplier of CuO mentioned by the literature is Merck.</p>	Molar mass	79.5 g/mol	Relative density	6390 kg/m ³	Bed Apparent density	1810 - 1813 kg/m ³	Bed porosity	0.6	Internal particle porosity	0.5	Pore diameter	1.2 × 10 ⁻¹⁰ m	Particle mean diameter	0.8 - 2 × 10 ⁻³ m	Grain mean diameter	1.9 × 10 ⁻⁷ m
Molar mass	79.5 g/mol																			
Relative density	6390 kg/m ³																			
Bed Apparent density	1810 - 1813 kg/m ³																			
Bed porosity	0.6																			
Internal particle porosity	0.5																			
Pore diameter	1.2 × 10 ⁻¹⁰ m																			
Particle mean diameter	0.8 - 2 × 10 ⁻³ m																			
Grain mean diameter	1.9 × 10 ⁻⁷ m																			

Cooler and Moisture separator	Cooling of the helium coolant and moisture separation.	From 250 °C to 20 - 40 °C	HTR-10, MHTGR, FSV, RDE.	Moisture separation is normally unimportant during normal operation as the relative humidity of the primary helium coolant is very low, even if the flow is cooled to 20 °C as in the HTR-10. Moisture separation plays a role during operation even though its operation is more relevant in case of tube ruptures. In the FSV reactor, the water collected in the tank is then dumped to the radiological waste system. An additional moisture separator and cooler can be also added for increased safety in case of water entry in the primary circuit as it has been done in RDE. Such solution has been considered in the economical calculations performed later.												
Molecular sieve trap	Captures H ₂ O and CO ₂ , NO _x and CH ₄ .	Between 20 (ambient temperature) and 49 °C	HTTR, HTR-10, HELITE, RDE, Peach Bottom, FSV, NRI Rez.	<p>The molecular sieve is designed to adsorb the impurities. Some of the molecular sieve characteristics have been reported below:</p> <table border="1" data-bbox="889 842 1425 1052"> <tr> <td>Pore volume</td> <td>0.3 cm³/g</td> </tr> <tr> <td>Mean pore diameter</td> <td>5 Å</td> </tr> <tr> <td>Particle size</td> <td>1.6 mm</td> </tr> <tr> <td>Specific surface</td> <td>700 - 800 m²/g</td> </tr> <tr> <td>Internal porosity</td> <td>50%</td> </tr> <tr> <td>Apparent density</td> <td>700 kg/m³</td> </tr> </table> <p>Based on the information provided by a test loop at CEA, the maximum amount adsorbed on the molecular sieve is about:</p> <ol style="list-style-type: none"> 1. 150 g of water per kg of molecular sieve 2. 50 g of CO₂ per kg of molecular sieve 3. 30 g of NO_x per kg of molecular sieve <p>Such data has been used for the calculation of the required mass of CuO in the modelled HPS for economic calculations, in the following sections. More information over the modelling of the sieve is present at the same source. Regeneration for a molecular sieve is accomplished by reducing the pressure around the trap and heating it to temperatures above the normal operating temperatures (approx. 300 °C). The elevated temperature is maintained for an extended period of time until the carbon dioxide and water are extracted. Possible suppliers are various. Zeochem Z5-01 was used by KAERI while Sylobead (Grace) was used by ENEA. After a compared study between 1/8 inch and 1/16 inches (3.2 – 1.6 mm) pebbles, the ENEA designers have selected the</p>	Pore volume	0.3 cm ³ /g	Mean pore diameter	5 Å	Particle size	1.6 mm	Specific surface	700 - 800 m ² /g	Internal porosity	50%	Apparent density	700 kg/m ³
Pore volume	0.3 cm ³ /g															
Mean pore diameter	5 Å															
Particle size	1.6 mm															
Specific surface	700 - 800 m ² /g															
Internal porosity	50%															
Apparent density	700 kg/m ³															

				second option to allow a more compact design of the column.												
Cold charcoal trap	Adsorption of noble gases such as krypton and xenon other than residual CO ₂ , CH ₄ , N ₂ , H ₂ .	Between -160 and -190 °C	HTTR, HTR-10, FSV, MHTGR, HCPB and HCLL TBMs, HELITE, FSV, Peach Bottom, NRI Rez	<p>Some of the activated carbon bed characteristics have been reported below:</p> <table border="1"> <tr> <td>Pore volume</td> <td>0.6 cm³/g</td> </tr> <tr> <td>Mean pore diameter</td> <td>24 Å</td> </tr> <tr> <td>Particle size</td> <td>2 - 5 mm</td> </tr> <tr> <td>Specific surface</td> <td>1100 m²/g</td> </tr> <tr> <td>Internal porosity</td> <td>55 - 75%</td> </tr> <tr> <td>Apparent density</td> <td>450 kg/m³</td> </tr> </table> <p>For an effective removal of fission products, the helium flow has to be cooled below -70°C. At very low temperatures, around -190°C, many noble gases are removed from the coolant and the beds can effectively remove hydrogen from the helium coolant. For regeneration purposes, helium is extracted from the bed, and a vacuum pump reduces the pressure to 10 kPa in the cold trap columns. Subsequently, the column heating process is performed in two stages to minimize thermal stress. Initially, liquid nitrogen is removed, and room temperature air is introduced into the external chamber until the column temperature reaches 0°C. Next, the air is heated using a resistance to raise the column temperature to 150°C, facilitating the regeneration of the adsorbent.</p>	Pore volume	0.6 cm ³ /g	Mean pore diameter	24 Å	Particle size	2 - 5 mm	Specific surface	1100 m ² /g	Internal porosity	55 - 75%	Apparent density	450 kg/m ³
Pore volume	0.6 cm ³ /g															
Mean pore diameter	24 Å															
Particle size	2 - 5 mm															
Specific surface	1100 m ² /g															
Internal porosity	55 - 75%															
Apparent density	450 kg/m ³															
Heated getter	Adsorption of impurities at high temperature and diffusion towards the bulk.	400 °C or less.	-	<p>The use of a heated getter has been proposed for HPS of fusion systems. Their introduction into the nuclear fusion research has been facilitated as the temperature of operation of these getters has been lowered from 700 °C to 400 °C or less. In the getters all impurities react on the surface forming stable compounds which then diffuse toward the bulk of the material. Increasing the temperature, hydrogen and its isotopes (tritium included) can be extracted from the getter while the extraction of other elements cannot be performed. The getter material can run also at room temperature, but its capacity would be reduced as the diffusion towards the bulk is slower and the surface adsorption could be saturated. Complete regeneration is not possible and the column has to be replaced. SAES has patented a heated getter which has been considered for fusion applications by the literature.</p>												

				The use of a heated getter for HTGRs could be evaluated as well based on the properties of the material and the capacity of adsorbing fission products and tritium as well.
Hydrogen getters	Remove hydrogen and tritium.	40 °C	FSV	FSV had two parallel hydrogen getters made of hot titanium sponge material. Their scope was to remove hydrogen and tritium by adsorption. Gettering often involves the use of a base metal, such as titanium, which is able to dissolve hydrogen and form metal-hydrogen phases or hydrides within the base metal. Hydrogen getters use base metals that strongly bond with hydrogen and have a low equilibrium pressure of hydrogen at the operating temperature. Other materials have been identified as good potential base materials for getters are zirconium, lanthanum, cerium, yttrium, and uranium. Material cost is a major consideration for use in hydrogen getters. The sponges did not work well for FSV as they were frequently deactivated by N ₂ impurities at FSV. Nevertheless, there were no operational consequences because H ₂ and H ₃ were absorbed in core graphite. The titanium getters were highly ineffective in FSV and are not expected to be used again.

In addition to the subsystems listed in Table 46, some others have been recurrently recognized in different HTGR designs even if not strictly relevant to the purification of helium. Those are the gas chromatograph, dew point analyzer, helium circulator, an emergency circuit for humidity dispersion in case of water ingress (as suggested by RDE development), heat exchangers, valves. The gas chromatograph and the impurity sensor are essential for HPS operation and could be placed at selected locations in the helium purification tram. Quantities of impurities have to be analyzed by a gas chromatograph every two hours during any reactor power level change, and at intervals as long as four hours at steady state levels (Yao, Wang, Liu, He, & Li, 2002). The emergency circuit is not always present in every HPS but can help in dealing with the entry of a great quantity of moisture from the external environment by working on its removal. This circuit is composed by a moisture separator and a molecular sieve which can withstand a large quantity of water entry in the primary circuit. Heat exchangers are useful to decrease/increase the temperature of the helium flow and allow certain chemical processes in the respective subsystems so that impurities can be effectively removed. Given that some of the components mentioned in Table 46 are redundant and positioned in parallel lines (so that continuous operation and regeneration of one of the two are possible), on-off valves are necessary to block or allow the flow in one of the units. Moreover, a specific and safety relevant (ASME III proven) valve must be positioned at the entry of the loop so that the HPS can be isolated if a pipe leak occurred. Finally, a circulator must also be installed to cope with the pressure losses of the HPS traps.

The HPS can be installed at different locations in a HTGR. A choice can be made by analyzing the areas of major impurity ingress or accumulation in the primary circuit. The purified helium can then re-enter the system in some selected locations by having it blown over seals to remove debris from various areas. Various choices have been made in past operational HTGR as displayed in Table 47 (Castle, 2010).

Table 47 Location of HPS installation in different HTGRs

Reactor	Location of Helium Removal
HTTR	Auxiliary heat Exchanger
Peach Bottom	Reactor and SG
FSV	Reactor inlet plenum
GT-MHR	Outlet of high-pressure compressor

As part of the NGNP project, the locations of greatest promise were recognized to be the reactor and in the SG. The reactor location is ideal as it can help in continuously removing the contaminants born in the core and escaping from it. On the other hand, siphoning off helium from the SG creates a great advantage in removing possible moisture ingress from the secondary side and allows the removal of water in case a SG tube break would happen preventing humidity to reach other parts of the primary system. FSV and Peach Bottom HPSs have both been designed to remove helium from the core and both have been operating successfully, suggesting the choice for the syphoning off could be done in those locations for future builds (Castle, 2010).

Other design factors for a HPS are the size and the flow rate. As mentioned before, the HTGRs are required to filter and store the entire capacity of the primary circuit in a 24-hour period i.e., roughly 4% of the primary circuit volume per hour (Castle, 2010). In this selection, there are advantages and drawbacks to be considered. In case the HPS was over-designed (providing excess purification capacity) the helium chemistry would indeed be maintained with a higher accuracy and reliability but the front capital costs will increase and the efficiency of the HTGR would also be lower due to the removal of additional helium coolant from the primary system. On the other hand, in case the HPS was under-designed the cost of maintenance could increase during the HTGR operation and difficulties may arise during operation. In any case, the HPS design must always meet the minimum required purification requirements to guarantee a certain purity level.

To determine the capital investment cost for the realization of a HPS in a HTGR, a reference HPS must be selected. This is because both the selection of the components differs between HTGRs but also because they have a different size which leads to a different pricing. Nevertheless, as discussed in the preceding sections, different reactors might use different subsystems for helium purification. This complicates the cost estimation of a “reference” plant which could be representative of HPS costs. Therefore, we designed a new, “potentially installable” HPS to be able to categorize each component and evaluate the cost of each subsystem. The design of the HPS has been done by considering the recurrent techniques in the operational HTGRs, test loops and planned HPS for fusion applications. It can be stated that the considered HPS could be installed in a newly built HTGR if the technical and engineering details are further developed. In fact, the design of such system, is beyond the scope of this project. Consequently, some technical information regarding the components is currently missing and would require further research for completeness. For this reason, the cost of some components presents uncertainties or might be identified within a range of values. The composition and structure of the selected HPS are developed mostly based on three main HPS designs: FSV, HTR-10 and HTTR.

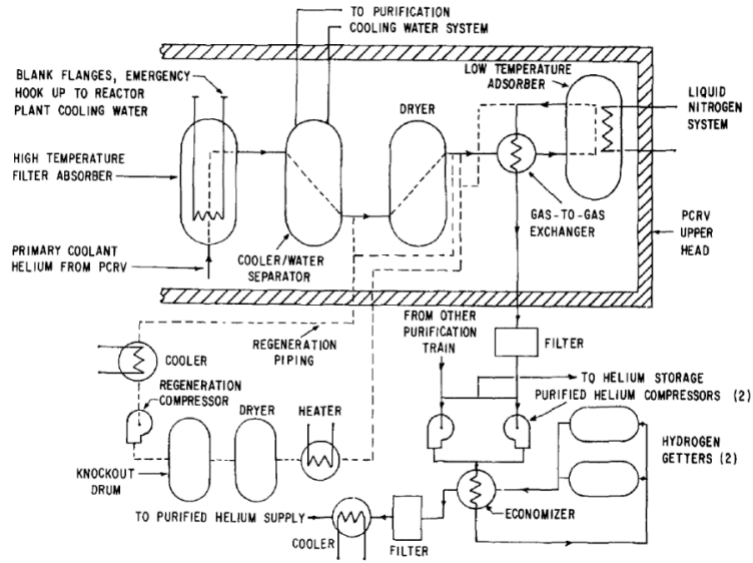


Figure 19 Schematic of the Fort St Vrain HPS (Olson, Brey, & Swart, 1980).

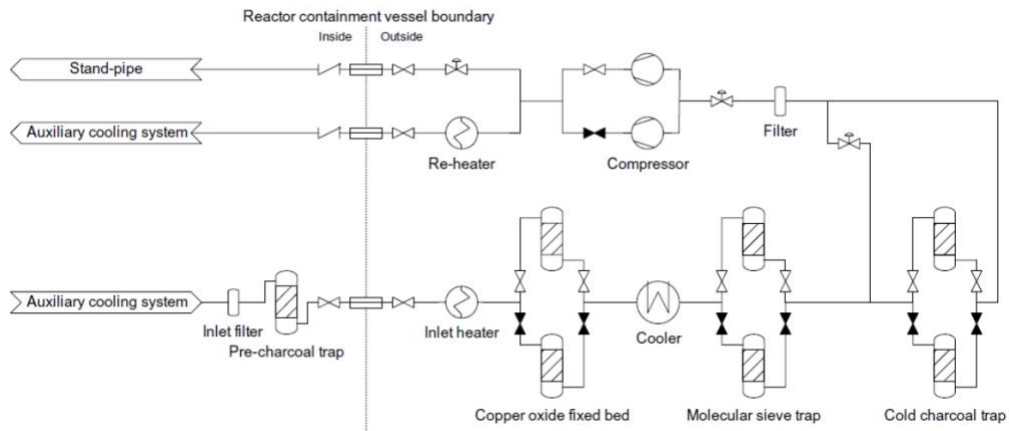


Figure 20 Schematic of the HTTR HPS (Fujiwara, 2021).

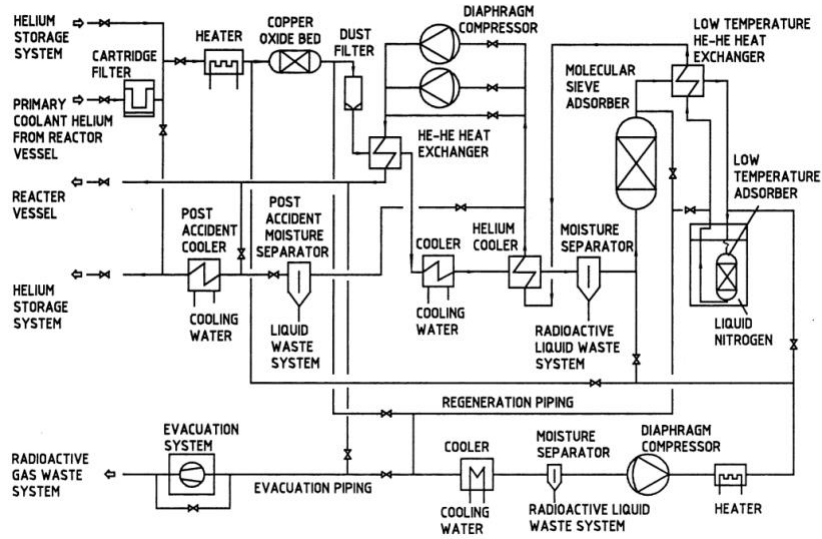


Figure 21 Schematic of the HTR-10 HPS (Yao, Wang, Liu, He, & Li, 2002).

The HPS scheme considered for the subsequent economic analysis is the following:

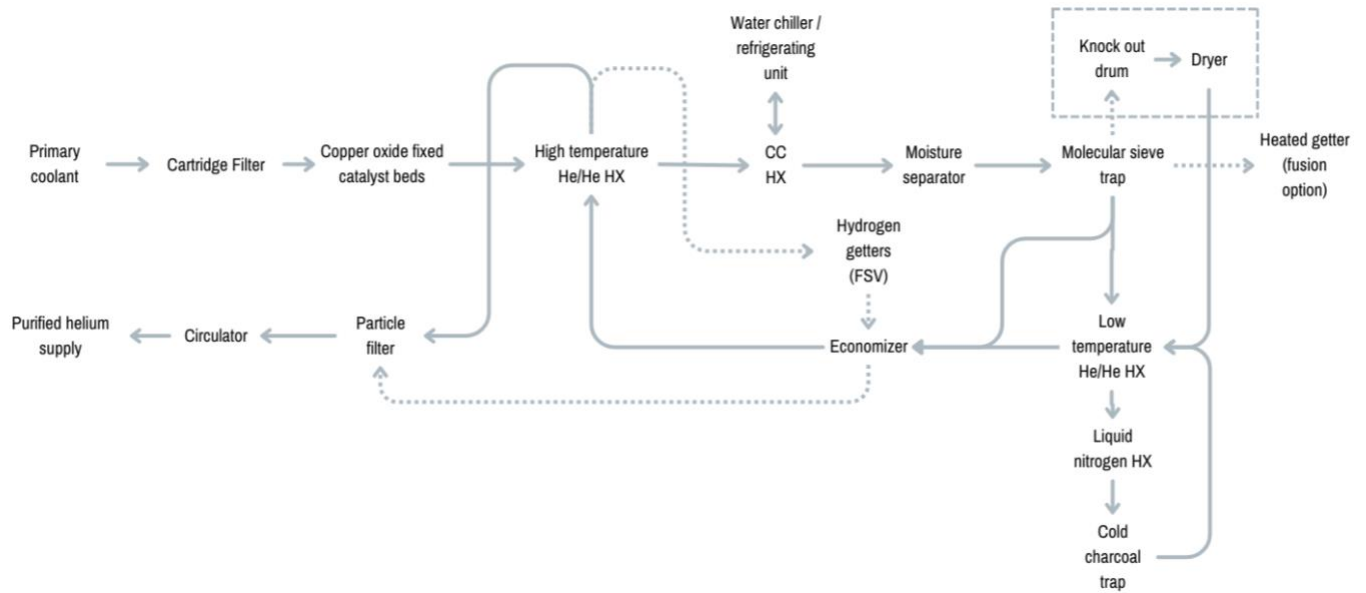


Figure 22 Designed HPS considered for subsequent economic evaluation.

As it can be seen from Figure 22, the helium flow will enter the HPS loop firstly encountering the 5 μm cartridge filter. The HPS has been designed so that it can nominally purify a flow rate of 200 kg/h of helium coolant entering at a temperature and pressure conditions respectively of 250 - 280 $^{\circ}\text{C}$ and 4 MPa. The same flow rate has been used for the HTR HPS which can purify 10% of the total helium inventory in an hour. After passing through the one-meter-long

cartridge filter for the removal of possible metallic debris, a CuO bed will convert the major impurities such as H and CO into CO₂ and H₂O. The conversion process, common to the majority of the analyzed HTGRs, will happen at a temperature between 250 and 280 °C. The oxidation of the impurities is necessary for them to be later adsorbed in the molecular sieve trap. Before that, the flow is cooled down to 90 °C in a high temperature counter current He/He HX. The HX, given the presence of highly pressurized gases on both sides, is a shell and tube heat exchanger. The helium flow is then further cooled down to ambient temperature by passing through a water-He counter current HX. The water, running through a closed loop, is being cooled by a water chiller using 513A as refrigerator. The flow is then ready to pass through a moisture separator and a molecular sieve so that CO₂ and H₂O are effectively removed. Please note that the efficiency of the traps in the removal of the impurities is strictly dependent on the velocity of the flow and the configuration of the beds. When designing an HPS for an existing HTGR, such conditions have to be accounted to maintain the target chemistry inside the primary circuit. Such level of technical detail was considered to be beyond the scope of the report which mainly focused on the calculation of the necessary mass of reactant on every trap to calculate the related cost. After the molecular sieve trap an emergency system has also been designed to additionally filter off the helium flow in case of major water entries. The emergency line, which activates in case of pipeline break and detection of a high level of moisture in the system, is composed of a knock out drum and an additional moisture separator (dryer). The emergency system has been designed to be able to conservatively remove 600 kg of water as described in the proceedings of (Zhipeng, Yan, & Yanhua, 2020). A dashed line from the molecular sieve shows the path that is currently being investigated for fusion HPS development, going to the heated getters (which will probably include a heating system to get to the necessary temperature of 400 °C (Ciampichetti, et al., 2010). Getting back to the designed path of the HPS, the flow of the HPS is split at this point. From the 200 kg/h flow, 50 kg/h of the main flow will be directed to a cryogenic system while the rest will recombine with the cold helium at the output of the cold trap. The helium entering the cryogenic trap is to be cooled in two consecutive steps first to -170 and then to -190 °C. The first step of the cooling leverages of a low temperature 45-50 kW He/He HX which uses the helium at the output of the cold trap to cool the input flow. Getting to the required -190 °C is then possible thanks to a liquid nitrogen HX. The goal of the subsequent cold bed, operating at a maximal pressure of 4 MPa and a minimal pressure of 3.3 MPa (accounting a maximum pressure loss of 0.7 MPa (Gastaldi, Liger, Robin, & Poletiko, 2006)) is to remove noble gases such as krypton, xenon, nitrogen and hydrogen gases by liquifying them at a temperature lower than their boiling point at their corresponding partial pressure. After filtration, the flow is heated in the He/He counter current HX before rejoining the rest of the flow rate at a temperature of approximately 0 °C. The total helium flow will again be heated up to 180 °C by first entering into an economizer to reach ambient temperature, and then going into the high temperature He/He HX. The flow goes into another 40" (~ 1 meter), 5 µm cartridge filter to finally enter the helium circulator. The blower has been sized considering a maximum pressure head loss of 0.7 MPa (Gastaldi, Liger, Robin, & Poletiko, 2006). Its final cost has been later estimated using the correlations mentioned in (Stewart, Velez-Lopez, Wiser, & Shirvan, 2021). As it can be seen from the scheme of the HPS proposed in Figure 22, a dashed line has been added after the high temperature He/He HX to highlight the path that the HPS loop would follow in case the hydrogen getters adopted in FSV are to be included in the system. As mentioned in Table 46, the getters are no longer foreseen to be used in new builds as they proved ineffective (Castle, 2010). The molecular sieve as well as the CuO bed and the cold trap are redundant so that regeneration and maintenance are possible while operating. The number of valves which could be installed in the proposed system is between 12 and 14. Given the need for operating in on/off conditions, gate valves have been considered.

Table 48 summarizes the cost of the components included in the HPS or related to its functioning:

Table 48 Capital cost estimation for a HPS capable of filtering a helium flow of 200 kg/h at an input pressure and temperature of 4 MPa and 280 °C.

System	Subsystem	Unit Cost [2024 USD]	Supplier	Units needed	Comments
Main HPS loop	Filter	9500 + custom high temperature gasket	Pall Corporation (US)	2	High uncertainty on the cost of the HT gasket as it should be customized based on the technical specifics of the loop. The cost of the gasket can vary between 2 and 100K \$.
	Copper oxide pellets	800 – 3100 /cycle	-	2	The cost of the copper oxide and the molecular sieve is conservatively calculated assuming the helium goes in the loop with the highest operational impurity levels previewed for NGNP HTGR and goes out at the minimum level. Given the planned cycle is 2000 hours, power re-start represents just a small contamination for the beds based on data from HTTR (Japan Atomic Energy Agency, 2010). For the molecular sieve, Zeolite 5A 1.6 – 2.5 mm pebbles and 1/16 pellets are considered.
	Molecular sieve	900 – 950 /cycle	Jalon (CHN), Zeochem (US), Grace WR & Co (US).	2	
	Moisture separator	20,000	Factory Direct Pipeline Products (US)	1	The moisture separator complies with ASME VIII requirements (the HPS is not safety relevant). The minimum efficiency for the moisture separator is assumed to be 90% for designing the other components.
	Water chiller	290,000	Ellis & Watts (US)	1	The chiller is provided with a water-cooled condenser and reciprocating compressor. It is designed to operate on R-513A refrigerant on 480V and 60 Hz power. The condenser will be a shell and tube HX in copper/carbon steel complying with ASME VIII. The water flow rate is 30 gallons (~ 0.11 m ³) per minute. The evaporator is set to be a copper/carbon steel shell and tube HX as well compliant with ASME VIII. The compressor

					comprehends four cylinders, with unloaders on two of them to allow for operation at 50% capacity.
Cold bed	35 /lb	HI-Q (US)	2		Cost of the impregnated carbon which main characteristics were mentioned in Table 46.
	>700,000	Criotec Impianti Criogenici (ITA)			The cost refers to a similar unit built by Criotec for the nuclear fusion industry with a flow rate of 200 Nm ³ /h at a pressure of 300 bar. The price for the unit requirements which are analyzed here is projected to be higher.
Heat exchangers	160,000 – 250,000	Precision Custom Components (US) – Radiological solutions (US)	3		Counter-current shell and tube HX complying with ASME VIII code.
Economizer	4500	-	1		The price is taken as a reference from the cost analysis of sodium.
ASME III Valve	80,000 – 100,000	Conval Inc. (US)	1		A certified ASME III valve has to be placed at the entry of the HPS to isolate the loop in case of pipeline break. The other valves are gate valves working in on-off condition based on the status of the traps which can be either in operation or regeneration.
ASME VIII Valve	25,000 – 40,000	Velan Inc. (CAN)	12 - 14		
Helium Blower	790,000 – 800,000	-	1		Conservatively estimated using estimations coming from (Stewart, Velez-Lopez, Wiser, & Shirvan, 2021). The circulator power is calculated with: $P [W] = \frac{Q * F}{\eta}$ Where Q is the pressure head loss, F the mass flow rate and η the circulator efficiency.
Hydrogen getters (FSV)	11 – 19 /piece*	SAES getters (ITA, present in US as well)	-		Titanium based hydrogen getters were included in the HPS design of FSV even though they are not foreseen to be used again. The quote refers to SAES getter SG/COMBO3/28-7/31020. SAES has manufactured getters for nuclear applications in the past as described in (Nigrey, 2000). Nevertheless, their application at

					higher temperatures is still to be demonstrated.
Instrumentation	Dew Point analyzer	60,000 – 70,000	Mitchell Instruments (US)	2 (min)	This is the foreseen cost for 3-channel dew point analyzers for ALLEGRO development.
	Gas chromatograph	67,000 – 85,000	ThermoFisher Scientific (US)	1	-
Emergency circuit	Knock-out drum	90,000 – 95,000	Schultz Process Services Inc (US).	1	Stainless steel vertical gas separator compliant with ASME VIII code. The price is conservatively estimated based on the accident analysis described in (Zhipeng, Yan, & Yanhua, 2020).
	Dryer (MS)	80 - 100	-	1	The possible suppliers are the same pointed out above for the main molecular sieve.

*Every SG/COMBO3/28-7/31020 piece weighs 6.3 grams and it's made of BaLi₄/CaO/Co₃O₄ in a stainless steel container.

Summing up the costs analyzed in Table 48 considering the expected installed units, the total cost of such HPS installation is set to be in the range between 4,700,000 and 6,000,000 in 2024 USD considering a project contingency of 30% as assumed for the sodium coolant system.

By adjusting the helium purification cost calculations performed for the Modular Helium Reactor (MHR) Program, we get a price of 4,900,000 for the target plant (close to a FOAK) steam cycle MHR (SC-MHR) and a price of 5,000,000 for the target plant direct cycle gas turbine MHR (DC GT-MHR) (Gas-Cooled Reactor Associates, 1993). The plants are designed to produce respectively 693 MWe and 869 MWe. Even though the inflated prices from (Gas-Cooled Reactor Associates, 1993) fall within the calculated cost range for the HPS we designed, it is hard to compare the systems as the proposed HPS could be used for a smaller reactor like the HTTR (only 30 MWth) or a bigger one. This is because the modeling of the HPS depends on:

- The helium inventory. As it can be seen from Table 44, different reactors have a different helium inventory depending on their design and that influences the amount of helium which has to be purified and consequently the size of the HPS.
- The selected flow rate at the entry of the HPS. NGNP suggests to maintain a flow rate of 4%/h to be able to purify the entire inventory in 24 hours-time. Nevertheless, some reactors like the HTTR purify 10% of it every hour while others, like the MHTGR, just the 0.07%/h (Castle, 2010).

Given the reasons specified above, the cost estimation provided in this chapter cannot be normalized with the reactor's power output as the same system could be used for reactors of different sizes and designs.

8. Decommissioning costs

As stated in the Introduction, decommissioning costs for each coolant type have not been included in this report. This exclusion is primarily due to the fact that many reactor coolants and designs considered here have not yet been commercialized, and some have not even been demonstrated. Consequently, decommissioning acceptance criteria have some “gray areas” and vary by country. Moreover, the possible costs related to the decommissioning of the coolants have been found to have a relatively small impact on the total costs compared to the initial coolant purchase and installation of purification systems, which are also foreseen to have a relatively small impact on the total reactor cost, perhaps with the exception of microreactors or small demonstration plants.

The impact on the total costs was investigated considering the concepts of Net Present Value (NPV) and Future Value of Annuity (FVA). The NPV is a financial metric used to assess the profitability of an investment or project by calculating the difference between the present value of cash inflows and the present value of cash outflows over a period of time. For decommissioning calculations, the NPV calculation would determine the amount of money needed today to cover future decommissioning costs. So, if it is known that we require an amount V_n after n years (e.g., at the time of decommissioning), considering a discount rate of r , we can estimate the amount V_0 that has to be invested now (i.e., the NPV) of the amount V_n with the formula:

$$V_0 = \frac{V_n}{(1 + r)^n}$$

On the other hand, the FVA is the total value of a series of recurring payments at a specified date in the future, assuming a particular rate of return or interest rate. For decommissioning calculations, it shows how a series of equal payments will grow over time when invested at a given interest rate. The equation for the FVA is:

$$V_n = P * \frac{(1 + i)^n - 1}{i}$$

Where V_n is the amount required (e.g., at the time of decommissioning), P is the amount paid per period, n is the number of periods of time and i is the interest rate. To quantify the impact of decommissioning on the total costs, V_n was assumed to be equal to one tenth of the initial investment costs related to nuclear grade coolant purchase and purification systems installation. This hypothesis is formulated considering that the estimated decommissioning costs for a nuclear reactor in the U.S. range between 300 and 400 million USD, while installation costs for a medium to large-sized reactor are in the order of a few billion USD (World Nuclear Association, 2022). The results of the calculations can be displayed in Figure 23.

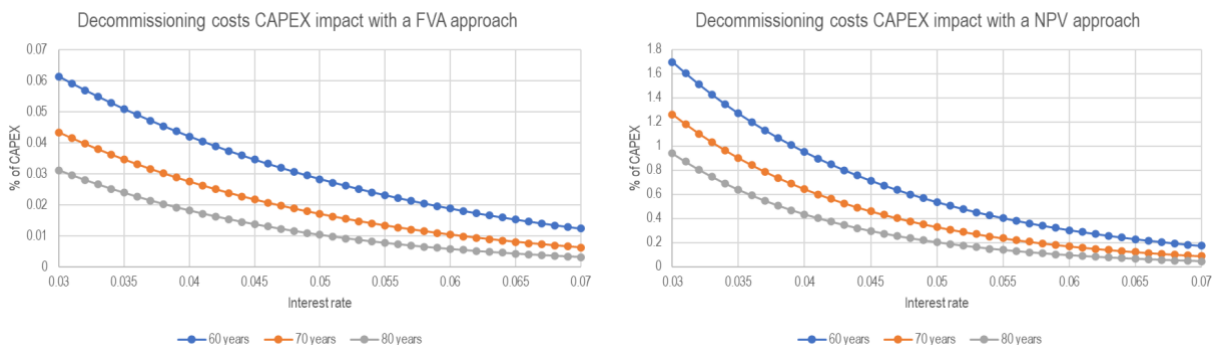


Figure 23 Decommissioning costs analyzed with FVA and NPV approaches

As shown in Figure 23, the FVA approach indicates that, with an interest rate varying between 0.03 and 0.07, the yearly investment required to cover decommissioning costs (assuming initial capital investments are equal to ten times the decommissioning costs) ranges from 0.06% to 0.003%. This variation depends on the interest rate and the reactor's lifetime. On the other hand, the NPV approach, with a discount rate varying between 0.03 and 0.07, indicates the total initial investment required to cover decommissioning costs ranging from 1.7% to 0.04%. This variation, as well, depends on the interest rate and the reactor's lifetime. Considering the most conservative approach possible, simulating a 60-year plant lifetime with a 0.03 discount/interest rate, the decommissioning costs could vary between the 1.6 and 3.7% of the initial CAPEX costs, considering respectively the NPV and FVA approach. Clearly, even considering the most conservative case, the costs of decommissioning have a relatively small impact with respect to the total required CAPEX. This justifies our assumption of not considering them while evaluating the costs related to the lifetime of advanced reactors' coolants.

9. Conclusion and future work

In conclusion, the costs associated with purchasing nuclear-grade coolants and maintaining the necessary purity of these throughout the reactor's lifetime have been analyzed. Overall, the capital investment required for the initial purchase of nuclear-grade coolants varies significantly among different types. Water, sodium, lead, terphenyls (organic coolant) and LBE are the least expensive, on a unit mass basis. Contrarily, helium and FLiBe are found to be considerably more expensive. The reasons for these cost differences are:

- Helium: Currently there is a very high demand, especially in the medical industry, of a naturally limited gas which production process is limited and inefficient because of the extremely high volatility of helium. Even though the world's overall production of helium is set to increase significantly in the next years to ensure lower consumer costs and some specific sectors development, there is currently a high uncertainty about the U.S. future trends.

- FLiBe: The cost of FLiBe is the highest among the coolants analyzed in this report, primarily due to the need for Lithium-7 enrichment, which lacks a substantial market in the U.S. However, the cost per kilogram of FLiBe is expected to decrease in the coming years, as companies like Kairos and Copenhagen Atomics are developing more efficient methods for salt production and coolant purification.

The cost of coolant purchase within different nuclear facilities/reactors decreases with the size of the facility as expected based on the economies of scale. On the other hand, the cost related to the purification systems installation is found to be in the order of units or tens of million USD for the coolants considered. The same costs, normalized in \$/kg, can widely differ between different reactor designs because of the different coolant’s mass and density. For this reason, a comparison within the cost of different purification systems installation is not relevant. This is also because they have different requirements in terms of frequency of operation, extracted coolant quantity, chemistry and purity, etc.

The main operating costs have also been analyzed. Overall, there is just a few historical operating data as the reactor types included in this report (except for LWRs) have never been built in the U.S. or have not been licensed in more than 50+ years. Nevertheless, the analyzed purification systems are not foreseen to require a high level of maintenance and the cost impact of preservation, reparation, and regeneration operation is not expected to be particularly high compared to other costs related to reactor operation. The most data on operating costs have been found for helium and organic coolants.

The main results of this research are summarized in Table 49. To highlight the cost differences associated with the installation of a purification system in an organic-cooled reactor, two cases were analyzed under the section “Organic Coolants.” the PNPf (left column) for which a CVCS is used, and the 15 MWth organic microreactor studied in (Shirvan, et al., 2023) (right), for which the entire coolant inventory is replaced periodically without requiring a purification system: the latter approach is far less expensive. To calculate the Levelized Cost of Coolant (LCOC) for helium, the CVCS costs were normalized using the 30 MWth HTR-PS as a reference for both the CVCS and LCOC calculations. This approach may lead to an overestimation, as the same HPS could support a larger reactor, as discussed in the relevant chapters.

Table 49 Summary of the main results.

Coolant	Lead	LBE	Sodium	FLiBe	Helium ^a	Water	Organic coolants ^b	
Target purity	99.97 %wt	99.97 %wt	99.9 %wt	99.76 %wt (99.995% enrichment)	99.999 %wt	Table 2	99.98 – 99.99 %wt	
Main impurities	O ₂ , CP ^c	Po, O ₂ , CP ^c	H ₂ , O ₂ , CP ^c	H ₂ , S, Cl ^d	H ₂ , H ₂ O, CO, CO ₂	Free radicals, Cl, F, S ₂ O ₄	HBs, O ₂ , H ₂ O	
Coolant weight [tons]	6,000 – 26,000	30 – 180	370 – 3,250	92	0.4 – 2	260	29 – 33	2.9
Capacity	400 – 2,800 MWth	30 – 210 MWth	62 – 1,500 MWe	100 MWe	115 – 400 MWth	1,144 MWth	45.5 MWth	15 MWth
Purchase cost [\$/kg]	2.2 – 3	6 – 15	2.6 – 13.6	1,530 – 2,670	170 – 205	0.21 – 0.32	22.5	

CVCS^e cost	0.44 – 0.57	0.48 – 0.62	17.32	57	2,380 – 3,000	138	47 – 72	0
Cost of makeup [\$/MW year]	-	-	-	-	1,000 – 6,300	-	20,000 – 28,000	880
LCOC^f [\$/MWh]	0.43 – 0.59	0.12 – 0.3	0.31 – 0.49	24 - 41	5.3 – 6.5	0.25	19 - 28	0.5

^aThe Helium costs are normalized using the 30 MWth HTTR-PS as a reference. This represents an overestimation as the designed HPS could potentially serve a bigger reactor. ^bPNPF reactor with the planned hydrocracking system (left) and the organic cooled microreactor analyzed in (Shirvan, et al., 2023) (right). Note that the microreactor has no purification system but replaces the complete coolant inventory every 5 years. The difference in the LCOC between these two organic-cooled concepts is partly attributed to the fact that the PNPF design (left) includes the costs of both the moderator and the coolant, whereas the microreactor design (right) excludes the cost of the moderator (which is heavy water in this concept). ^cCorrosion Products. ^dCarbonaceous Impurities. ^eChemistry and Volume Control System. ^fLevelized Cost Of Coolant.

Lastly, there are many possible improvements that can be considered as future work of this report, as follows:

- Calculation of the necessary operator costs for purification systems regeneration and maintenance;
- Evaluation of possible future trends for nuclear grade coolants costs, especially focusing on helium and LBE;
- Evaluation of the impact of purification costs on the total reactor costs at different reactor sizes.
- Evaluation of the possible strategies for Polonium-210 extraction in LFRs and the related costs;

Bibliography

- Akins, A., Kultgen, D., & Heifetz, A. (2023). Anomaly Detection in Liquid Sodium Cold Trap Operation with Multisensory Data Fusion Using Long Short-Term Memory Autoencoder. *Energies* 16, no. 13. Retrieved from <https://doi.org/10.3390/en16134965>
- Alemberti, A., Smirnov, V., Smith, C. F., & Takahashi, M. (2014). Overview of lead-cooled fast reactor activities. In *Progress in Nuclear Energy, Vol. 77* (pp. 300-307). Retrieved from <https://doi.org/10.1016/j.pnucene.2013.11.011>
- Ames, M. R. (2015). *Minor and Trace Elements in Flibe after Purification and Corrosion Testing*. Cambridge (MA), United States: Massachusetts Institute of Technology.
- Ames, M., & Hu, L. (2013). *Trace Elemental Analysis of Flibe by Neutron Activation Analysis in support of FHR Research*. Cambridge (MA), United States: Massachusetts Institute of Technology.

- Amy, J. (2023, May 25). *Georgia nuclear rebirth arrives 7 years late, \$17B over cost*. Retrieved from The Associated Press: <https://apnews.com/article/georgia-nuclear-power-plant-vogtle-rates-costs-75c7a413cda3935dd551be9115e88a64>
- Andreades, C., Cisneros, T., Choi, J. K., Chong, A. Y., Fratoni, M., Hong, S., . . . Peterson, P. F. (2014). *Technical Description of the "Mark 1" Pebble-Bed Fluoride-Salt-Cooled High-Temperature Reactor (PB-FHR) Power Plant*. University of California, Berkeley, Department of Nuclear Engineering.
- Aoto, K., Dufour, P., Hongyi, Y., Glatz, J. P., Kim, Y.-i., Ashurko, Y., . . . Uto, N. (2014). A summary of Sodium-Cooled Fast Reactor Development. In *Progress in Nuclear Energy, Vol. 77* (pp. 247-265). Retrieved from <https://doi.org/10.1016/j.pnucene.2014.05.008>
- Argonne National Laboratory. (2024). *Experimental Breeder Reactor-II*. Retrieved from Argonne National Laboratory: <https://www.anl.gov/eof/experimental-breeder-reactorii>
- Atomics International. (1960). *Final Safeguards Summary Report for the Piqua Nuclear Power Facility*. North American Aviation Inc. .
- Attarian, S., Morgan, D., & Szlufarska, I. (2022). Thermophysical properties of FLiBe using moment tensor potentials. In *Journal of Molecular Liquids, Vol. 368, Part B*. Retrieved from <https://doi.org/10.1016/j.molliq.2022.120803>.
- Ault, T., Brozek, K., Fan, L., Folsom, M., Kim, J., & Zeismer, J. (2012). *Lithium Isotope Enrichment: Feasible Domestic Enrichment Alternatives*. University of California, Berkeley, Department of Nuclear Engineering.
- Bassini, S. (2017). *Coolant Chemistry Control in Heavy Liquid Metal cooled Nuclear Systems*. Bologna, Italy.
- Beauchamp, F., Morier, O., Brissonneau, L., Courouau, J. L., Chabert, C., & Reyne, F. (2010). A review of lead-bismuth alloys purification systems with regard to the latest results achieved on STELLA loop. *OECD/NEA Workshop on Technology and Components of Accelerator Driven System*, (p. 20). Karlsruhe, Germany.
- Beck, J. M., & Pincock, L. F. (2011). *High Temperature Gas-cooled Reactors Lessons Learned Applicable to the Next Generation Nuclear Plant*. Idaho National Laboratory.
- Berganza, C., & Zhang, J. (2013). The role of helium gas in medicine. In *Med Gas Res 3, 18*. Retrieved from <https://doi.org/10.1186/2045-9912-3-18>
- Berka, J., Matěcha, J., Černý, M., Viden, I., Sus, F., & Hájek, P. (2012). New experimental device for VHTR structural material testing and helium coolant chemistry investigation – High Temperature Helium Loop in NRI Řež. In *Nuclear Engineering and Design, Vol. 251* (pp. 203-207). Retrieved from <https://doi.org/10.1016/j.nucengdes.2011.10.045>.
- Bite, R. (2021, August 27). *What is Helium and How is it Used in Welding and Other Industries?* Retrieved from Simcoegases: <https://www.simcoegases.com/post/what-is-helium-and-how-is-it-used-in-welding-and-other-industries>
- Bitelli, G., Martinelli, R., Orestano, F. V., & Santandrea, E. (1967). Analysis of Critical Experiments with Organic-Moderated Assemblies. In *Nuclear Science and Engineering, Vol. 28* (pp. 270-276).
- Bosworth, G., & Parkins, W. (1960). *Designs for Large Organic Reactor Power Plants*. United States.
- Brissonneau, L., Beauchamp, F., Morier, O., Schroer, C., Konys, J., Kobzova, A., . . . Courouau, J. L. (2011). Oxygen control systems and impurity purification in LBE: Learning from DEMETRA project. In *Journal of Nuclear Materials, Vol. 415, Issue 3* (pp. 348-360). Retrieved from <https://doi.org/10.1016/j.jnucmat.2011.04.040>

- Brumfiel, G. (2019, November 8). *The World Is Constantly Running Out Of Helium. Here's Why It Matters*. Retrieved from NPR: <https://www.npr.org/2019/11/01/775554343/the-world-is-constantly-running-out-of-helium-heres-why-it-matters>
- Bubelis, E. (2013). Gases, in Particular Helium, as Nuclear Reactor Coolant. *Fluides Caloporteurs Pour Reacteurs a Neutron Rapides*, (p. 37). Karlsruhe, Germany.
- Bureau of Land Management. (2024, June 27). *BLM completes sale of Federal Helium System*. Retrieved from U.S. Department of Interior Bureau of Land Management: <https://www.blm.gov/press-release/blm-completes-sale-federal-helium-system>
- Burke, A., Ogden, J., Fulton, L., & Cerniauskas, S. (2024). *Hydrogen Storage and Transport: Technologies and Costs*. Institute of Transportation Studies, UC Davis.
- Business Analitiq. (2024). *Hydrofluoric Acid price index*. Retrieved from Business Analitiq: <https://businessanalytiq.com/procurementanalytics/index/hydrofluoric-acid-price-index/>
- Cabet, C., & Rouillard, F. (2009). Corrosion of high temperature metallic materials in VHTR. *Journal of Nuclear Materials*, Vol. 392, Issue 2, 235-242.
- Cacuci, D. G. (2010). *Handbook of Nuclear Engineering*. Springer.
- Cadwallader, L. C., & Longhurst, G. R. (1999). *Flibe use in fusion reactors -- An initial safety assessment*. Idaho National Engineering and Environmental Laboratory, United States. Retrieved from <https://doi.org/10.2172/752080>
- Castle, B. (2010). *NGNP Reactor Coolant Chemistry Study*. Idaho National Laboratory.
- ChemRisk. (1999). *Mercury Releases from Lithium Enrichment at the Oak Ridge Y12 Plant - a Reconstruction of Historical Releases and Off-Site Doses and Health Risks*. Tennessee Department of Health.
- Cheng, H., Cheng, S., & Chen, S. (2024). Chapter 10 - Sodium fast reactors. In *Nuclear Power Reactor Designs* (pp. 185-208). Retrieved from <https://doi.org/10.1016/B978-0-323-99880-2.00010-2>
- Chung, C. K., Kim, I. H., Lee, S. K., & Lee, B. J. (2020). Innovative CVCS Design for SMRs. *Transactions of the Korean Nuclear Society Virtual Autumn Meeting*.
- Ciampichetti, A., Aiello, A., Coccoluto, G., Ricapito, I., Liger, K., Demange, D., & Moreno, C. (2010). The coolant purification system of the European test blanket modules: Preliminary design. In *Fusion Engineering and Design*, Vol. 85, Issues 10-12 (pp. 2033-2039). Retrieved from <https://doi.org/10.1016/j.fusengdes.2010.07.016>
- Cowgill, D. F. (2018). Measurement of Helium Diffusion in Metals. *40th Tritium Focus Group*. Albuquerque (NM), United States: Sandia National Laboratories.
- Dahlkamp, J. M., Quintero, C., Videla, A., & Rojas, R. (2024). Production processes for LiOH – A review. In *Hydrometallurgy*, Vol. 223. Retrieved from <https://doi.org/10.1016/j.hydromet.2023.106217>.
- Danabalan, D. (2017). On the hunt for helium. *2017 Physics World Focus on Vacuum and Instruments*.
- Dragunov, Y. G., Lemekhov, V. V., Moiseyev, A. V., & Smirnov, V. S. (2015). Lead-Cooled Fast-Neutron Reactor (BREST). *INPRO Dialog-Forum*, (p. 32). Vienna, Austria: Rosatom.

- Feng, J., Velez Lopez, E., Stewart, W. R., Wiser, R., Baglietto, E., & Shirvan, K. (2021). Heat Transfer Analysis of a Conceptual Horizontally-Oriented High Temperature Gas-Cooled Reactor. In *Volume 1: Operating Plant Challenges, Successes, and Lesson Learned*. Retrieved from <https://hdl.handle.net/1721.1/147083>
- Ferguson, C. D. (2015). *Lessons Learned from the History of Light Water Reactor*. Federation of American Scientists. Retrieved from <http://www.jstor.com/stable/resrep18925.5>
- Fermi, E., & Szilard, L. (1944). *United States of America Patent No. 2,708,656*.
- Flanagan, G. (2019). Overview of Past U.S. SFR Operations Experience. *Fast Reactor Technology Training U.S. Nuclear Regulatory Commission*, (p. 32).
- Forsberg, C., Peterson, P. F., & Pickard, P. S. (2003). Molten-Salt-Cooled Advanced High-Temperature Reactor for Production of Hydrogen and Electricity. In *Nuclear Technology, Vol.144* (pp. 289-302). Oak Ridge National Laboratory, managed by UT-Battelle, LLC. Retrieved from <https://doi.org/10.13182/NT03-1>
- Fruzzetti, K. (2017). *Potassium Hydroxide (KOH) Qualification Program Overview*. United States: EPRI.
- Fujiwara, Y. (2021). 2 - Design of High Temperature Engineering Test Reactor (HTTR). In *In JSME Series in Thermal and Nuclear Power Generation, High Temperature Gas-Cooled Reactors, Vol. 5* (pp. 17-177). Academic Press.
- Ganda, F., Hoffman, E., Taiwo, T. A., Kim, T. K., & Hansen, J. (2019). *Report on the ACCERT Cost Algorithms Tool*. Argonne National Laboratory.
- Ganda, F., Taiwo, T. A., & Kim, T. K. (2018). *Report on the Update of Fuel Cycle Cost Algorithms*.
- Gardner, L., & Hutchinson, W. (1964). *Reclamation of Damaged Nuclear Reactor Coolant by Catalytic Hydrocracking*.
- Gas-Cooled Reactor Associates. (1993). *Modular High Temperature Gas-Cooled Reactor Commercialization and Generation Cost Estimates*. Gas-Cooled Reactor Associates.
- Gastaldi, O., Liger, K., Robin, J. C., & Poletiko, C. (2006). Helium Purification. *3rd International Topical Meeting on High Temperature Reactor Technology*. Johannesburg, South Africa.
- Gierszewski, P., & Hollies, R. E. (1987). Organic coolants and their applications to fusion reactors. In *Nuclear Engineering and Design, Vol. 4* (pp. 223-236). Retrieved from [https://doi.org/10.1016/0167-899X\(87\)90006-1](https://doi.org/10.1016/0167-899X(87)90006-1)
- Gilbert, A., Penev, M., O'Dell, K., Howe, C., & Wu, C. (2024). *Summary of Electrolyzer Cost Data Synthesized from Applications to the DOE Clean Hydrogen Hubs Program*. DOE Hydrogen Program, Office of Clean Energy Demonstrations Program Record.
- Gokcek, O., Babka, P., Pavlenco, G., & Kemmerer, F. (1995). *The U.S. Advanced Liquid Metal Reactor Program (ALMR) Actinide Recycle System 1994 Capital and Busbar Cost Estimates*. GE Nuclear Energy. Retrieved from <https://doi.org/10.2172/1108730>
- Grabaskas, D. (2019). Operational Considerations. *Fast Reactor Technology Training U.S. Nuclear Regulatory Commission* (p. 28). Argonne National Laboratory.
- Griffith, J., & Russel, G. (1963). *Economics of Hydrocracking Damaged Coolant from Organic Reactors*. Idaho Operations Office, Reactor Technology Branch Nuclear Technology Division.

- Haas, C. (2009). *Pressurized Water Reactor Chemistry Monitoring and Assessment*. Palo Alto (CA), United States: EPRI.
- Holcomb, D. E., Peretz, F. J., & Qualls, A. L. (2011). *Advanced High Temperature Reactor Systems and Economic Analysis*. Oak Ridge National Laboratory, managed by UT-Battelle.
- Holt, M. (2023). *Advanced Nuclear Reactors: Technology Overview and Current Issues*. Congressional Research Service.
- Honeycutt, S. C., & O. Bach, R. (1971). *United States Patent No. 3597340*.
- Hopkins, C. (2024, January 25). *The U.S. just sold its helium stockpile. Here's why the medical world is worried*. Retrieved from NBC News: <https://www.nbcnews.com/health/health-news/us-just-sold-helium-stockpile-s-medical-world-worried-rcna134785>
- Huang, D. (2021). Status and prospects of China sodium-cooled fast reactor. *Ninth Joint IAEA-GIF Technical Meeting/Workshop on the Safety of Liquid Metal Cooled Fast Reactors*, (p. 16).
- Idaho National Laboratory. (2010, May 24-27). HTGR Technology Course for the Nuclear Regulatory Commission. United States.
- Institute for Energy Research. (2021, January 11). *Helium Is Instrumental in Semiconductor Manufacturing*. Retrieved from Institute for Energy Research: <https://www.instituteforenergyresearch.org/fossil-fuels/helium-is-instrumental-in-semiconductor-manufacturing/>
- International Atomic Energy Agency. (2012). *Liquid Metal Coolants for Fast Reactors Cooled by Sodium, Lead and Lead-Bismuth Eutectic*. Vienna, Austria: International Atomic Energy Agency.
- International Atomic Energy Agency. (2016). *Status Report – Mark 1 Pebble-Bed Fluoride-Salt-Cooled High-Temperature*. Retrieved from <https://aris.iaea.org/PDF/Mk1%20PB-FHR%20ARIS%20final.pdf>
- International Atomic Energy Agency. (2024). *Nuclear Power Reactors in the World*. Vienna, Austria: International Atomic Energy Agency.
- International Atomic Energy Agency. (2024, February 19). *Water cooled reactors*. Retrieved from International Atomic Energy Agency: <https://www.iaea.org/topics/water-cooled-reactors>
- International Energy Agency. (2022). *Nuclear Power and Secure Energy Transitions. From today's challenges to tomorrow's clean energy systems*. International Energy Agency.
- Japan Atomic Energy Agency. (2010). *Test Plan using the HTTR for commercialization of GTHTTR300C*. JAEA.
- Jiang, D., Zhang, D., Li, X., Wang, S., Wang, C., Qin, H., . . . Qiu, S. (2022). Fluoride-salt-cooled high-temperature reactors: Review of historical milestones, research status, challenges, and outlook. In *Renewable and Sustainable Energy Reviews, Vol. 161* (pp. 112-345). Retrieved from <https://doi.org/10.1016/j.rser.2022.112345>.
- Jones, S. B., Valkenburt, C., Walton, C. W., Elliott, D. C., Holladay, J. E., & Stevens, D. J. (2009). *Production of Gasoline and Diesel from Biomass via Fast Pyrolysis, Hydrotreating and Hydrocracking: A Design Case*. United States. Retrieved from doi:10.2172/950728
- Kasten, P. R., Adams, R. E., Roberts, J. T., Carlsnith, R. S., Salmon, R., Chapman, R. X., . . . Yeatts, L. B. (1967). *An Evaluation of Heavy-Water-Moderated Organic-Cooled reactors*. Oak Ridge National Laboratory, Reactor Division, Oak Ridge, Tennessee.

- Kawamura, H., Hirano, H., Katsumura, Y., Uchida, S., Mizuno, T., Kitajima, H., . . . Nishimura, T. (2016). BWR water chemistry guidelines and PWR primary water chemistry guidelines in Japan – Purpose and technical background. In *Nuclear Engineering and Design*, Vol. 309 (pp. 161-174). Retrieved from <https://doi.org/10.1016/j.nucengdes.2016.08.029>
- Kelleher, B. C., Dolan, K. P., Brooks, P., Anderson, M. H., & Sridharan, K. (2015, October). Batch-Scale Hydrofluorination of $7\text{Li}_2\text{BeF}_4$ to Support Molten Salt Reactor Development. *Journal of Nuclear Engineering and Radiation Science*. doi:10.1115/1.4030963
- Kim, T. K., Grandy, C., Natesan, K., Sienicki, J., & Hill, R. (2018). *Research and Development Roadmaps for Liquid Metal Cooled Fast Reactors - Draft for Public Comment*. Argonne National Laboratory, Nuclear Engineering Division.
- Kozlov, F. A., Bogdanovich, N. G., Zagorulko, Y. I., & Matveev, V. P. (2012). Sodium Coolant for Fast Reactors: Experience in Preparation and Delivery to BN-600; Problems for BN-800. *Atomic Energy*, Vol. 112, No. 4.
- Kugeler, K., & Zhang, Z. (2018). *Modular High-temperature Gas-cooled Reactor Power Plant*. Springer.
- Kwon, B., Lee, K., & Jang, A. (2018). The Estimation of Total Cost Through the Financial Assessment of Customized High Purity Industrial Water. *Journal of Korean Society of Environmental Engineers*.
- Lam, S., Li, Q., Ballinger, R., Forsberg, C., & Li, J. (2021). *Modeling LiF and FLiBe Molten Salts with Robust Neural Network Interatomic Potential*. American Chemical Society. Retrieved from <https://doi.org/10.1021/acscami.1c00604>
- Lee, J., & Pint, B. A. (2021). *Corrosion in Gas-Cooled Reactors*. Oak Ridge National Laboratory.
- Legros, F., Liger, K., Poletiko, C., Gastaldi, O., Troulay, M., & Ollivier, M. (2006). Helium Purification at Laboratory Scale. *3rd International Topical Meeting on High Temperature Reactor Technology*. Johannesburg, South Africa.
- Leiden, K. (2015, August 7). *The importance of helium for welding*. Retrieved from Zephyr: <https://zephyrsolutions.com/the-importance-of-helium-for-welding/>
- Levinsky, A., Franceschini, F., Ferroni, P., Stansbury, C., Ickes, M., & Liao, J. (2022). Activation of lead coolant in Westinghouse lead fast reactor. *PHYSOR 2022: International conference on physics of reactors* (p. 10). Pittsburg, US: Westinghouse.
- Li, X., Damartzis, T., Stadler, Z., Moret, S., Meier, B., Friedl, M., & Maréchal, F. (2020). Decarbonization in Complex Energy Systems: A Study on the Feasibility of Carbon Neutrality for Switzerland in 2050. In *Frontiers in Energy Research*, Vol. 8. doi:10.3389/fenrg.2020.549615
- Liger, K., Lefebvre, X., Ciampichetti, A., Aiello, A., & Ricapito, I. (2011). HCLL and HCPB coolant purification system: Design of the copper oxide bed. In *Fusion Engineering and Design Vol. 86* (pp. 1859-1862).
- Lister, D., & Uchida, S. (2014). Determining water chemistry conditions in nuclear reactor coolants. In *Journal of Nuclear Science and Technology*, Vol. 52 (pp. 451–466). Retrieved from doi:10.1080/00223131.2014.973460
- Liu, P., Chen, X. N., Gabrielli, F., Flad, M., Maschek, W., Rineiski, A., . . . Ege, Y. (2009). Analyses of Transients for 400 MWth-Class EFIT Accelerator Driven Transmuter with the SIMMER-III Code. *International Topical Meeting on Nuclear Research Applications and Utilization of Accelerators*. Vienna, Austria.

- Lucoff, D. M., Waltar, A. E., Sackett, J. I., Salvatores, M., & Aizawa, K. (1992). Experimental and design experience with passive safety features of liquid metal reactors. *International Conference on Design and Safety of Advanced Nuclear Power Plants*, (p. 11). Washington (DC), United States.
- Luo, C., & Zhang, T. (2024). Chapter 11 - Lead fast reactors. In *Nuclear Power Reactor Designs* (pp. 209-244). Academic Press. Retrieved from <https://doi.org/10.1016/B978-0-323-99880-2.00011-4>
- Ivanenko, F. A. (1996). Sodium -- Coolant for Nuclear Power Plants with Fast Reactors. In *Atomic Energy, Vol. 80, No. 5*.
- Maeda, H., Kobayashi, T., Ishiyama, S., & Motonaga, T. (1987). *Argon Cover Gas Purity Control on LMFBR*.
- Makens, R. F. (1964). *Organic Coolant Summary Report*. Idaho Operations Office, U.S Atomic Energy Commission.
- Martinelli, L., Courouau, J., & Balbaud-Célérier, F. (2011). Oxidation of steels in liquid lead bismuth: Oxygen control to achieve efficient corrosion protection. In V. 2. Nuclear Engineering and Design. Retrieved from <https://doi.org/10.1016/j.nucengdes.2010.07.039>
- Martynov, P. N., Askhadullin, R. S., Simakov, A. A., Chaban', A. Y., & Legkikh, A. Y. (2008). Designing Mass Exchangers for various control of Oxygen Content in Pb-Bi (Pb) coolants in various research facilities. *17th International Conference on Nuclear Engineering*, (p. 7). Brussels, Belgium.
- Massachusetts Institute of Technology. (2018). *The Future of Nuclear Energy in a Carbon-Constrained World*. Massachusetts Institute of Technology.
- Mechanisms Engineering Test Loop Facility*. (2018). Retrieved from Argonne National Laboratory: <https://www.anl.gov/nse/metl>
- Mohamed, H., & Parks, G. T. (2017). The effect of variations in lithium (⁷Li) and Uranium (²³⁵U) isotope levels on a small fluoride salt-cooled, high temperature reactor with UO₂ fuel pins. In *Journal of Nuclear And Related Technologies, Vol. 14, No.1*.
- Moir, R., House, P., & Leber, R. (1994). *HYLIFE-II: An approach to a long-lived, first-wall component for inertial fusion power plants*. Retrieved from <https://digital.library.unt.edu/ark:/67531/metadc626683/>
- Moriyama, H., Sagara, A., Tanaka, S., Moir, R. W., & Sze, D. K. (1998). Molten salts in fusion nuclear technology. In *Fusion Engineering and Design, Vol. 39-40* (pp. 627-637). Retrieved from [https://doi.org/10.1016/S0920-3796\(98\)00202-6](https://doi.org/10.1016/S0920-3796(98)00202-6).
- Murakami, T. (2021). A historical review and analysis on the selection of nuclear reactor types and implications to development programs for advanced reactors; A Japanese study. In *Energy Reports, Vol. 7* (pp. 3428-3436). Retrieved from <https://doi.org/10.1016/j.egy.2021.05.049>
- NASA. (2024, June). *Carbon Dioxide*. Retrieved from NASA: <https://climate.nasa.gov/vital-signs/carbon-dioxide/?intent=121>
- Natesan, K., Purohit, A., & Tam, S. W. (2003). *Materials Behavior in HTGR Environments*. Argonne National Laboratory.
- National Research Council. (2000). *The Impact of Selling the Federal Helium Reserve*. Washington (DC), United States: The National Academies Press. Retrieved from doi: 10.17226/9860.
- Nigrey, P. (2000). *An Issue Paper on the Use of Hydrogen Getters in Transportation Packaging*. Sandia National Laboratories.

- Nordrum, A. (2024, February 25). *The era of cheap helium is over—and that's already causing problems*. Retrieved from MIT Technology Review: <https://www.technologyreview.com/2024/02/25/1088930/global-helium-market-semiconductors/>
- Nuclear Energy Agency. (2015). *Handbook on lead-bismuth Eutectic Alloy and Lead Properties, Materials Compatibility, Thermal Hydraulics and Technologies - 2015 Edition*. Paris, France: OECD Publishing.
- Nuclear Engineering International. (2020, June 22). *Rosatom considers life extension for BN-600 fast reactor to 2040*. Retrieved from Nuclear Engineering International: <https://www.neimagazine.com/news/rosatom-considers-life-extension-for-bn-600-fast-reactor-to-2040-7986394/?cf-view>
- Nuclear Engineering International. (2024, June 12). *TerraPower breaks ground on planned Sodium NPP*. Retrieved from Nuclear Engineering International: <https://www.neimagazine.com/news/terrapower-breaks-ground-on-planned-sodium-npp/?cf-view>
- Oak Ridge National Laboratory. (2004). *Fort Saint Vrain Gas Cooled Reactor Operational Experience*. Washington (DC), United States.
- Oak Ridge National Laboratory. (2020, October 22). *ORNL scientists solve the mystery of mercury*. Retrieved from Oak Ridge National Laboratory: <https://www.ornl.gov/blog/ornl-review/ornl-scientists-solve-mystery-mercury>
- Ohshima, H., & Kubo, S. (2023). Chapter 5 - Sodium-cooled Fast Reactors (SFRs). In *Woodhead Publishing* (pp. 173-194). Woodhead Publishing. Retrieved from <https://doi.org/10.1016/B978-0-12-820588-4.00006-2>.
- Olson, H. G., Brey, H. L., & Swart, F. E. (1980). The Fort St. Vrain High Temperature Gas-cooled Reactor VI: Evaluation and removal of primary coolant contaminants. In *Nuclear Engineering and Design Vol. 61* (pp. 315-322). North-Holland Publishing Company.
- Orlov, Y. I., Efanov, A. D., Martynov, P. N., Gulevsky, V. A., Papovyants, A. K., Levchenko, Y. D., & Ulyanov, V. V. (2007). Hydrodynamic problems of heavy liquid metal coolants technology in loop-type and mono-block-type reactor installations. In *Nuclear Engineering and Design, Vol. 237, Issues 15-17* (pp. 1829-1837). Retrieved from <https://doi.org/10.1016/j.nucengdes.2007.03.008>
- Ortiz Amaya, L., & Braet, J. (2009). Purification of Lead-Bismut Eutectic Used in Accelerator Driven Systems - 9411. *WM2009 Conference*. Phoenix (AZ), United States.
- Parkins, W., & Weisner, E. (1959). Organic Moderated Reactors for Central Station Power. *Transactions of the American Institute of Electrical Engineers, Part I: Communication and Electronics*, 77(6), pp. 985-993. doi:10.1109/TCE.1959.6372928
- Patel, S. (2024, April 2). *Long-Awaited Milestone: Fuel Loading Begins at India's Prototype Fast Nuclear Reactor*. Retrieved from Power: <https://www.powermag.com/long-awaited-milestone-fuel-loading-begins-at-indias-prototype-fast-nuclear-reactor/>
- Pearson, R. J. (2022). The Availability & Supply of Critical Natural Resources for the Realization of a Fusion Pilot Plant: Fuels for Fusion. *U.S. DoE Fusion Workshop* (p. 23). Washington (DC), United States: Fusioneering, Kyoto.
- Pei, H., Yan, F., Liu, H., He, B., & Li, J. (2024). The selective complexation of crown ethers for lithium isotope separation: A critical review. In *Separation and Purification Technology, Vol. 341*. Retrieved from <https://doi.org/10.1016/j.seppur.2024.126857>

- Pioro, I. (2016). 2 - Introduction: Generation IV International Forum. In *Handbook of Generation IV Nuclear Reactors* (pp. 37-54). Woodhead Publishing.
- Polushkin, K. K., Enelyanov, I. Y., Delens, P. A., Zvonov, N. V., Aleksenko, U. N., Grozdov, I. L., . . . Popov. (1964). THE ATBYC ORGANIC COOLED AND MODERATED NUCLEAR POWER STATION. *Third United Nations International Conference on the Peaceful Uses of Atomic Energy*.
- Priambodo, D., Pancoko, M., Sriyono, & Setiadipura, T. (2018). Design of Helium Purification System for Indonesia Experimental Power Reactor-Reaktor Daya Eksperimental. *International Journal of Mechanical Engineering and Technology (IJMET)*, Vol. 9, Issue 6, 873-880.
- Prosser, J., Graham, M., Acevedo, Y. M., Jensen, M., James, B., & Abou Jaoude, A. (2023). *First-Principles Cost Estimation of a Sodium Fast Reactor Nuclear Plant*. doi:10.2172/2007008
- Ragheb, M. (2015). *Isotopic Separation and Enrichment*. Retrieved from <https://www.semanticscholar.org>
- Rahmatullah, H. F., Sigit, R., Ismarwanti, S., Noerpitasari, E., Ajiriyanto, M. K., & Setiawan, J. (2019). Analysis of Irradiated Pebble Bed Fuel Transfer System in Hot Cell 101 Radiometallurgy Installation. *Journal of Physics: Conf. Series 1198*. Retrieved from doi:10.1088/1742-6596/1198/2/022025
- Rainer, S. (2005). The Primary Circuit of the Dragon High Temperature Reactor Experiment. *18th International Conference on Structural Mechanics in Reactor Technology (SMiRT 18)*. Beijing, China.
- Reister, R. (2013). *Li-7 Supply*. U.S. Department of Energy, Office of Light Water Reactor Technologies, Office of Nuclear Energy.
- Rennie, C. A. (1978). Achievements of the Dragon Project. In *Annals Of Nuclear Energy, Vol.5* (pp. 305 - 320). Pergamon Press.
- Ricapito, I., Aiello, A., Galabert, J., Poitevin, Y., & Tincani, A. (2017). Water and pressurized Helium as coolants of fusion reactor breeding blankets: chemistry issues and purification technologies. *IAEA Workshop on "Challenges for Coolants in Fast Neutron Spectrum Systems"*, (p. 12). Vienna, Austria.
- Rittenhouse, P. L., & Morgan, C. S. (1976). *Status report on structural materials of HTGR primary system components*. United States. Retrieved from <https://doi.org/10.2172/4081838>
- Rocky Mountain Air Solutions. (2024). *Rocky Mountain Air Solutions*. Retrieved from How Is Helium Extracted, and Are We Running Out?: <https://rockymountainair.com/blog/how-is-helium-extracted/>
- Romatoski, R., & Hu, L. (2017). Fluoride salt coolant properties for nuclear reactor applications: A review. In *Annals of Nuclear Energy, Vol. 109* (pp. 635-647). Retrieved from <https://doi.org/10.1016/j.anucene.2017.05.036>
- Romero, J. B. (1980). *Evaluation of Organic Moderator/Coolants for Fusion Breeder Blankets*. Argonne National Laboratory.
- Rustagi, N., Elgowainy, A., & Vickers, J. (2018). *Current Status of Hydrogen Delivery and Dispensing Costs and Pathways to Future Cost Reductions*. U.S. Department of Energy.
- Salam, M. N., & Rokonzaman, M. (2023). *Water Chemistry in Nuclear Power Plant*. doi:10.5772/intechopen.1002246
- Sato, H., Yan, X. L., Tachibana, Y., & Kunitomi, K. (2014). GTHT300—A nuclear power plant design with 50% generating efficiency. In *Nuclear Engineering and Design, Vol. 275* (pp. 190-196). Retrieved from <https://doi.org/10.1016/j.nucengdes.2014.05.004>

- Scheibner, K. (2004). *Cost Estimate for Laser Isotope Separation for RIA*. United States. Retrieved from <https://doi.org/10.2172/15014826>
- Schulenberg, T. (2022). *The fourth generation of nuclear reactors. Fundamentals, Types, and Benefits Explained*. Springer.
- Seifried, J. E., Scarlat, R. O., Peterson, P. F., & Greenspan, E. (2019). A general approach for determination of acceptable FLiBe impurity concentrations in Fluoride-Salt Cooled High Temperature Reactors (FHRs). In *Nuclear Engineering and Design*, Vol. 343 (pp. 85-95). Retrieved from <https://doi.org/10.1016/j.nucengdes.2018.09.038>.
- Serra Leal, J. S., Incer-Valverde, J., & Morosuk, T. (2023). Helium: Sources, Applications, Supply, and Demand. *Gases*, Vol. 3, 181-183. Retrieved from <https://doi.org/10.3390/gases3040013>
- Shaffer, J. H. (1971). *Preparation and Handling of Salt Mixtures for the Molten Salt Reactor Experiment*. United States. Retrieved from <https://doi.org/10.2172/4074869>
- Shin, C. W., Son, S. K., Lee, Y., Kim, S. K., Jin, H. G., Lee, D. W., & Ahn, M. Y. (2023). Experimental validation of bed depth service time model using vapor adsorption bed for coolant purification system of fusion research. In *Fusion Engineering and Design*, Vol. 192. Retrieved from <https://doi.org/10.1016/j.fusengdes.2023.113716>
- Shirvan, K., & Forrest, E. (2016). Design of an Organic Simplified Nuclear Reactor. *Nuclear Engineering and Technology*, 48(4), pp. 893-905. Retrieved from <https://doi.org/10.1016/j.net.2016.02.019>
- Shirvan, K., Buongiorno, J., MacDonald, R., Dunkin, B., Cetiner, S., Saito, E., . . . Forsberg, C. (2023). UO₂-fueled microreactors: Near-term solutions to emerging markets. In *Nuclear Engineering and Design*, Vol. 412. United States. Retrieved from <https://doi.org/10.1016/j.nucengdes.2023.112470>
- Siddhantakar, A., Santillán-Saldivar, J., Kippes, T., Sonnemann, G., Reller, A., & Young, S. B. (2023). Helium resource global supply and demand: Geopolitical supply risk analysis. In *Resources, Conservation and Recycling*, Vol. 193. Retrieved from <https://doi.org/10.1016/j.resconrec.2023.106935>.
- Singh, R., & Hankins, N. P. (2016). Chapter 2 - Introduction to Membrane Processes for Water Treatment. In *Emerging Membrane Technology for Sustainable Water Treatment* (pp. 15-52). Retrieved from <https://doi.org/10.1016/B978-0-444-63312-5.00002-4>
- Smith, C. F., & Cinotti, L. (2023). Chapter 6 - Lead-cooled Fast Reactors (LFRs). In *Handbook of Generation IV Nuclear Reactors (Second Edition)* (pp. 195-230). Woodhead Publishing. Retrieved from <https://doi.org/10.1016/B978-0-12-820588-4.00018-9>
- Smith, C. F., Halsey, W. G., Brown, N. W., Sienicki, J. J., Moiseyev, A., & Wade, D. C. (2008). SSTAR: The US lead-cooled fast reactor (LFR). In *Journal of Nuclear Materials*, Vol. 376, Issue 3 (pp. 255-259). Retrieved from <https://doi.org/10.1016/j.jnucmat.2008.02.049>
- Smith, C. R., & Holmes, J. T. (1975). *Purity of EBR-II Sodium: 1967-1974*. Argonne National Laboratory.
- Sofu, T. (2019). Overview of Lead-Cooled Fast reactor (LFR) Technology. *Fast Reactor Technology Training, U.S. Nuclear Regulatory Commission* (p. 24). Argonne National Laboratory.
- Sorbom, B. N., Ball, J., Palmer, T. R., Mangiarotti, F. J., Sierchio, J. M., Bonoli, P., . . . Whyte, D. G. (2015). ARC: A compact, high-field, fusion nuclear science facility and demonstration power plant with demountable magnets.

- Statista. (2024, June 28). *Capacity factor of nuclear power plants in the United States from 1975 to 2023*. Retrieved from Statista: <https://www.statista.com/>
- Stepanov, V. S., Legyuenko, S. K., Grigoriev, O. G., Gromov, B. F., Dedul, A. V., Leonchyk, M. P., . . . Skorikov, D. E. (1998). The ANGSTREM project: present status and development activities. *Advisory group meeting on technology, design and safety aspects of non-electrical application of nuclear energy*. Obninsk (Russian Federation).
- Stewart, W. R., Velez-Lopez, E., Wisner, R., & Shirvan, K. (2021). Economic solution for low carbon process heat: A horizontal, compact high temperature gas reactor. In *Applied Energy*, Vol. 304. Retrieved from <https://doi.org/10.1016/j.apenergy.2021.117650>
- Strydom, H. (1999). *Mass spectrometry characterisation of laser produced products*. United States.
- Sze, A. K., Sviatoslavsky, I., Sawan, M., Gierszewski, P., Hollies, R., Sharafat, S., & Herring, S. (1991). Organic coolant for ARIES-III. In *Fusion Engineering and Design* (Vol. 18, pp. 435-441). Retrieved from [https://doi.org/10.1016/0920-3796\(91\)90160-R](https://doi.org/10.1016/0920-3796(91)90160-R)
- The American Society of Mechanical Engineers. (1979). *Experimental Breeder Reactor I, Idaho National Engineering Laboratory*. The American Society of Mechanical Engineers.
- Tillack, M. S., Humrickhouse, P. W., Malang, S., & Nygren, R. E. (2014). *Technology readiness of helium as a fusion power core coolant*. University of California, San Diego, Center for Energy Research, La Jolla (CA), United States.
- Tincani, A., Aiello, A., Ferrucci, B., Granieri, M., Voukelatou, K., Ricapito, I., . . . Forte, R. (2019). Conceptual design of the enhanced coolant purification systems for the European HCLL and HCPB test blanket modules. In *Fusion Engineering and Design*, Vol. 146 Part A (pp. 365-368). Retrieved from <https://doi.org/10.1016/j.fusengdes.2018.12.069>
- Tochio, D., Shimizu, A., Hamamoto, S., & Sakaba, N. (2014). Helium leak and chemical impurities control technology in HTTR. *Journal of Nuclear Science and Technology*, Vol. 51, 1407-1412.
- Trester, P. W., Johnson, W. R., Simnad, M. T., Burnette, R. D., & Roberts, D. I. (1982). *Assessment of effects of Fort St. Vrain HTGR primary coolant on Alloy 800. Final report*. United States.
- U.S. Department of Defence. (2022, April 13). *DoD to Build Project Pele Mobile Microreactor and Perform Demonstration at Idaho National Laboratory*. Retrieved from U.S. Department of Defence: <https://www.defense.gov/News/Releases/Release/Article/2998460>
- U.S. Department of Energy. (1987). *PRISM - Preliminary Safety Information Document (PSID) - GEFR-00795, Vol. III, Chapters 9-14*. Washington (DC), United States.
- U.S. Department of Energy. (2015). *Quadrennial Technology Review 2015*. U.S. Department of Energy.
- U.S. Department of Energy. (2023, December 12). *NRC Approves Construction for Hermes Reactor*. Retrieved from Office of Nuclear Energy: <https://www.energy.gov/ne/articles/nrc-approves-construction-hermes-reactor>
- U.S. Department of Energy. (n.d.). *The History Of Nuclear Energy*. Washington (DC), United States: U.S. Department of Energy.
- U.S. Geological Survey. (2024). *Mineral Commodity Summaries: Helium*. U.S. Geological Survey.

- U.S. National Regulatory Commission. (2023, October 19). *Power Reactors*. Retrieved from U.S. National Regulatory Commission: <https://www.nrc.gov/reactors/power.html>
- U.S. Nuclear Regulatory Commission. (2024, March 27). *Next Generation Nuclear Plant (NGNP)*. Retrieved from U.S. NRC: <https://www.nrc.gov/reactors/new-reactors/advanced/who-were-working-with/licensing-activities/ngnp.html>
- U.S. Nuclear Regulatory Commission. (n.d.). Chapter 3: LWR Chemistry. In U. T. Center, *Radioactive Waste Management Technology*.
- U.S. Nuclear Regulatory Commission. (n.d.). *Module 3.0: Laser Enrichment Methods (AVLIS and MLIS)*. United States: USNRC Technical Training Center.
- U.S. Nuclear Regulatory Commission. (n.d.). Section 4.1 Chemical and Volume Control System. In *Westinghouse Technology Systems Manual*.
- United Nations. (2015). *Paris Agreement*. Paris, France: United Nations. Retrieved from United Nations Climate Change.
- United States Geological Survey. (2024). *2024 Mineral Commodity Summaries - Bismuth*. United States Geological Survey.
- United States Geological Survey. (2024). *2024 Mineral Commodity Summaries - Lead*. United States Geological Survey.
- United States Government Accountability Office. (2013). *MANAGING CRITICAL ISOTOPES Stewardship of Lithium-7 Is Needed to Ensure a Stable Supply*. United States: United States Government Accountability Office.
- University of California, Berkeley. (2013). *Fluoride-Salt-Cooled, High-Temperature Reactor (FHR) Subsystems Definition, Functional Requirement Definition, and Licensing Basis Event (LBE) Identification White Paper*. University of California, Berkeley, Department of Nuclear Engineering.
- Vaaler, L. E. (1979). *Survey of electrochemical metal winning processes. Final report*. United States. Retrieved from <https://doi.org/10.2172/6063735>
- Van den Eynde, G., Malambu, E., Stankovskiy, A., Fernandez, R., & Baeten, P. (2015). An updated core design for the multi-purpose irradiation facility MYRRHA. In *Journal of Nuclear Science and Technology*, Vol. 52 (pp. 1053-1057). Retrieved from <https://doi.org/10.1080/00223131.2015.1026860>
- Waltar, A. E., Todd, D. R., & Tsvetkov, P. V. (2012). *Fast Spectrum Reactors*. Springer.
- Wang, H., & Zhong, X. (2024). Chapter 8 - An overview of high-temperature gas-cooled reactors. In *Nuclear Power Reactor Designs* (pp. 135 - 162). Academic Press. Retrieved from <https://doi.org/10.1016/B978-0-323-99880-2.00008-4>.
- Wang, Y., Li, X., Liang, R., Zhu, H., Liu, F., Liu, Y., & Niu, F. (2022). Simulation of a solid-phase oxygen control scheme in lead-bismuth eutectic system. In *Nuclear Engineering and Design*, Vol. 394. Retrieved from <https://doi.org/10.1016/j.nucengdes.2022.111821>
- Wiedenmann, D., & Cook, K. (2020). *The Benefits of Using Enriched Boric Acid in Commercial Nuclear Power Plants*. 3M Technical Ceramics, Inc., USA.
- World Nuclear Association. (2022, November 23). Retrieved from Lithium current and future generation: <https://world-nuclear.org/information-library/current-and-future-generation/lithium>

- World Nuclear Association. (2022, May 3). *Decommissioning Nuclear Facilities*. Retrieved from World Nuclear Association: <https://world-nuclear.org/information-library/nuclear-fuel-cycle/nuclear-waste/decommissioning-nuclear-facilities>
- World Nuclear Association. (2024, April 30). *Nuclear Power Reactors*. Retrieved July 29, 2024, from World Nuclear Association: <https://world-nuclear.org/information-library/nuclear-fuel-cycle/nuclear-power-reactors/nuclear-power-reactors>
- World Nuclear Association. (2024, February 16). *Small Nuclear Power Reactors*. Retrieved from World Nuclear Association: <https://world-nuclear.org/information-library/nuclear-fuel-cycle/nuclear-power-reactors/small-nuclear-power-reactors>
- World Nuclear News. (2017, December 29). *China begins building pilot fast reactor*. Retrieved from World Nuclear News: <https://www.world-nuclear-news.org/NN-China-begins-building-pilot-fast-reactor-2912174.html>
- World Nuclear News. (2020, December 29). *China starts building second CFR-600 fast reactor*. Retrieved from World Nuclear News: <https://www.world-nuclear-news.org/Articles/China-starts-building-second-CFR-600-fast-reactor>
- World Nuclear News. (2022, December 9). *China's demonstration HTR-PM reaches full power*. Retrieved from World Nuclear News: <https://www.world-nuclear-news.org/Articles/China-s-demonstration-HTR-PM-reaches-full-power>
- World Nuclear News. (2022, October 21). *Defuelling completed at Japan's Monju reactor*. Retrieved from World Nuclear News: <https://www.world-nuclear-news.org/Articles/Defuelling-completed-at-Japan-s-Monju-reactor>
- World Nuclear News. (2022, December 14). *Uranium-plutonium nitride fuel tested for BN-1200 fast reactor*. Retrieved from World Nuclear News: <https://www.world-nuclear-news.org/Articles/Uranium-plutonium-nitride-fuel-tested-for-BN-1200>
- World Nuclear News. (2024, January 17). *First lead-cooled fast neutron reactor's installation under way*. Retrieved from World Nuclear News: <https://www.world-nuclear-news.org/Articles/First-lead-cooled-fast-neutron-reactor-s-installat>
- Wright, R. N. (2006). *Kinetics of Gas Reactions and Environmental Degradation in NGNP Helium*. Idaho National Laboratory.
- Wu, Y. (2016). Design and R&D Progress of China Lead-Based Reactor for ADS Research Facility. In *Engineering, Vol.2, Issue 1* (pp. 124-131). Retrieved from <https://doi.org/10.1016/J.ENG.2016.01.023>
- Wu, Z., Lin, D., & Zhong, D. (2002). The design features of the HTR-10. In *Nuclear Engineering and Design, Vol. 218, Issues 1–3* (pp. 25-32). Retrieved from [https://doi.org/10.1016/S0029-5493\(02\)00182-6](https://doi.org/10.1016/S0029-5493(02)00182-6).
- X-energy. (2021, March 1). *X-energy signs Department of Energy's Advanced Reactor Demonstration Program (ARDP) Cooperative Agreement*. Retrieved from X-energy: <https://x-energy.com/media/news-releases/x-energy-signs-department-of-energys-advanced-reactor-demonstration-program-ardp-cooperative-agreement>
- Y-12 National Security Complex. (2014). *Dr. Googin and the Y-12 COLEX Process — Recalling the Y-12 COLEX (column exchange) process*. Retrieved from <https://www.y12.doe.gov/>

- Yao, M. S., Wang, R. P., Liu, Z. Y., He, X. D., & Li, J. (2002). The helium purification system of the HTR-10. In *Nuclear Engineering and Design Vol. 218, Issues 1-3* (pp. 163-167). Elsevier Science B.V. Retrieved from [https://doi.org/10.1016/S0029-5493\(02\)00187-5](https://doi.org/10.1016/S0029-5493(02)00187-5)
- Yoshida, E., & Furukawa, T. (2012). 21 - Corrosion issues in sodium-cooled fast reactor (SFR) systems. In *Nuclear Corrosion Science and Engineering* (pp. 773-806). Woodhead Publishing.
- Zhipeng, C., Yan, W., & Yanhua, Z. (2020). Discussion on the accident behavior and accident management of the HTGR. In *Nuclear Engineering and Design, Vol. 360*. Retrieved from <https://doi.org/10.1016/j.nucengdes.2019.110497>
- Zhu, G., Zou, Y., Yan, R., Tan, M., Zou, C., Kang, X., . . . Dai, Y. (2019). Low enriched uranium and thorium fuel utilization under once-through and offline reprocessing scenarios in small modular molten salt reactor. *International Journal of Energy Research*.

Appendix A

For the purpose of report's completeness, the recommended guidelines for PWR's secondary circuit and for BWRs are included in the Appendix. As mentioned in the previous paragraphs, the recommended chemical conditions values are intended to enhance safety and reliability of the plant. If a utility does not meet these recommended values, water chemistry experts are supposed to identify and assess the root cause of the deviation and discuss appropriate corrective actions.

Table 50 PWR secondary circuit water chemistry indications (Salam & Rokonzaman, 2023).

Parameter	Unit	Recommended values PWR secondary circuit
pH		4.5–10
Electrical conductivity (EC) at 25°C	µS/cm	0
TDS	ppm	0
Chloride	ppm	<0.1

Total hardness	ppm	0
Total alkalinity	ppm	0
Silica (SiO ₂)	ppm	—

Table 51 Control parameters for reactor coolant of BWR during power operations (Kawamura, et al., 2016).

Control parameter	Recommended value	Monitoring frequency
Conductivity at 25 °C, $\mu\text{S}/\text{m}$ ($\mu\text{S}/\text{cm}$)	< 10 (< 0.1)	Continuously
Chloride, $\mu\text{g}/\text{L}$	< 1	Weekly
Sulfate, $\mu\text{g}/\text{L}$	< 2	

Appendix B

In the chapter *Purity requirements of Sodium*, several impurities are analyzed. With them, their potential source in a SFRs is described. Between impurity origins, stainless steels and structural materials represent the major sources of sodium impurities as historically demonstrated during SFR operation. For the sake of completeness, a list of the typically used core and structural materials is reported here from existing and planned SFRs:

Table 52 Materials used in SFRs in different countries (Yoshida & Furukawa, 2012).

Country	Japan		England	France		Germany	Russia
Reactor name	Monju	JSFR	PFR	Phenix	Super Phenix	SNR300	BN-350
Reactor type	Loop	Loop	Pool	Pool	Pool	Loop	Loop
Fuel cladding	PNC316 (20%CW)	ODS	PE16	Cr17-Ni13-Mo2.5-Mn1.5-Ti-Si	316L(N)	304SS	304SS
Reactor vessel	304SS	316FR	321SS	316SS	316L(N)	304SS	304SS
IHX	304SS	Mod.9Cr-1Mo	321SS	316SS	316L(N)	304SS	304SS
Primary pipes	304SS	Mod.9Cr-1Mo	-	-	-	304SS	304SS
Secondary pipes	304SS	Mod.9Cr-1Mo	321SS	321SS,304SS	316L(N)	304SS	304SS
SG	2.25Cr-1Mo 321SS	Mod.9Cr-1Mo	2.25Cr-MoNb 316SS (9Cr-1Mo)	2.25Cr-1MoNb 321SS	Alloy 800	2.25Cr-1MoNbNi	2.25Cr-Mo

In the following table, the impurities collected during initial sodium loading, reactor operation and maintenance for the GE PRISM reactor is reported, similarly to the data available for the BN-350 and BN-600 in the chapter *Purity requirements of Sodium*:

Table 53 Intensity of impurity contamination in primary sodium for PRISM case (U.S. Department of Energy, 1987).

Source or activity	Oxygen [kg]	Hydrogen [lbs]	Theoretical Volume of Na ₂ O + NaH [dm ³]
1. Initial			
Sodium	0.86	0.072	3.4
Piping/Vessel	3.9	0.45	18

2. Operational			
New surfaces/cycle Fuel Cladding: (if) Stainless Steel (if) HT-9	0.02	0.027	0.73
	0.02	0.027	0.73
Inadvertent Air In-Leakage/Cycle	0.10	0.045	1.4
H2 Core Generation/Cycle	-	0.48	13
3. Maintenance (60 years)			
Total, 60 Years at 1 Cycle/2 Years	14	17	0.49

Appendix C

As mentioned in the section *Operational and Purification costs for Organic fluids*, the HB formation rate at the PNPf is set to vary linearly between 90 lb/h (40.8 kg/h) and 50 lb/h (22.7 kg/h) depending on the already existent equilibrium HB concentration. This assumption has been used by (Griffith & Russel, 1963) to estimate the cost of hydrocracker installation at Piqua as shown in Figure 24 below.

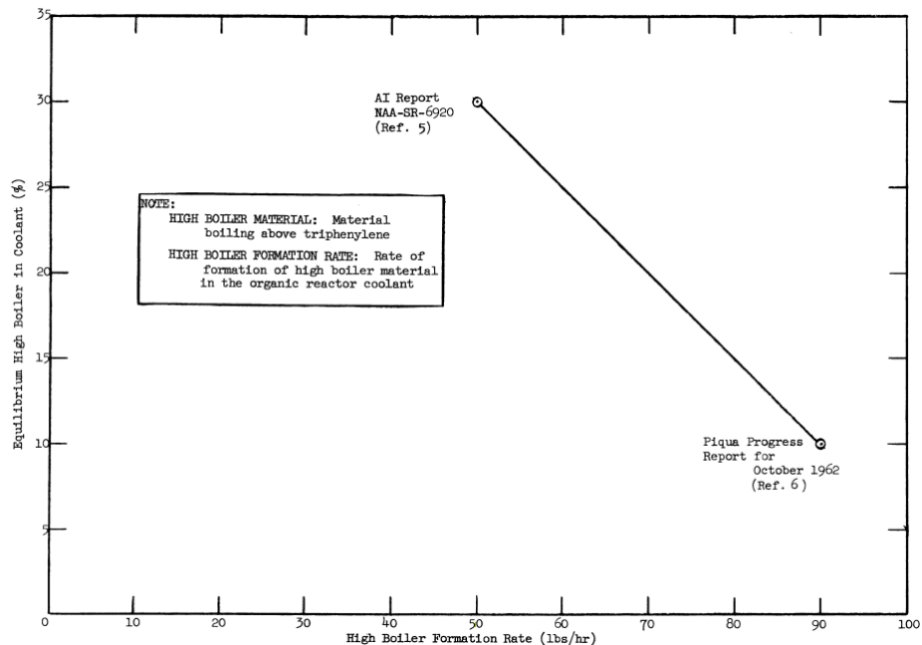


Figure 24 Rate of HB formation in the coolant based on HB equilibrium concentration (J.L. Griffith, 1963).

Appendix D

In this Appendix, the economics of the possible installation of two lithium enrichment facilities based on the Crown Ether (CE) enrichment technique are included based on data found from the UCBTH-12-005 report. The capital costs included initial procurement of chemicals, equipment costs, facility costs, construction, and installation costs for all the

systems. The operating costs included chemicals for makeup, employee wages, and utilities to run the plant. Here are the resuming tables as found in UCBTH-12-005 report.

Table 54 Plant Economics for a 400 kg/year Li-7 throughput (Ault, et al., 2012).

Capital Costs	Quantity	Cost (each) [\$]	Total
RO Water Systems (GPM)	5	100,000	500,000
Dryers (each)	2	100,000	200,000
Facility (ft)	10000	120	1,200,000
Electrical equipment (MCC)	1	500,000	500,000
Electrical Equipment (Substation)	1	180,000	180,000
Other Equipment	1	500,000	500,000
Refrigeration System	300	300,000	300,000
Mixer-settler Cells	260	Size dependent	1,400,000
Analytical lab	1	200,000	200,000
Organic Recovery system	2	100,000	200,000
Benzo-15-crown-5 (kg)	370	1,000	370,000
Chloroform	6200	2	12,400
Engineering	1	3,000,000	3,000,000
Installation	1	75% equipment	2,800,000
Total Capital Cost			11,500,000
Operating Costs Per Year:			
Employees	8	150,000	1,200,000
Electricity Usage Mixers (assume 1 HP Agitators, 80% efficiency) kwh	2300000	0.10	230,000
Electricity Usage - refrigerant system	750000	0.10	750,000
Electricity Usage - Brine concentration	260000	0.10	26,000
Electricity Usage - Other	100000	0.10	10,000
Chloroform	5000	2.00	10,000
Crown Ether (kg)	92.5	1,000	92,500
Water (liters)	1600000	0.00040	640
LiCl Feed (kg)	14607	1	14,607
Total Operating costs			2,400,000
Profits			
Enriched LiCl Sales (kg)	2430	1,650	4,000,000
Depleted LiCl sales (kg)	12177	0.15	1,830
Net Yearly Profit			1,600,000
Payback Time (years)	7.2		

Table 55 Plant Economics for a 20 ton/year Li-7 throughput (Ault, et al., 2012).

Capital Costs	Quantity	Cost (each) [\$]	Total
Mixer Settlers, C1-1	218	4	24,100,000
Mixer Settlers, C1-2	40	91,208	3,650,000
Mixer Settlers, C1-3	19	75,486	1,400,000
Mixer Settlers, C1-4	24	62,807	1,500,000

Mixer Settlers, C2	25	110,632	2,770,000
Mixer Settlers, C3	25	112,251	2,800,000
Ro systems (GPM)	500	5,000	2,500,000
Spray Dryers	3	2,500,000	7,500,000
Kiln Dryers	2	500,000	1,000,000
Chillers	2	180,000	360,000
MCC	1	3,500,000	3,500,000
Substation	1	775,000	775,000
Misc. and laboratory	1	3,000,000	3,000,000
Organic Recovery Units	2	1,000,000	2,000,000
Installation	1	41,198.187	42,600,000
Facility	47,500	120	5,700,000
chloroform (kg)	37,500,000	2	75,000,000
Crown Ether (kg)	222,000	1,000	222,000,000
Total Capital Costs:			
Yearly Operating Costs:			
Employees	15	150,000	2,250,000
Electricity kWh	39,420,000	0.1	3,942,000
Natural Gas (mmBTU)	50,000	2	100,000
Chloroform (kg)	1,170,000	2	2,340,000
Crown Ether (kg)	55,500	1,000	55,500,000
Water (m ³)	50,000	0	20,000
LiCl Feed (kg)	7,500,000	1	7,500,000
Maintenance / consumables	1	2,750,000	2,750,000
Total Operating costs:			74,400,000
Yearly Income:			
Enriched LiCl (kg)	1,200,000	83.33	101,000,000
Depleted LiCl (kg)	6,300,000	1	6,300,000
Total Yearly Income:			
Net Yearly Profit:			32,500,000
Payback Period (years)	12,4		

Appendix E

For the sake of the report's completeness, the emitted impurities at different stages of a helium-cooled reactor power-up and temperature escalation are reported in the following graph as registered during HTTR operation (Japan Atomic Energy Agency, 2010).

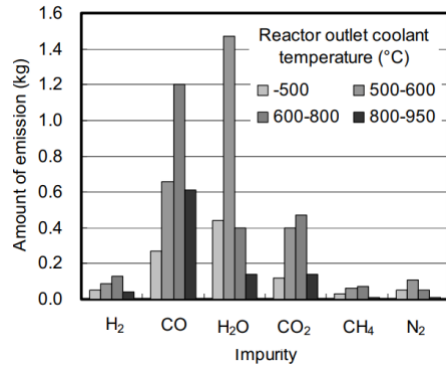


Figure 25 Impurity emission from primary circuit structures in the HTTR at different temperature ranges (Japan Atomic Energy Agency, 2010).

The main reason for an increase of impurity release with temperature is the impurity emission from the graphite material used in the core and as an insulator in the concentric hot gas duct (Japan Atomic Energy Agency, 2010) other than the chemical equilibrium in the core which converts the impurities (especially splitting water and carbon dioxide) given the temperature and pressure conditions.